

The Petrology and Petrogenesis of three Late Archean K-rich  
granites in the Archean Wyoming Province U.S.A.

by  
Maureen E. Wilks

GEOSCIENCE DEPARTMENT  
N.M.I.M.T  
SOCORRO, N.M. 87801

Submitted in Partial Fulfillment  
of the Requirements for the Degree  
Doctor of Philosophy in Geochemistry

New Mexico Institute of Mining and Technology  
Socorro, New Mexico

1991

## Table of Contents

Abstract	iv
Acknowledgements	vi
List of Figures	viii
List of Tables	xiii
List of Plates	xvi
Chapter 1. Introduction	1
Chapter 2. Geology	
2.1. Wind River Range	11
2.1.1. Previous Investigations	11
2.1.2. Summary of Archean History	12
2.1.3. Age Constraints	15
2.1.4. Description of Late Archean Granites	16
2.2. Teton Range	31
2.2.1. Previous Investigations	31
2.2.2. Summary of Archean History	31
2.2.3. Age Constraints	32
2.2.4. Description of Late Archean Granite	32
Chapter 3. Geochemistry and Classification of Plutons	
3.1. Introduction	37
3.2. Sampling Methods	38
3.3. Major Element Data	39
3.4. Trace Element Data	63
3.5. Tectonic Discriminant Diagrams	83
3.6. Comparison to other Late Archean Granites and Post Archean Granites	94
3.7. Conclusion	101
Chapter 4. Petrogenesis	
4.1. Introduction	103
4.2. Constraints	
4.2.1. Field Evidence Constraints	103
4.2.2. Major and Trace Element Constraints	104
4.2.3. Isotopic Constraints	105
4.3. Models	110
4.3.1. Controls on Models	112
4.3.1.1. Partition Coefficients	112
4.3.1.2. Source and Melt Modes	113
4.3.1.3. Melt Fraction-F	114
4.3.1.4. Accessory Phases	115

4.4. Results	116
4.5. Conclusion	137
Chapter 5. Discussion	140
Chapter 6. Conclusion	148
References	150

### Appendices

Appendix A. Data	163
Appendix B. Sample Locations	188
Appendix C. Analytical Techniques	
C1. Initial Sample Processing	191
C2. X-Ray fluorescence	191
C3. Instrumental Neutron Activation Analyses	191
Appendix D. Effects of Partition Coefficients ( $K_D$ ) on Geochemical Models.	209
Appendix E. Effects of source and melt modes on melt composition.	213
Appendix F. Effects of Degree of Partial Melt on magma composition.	216
Appendix G. Effects of Accessory Phases (Zircon, Apatite, Allanite, Sphene, Monazite) on geochemical models.	218
Appendix H. Fine tuning models.	235
Appendix I. Source and Melt Modes for Middle Mountain Pluton.	239
Appendix J. Source and Melt Modes for Dome Peak Pluton.	241
Appendix K. Source and Melt Modes for Mount Owen Pluton.	243

**Abstract**

The late Archean (2.7-2.5 Ga) was a period of worldwide K-rich granite plutonism. In this study three late Archean K-rich granites (Middle Mountain, Dome Peak and Mount Owen plutons) exposed in the Archean Wyoming Province were sampled and analysed in order to understand their petrogenesis and tectonic setting. Middle Mountain and Dome Peak plutons, part of the Bears Ear batholith, are exposed in the northern Wind River Range where they intrude an older migmatite-gneiss terrane. Contacts between the plutons and the country rock are variable, from sharp to gradational over fifty meters. Mount Owen pluton is exposed in the central Teton Range, where it intrudes an older amphibolite-grade metamorphic terrane. Contacts of the pluton are highly irregular, and grade imperceptibly from quartz monzonite with inclusions of wallrock into wallrock containing cross-cutting quartz monzonite dikes. From major element, trace element, and isotopic data, Middle Mountain pluton is a granite with both I-type and S-type source characteristics, Dome Peak pluton is a quartz monzonite with both I-type and A-type source characteristics, and Mount Owen is a quartz monzonite with S-type source characteristics.

All three plutons are interpreted as crustally derived melts. Petrogenetic modelling indicates that Middle Mountain pluton can be generated by 40% partial melting of an older HREE (heavy rare earth) depleted tonalite/trondhjemite source, followed by assimilation of amphibolite with up to 50% fractional crystallisation. The more REE enriched Dome Peak pluton can be

generated by 20% partial melting of an older HREE depleted tonalite/trondhjemite source, followed by up to 50% fractional crystallisation. Mount Owen pluton can be generated by 40% partial melting of an Archean greywacke followed by variable degrees of assimilation of felsic orthogneiss, and up to 50% fractional crystallisation. Their major and trace element geochemistry cannot be used within the framework of Phanerozoic granitoid tectonic discriminant diagrams to confidently determine their environment of genesis.

The fragmented nature of Archean terranes makes it difficult to reconstruct late Archean orogenic events. However, the worldwide late Archean felsic plutonism may either represent the accretion of magmatic terranes to form a supercontinent or global mantle overturn with extensive upwelling of deep mantle plumes. In both cases anatexis will occur in the lower crust to produce granites.

### Acknowledgements

This thesis would not have been possible without the support of my parents, Drs. John and Eileen Wilks, who have always encouraged my globe trotting in pursuit of unravelling Archean crustal evolution.

I thank my advisor Dr. Kent C. Condie for his constructive comments and assistance in the field. A special thanks goes to my other committee members, Drs. Marshall Reiter, Antonius Budding and Andrew Campbell.

I have benefitted from many hours of fruitful discussion with Mark Boryta, Mike Knoper and Bruce Hallett on Precambrian crustal evolution. Mark and Mike are warmly thanked for all their assistance with instrumental neutron activation analyses, and guiding me through the elementary hoops on the road to becoming a semi-literate dweeb. Chris Mckee is thanked for all his help and patience in the preparation and analyses of samples in the XRF lab. Bruce and Davy Pattison, and Mathew Tilman are thanked for their lively assistance in the field.

Financial support for this project came from a teaching assistantship at New Mexico Tech, a Geological Society of America Research Grant (1988/1989), New Mexico Tech Richard A. Matuzeski Graduate Scholarship (1988/1989), J.D. Love Wyoming Geological Society Scholarship (1989), La Luz American Association of Business Women Scholarship (1989), and the Roswell Geological Society

Scholarship (1989).

I am also indebted to Drs. Paul Bauer and Jamie Robertson, and the New Mexico Bureau of Mines for their support of my research in granite petrogenesis in northern New Mexico. Financial support for this project came from a New Mexico Bureau of Mines Research Grant and the New Mexico Geological Society Wellnitz Scholarship.

Part of this thesis was presented at the Third International Archean Symposium in Perth, Australia. I thank Dr. Kent C. Condie, Dr. Al Smoake and the Graduate Office, Dr. Fred Kuellmer and the Research and Development Office, Dr. John Schlue and the Geoscience Department and Dr. Larry Lattman for supporting my way to Perth. I also thank the organisers of the symposium for financial support in Australia. Drs. Dave Johnson and Don Wolberg are thanked for their help in preparation of photomicrographs and slides.

Finally I would like to thank Diane Bellis, Carol Rison, Ruta Bastian, Ricky and Soledad Sanchez, Helen Sanchez and Dr. Bob for their friendship, support, encouragement and most of all refreshments when needed!

## Figures

Figure 1.1:	Map of the distribution of Archean rocks in the Wyoming Province.	5
Figure 1.2:	Cross-section through the Wind River Range.	9
Figure 2.1:	Geological map of the Wind River Range.	13
Figure 3.1:	Shand's index for Middle Mountain, Dome Peak and Mount Owen plutons.	41
Figure 3.2a:	CIPW normative classification of granites (Middle Mountain, Dome Peak and Mount Owen plutons).	44
Figure 3.2b:	CIPW normative classification of granites (Bridger and Louis Lake batholiths).	45
Figure 3.3a:	Ab-Or-Q plots of Middle Mountain, Dome Peak and Mount Owen plutons.	46
Figure 3.3b:	Ab-Or-Q plots of the Bridger and Louis Lake batholiths.	47
Figure 3.4:	Harker variation diagrams of major elements for Middle Mountain pluton.	50
Figure 3.5:	Qz-Ab-Or plots for Middle Mountain, Dome Peak and Mount Owen plutons.	51
Figure 3.6:	Harker variation diagrams of major elements for Dome Peak pluton.	52
Figure 3.7:	Harker variation diagrams of major elements for Mount Owen Pluton.	55
Figure 3.8:	Shand's index for the Bridger and Louis Lake batholiths.	57
Figure 3.9:	Harker variation diagrams of major elements for Bridger batholith.	60
Figure 3.10:	Harker variation diagrams of major elements for Louis Lake batholith.	61
Figure 3.11:	Harker variation diagrams of trace elements for Middle Mountain pluton.	64
Figure 3.12:	Harker variation diagrams of trace elements for Dome Peak pluton.	65



Figure 3.13:	Harker variation diagrams of trace elements for Mount Owen pluton.	66
Figure 3.14a:	REE plots for Middle Mountain pluton.	67
Figure 3.14b:	REE plots for Dome Peak pluton.	68
Figure 3.14c:	REE plots for Mount Owen pluton.	69
Figure 3.15a:	Primordial mantle-normalised plots for Middle Mountain pluton.	71
Figure 3.15b:	Primordial mantle-normalised plots for Dome peak pluton.	72
Figure 3.15c:	Primordial mantle-normalised plots for Mount Owen pluton.	73
Figure 3.16:	Harker variation diagrams of trace elements for Bridger batholith.	75
Figure 3.17:	Harker variation diagrams of trace elements for Louis Lake batholith.	76
Figure 3.18a:	REE plots for Bridger batholith.	77
Figure 3.18b:	REE plots for Louis Lake batholith.	78
Figure 3.19a:	Primordial mantle-normalised plots for Bridger batholith.	80
Figure 3.19b:	Primordial mantle-normalised plots for Louis Lake batholith.	81
Figure 3.20:	Rb-Y-Nb tectonic discriminant diagram for Middle Mountain, Dome Peak and Mount Owen plutons.	84
Figure 3.21:	Rb-Hf-Ta tectonic discriminant diagrams for Middle Mountain, Dome Peak and Mount Owen plutons.	86
Figure 3.22:	Rb-Y-Nb tectonic discriminant diagrams for Bridger and Louis Lake batholiths.	87
Figure 3.23:	Rb-Hf-Ta tectonic discriminant diagrams for Bridger and Louis Lake batholiths.	88
Figure 3.24:	Gallium (Ga) discriminant diagrams for Middle Mountain, Dome Peak and Mount Owen plutons.	90
Figure 3.25:	Ga and ZNCY discriminant diagrams for Middle Mountain, Dome Peak and Mount Owen plutons.	91

Figure 3.26:	Gallium (Ga) discriminant diagrams for Bridger and Louis Lake batholiths.	92
Figure 3.27:	Ga and ZNCY discriminant diagrams for Bridger and Louis Lake batholiths.	93
Figure 3.28:	REE plots for selected late Archean granites.	95
Figure 3.29:	Rb-Y-Nb tectonic discriminant diagrams for selected late Archean granites.	96
Figure 3.30:	ZNCY discriminant plots for selected late Archean granites.	97
Figure 3.31:	REE plots for selected Proterozoic granites.	99
Figure 3.32:	Primordial mantle-normalised plot of selected Proterozoic granites and Middle Mountain, Dome Peak and Mount Owen plutons.	100
Figure 4.1:	REE and Primordial mantle-normalised plots for range of melts produced by 40% batch melting of the older granitoids.	118
Figure 4.2:	Ba versus Sr plot of the FXL trend of a melt produced by 40% partial melt of the older granitoids.	119
Figure 4.3:	La/Yb versus Yb plot of the FXL trend of a melt produced by 40% partial melt of the older granitoids.	119
Figure 4.4a:	La versus SiO <sub>2</sub> plot for Middle Mountain pluton.	120
Figure 4.4b:	La/Yb versus SiO <sub>2</sub> plot for Middle Mountain pluton.	120
Figure 4.5:	La/Yb versus Yb plot of AFC trends for Middle Mountain pluton.	122
Figure 4.6:	Ba versus Sr plot of an AFC trend for Middle Mountain pluton.	122
Figure 4.7:	Nb versus Y tectonic discriminant plot to show FXL and AFC trends for Middle Mountain pluton.	124

Figure 4.8a/b:	REE element and Primordial mantle-normalised plots for the range of melt generated by 20% batch melting of the minimum and maximum values of Bridger/Louis Lake batholiths.	126
Figure 4.9:	FXL trend of a melt produced by 20% batch melting of the older granitoids on a Ba versus Sr plot.	127
Figure 4.10:	FXL trend of a melt produced by 20% batch melting of the older granitoids on a La/Yb versus Yb plot.	127
Figure 4.11a:	La versus SiO <sub>2</sub> plot for Dome Peak pluton.	128
Figure 4.11b:	La/Yb versus SiO <sub>2</sub> plot for Dome Peak pluton.	128
Figure 4.12:	FXL trend of melt produced by 20% batch melting of the older granitoids on a Rb-Y-Nb discriminant diagram.	129
Figure 4.13:	REE plot of produced by 40% batch melting of an Archean greywacke.	132
Figure 4.14:	FXL trend of a melt produced by 40% batch melting an Archean greywacke on a Ba versus Sr plot.	134
Figure 4.15:	FXL trend of a melt produced by 40% batch melting of an Archean greywacke on a La/Yb versus Yb plot.	134
Figure 4.16a/b:	AFC trends for a melt produced by 40% batch melting of an Archean greywacke on La/Yb versus Yb plots.	135
Figure 4.17a/b:	AFC trends for a melt produced by 40% batch melting of an Archean greywacke on Ba versus Sr plots.	136
Figure 4.18:	FXL and AFC trends for a melt produced by 40% batch melting of an Archean greywacke on a RB-Y-Nb discriminant diagram.	138
Figure D1:	Effect of maximum and minimum K <sub>D</sub> values on the REE concentration in the melt.	212
Figure D2:	Effect of varying only the K <sub>D(Eu/Plag)</sub> on the REE concentration in the melt.	212

Figure E1:	Effect of varying the source mode on the REE concentration in the melt.	215
Figure E2:	Effect of Opx and Hbl on the concentration of REE in the melt.	215
Figure F1:	Effect of degree of partial melt on REE concentration in the melt.	217
Figure G1:	Results of hydrothermal zircon saturation/solubility experiments.	221
Figure G2:	Effect of varying source and melt modes on the REE and Zr concentration in the melt.	224
Figure G3:	Plot of $\ln D_{Zr}^{zircon/melt}$ for different M values.	224
Figure G4:	Effect of varying source and melt modes on the REE and $P_2O_5$ concentration in the melt.	227
Figure G5:	Effect of different apatite $K_D$ values on REE content in melt.	227
Figure G6:	Effect of varying source and melt modes for allanite on the REE concentration in the melt.	230
Figure G7:	Effect of different $K_D$ values for allanite on REE concentration in the melt.	230
Figure G8:	Effect of different $K_D$ values for sphene on the REE concentration in the melt.	233
Figure G9:	Effect of varying the source and melt modes of monazite on the REE concentration in the melt.	233
Figure H1:	REE patterns produced by 40% batch melting, with varying source and melt modes of accessory phases.	237
Figure H2:	REE pattern of average Middle Mountain pluton with Figure H1.	238

## Tables

Table 1.1:	Summary of radiometric ages for the Wyoming Province.	6
Table 2.1:	Geochronological data for the Wind River and Teton Ranges.	14
Table 3.1:	Average major and trace element contents of granites from Middle Mountain, Dome Peak and Mount Owen plutons.	42
Table 3.2:	I/S-type classification of granites.	48
Table 3.3:	Average major and trace element contents of granites from Bridger and Louis Lake batholiths.	58
Table 4.1:	Summary of isotopic data for the Wind River Range.	106
Table 4.2:	Summary of isotopic data for the Teton Range.	131
Table C1:	Information for X-Ray Fluorescence Analyses.	192
Table C2:	Major (XRF) and trace (INNA) element analyses of standard BCR-1 (basalt).	194
Table C3:	Trace element analyses (XRF) of standard GS-N (granite)	196
Table C4:	Trace element analyses (XRF) of standard AN-G (anorthosite).	197
Table C5:	Trace element analyses (XRF) of standard NIM-G (granite).	198
Table C6:	Trace element analyses (XRF) of standard W-2 (diabase).	199
Table C7:	Information for Instrumental Neutron Activation Analyses (INNA).	201
Table C8:	Table of uncorrected and corrected INNA data.	204

Table C9:	Trace element analyses (INNA) of Fly Ash standard NBS1633a.	205
Table C10:	Trace element analyses (INNA) of standard G-2 (granite).	206
Table C11:	Trace element analyses (INNA) of standard AGV-1 (andesite).	207
Table D1:	Average felsic $K_D$ values for major rock forming minerals.	210
Table D2:	Minimum and maximum felsic $K_D$ values of REE for major rock forming minerals.	211
Table E1:	Source and melt modes for partial melt models.	214
Table G1:	$K_d$ values for REE in accessory phases.	219
Table G2:	Calculation of whether zircon is a residual phase on melting the older granitoids.	222
Table G3:	Calculation of whether zircon is a residual phase on melting an Archean greywacke.	222
Table H1:	Source and melt modes for 40% batch melting of the older granitoids.	236
Table I1:	Composition of sources used in batch melting, FXL and AFC models for Middle Mountain pluton.	239
Table I2:	Crystallising modes for FXL and AFC models for Middle Mountain pluton.	240
Table J1:	Composition of sources used in batch melting, and FXL models for Dome Peak pluton.	241
Table J2:	Sources and melt modes for batch melting models for Dome Peak pluton.	242

Table J3:	Crystallising modes for FXL models for Dome Peak pluton.	242
Table K1:	Composition of sources used in batch melting, FXL, and AFC models for Mount Owen pluton.	243
Table K2:	Source and melt modes for batch melting an Archean greywacke.	244
Table K3:	Crystallising modes for FXL and AFC models for Mount Owen pluton.	244

**Plates**

Plate 1	Hand specimen of the Bridger batholith	17
Plate 2	Photomicrograph of the Bridger batholith.	18
Plate 3	Hand specimen of the Louis Lake batholith.	20
Plate 4	Photomicrograph of the Louis Lake batholith.	21
Plate 5	Hand specimen of Middle Mountain pluton.	24
Plate 6	Photomicrograph of Middle Mountain pluton.	25
Plate 7	Contact between Middle Mountain pluton and country rock.	26
Plate 8	Contact between Middle Mountain pluton and country rock.	27
Plate 9	Hand specimen of Dome Peak pluton.	29
Plate 10	Photomicrograph of Dome Peak pluton.	30
Plate 11	Hand specimen of Mount Owen pluton.	34
Plate 12	Photomicrograph of Mount Owen pluton.	35
Plate 13	Contact between Mount Owen pluton and country rock.	36



## Chapter 1

### Introduction

#### General Background

The formation of continents began in the Archean (4.6 Ga to 2.5 Ga ago). Proterozoic and Phanerozoic rock sequences can be interpreted within the framework of modern plate tectonics by direct analogy to present-day environments (Hoffman, 1980; Windley, 1984). However in the Archean, the fragmentary nature of the rock record, coupled with theoretical and observational evidence (Richter, 1985; Bickle, 1982) that Archean mantle temperatures were 200°C to 400°C hotter than today render a uniformitarian approach less tenable. Igneous-rock compositions depend both upon the tectonic processes and thermal state within the source region. One may therefore expect a secular evolution of magmatic processes as global tectonic processes change with cooling interior temperatures.

Many Archean igneous rocks are compositionally and petrologically similar to modern igneous rocks. However, distinct differences include:

- 1) Presence of komatiites derived from high temperature ( $\geq 1600^\circ\text{C}$ ) liquids with  $>20\%$  MgO (Arndt, 1986).
- 2) Calc-alkali suites characterised by higher Ni, Cr and highly fractionated REE contents (Taylor and McLennan, 1985; Bickle, 1990).
- 3) The lack of undisputed Ocean Ridge Basalts (MORB) (Bickle, 1990).

4) The lack or paucity of alkali and alkaline volcanics and plutonics (Taylor and McLennan, 1985; Bickle, 1990).

1) and 4) are taken as evidence of higher temperature source regions and higher degrees of partial melting.

Three problems dominate Archean geology:

1) Discovering the tectonic systems by which the surface of the Earth was constructed;

2) The rate of growth of continental crust with time; and

3) The origin of life.

This thesis study concentrates on addressing the first issue.

### **Purpose of Investigation**

The dominant crustal component in Archean cratons is I-type HREE (heavy rare earth element) depleted tonalites (Windley, 1984; Taylor and McLennan, 1985; Nisbet, 1987). Minor amounts of potassic granites are known to occur in the early and middle Archean, e.g. Mount Edgar batholith, Pilbara craton (Collins, 1988), but it is not until the late Archean 2.7-2.5 Ga that voluminous amounts of K-rich granites occur (Windley, 1984; Taylor and McLennan, 1986).

Much work has focused on the origin of HREE depleted tonalites (Arth et al., 1978; Martin, 1987; Rudnick and Taylor, 1987) with partial melting of eclogite, garnet/hornblende amphibolite and garnet granulite as viable sources. An important constraint for these sources is the retention of

garnet and/or hornblende in the source region to retain the HREEs. Little work has focused on the origin of late Archean K-rich granites, in part because it is only in the last ten years that combined regional mapping and geochronology has revealed their sizeable volume in individual cratons. Notable examples occur in the Slave (Kusky, 1989; Davies et al., 1990), Pilbara (Collins, 1988; Bickle, 1989), Dawar (Allen et al., 1986; Oak and Friend, 1990) and Wyoming (Peterman, 1979; Stuckless, 1989) Cratons.

Most Archean cratons record a major period of crustal growth, metamorphism, deformation, and plutonism around 2.7Ga, with the final magmatic event being the emplacement of K-rich granites. This worldwide event may represent

- 1) The final stabilisation of individual cratons;
- 2) The amalgamation of the Archean cratons to form a supercontinent; or
- 3) Major hot spot-plume tectonics due to either the breakup of a supercontinent similar to the breakup of Pangaea (Anderson, 1983), the incipient breakup of Laurentia in the late Early Proterozoic (Hoffman, 1989) or core-mantle cooling causing major instabilities (plumes) at this boundary.

The purpose of this study is to understand the origin and petrogenesis of three late Archean granites exposed in the Wyoming Craton, and to compare their geochemistry with post-Archean granites and thereby determine any secular variations in granitoid (crustal) evolution through time.

## Regional Geology

The Precambrian rocks of the Wyoming Province occur in the cores of major crustal blocks uplifted during the Laramide orogeny from Late Cretaceous to Early Tertiary time. These blocks (Figure 1.1) are separated by basins containing thick sequences of Phanerozoic sedimentary rocks. The structural relief on the surface of the Precambrian is locally as much as 12,500m. The boundaries of the Wyoming Province are ill defined except along the southern margin in the Sierra Madre, Medicine Bow and Laramie Ranges where Proterozoic rocks overlie the Archean basement along the Cheyenne Shear Zone (Karlstrom and Houston, 1984; Dubendorfer and Houston, 1986). The known limits suggest a province as large as  $5 \times 10^5 \text{ km}^2$ . Geological and geochronological data for the Archean basement uplifts is summarised in Table 1.1.

The Wyoming Province can be divided broadly into a northern and southern region. In the northern region the North Snowy Mobile Block separates an older high-grade metasedimentary terrane exposed in the Madison and Gallatin Ranges from a younger tonalite and tonalite gneiss terrane exposed in the western Beartooth and Bighorn Mountains (Figure 1.1). The high-grade metasedimentary terrane is interpreted as a passive margin sequence with later tonalites generated by subduction of oceanic crust (Mogk et al., 1988).

The southern region including the Teton, Owl Creek, Wind River, Granite, Sierra Madre, Medicine Bow, and Laramie Ranges

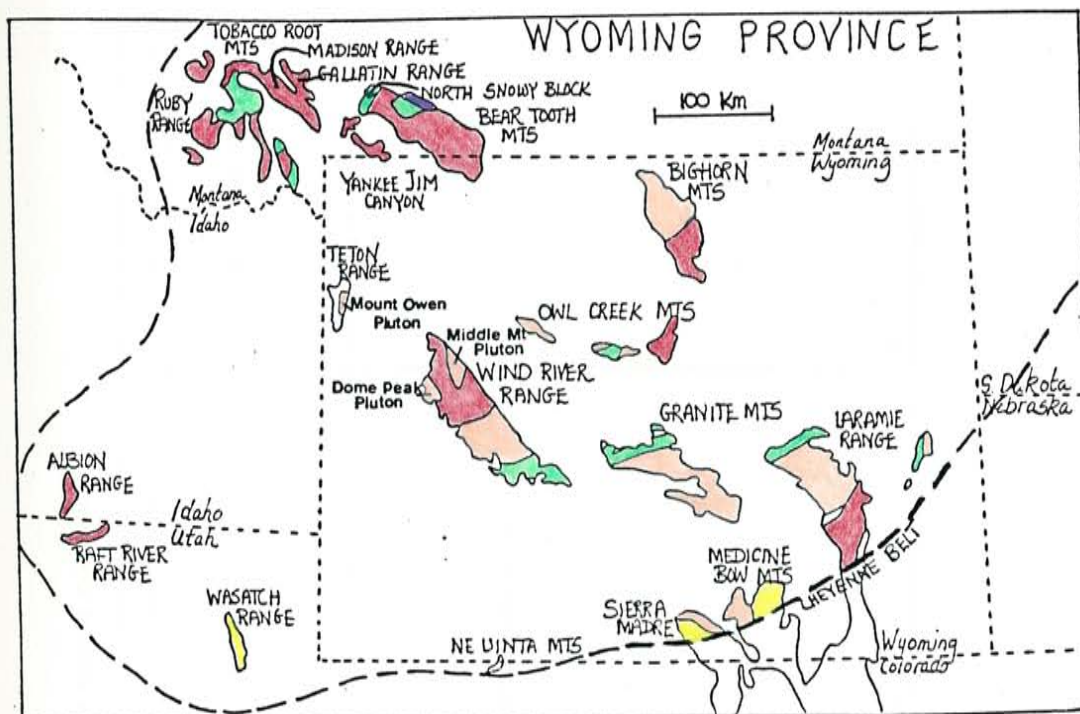


FIGURE 1.1: The Archean age Wyoming Province, USA. Precambrian rocks occur in the cores of major Laramide uplifts.

- Greenstones
- Gneisses (dominantly tonalite)
- Granites
- Metasediments
- Stillwater Complex

Table 1.1: Summary of radiometric ages for the Wyoming Province

	Wind River Range	Granite Mountains	Medicine Bows & Sierra Madres	N. Laramie Range
2.4Ga	+++Bears Ear Batholith	+++ Lankin Dome Batholith	+++ Baggots Rock Granite	+++ Laramie Granite
2.6Ga	+++Louis Lake Batholith			+++ Leucogranite
2.8Ga	xxxBridger Batholith	xxx Qtz-Fsp-Gneiss	xxx Tonalite gneiss	--- Migmatite
3.0Ga				
3.2Ga	*** xenocrystic zircon from orthogneiss	xxx Tonalite gneiss		
3.4Ga	xxx Orthogneiss			
3.6Ga	*** xenocrystic zircon from orthogneiss			
3.8Ga	*** xenocrystic zircon			
4.0Ga				
Refs	1,4,7,10	8,11	8	8

Table 1.1 cont.

	Madison & Gallatin Mts	Beartooths	Big Horns	Grand Tetons
2.4Ga		+++ Felsic gneissic sills		+++ Mt. Owen Qtz Monzonite
2.6Ga		+++ Long Lake Granite		
2.8Ga	xxx Tonalite gneiss	^^^ Amphibolite (Andesite)	xxx Tonalite gneiss	xxx Amphibolite/Felsic gneiss
3.0Ga			xxx Tonalite gneiss	
3.2Ga	xxx Tonalite gneiss xxx Tonalite gneiss			
3.4Ga				
3.6Ga				
3.8Ga				
Refs	3, 5, 6	3, 5, 6	2, 8	9

References: 1: Aleinikoff et al. (1989); 2. Arth et al. (1980); 3. Henry et al. (1982); 4. Koesterer et al. (1987); 5. Mogk et al. (1988); 6. Mueller et al. (1983); 7. Naylor et al. (1970); 8. Peterman (1979); 9. Reed and Zartman (1973); 10. Stuckless et al. (1985); 11. Stuckless et al. (1986).

+++ unfoliated granite/tonalite  
xxx foliated tonalite gneiss  
^^^ amphibolite  
--- migmatite  
\*\*\* xenocrystic zircon

are dominated by syn- and post-tectonic granites (2.7-2.5Ga).

## **Local Geology**

### **Wind River Range**

The Wind River Range in western Wyoming is a Laramide uplift approximately 200km long and 70km wide (Figure 1.1). The NW-SE trending massif is composed almost entirely of Archean granites and high-grade Archean gneisses, which were thrust to the west over Paleozoic and Mesozoic sedimentary rocks during the Laramide orogeny (Figure 1.2). The Wind River uplift is the largest Laramide structure in Wyoming with maximum structural relief between the Precambrian peaks and the crystalline basement in the Green River basin to the east of about 13km (Figure 1.2), (Hurich and Smithson, 1982). On the eastern side of the range, Phanerozoic sediments rest directly on the Precambrian basement. The Archean block was tilted during thrusting so that there is a general increase in depth of exposure as one goes from east to west across the range (Mitra and Frost, 1981).

Estimates from reconnaissance mapping indicate that approximately 80% of the range is composed of late Archean granitoids (Worl et al., 1986). The remaining 20% of the area consists of high-grade gneisses with a large supracrustal component into which the late Archean granites were emplaced.



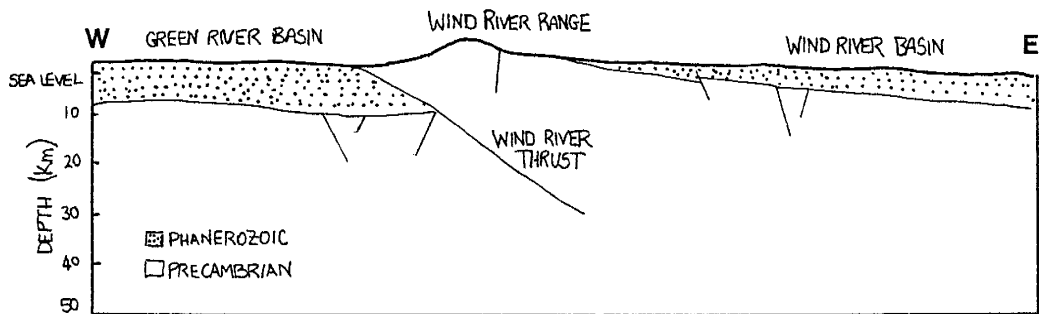


Figure 1.2: E-W cross section through Wind River Range from Smithson and Hurich (1982)

**Teton Range**

The Teton Range is a fragment of a large northwest trending Laramide uplift that was sundered in late Pliocene or Pleistocene time by a zone of major north-south normal faults along which the eastern edge of the Teton block was uplifted and the floor of Jackson Hole was dropped. The total vertical displacement on the fault zone is estimated to be as much as 10km (Love and Reed, 1968). The area of exposed Archean rocks is only 450km<sup>2</sup> and the precipitous eastern face of the range provides a nearly continuous vertical cross section with a maximum relief of nearly 2100m. The oldest rocks comprise a metamorphic complex of migmatite, hornblende gneiss, amphibolite, trondhjemite gneiss and minor iron formation (Reed, 1963). The metamorphic complex is intruded by an unfoliated late Archean (2.49Ga) granite (Reed and Zartman, 1973).

## CHAPTER 2

### LOCAL GEOLOGY

#### 2.1: Wind River Range

##### 2.1.1: Previous Investigations

The first descriptive account of the Wind River Range was made by St. John (1878) from the Hayden surveys of the Territories. For an excellent review of subsequent investigations prior to 1970 the reader is referred to Anderson (1986).

The Wind River Range includes the Bridger Wilderness, Fitzpatrick Wilderness (formerly Glacier Primitive Area), Popo Agie Primitive Area and the Wind River Reservation. Individual areas have been mapped on a reconnaissance scale. The Popo Agie (1:62,500) by Pearson et al. (1971), Glacier Primitive Area (1:62,500) by Granger et al. (1971) and the Bridger Wilderness (1:100,000) by Worl et al. (1986). A few detailed field studies (Link et al., 1985; Anderson, 1986; Koesterer, 1986) have been done in the west-central Wind River Range to unravel the geological history as exposed in the older gneiss terrane. Two field based studies within the late Archean granites were done, one in the southern Wind River Range by Benedict (1982) who looked at the mineral potential of the Schiestler Peak area and one in the northern Wind River Range by Marshall (1987) who concentrated on the structure and petrology of an Archean shear zone. These studies provided the

basis of the geological framework for this geochemical study of the late Archean granites.

### 2.1.2: Summary of Archean History

In the west-central part of the Range detailed mapping in the older gneiss terrane (Link et al., 1985; Anderson, 1986; Koesterer, 1986) and geochronology (Koesterer et al., 1987; Aleinikoff et al., 1989) has revealed an extensive Archean crustal history. A summary of this early to late Archean history taken from Koesterer et al. (1987) is outlined below. All unit abbreviations are modified from Worl et al. (1986) and refer to Figure 2.1.

#### Early to Middle Archean

- 1: Deposition of oldest supracrustal rocks accompanied by intrusion of layered basic and ultrabasic rocks.
- 2: Deformation, granulite facies metamorphism ( $M_1$ ): Intrusion of older granitoids.
- 3: Intrusion of narrow porphyritic dikes (Victor dikes).
- 4: Deposition of Medina Mountain supracrustal rocks.
- 5: Deformation to form tight isoclinal structures, amphibolite facies metamorphism ( $M_2$ ), locally reaching granulite grade.

#### Late Archean

- 6: Emplacement of Bridger and Europe Canyon batholiths

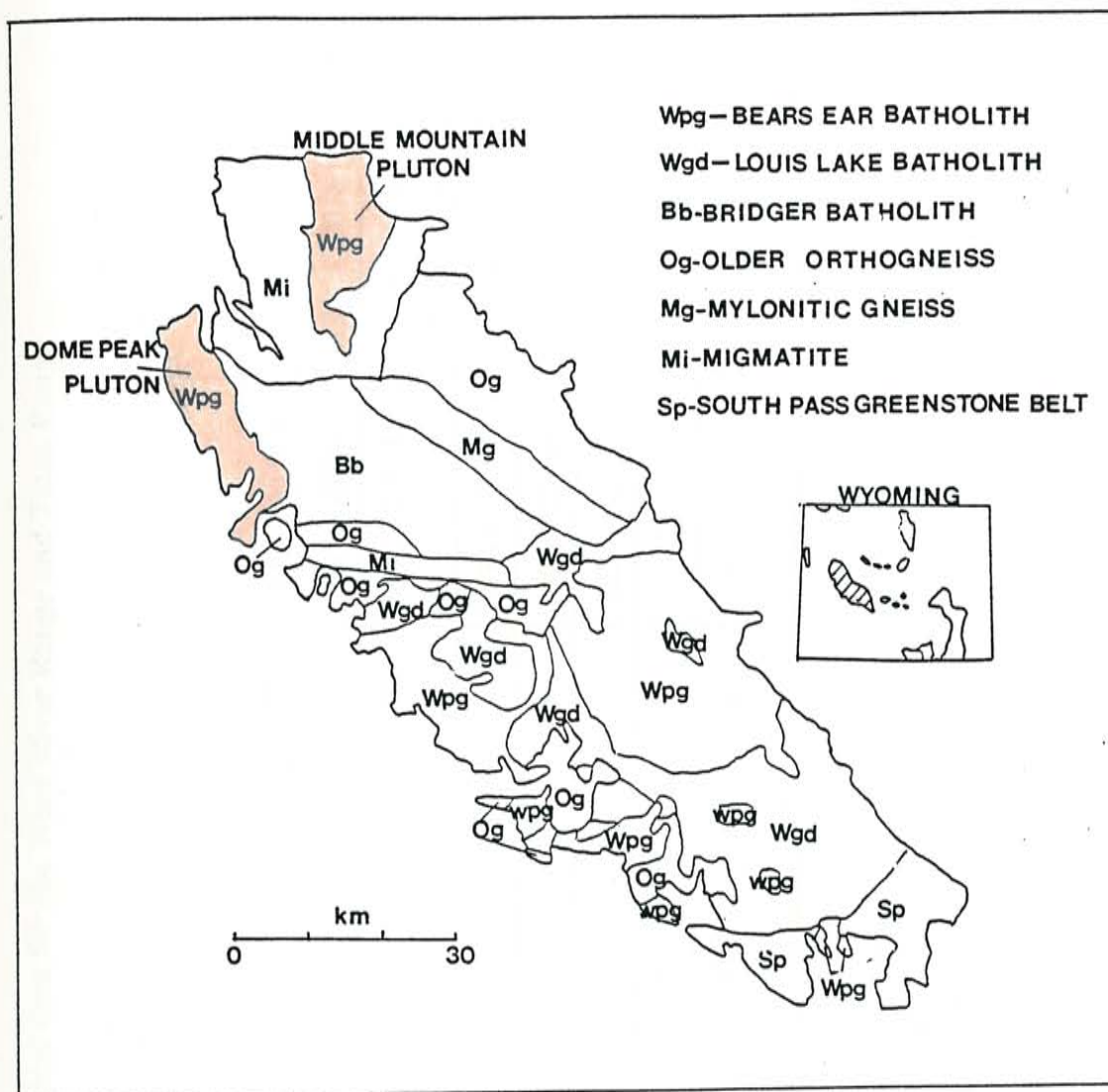


Figure 2.1: Geological map of the Wind River Range simplified from Worl et al. (1986). The Bears Ear batholith (Wpg--2.5Ga) intrudes an older (3.8-2.7Ga) complex of migmatite, granulite to amphibolite orthogneiss and paragneiss including the Bridger (Bb--2.7Ga) and Louis lake (Wgd--2.63Ga) batholiths.

Table 2.1: Geochronological data for the Wind River Range and Teton Range

	OLDER GNEISSES	BRIDGER	LOUIS LAKE	BEARS EAR	MOUNT OWEN
Rb/Sr Age	-----	2655 + 35 Ma	2631 + 35 Ma	2511 +34 Ma	2495 +75 Ma
( <sup>87</sup> Sr/ <sup>86</sup> Sr) <sub>i</sub>	-----	.701 to .704	.7017 +.0005	.7038 + .0018	.7320
U-Pb zircon	3.8,3.65 and 3.3Ga	2670 + 13 Ma 2699 + 7 Ma	2642 + 13 Ma	2575 + 50 Ma 2562 + 75 Ma	-----
U-Pb whole rock	-----	-----	2633 + 33 Ma	2555 + 22 Ma	-----
Th-Pb	-----	-----	2620 + 27 Ma	2543 + 42 Ma	-----
Pb-Pb	-----	-----	2629 + 21 Ma	2572 + 19 Ma	-----
Sm-Nd E <sub>Nd</sub>	Mean -3.71	+3.95 to 3.35	-----	-----	-----
Crustal residence age	3.41-2.94 Ga	3.09 -2.69 Ga	-----	-----	-----

References: Aleinikoff et al., 1989  
Hulsebosch and Frost, 1989  
Koesterer et al., 1987  
Reed and Zartman, 1973  
Stuckless et al., 1985

(BB), accompanied by renewed or continued deformation, extensive migmatization, and formation of partial melts in psammitic and pelitic rocks.

7: Emplacement of the late Archean Louis Lake (Wgd) and Bears Ear batholiths (Wpg).

In the southern end of the Range the late Archean granites intrude the South Pass Greenstone belt. The greenstone belt clearly shows evidence of two episodes of folding and several episodes of faulting (Bayley et al., 1973).

### **2.1.3: Age Constraints**

Numerous geochronological studies have been carried out on the various rock types to better constrain ages of metamorphism, deformation, and emplacement of the late Archean granites, summarised in Table 2.1.

Barker et al. (1979) obtained Rb-Sr whole-rock ages of 2800-3000 Ma for orthogneisses in the northeastern part of the Range (Paradise quadrangle, Wind River Reservation). Aleinikoff et al. (1989) obtained a conventional U-Pb zircon age of  $2670 \pm 13$  Ma for the Bridger batholith, and a granulite related to the intrusion of the Bridger batholith yielded an age of  $2699 \pm 7$  Ma. Ion microprobe data on xenocrystic zircons in an early migmatite granulite yielded ages of 3.3, 3.65 and 3.8 Ga (Aleinikoff et al. 1989). Koesterer et al. (1987) determined an Rb-Sr whole rock age of  $2650 \pm 150$  Ma for the

Bridger batholith.

The Louis Lake batholith has been dated at  $2642 \pm 13$  (Naylor et al. 1970),  $2630 \pm 20$  Ma (Stuckless et al. 1985) by Rb-Sr methods and at  $2642 \pm 13$  Ma (U-Pb zircon, Stuckless et al., 1985). The Bears Ear batholith has been dated (Rb-Sr whole-rock, U-Pb zircon and Pb-Pb whole rock) at about  $2545 \pm 30$  Ma (Naylor et al. 1970; Stuckless et al. 1985).

A metavolcanic unit in the South Pass Greenstone belt yields a Rb-Sr whole rock age of  $2800 \pm 100$  Ma (Peterman, 1982).

#### **2.1.4: Description of the Late Archean Granites**

##### **Bridger Batholith**

The Bridger batholith (Bb) has an outcrop area of 24km by 32 km and it has been correlated with the Europe Canyon granodiorite in the Medina Mountain area (Koesterer et al. 1987). Both the Bridger and Europe Canyon batholiths are composite intrusions with irregular contacts. The bodies are strongly foliated parallel to the regional foliation near the contacts, but appear homogeneous in their cores. Recrystallisation of feldspars is pervasive throughout the plutons and plagioclase grains are locally bent, suggesting the bodies were ductily deformed in a solid state at high temperatures (Koesterer et al. 1987).

In the field the Bridger batholith is a white to light grey, medium grained, equigranular biotite-quartzo-feldspathic gneiss with variable composition (Plate 1). The dominant



## Plate 1

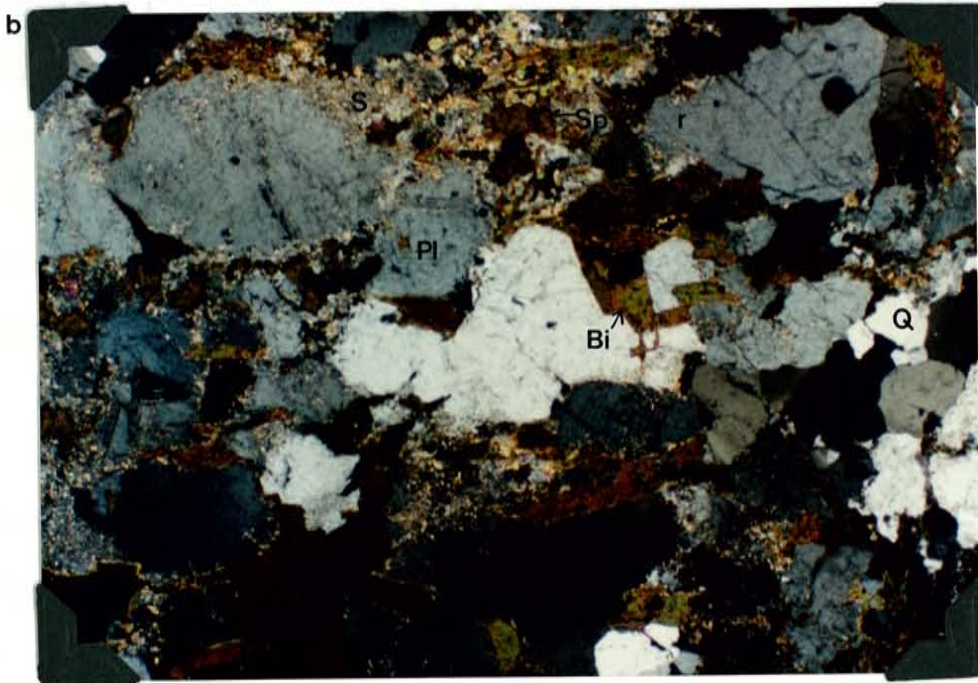
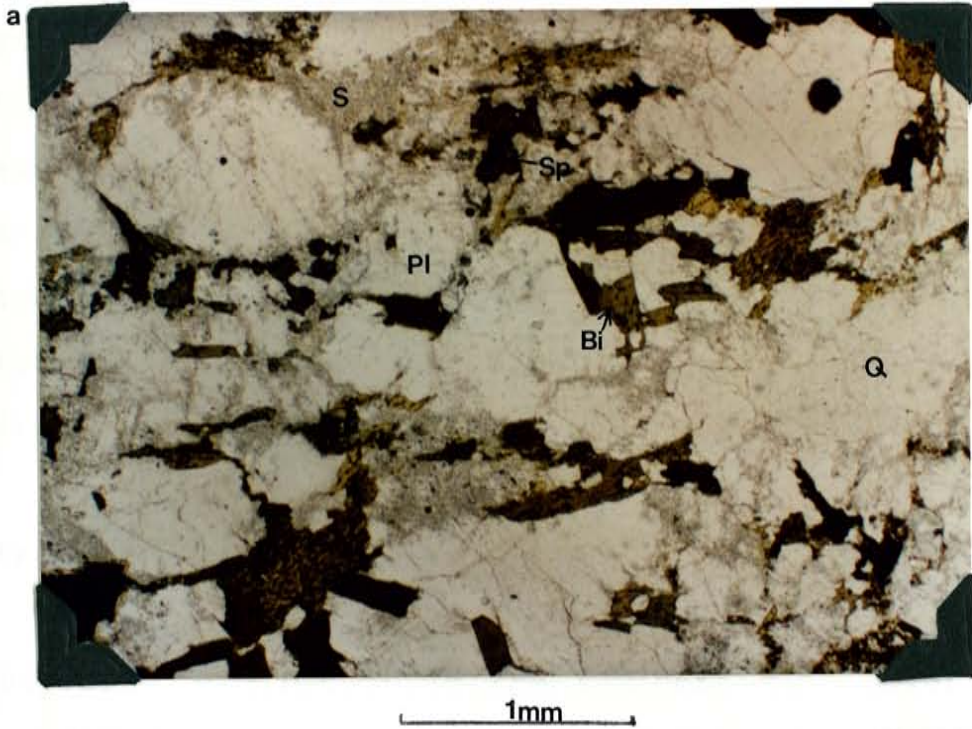
## Hand Specimen from the Bridger Batholith



Bridger batholith: Characteristically this is a light grey medium grained equigranular biotite-quartzo-feldspathic gneiss, with a foliation defined by biotite-rich and quartzo-feldspathic-rich layers.

## Plate 2

## Photomicrograph of the Bridger batholith



a) Plane light b) Crossed-nicols. Q=Quartz, Pl=Plagioclase (Oligoclase) S=Sericite (feldspar alteration), Bi=Biotite, Op=Opauques (ilmenite, magnetite), Sp=Sphene.

phase is granodiorite based on modal analyses by Koesterer (1986), with some tonalitic phases. The rock is composed of plagioclase (25-50%), quartz (25-30%), microcline (5-15%), biotite (3-25%) and hornblende (2-9%) (Koesterer, 1986). Accessory minerals include magnetite, zircon, apatite, allanite and sphene (Plate 2). Biotite defines a weak irregular foliation. This unit contains numerous deformed bodies of metagabbro, metadiorite and amphibolite (Worl et al. 1986).

#### **Louis Lake Batholith (Wgd)**

The Louis Lake batholith was first mapped and described by Bayley (1965a,b,c,d) in the southern Wind River Range, where it is exposed over an area of about 640km<sup>2</sup>. Like the Bridger batholith, the Louis Lake batholith is a composite intrusion and crops out in the southern and central part of the Range (Figure 2.1), where it forms relatively uniform granodiorite bodies with a weak to moderate foliation defined by biotite and hornblende.

The granodiorite is commonly grey, medium grained (Plate 3), with a monzonitic texture and anhedral microcline enclosing euhedral plagioclase. Modal analyses (Bayley et al., 1973; Benedict, 1982) show that it is composed of plagioclase (An<sub>24-29</sub>, 25-60%), quartz (25-30%), microcline (15-9%), biotite (2-25%) and hornblende (0-9%). Pigeonite was found in one sample in the northwest corner of the Temple Peak quadrangle

## Plate 3

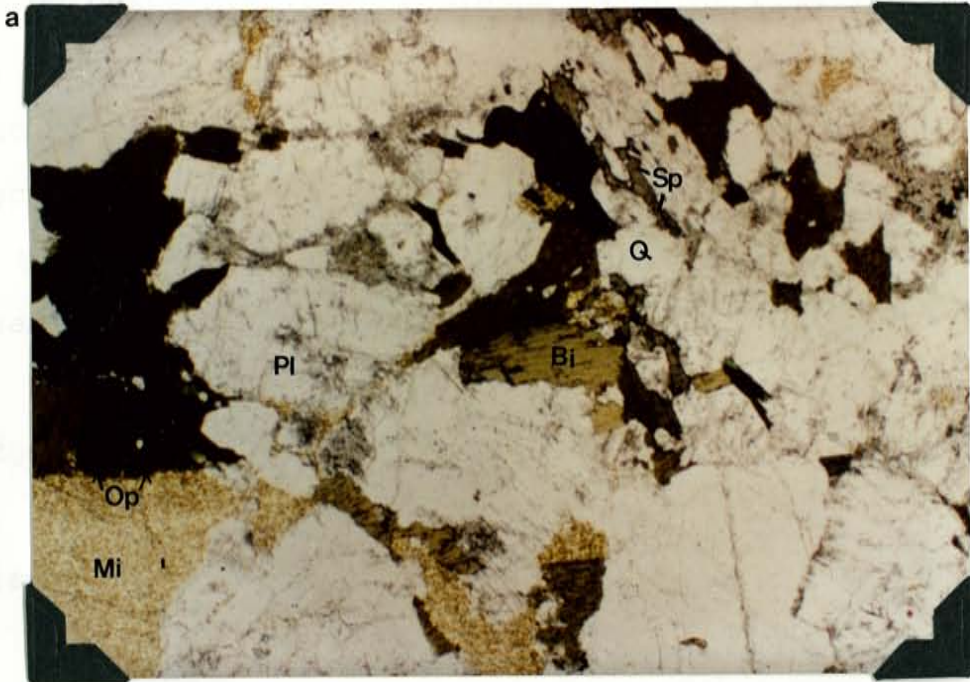
Hand Specimen from the Louis Lake Batholith



Louis Lake granodiorite: A whitish-grey medium grained equigranular rock composed of plagioclase, quartz, pinkish microcline, biotite and minor hornblende.

## Plate 4

## Photomicrograph of the Louis Lake batholith



1mm



a) Plane light, b) Crossed-nicols. Q=Quartz, Pl=Plagioclase (oligoclase, locally altered to sericite), Mi=Microcline, Bi=Biotite, Op=Opagues (ilmenite, magnetite), Sp=Sphene.

(Benedict, 1982). In the west-central part of the Range, orthopyroxene is present as relicts surrounded by cummingtonite-biotite-hornblende reaction rims (Koesterer et al., 1987). Accessory minerals include allanite, sphene, zircon, apatite and magnetite. Low grade alteration has affected most specimens. Plagioclase is commonly sericitised, and mafic minerals are partly chloritised and epidote is disseminated throughout the rock (Plate 4).

Lithologically the Louis Lake batholith is similar to the Bridger batholith, but has not been so highly deformed.

### **Bears Ear Batholith**

The Bears Ear batholith is a composite intrusion that occurs throughout the Wind River Range (Figure 2.1). A body of the batholith was first described by Naylor et al. (1970) from the southern Wind River Range, who named it the Bears Ear pluton, after Bears Ear Mountain. Subsequent workers in other parts of the Range have variously called it the Popo Agie batholith (Pearson et al., 1971), the Middle Mountain batholith (Granger et al., 1971), and in the Bridger Wilderness it corresponds to map unit Wpg (Worl et al., 1986). Stuckless et al. (1985) in a regional geochronological study of the late Archean granites gave the entire unit the name Bears Ear batholith.

The unit is dominantly a quartz monzonite. Two distinct lithologies occur forming individual plutons, although there

are gradations between the two. In the northern Wind River Range these two lithologies form two separate plutons, the Middle Mountain pluton (formerly Middle Mountain batholith of Granger et al., 1971) and Dome Peak pluton (Figure 2.1). These two plutons were chosen for detailed chemical analysis to elucidate the petrogenesis of late Archean K-rich granites.

In the southern Wind River Range, which is dominated by exposures of the Louis Lake and Bears Ear batholiths, further detailed mapping (1:24,000 to 1:5000) is needed to delineate individual plutons before further geochemical study is carried out.

#### **Middle Mountain Pluton**

This north-trending pluton is approximately 20km wide and 30km long (Figure 2.1). The body is composed of granitic rocks that are heterogeneous in texture but generally similar in composition (Appendix A). Two distinct phases were observed (Plate 5a and b), but there is no distinct separation between these phases and they are intermixed throughout much of the pluton.

The most characteristic rock type is a grey to pale-pink biotite granite containing scattered, randomly oriented microcline megacrysts .5 to 1.5cm long. In some places, the porphyritic granite phase grades into a simple pegmatite phase of quartz and microcline. A more equigranular grey granite, similar in composition to the porphyritic granite is also

## Plate 5

## Hand Specimens of Middle Mountain Pluton

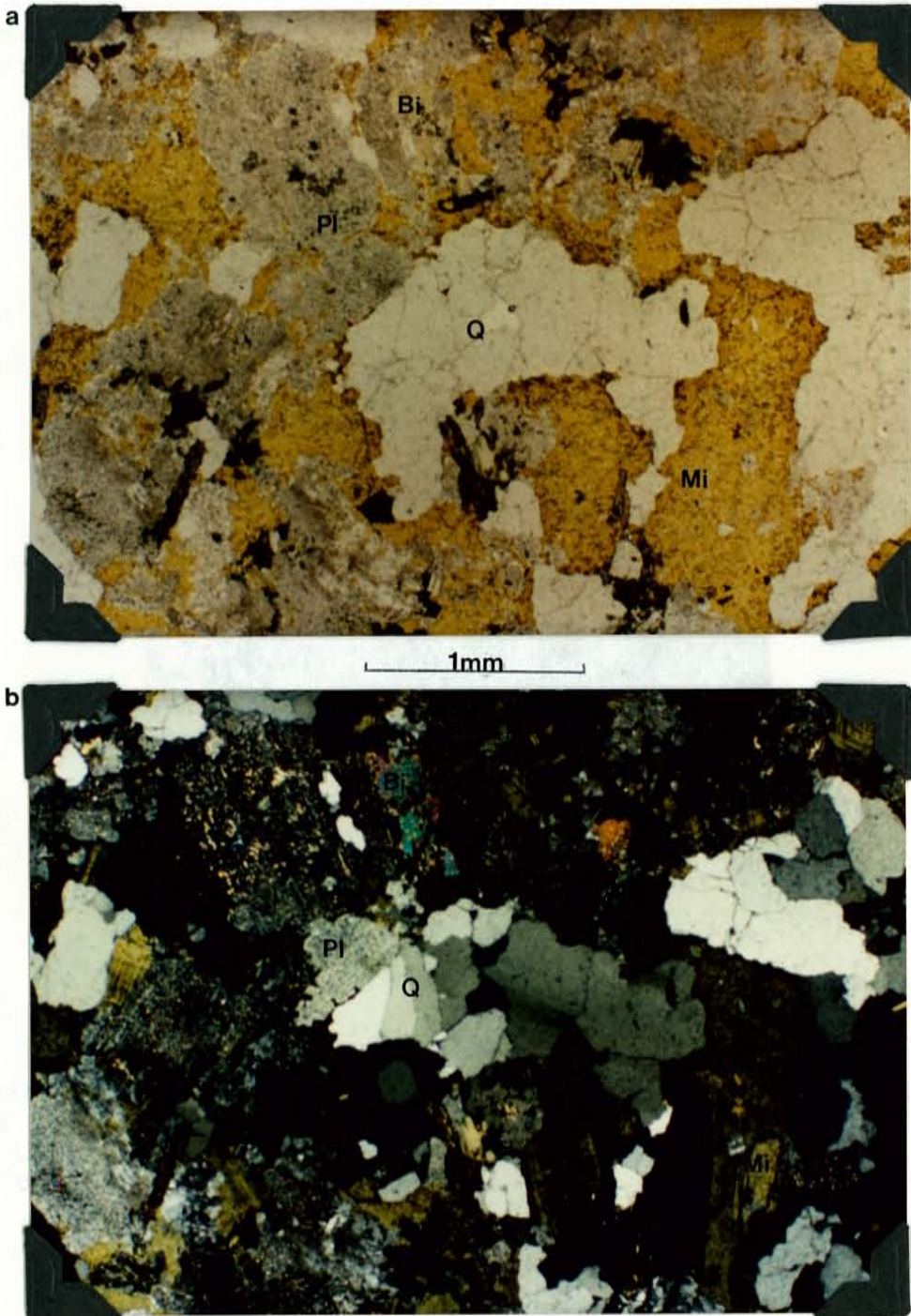


Middle Mountain pluton: a) A grey to pale pink biotite granite, containing scattered randomly oriented microcline megacrysts (.5-1cm long) in a groundmass of plagioclase, quartz, microcline, and biotite. b) a more equigranular grey granite of similar composition to (a).



## Plate 6

## Photomicrograph of Middle Mountain pluton



a) Plane light, b) Crossed-nicols. Q=Quartz, Pl=Plagioclase (oligoclase, locally altered to sericite), Mi=Microcline, Bi=Biotite.

## Plate 7

Contact relationship between the late-granites and older gneisses.



A sharp contact between Middle Mountain granite (MM) and older amphibolite gneiss (AM). Multiple veins and dikes of the granite have invaded the amphibolite. Xenoliths of amphibolite (XM) occur up to 30m from the contact.

## Plate 8

Contact relationship between the late-granites and older gneisses.



A diffuse contact between Middle Mountain granite and the older amphibolite gneiss on the northeastern margin of the pluton, where pinkish fine grained granite both parallels and crosscuts the wavy foliation of the biotite-rich aggregations.

abundant.

The Middle Mountain granite is composed of quartz (20-30%), microcline is commonly perthitic (20-50%), albite or oligoclase is commonly clouded with sericite (15-40%) (Granger et al., 1971) (Plate 6). Biotite can make up to 15% of the rock, but may be sparse or absent. Hornblende occurs only adjacent to amphibolite inclusions (Granger et al., 1971). Accessory minerals include magnetite, zircon, allanite, sphene, and apatite, and alteration products include chlorite, epidote and sericite.

The contacts with the surrounding country rocks vary from sharp to diffuse. Near Louise Lake on the northeastern margin of the pluton the contact with the older amphibolite gneiss is sharp with no evidence of a chilled margin (Plate 7). Along the eastern margin, there is a migmatite zone characterised in different places by lit-par-lit intrusion, partly assimilated blocks of migmatite gneiss, and a network of granitic and pegmatitic dikes (Plate 8). The southern margin of the pluton is terminated abruptly against a northwest-trending Archean fault zone (Granger et al., 1971).

### **Dome Peak Pluton**

The Dome Peak pluton mapped by Worl et al. (1986) and named by the author after Dome Peak which is on the western margin of the pluton is about 8km wide and 30km long. The pluton is dominantly a coarse grained grey porphyritic granite

Plate 9

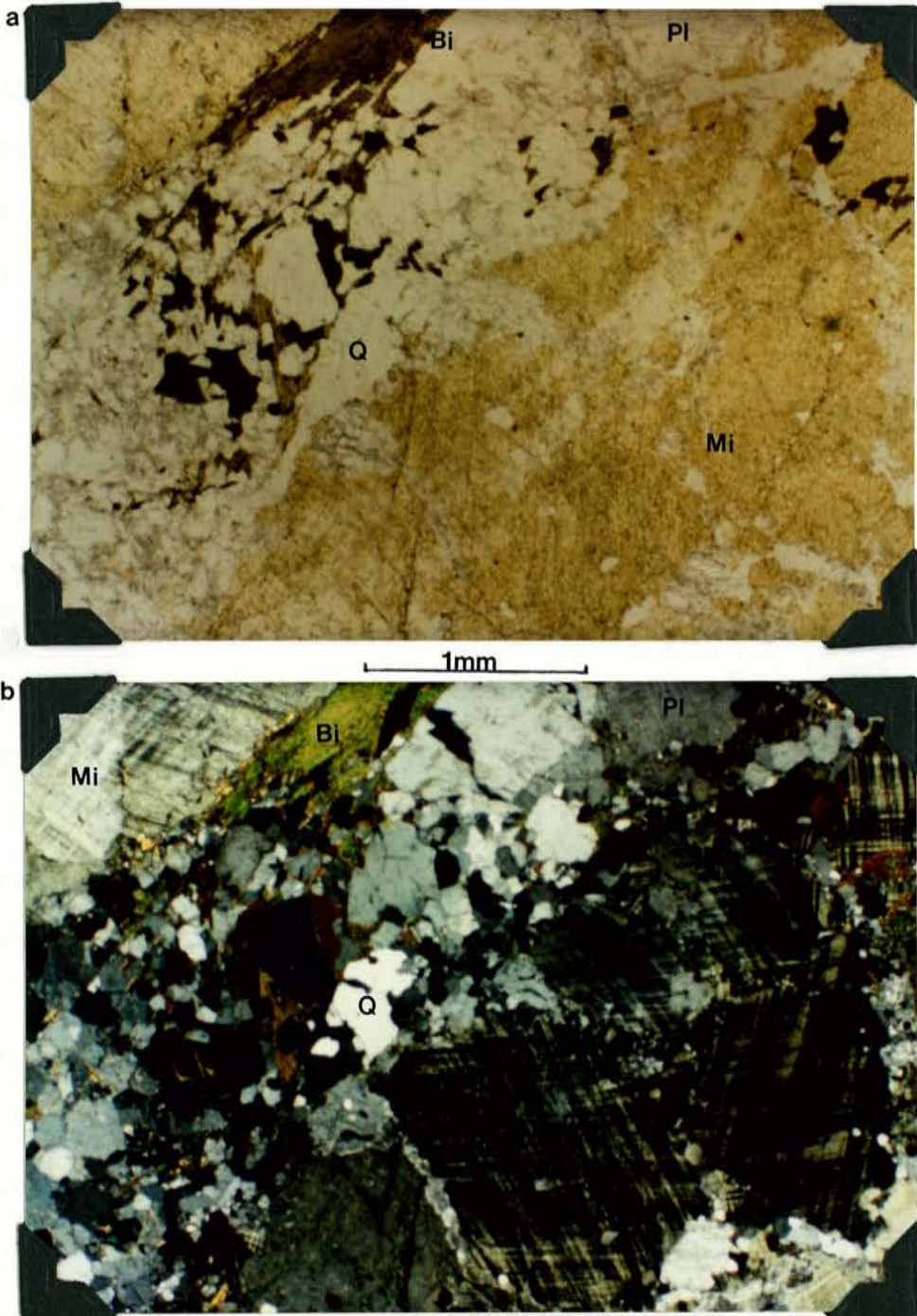
Hand Specimen of Dome Peak Pluton



Dome Peak pluton is a coarse grained porphyritic granite, composed of microcline megacrysts 1.5-5cm long, set in a groundmass of plagioclase, quartz, and biotite.

## Plate 10

## Photomicrograph of Dome Peak pluton



a) Plane light, b) Crossed-nicols. Q=quartz, Pl=Plagioclase (oligoclase), Mi=Microcline, Bi=Biotite.

(Plate 9) with megacrysts of microcline 8cm to 1cm long where they begin to merge with the groundmass of oligoclase (15-40%), quartz (20-30%), biotite (10-25%) and locally, hornblende. Accessory minerals include magnetite, allanite, zircon and apatite, and sphene which is megascopically conspicuous (Plate 10). Locally, the megacrysts are aligned, and the linear character is interpreted as flow structure, which is not apparent in the groundmass.

## **2.2: Teton Range**

### **2.2.1: Previous Investigations**

The Precambrian crystalline rocks of the Teton Range were first described by members of the Hayden survey (Bradley, 1873; St. John, 1879), and Reed (1963) summarises previous investigations. Up to the 1960's the Precambrian rocks had received little attention, although the surrounding Paleozoic and younger rocks had been well studied. The Precambrian core was mapped (1:62,500) by Reed (1973, unpublished).

### **2.2.2: Summary of Archean History**

The oldest rocks in the Teton range are biotite gneiss, plagioclase gneiss, amphibole gneiss and amphibolite (Reed and Zartman, 1973). Within these rocks there are concordant bodies of strongly lineated quartz monzonite (Webb Canyon Gneiss). Coarse metagabbro has intruded the layered gneiss sequence and

is metamorphosed and deformed along with the enclosing rocks. The deformed gneissic rocks display at least two generations of folds (Reed, 1963). Earliest folds are rootless isoclinal. Superimposed on the early isoclinal folds are more open folds with diverse axial orientations, which may be of several generations. Mineral lineations are generally parallel to the axes of the younger folds, suggesting their growth was synchronous with the younger folding.

The deformed layered gneisses are cut by discordant plutons and swarms of undeformed dikes of quartz monzonite and associated pegmatite. This quartz monzonite, which makes up much of the central part of the Teton Range, is one of the plutons analysed as part of this study. Reed and Zartman (1973) named the pluton the Mount Owen Quartz Monzonite.

### 2.2.3: Age Constraints

There has been limited isotopic work on the Teton Range. Rb-Sr whole-rock isochrons on the Webb Canyon Gneiss and Rendezvous Metagabbro indicate that these rocks were metamorphosed at  $2875 \pm 150$  Ma (Reed and Zartman, 1973). The initial  $^{87}\text{Sr}/^{86}\text{Sr}$  isotopic ratio of 0.7000 suggests that the original rocks were probably not significantly older than the metamorphic event.

The Mount Owen pluton has a Rb-Sr whole-rock age of  $2495 \pm 75$  Ma and a high initial  $^{87}\text{Sr}/^{86}\text{Sr}$  isotopic ratio of 0.7320 (Table 2.1) (Reed and Zartman, 1973).



#### 2.2.4: Mount Owen Pluton

The Mount Owen Pluton is a medium to fine grained equigranular light coloured rock (Plate 11), consisting of 30-40% quartz, 20-30% microcline and/or microperthite, 25-35% finely twinned unzoned sodic oligoclase, 5% or less biotite and 1% muscovite (Reed and Zartman, 1973), (Plate 12).

The contacts of the pluton are highly irregular. Xenoliths of wallrocks a few meters to several meters across are common throughout the pluton, as the margins are approached these become more abundant and one passes imperceptibly from quartz monzonite and pegmatite containing abundant inclusions of wallrock into wallrocks containing a myriad of cross-cutting dikes of quartz monzonite and pegmatite (Plate 13).

Contacts of individual dikes are generally sharp, with no evidence of local contact metamorphic effects on the wallrocks and only local evidence of digestion of xenoliths. The pluton was emplaced in rather brittle country rocks by some combination of dilation of fractures and magmatic stoping, without appreciable deformation of the country rocks (Reed and Zartman, 1973).

## Plate 11

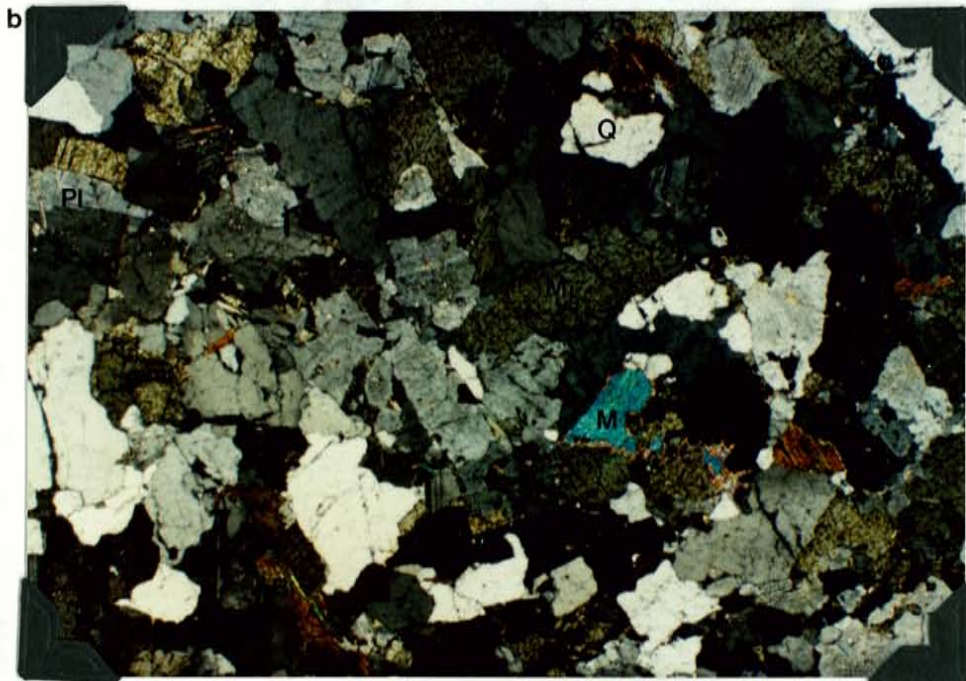
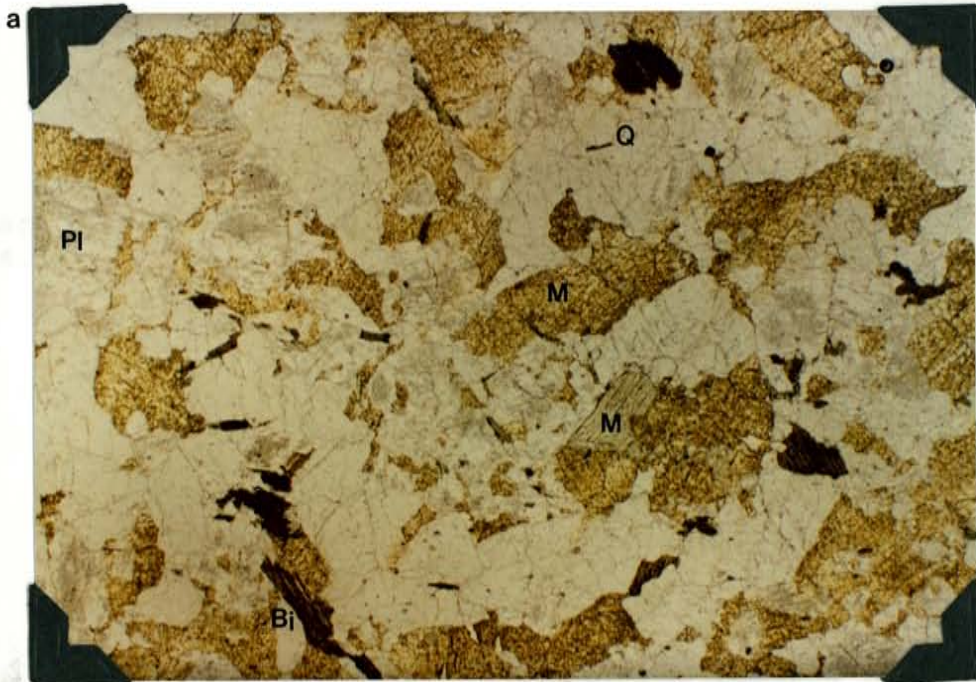
## Hand Specimen of Mount Owen Pluton



Mount Owen pluton is a medium to fine grained whitish quartz monzonite, composed of K-feldspar, plagioclase, quartz, biotite, and minor muscovite.

## Plate 12

## Photomicrograph of Mount Owen pluton



a) Plane light, b) Crossed-nicols. Q=Quartz, Pl=Plagioclase (oligoclase, locally altered to sericite), Bi=Biotite, M=Muscovite.

## Plate 13

Contact relationship between Mount Owen pluton and country rocks.



Mount Owen quartz monzonite (MO-light colored) intrudes as a veined network into older amphibolite gneiss (AM).

## CHAPTER 3

## GEOCHEMISTRY AND CLASSIFICATION OF PLUTONS

**3.1: Introduction**

In classifying granitic rocks the "mineralogy and mode remain of first importance" Pitcher (1987), as it is the stability of the mineral phases that controls the nature of both partial melting and crystal differentiation. The mode and mineralogy described in the previous chapter for all plutons analysed in this study, can chart evolutionary processes. However magmas originating by mechanisms as diverse as batch melting, fractional melting, assimilation and fractional crystallisation, liquid unmixing and selective metasomatism may evolve towards similar end members. From the availability of a great variety of geochemical parameters further constraints can be placed on granitoid genesis. Trace element data can more precisely chart the consanguinity of rock types and enable one to distinguish between different generative processes (i.e. partial melt versus fractional crystallisation) (Allegre and Minster, 1978; Hanson, 1978). Trace element ratios, which are largely unaffected by crystal differentiation processes, can be plotted to discriminate granite composition in terms of source rock and by implication, tectonic environment (Pearce et al., 1984).

### 3.2: Sampling and Analytical Methods

Previous workers (Pearson et al., 1971; Granger et al., 1971, Stuckless et al., 1985; Worl et al., 1986) identified the Bears Ear batholith as a late Archean K-rich granite in the Wind River Range. In the first field season, representative samples of the Bears Ear batholith were collected from throughout the range. However, the batholith was found to be a composite of distinct plutons, and for any meaningful geochemical study one has to be able to delineate individual plutons. This is not possible in the southern Wind River Range where the Bears Ear batholith and older Louis Lake batholith are intermingled and detailed field mapping was required to unravel pluton boundaries has not been done. In the second field season, sampling was concentrated in the northern Wind River Range where two of the distinct lithologies of the Bears Ear batholith are exposed to form two separate plutons (Middle Mountain and Dome Peak plutons). These intrude an older gneiss terrane and the Louis Lake batholith is absent. Samples of the older Bridger and Louis Lake batholiths were also collected. Samples of the Mount Owen Quartz Monzonite were collected from the Teton Range.

All samples were analysed for major and trace elements using XRF and INNA techniques and the data are presented in Appendix A. Sample localities are listed in Appendix B, and analytical methods and precision are reported in Appendix C.

### 3.3: Major Element Data Late Archean K-rich granites

#### Middle Mountain Granite

The Middle Mountain granite is a true granite (Streckeisen, 1976) with  $K_2O/Na_2O > 1$ . The granite is peraluminous (Figure 3.1a) with high  $SiO_2$  (72-76%), high  $K_2O$  and low to moderate  $CaO$  (Table 3.1), varies from corundum to diopside CIPW normative, and plots in the granite field (Figure 3.2a) on the Ab-An-Or discriminant diagram of Barker (1979). The granite follows a calc-alkali trend (Figure 3.3a). On Harker Variation diagrams (Figure 3.4)  $TiO_2$ ,  $Fe_2O_3$  and  $CaO$  show decreasing with increasing  $SiO_2$  content ( $R^* = .88$   $TiO_2$ ,  $R = .85$   $Fe_2O_3$ ,  $R = .70$   $CaO$ ), whilst  $K_2O$  shows increasing with increasing  $SiO_2$  content ( $R = .80$ ), implying the pluton has undergone some degree of fractional crystallisation. Three samples BL-1, BL-4 and BL-5 form a separate group with lower  $SiO_2$  (68-70wt%) than the main trend (circled in Figure 3.4). These samples come from the eastern margin of the pluton, where assimilation of the surrounding amphibolite gneisses may have occurred.

The Middle Mountain granite does not readily fall into either the I- or S-type classification for granites of Chappell and White (1974), but shows features of each (Table 3.2). It has relatively high  $Na_2O$  and shows near linear

(\* $R$ =Coefficient of Determination, used in linear regressions)

1924-1925. The following table shows the results of the  
1924-1925. The following table shows the results of the



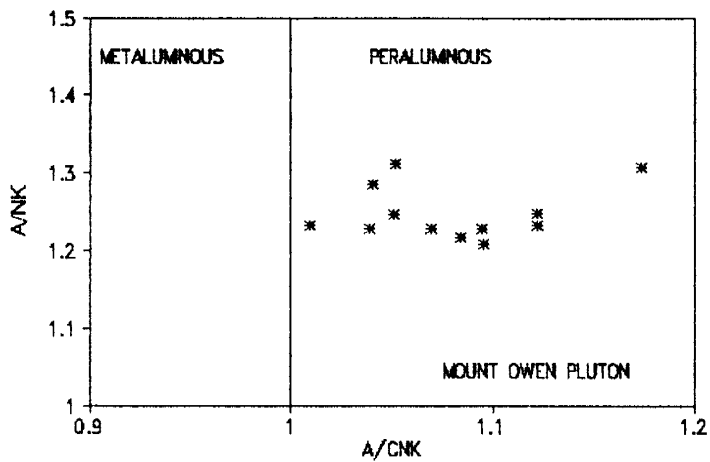
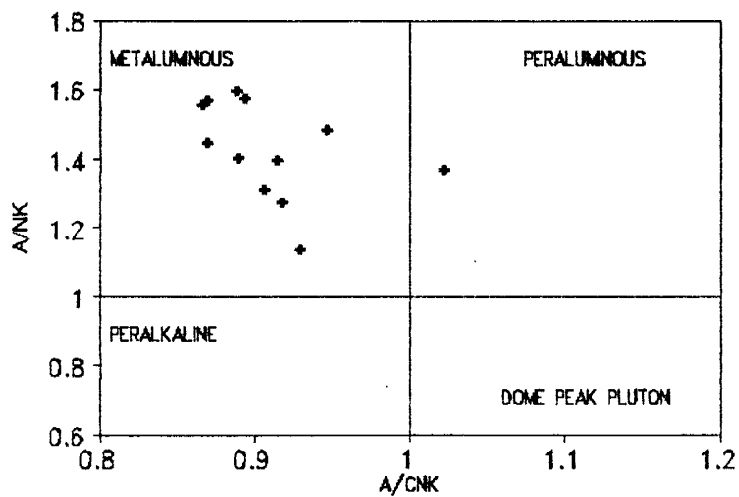
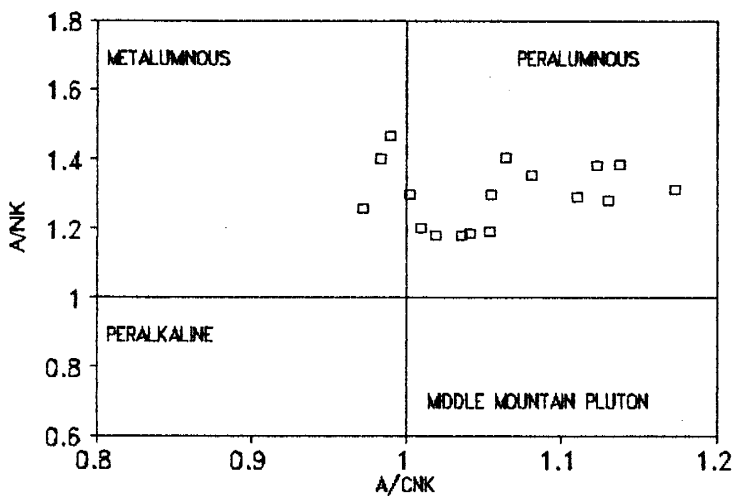


**Table 3.1: Average major and trace element contents of granites from Middle Mountain, Dome Peak and Mount Owen Plutons**

Sample	Middle Mountain Pluton		Dome Peak Pluton		Mount Owen Pluton	
	n=19	STD	n=13	STD	n=12	STD
SiO <sub>2</sub>	72.69	2.00	65.68	3.75	75.25	0.95
TiO <sub>2</sub>	0.26	0.12	0.77	0.20	0.10	0.04
Al <sub>2</sub> O <sub>3</sub>	14.92	0.81	15.62	1.08	13.92	0.27
Fe <sub>2</sub> O <sub>3</sub> -T	1.86	0.72	4.56	1.21	1.32	0.30
MgO	0.51	0.33	1.51	0.53	0.24	0.10
CaO	1.46	0.66	3.31	1.00	1.57	0.36
Na <sub>2</sub> O	3.78	0.60	3.84	0.82	3.70	0.33
K <sub>2</sub> O	4.76	0.87	4.07	0.98	4.67	0.47
MnO	0.02	0.01	0.05	0.02	0.02	0.01
P <sub>2</sub> O <sub>5</sub>	0.06	0.03	0.29	0.13	0.05	0.02
LOI	0.60	0.17	0.72	0.27	0.47	0.16
TOTAL	100.96	0.97	100.23	1.26	100.78	0.63
Rb	152.87	32.40	91.55	21.47	179.67	58.51
Ba	992.89	381.98	1385.2	808.69	487.54	207.06
Cs	0.89	0.47	0.25	0.20	4.25	2.95
Sr	191.71	95.06	490.51	174.43	58.15	23.05
Pb	44.25	9.43	24.56	6.72	42.95	11.46
Th	45.84	15.38	46.53	22.83	23.41	11.77
U	6.01	3.04	2.02	1.03	3.58	0.96
Sc	3.13	1.05	8.80	1.84	2.63	0.44
V	21.51	13.32	73.53	20.10	6.26	2.74
Cr	7.14	6.51	20.49	16.84	9.65	6.53
Co	2.34	1.89	10.14	3.48	1.15	0.56
Cu	BD	0	5.21	8.26	0.35	1.12
Zn	21.38	12.16	55.96	29.67	25.65	12.35
Ga	21.34	2.77	22.38	3.23	19.54	2.10
Y	18.22	14.90	35.00	5.42	38.93	35.14
Zr	173.25	63.21	356.21	51.19	96.65	45.79
Nb	7.28	3.13	12.92	2.31	10.37	6.70
Hf	6.20	1.67	13.32	2.80	3.37	1.27
Ta	0.45	0.23	0.70	0.21	1.11	0.54

Sample	Middle	Mountain	Peak		Mount	Owen
	n=19	STD	n=13	STD	n=12	STD
La	70.26	20.12	167.68	43.51	30.80	16.25
Ce	127.94	36.69	313.55	82.34	61.82	33.74
Nd	40.11	12.19	106.28	31.12	24.52	14.55
Sm	7.32	2.83	20.22	4.32	6.69	3.45
Eu	1.14	0.42	3.25	0.59	0.65	0.23
Tb	0.70	0.57	1.44	0.26	0.84	0.33
Yb	2.36	2.91	2.87	0.44	2.65	0.92
Lu	0.25	0.46	0.50	0.60	0.32	0.11
K2O/Na2	1.32	0.42	1.13	0.36	1.28	0.23
K/Rb	264.02	51.31	368.06	58.15	233.87	59.21
Ba/Sr	5.75	1.75	2.88	1.50	8.56	2.41
Rb/Sr	1.13	0.81	0.22	0.09	4.01	2.71
La/Yb	40.68	14.08	58.76	13.22	12.25	6.32
La/Sm	10.13	1.89	8.25	1.01	4.94	2.12
Eu/Eu*	0.60	0.30	0.57	0.09	0.37	0.21

Table 3.1 cont'd: Average major and trace element contents for granites from Middle Mountain, Dome Peak, and Mount Owen Plutons.

BD=Below detection

STD=1 standard deviation of the mean

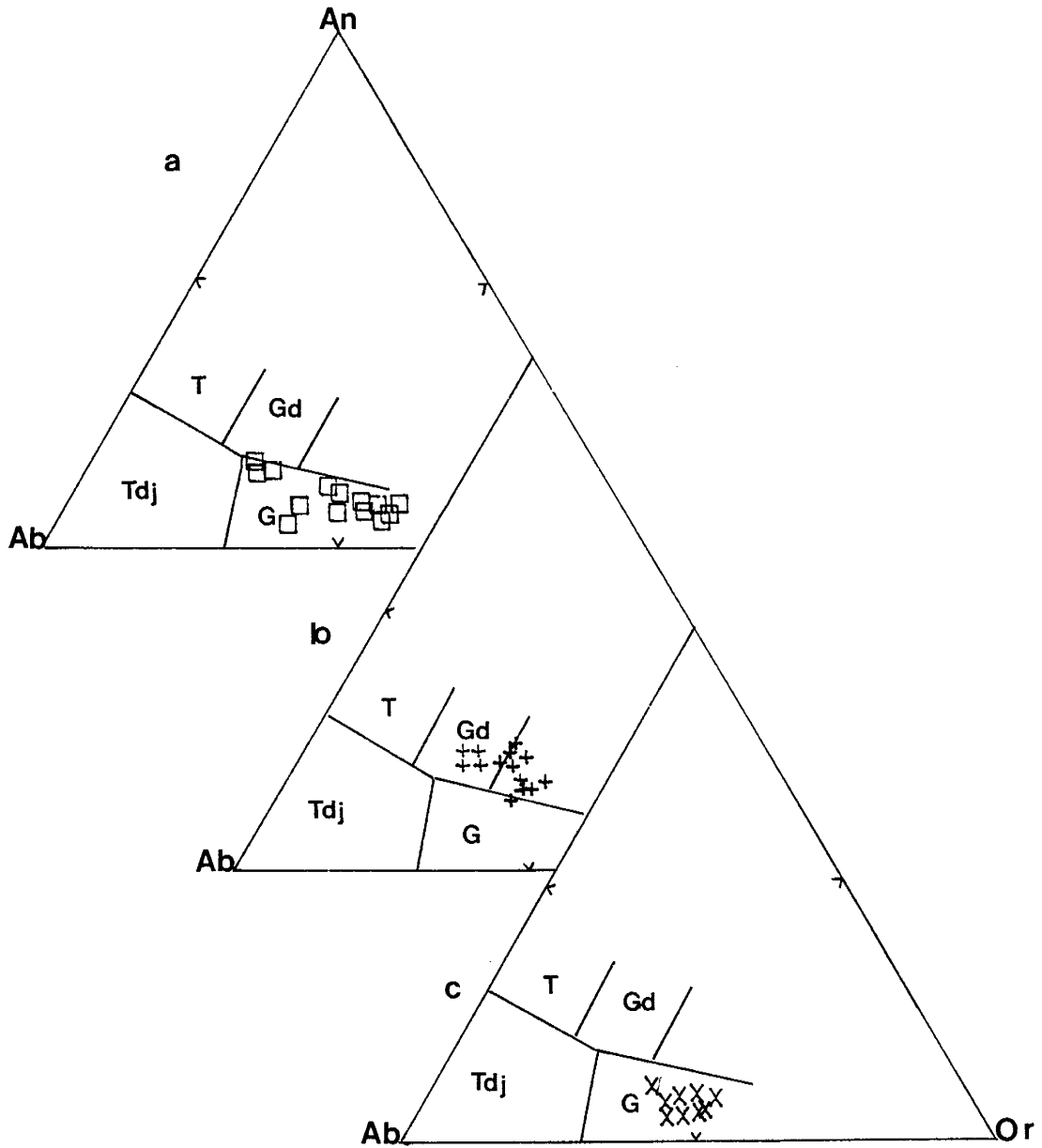


Figure 3.2a: CIPW normative classification of granites from Barker (1979). T=Tonalite, Tdj=Trondhjemite, Gd=Granodiorite, G=Granite. a) Middle Mountain pluton, b) Dome Peak pluton and c) Mount Owen pluton.

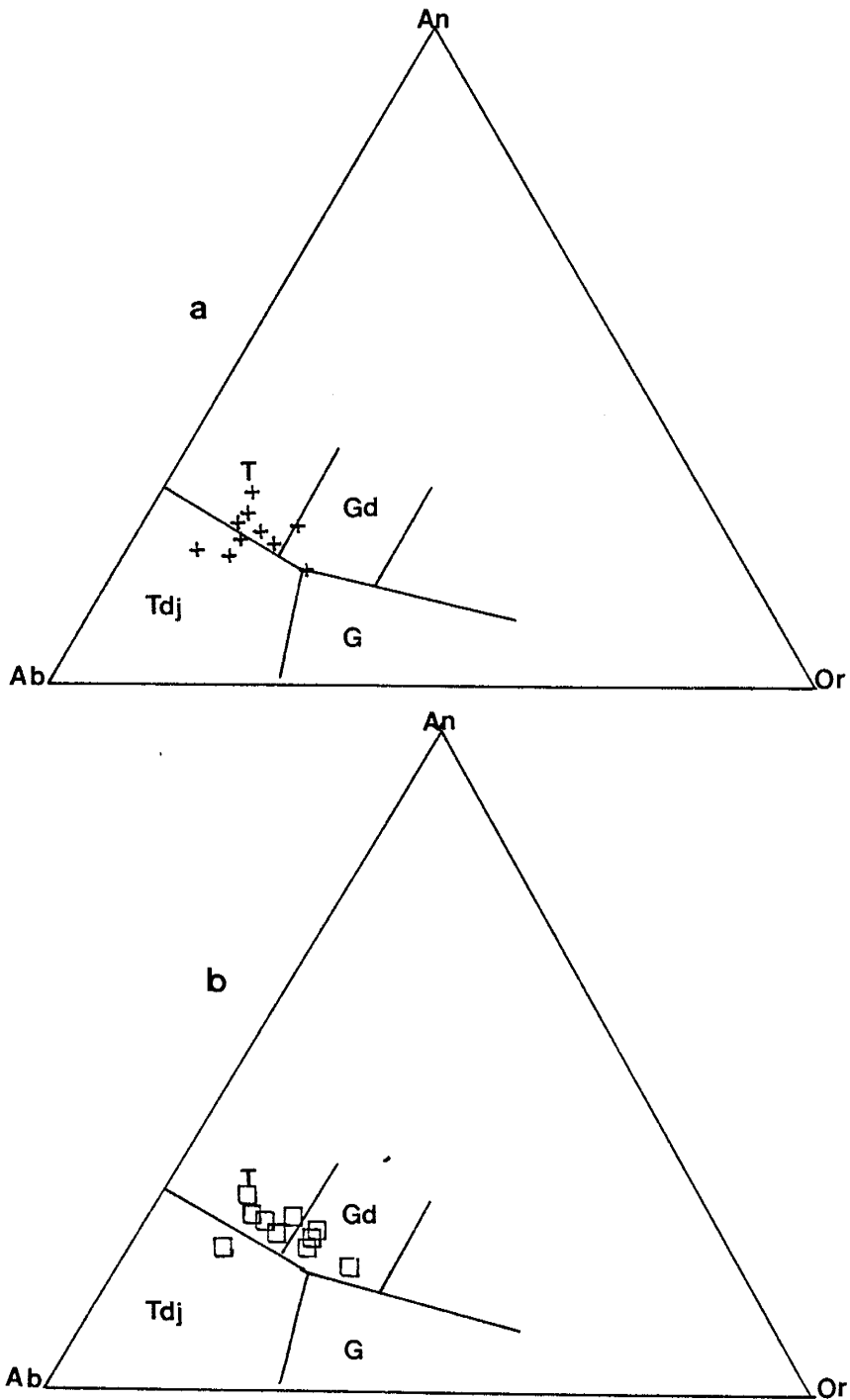


Figure 3.2b: CIPW normative classification of granites from Barker (1979). T=Tonalite, Tdj=Trondhjemite, Gd=Granodiorite, G=Granite. a) Bridger batholith and b) Louis Lake batholith.

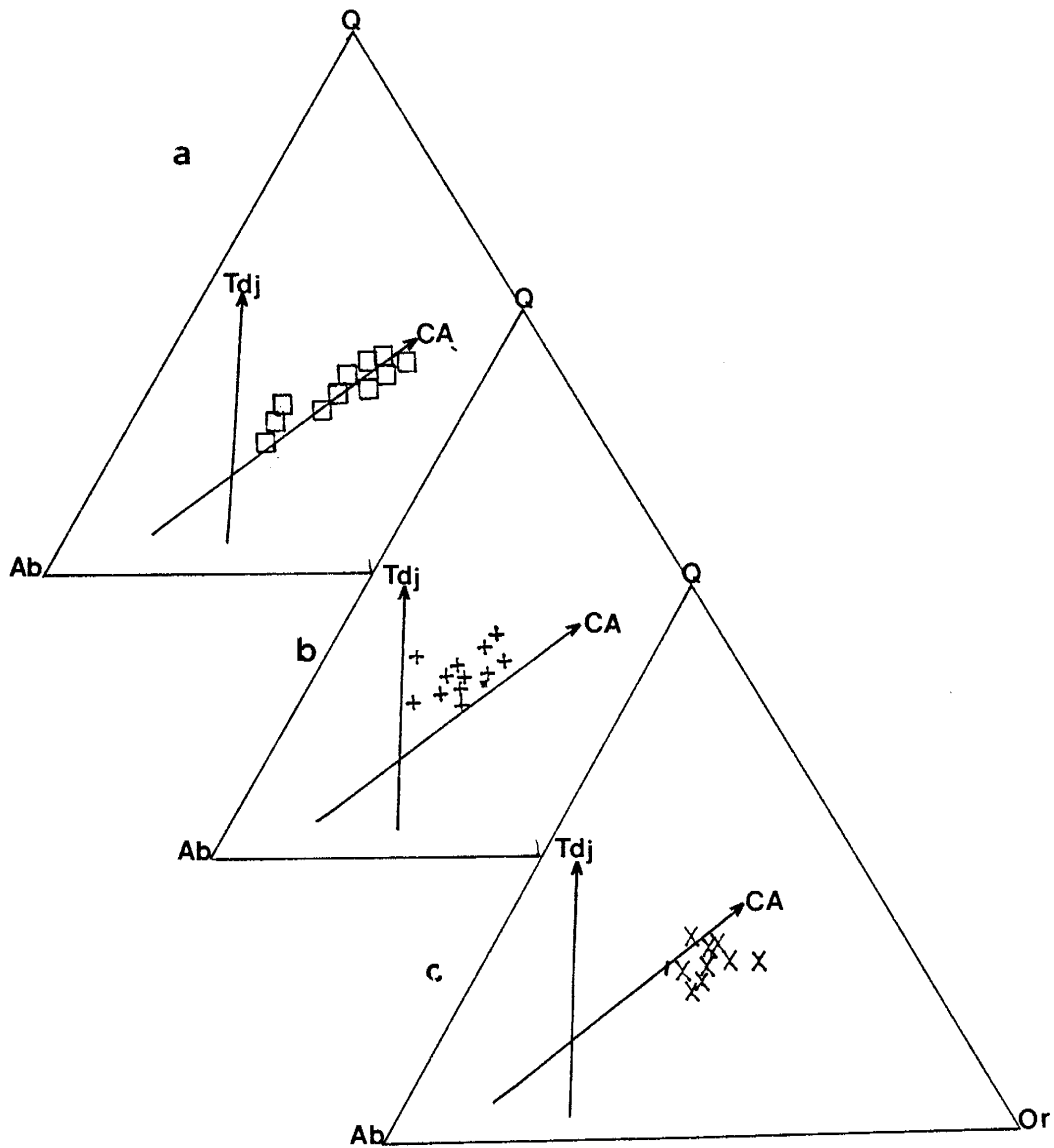


Figure 3.3a: Ab-Or-Q normative plots to distinguish between Calc-alkali (CA) trondjemite (Tdj) trends from Barker and Arth (1976). a) Middle Mountain pluton, b) Dome Peak pluton and c) Mount Owen pluton

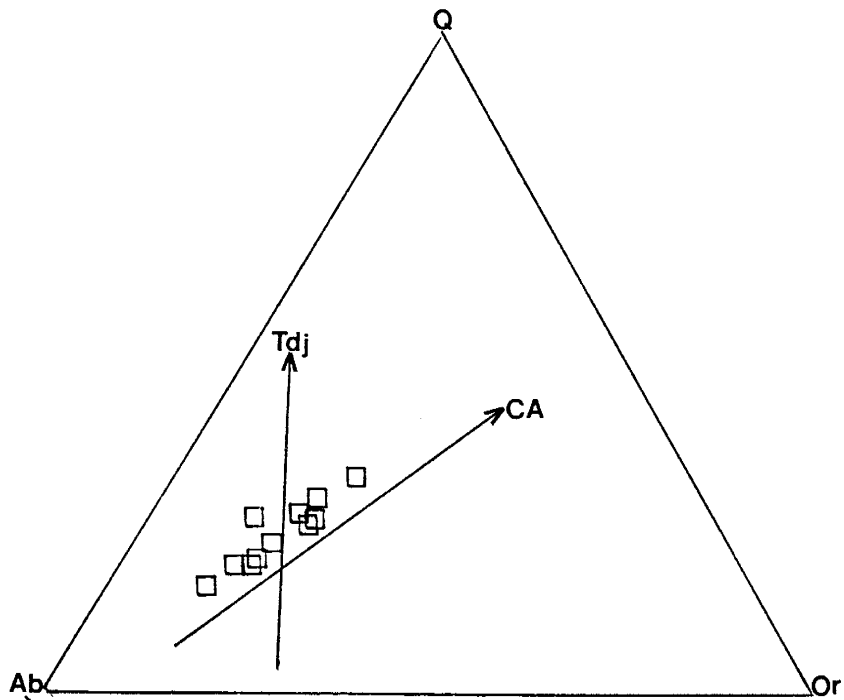
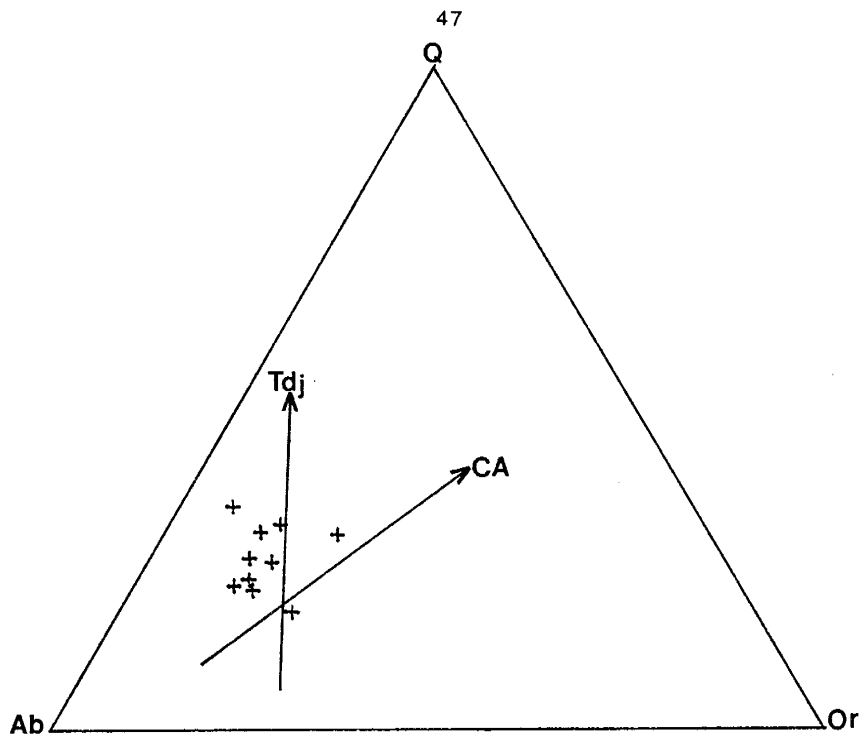


Figure 3.3b: Ab-Or-Q normative plots to distinguish between Calc-alkali (CA) and trodhjemite (Tdj) trends from Barker and Arth (1976). a) Bridger batholith and b) Louis Lake batholith.

Table 3.2: I/S-type classification of granites from Chappell and White (1974).

I-types	BB	LLB	MM	DP	MO
Rel. high Na <sub>2</sub> O, >3.2% in felsic varieties, decreasing to >2.2% in more mafic types	X	X	X	X	
Mol Al <sub>2</sub> O <sub>3</sub> / (Na <sub>2</sub> O+K <sub>2</sub> O+CaO) <1.1	X	X	X	X	
CIPW normative diopside or <1% normative corundum	X	X	X	X	
Broad spectrum of compositions from felsic to mafic	-----	-----	-----	-----	
Regular inter-element variations within plutons; linear or near-linear variation diagrams.	X	X	X	X	
S-type	BB	LLB	MM	DP	MO
Rel. low Na <sub>2</sub> O normally <3.2% in rocks with approx. 5% K <sub>2</sub> O, decreasing to <2.2% in rocks with approx. 2% K <sub>2</sub> O					X
Mol Al <sub>2</sub> O <sub>3</sub> / (Na <sub>2</sub> O+K <sub>2</sub> O+CaO) >1.1			X		X
>1% CIPW normative corundum			X		X
Rel. restricted in composition to high SiO <sub>2</sub> types					X
Variation diagrams more irregular					X



variation diagrams (I-type), but also has  $\text{Al}_2\text{O}_3/(\text{Na}_2\text{O}+\text{K}_2\text{O}+\text{CaO}) > 1.1$  and  $> 1\%$  CIPW normative corundum (S-type). Mesonorm data are shown on a Qz-Ab-Or plot, with a compilation in the form of a grid for all existing minimum melt points over a range of pressures and Ab/An ratios from Anderson and Cullers (1978) (Figure 3.5a). The compositions of undifferentiated plutons can be utilised to determine depth of fusion. Extremely differentiated plutons should depict a trend toward an appropriate minimum for their level of emplacement. The broad spread shown by Middle Mountain, with Ab/An ratios from 11.7 to 3.5 would suggest that the magma has undergone differentiation and possible assimilation of country rock subsequent to its formation. The trend of the data points would imply depths of emplacement around 4kb.

### **Dome Peak Pluton**

The Dome Peak pluton is classified as a quartz monzonite from the mode (Pearson et al., 1971). It is metaluminous (Figure 3.1b) with moderate  $\text{SiO}_2$  (65%), high  $\text{K}_2\text{O}$  and moderate CaO (Table 3.1). It is diopside CIPW normative, and plots in the granodiorite to quartz monzonite fields on the Ab-An-Or discriminant diagram (Figure 3.2b). It does not clearly define either a calc-alkali or trondhjemite trend (Figure 3.3b).

On Harker Variation diagrams,  $\text{TiO}_2$ ,  $\text{Al}_2\text{O}_3$ ,  $\text{Fe}_2\text{O}_3$ , and CaO show moderate linear variations with  $\text{SiO}_2$  content ( $R=.70$   $\text{TiO}_2$ ,  $R=.82$   $\text{Al}_2\text{O}_3$ ,  $R=.70$   $\text{Fe}_2\text{O}_3$ ,  $R=.81$  CaO), similar to Middle

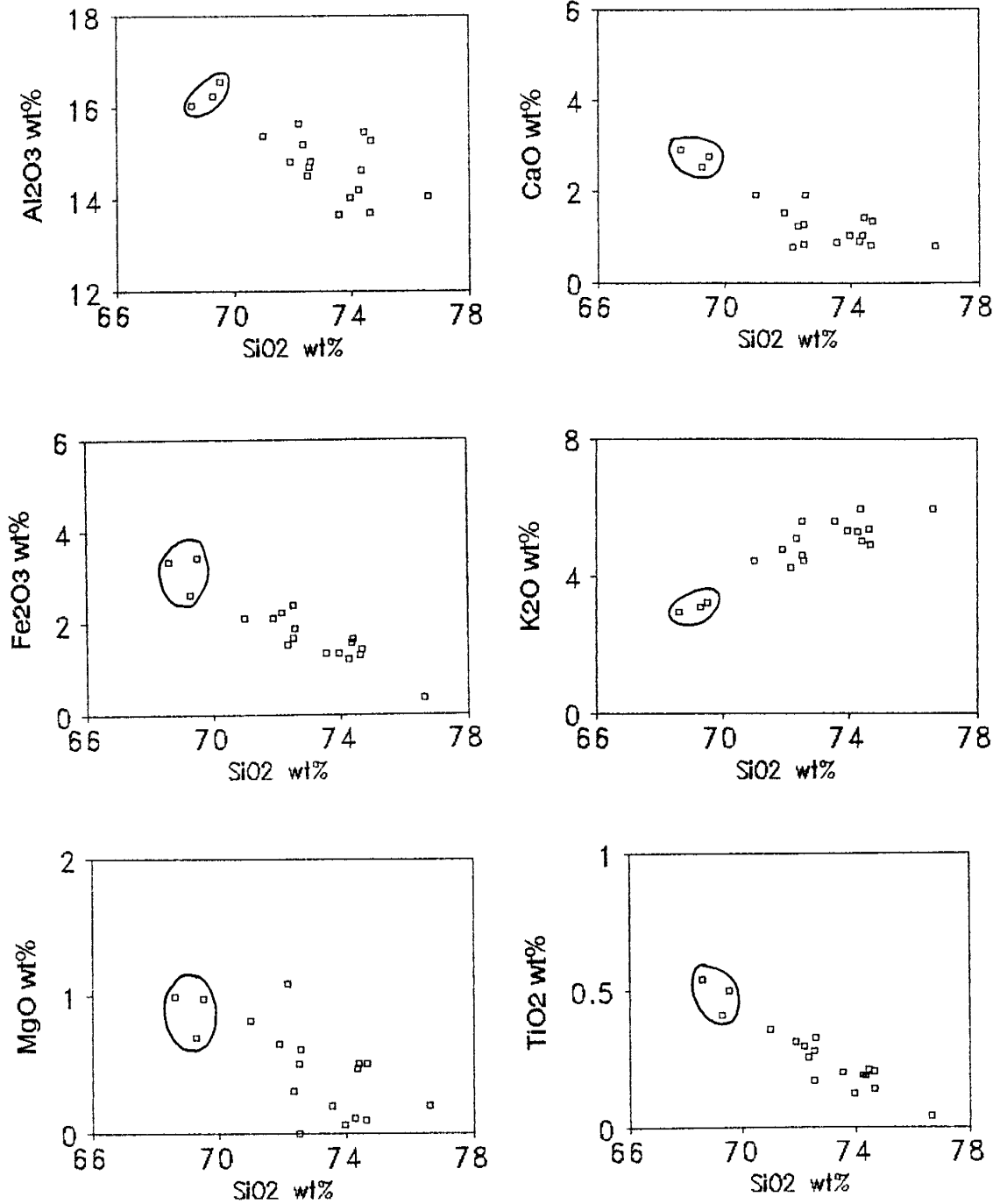


Figure 3.4: Harker variation diagrams showing the distribution of major elements in Middle Mountain pluton. Circled data points come from the margins of the pluton.

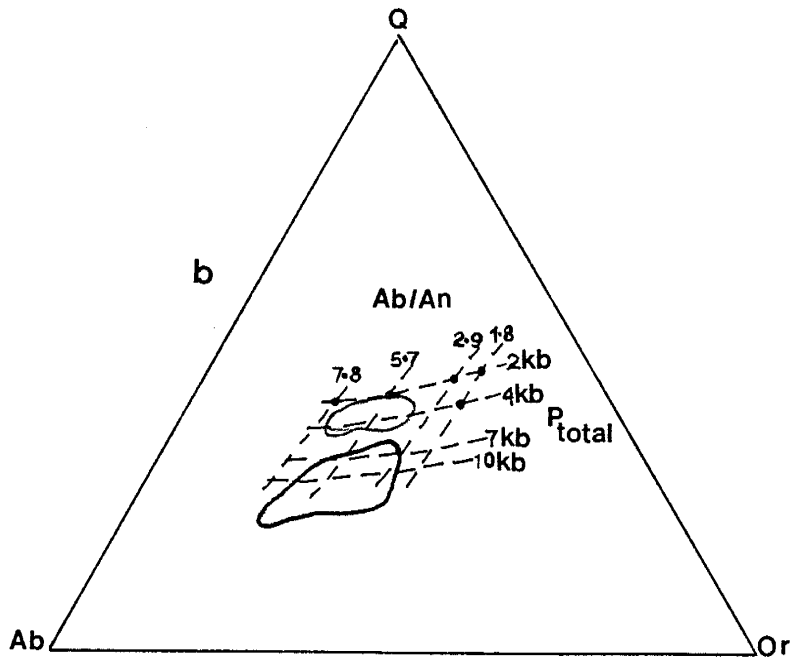
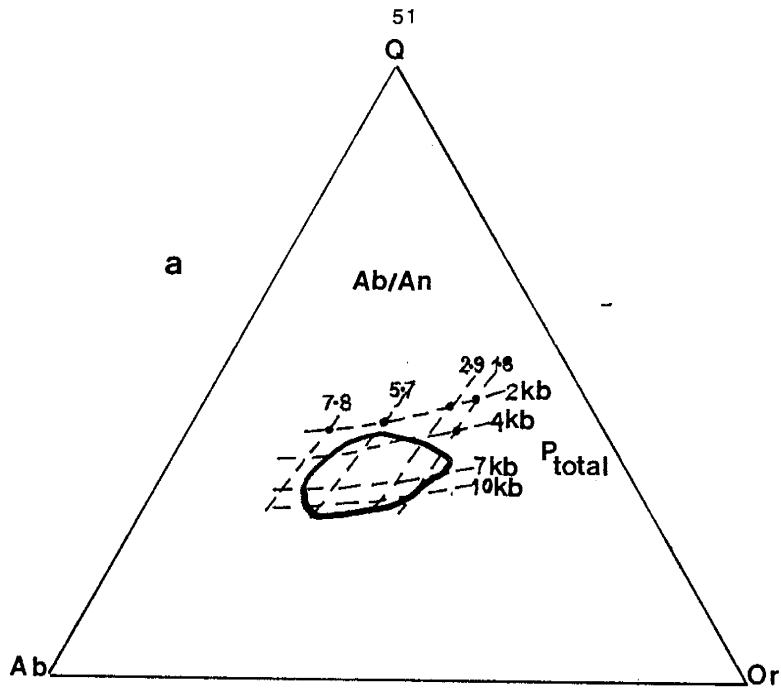


Figure 3.5: Normative quartz, albite and orthoclase for a) Middle Mountain pluton and b) Dome Peak and Mount Owen plutons, with comparison to experimental minimum melt compositions. Minimum melt experimental grid from Anderson and Cullers (1978).

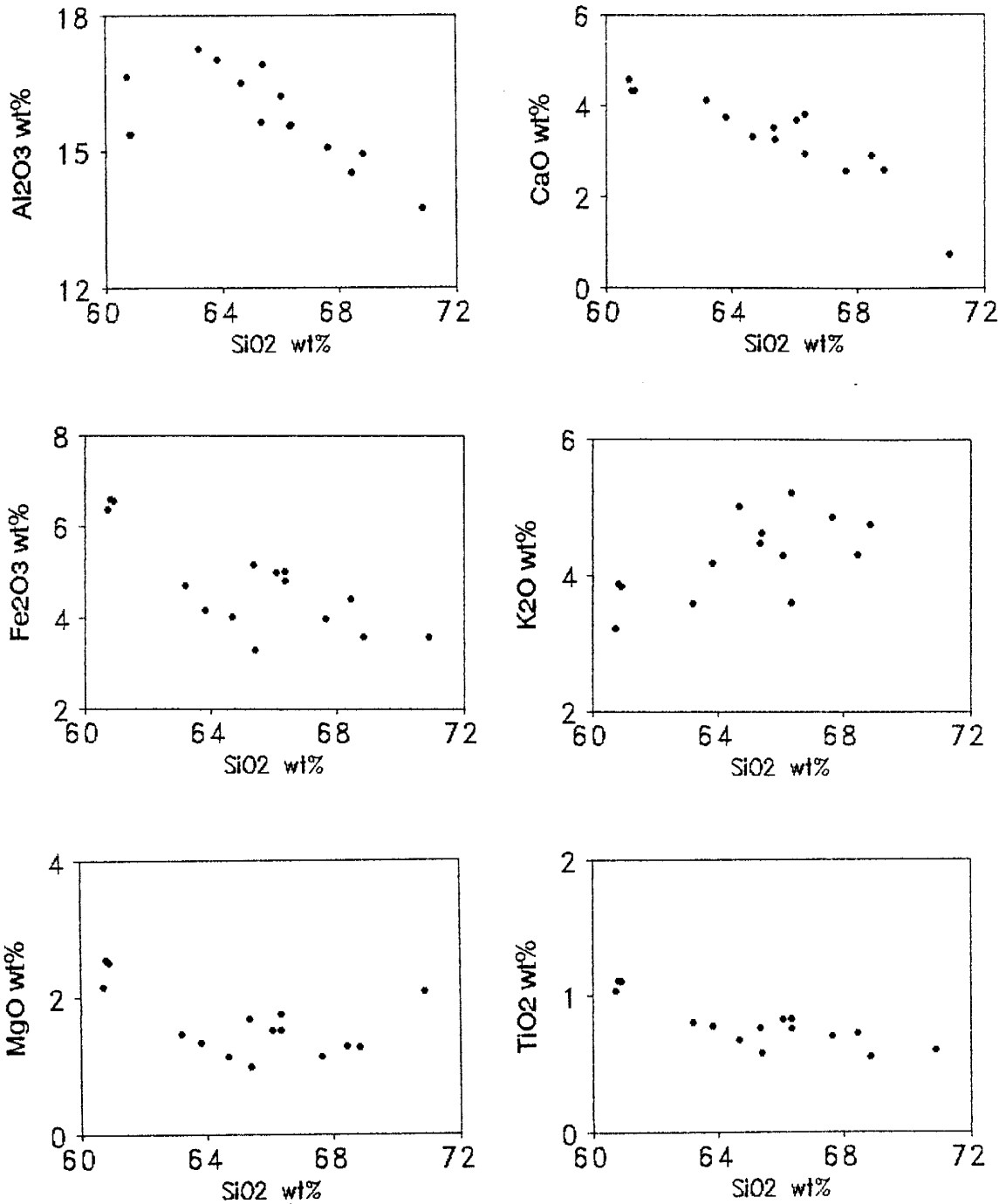


Figure 3.6: Harker variation diagrams showing the distribution of major elements in Dome Peak pluton.

Mountain pluton (Figure 3.6). It is an I-type granite with relatively high  $\text{Na}_2\text{O}$  ( $>3.2\%$ ),  $\text{Mol Al}_2\text{O}_3 / (\text{Na}_2\text{O} + \text{K}_2\text{O} + \text{CaO}) < 1.1$ , CIPW normative corundum  $< 1\%$  (Table 3.2). Most samples have between 63-68wt%  $\text{SiO}_2$ , three samples (FL-1, FL-1A, FL-7) have slightly lower  $\text{SiO}_2$  content (60-61wt%) and these samples come from the southern margin of the pluton, whereas all other samples come from the interior. Another sample NFL-5 falls significantly away from the main trend, with lower CaO and  $\text{K}_2\text{O}$ . In this sample, the feldspars are extensively sericitised and there are small fractures filled with epidote suggesting the rock has been altered, perhaps associated with later fault movements.

Mesonorm data for the Dome Peak pluton plot over a wide area on a Qz-Ab-Or plot (Figure 3.5b). There is a broad trend as indicated, suggesting emplacement depths around 7kb. The Dome Peak pluton is a coarse grained pluton implying either crystallisation in the water vapor-undersaturated region with longer temperature ranges of crystallisation (Whitney, 1988), or slower cooling due to emplacement at greater depths. At greater depths, heat loss by both convection and conduction is slower, as the thermal gradient is less. The Middle Mountain granite by comparison is relatively fine grained implying rapid crystallisation over a short temperature range (Whitney, 1988).

### Mount Owen Pluton

Mount Owen Pluton is classified as a quartz monzonite from the mode (Reed and Zartman, 1973). The pluton is peraluminous (Figure 3.1c) with a narrow range of  $\text{SiO}_2$  (72-76%), high  $\text{K}_2\text{O}$ , low  $\text{CaO}$  and  $\text{MgO}$  (Table 3.1). It is a corundum CIPW normative 2-mica granite, plots in the granite field on the Ab-An-Or granitoid discriminant diagram (Figure 3.2c), and also defines a calc-alkali trend (Figure 3.3c). On Harker Variation diagrams there is poor linear correlation between  $\text{Al}_2\text{O}_3$  ( $R=.29$ ),  $\text{Fe}_2\text{O}_3$  ( $R=.38$ ),  $\text{MgO}$  ( $R=.08$ ),  $\text{K}_2\text{O}$  ( $R=.07$ ) and  $\text{SiO}_2$  content, although  $\text{TiO}_2$  ( $R=.66$ ) and  $\text{CaO}$  ( $R=.49$ ) do show a moderate negative correlation with  $\text{SiO}_2$  content (Figure 3.7). It is a S-type granite with a relatively restricted  $\text{SiO}_2$  range,  $\text{Mol Al}_2\text{O}_3/(\text{Na}_2\text{O}+\text{K}_2\text{O}+\text{CaO}) >1.1$ , and  $>1\%$  CIPW normative corundum (Table 3.2).

The mesonorm data form a tighter cluster on a Qz-Ab-Or plot than either Middle Mountain or Dome Peak plutons. The trend of the data points would imply depth of emplacements around 4kb (Figure 3.5b). The relatively shallow depth of emplacement implied by the mesonorm data is supported by the fine grain size of the pluton, which indicates rapid cooling at shallow depth (Whitney, 1988). The veined network of quartz monzonite dikes with no evidence of chilled margins implies the pluton was emplaced in rather brittle country rocks (Reed and Zartman, 1973).

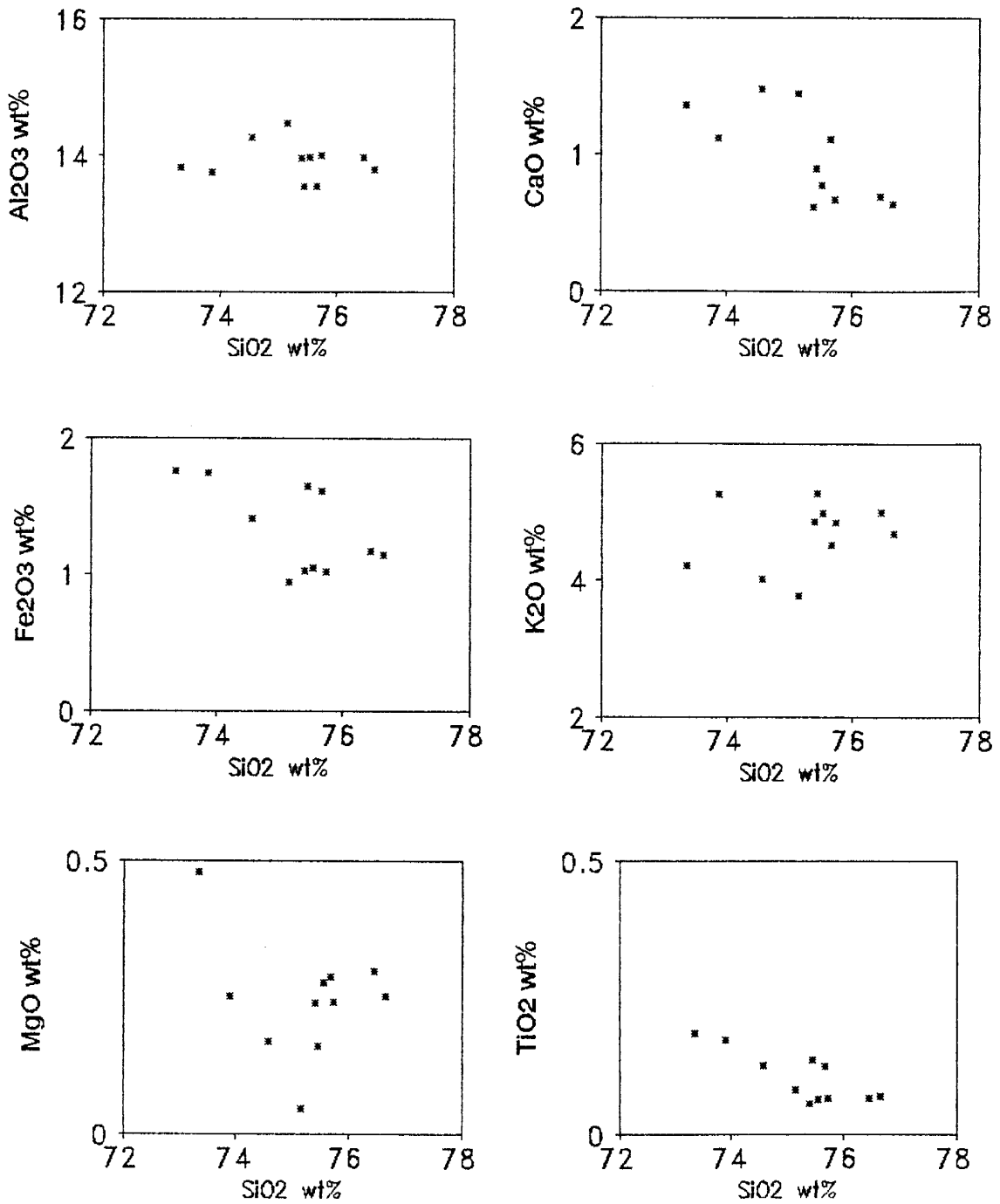


Figure 3.7: Harker variation diagrams showing the distribution of major elements in Mount Owen pluton.

## Older Granitoids

### Bridger Batholith

The Bridger batholith has a variable mode and ranges from tonalite to granodiorite (Koesterer et al., 1987) with  $K_2O/Na_2O < 1$ . It is metaluminous (Figure 3.8) with moderate  $SiO_2$  content (Table 3.3), and plots in the trondhjemite and tonalite fields on the CIPW normative Ab-An-Or discriminant diagram (Figure 3.2d), and weakly defines a trondhjemite trend (Figure 3.3b). The Bridger batholith is an I-type granite, with relatively high  $Na_2O$  content ( $>3.2\%$  in felsic varieties, decreasing to  $>2.2\%$  in more mafic types), and  $<1\%$  CIPW normative corundum (Table 3.2). On Harker Variation diagrams there is a moderate linear correlation for  $TiO_2$  ( $R=.90$ ),  $Al_2O_3$  ( $R=.74$ ),  $Fe_2O_3$  ( $R=.72$ ), and  $MgO$  ( $R=.75$ ) with  $SiO_2$  content (Figure 3.9).

### Louis Lake Batholith

The Louis Lake batholith has a more restricted range of composition than the Bridger batholith, and is dominantly a granodiorite (mode-Bayley et al., 1973) with moderate  $SiO_2$  (Table 3.3). The granodiorite is metaluminous with  $K_2O/Na_2O < 1$  (Figure 3.1d), and plots in the tonalite and granodiorite fields on the CIPW normative Ab-An-Or diagram (Figure 3.2e). The granodiorite does not clearly define either a calc-alkali or trondhjemite trend (Figure 3.3e).

On Harker Variation diagrams there is moderate linear



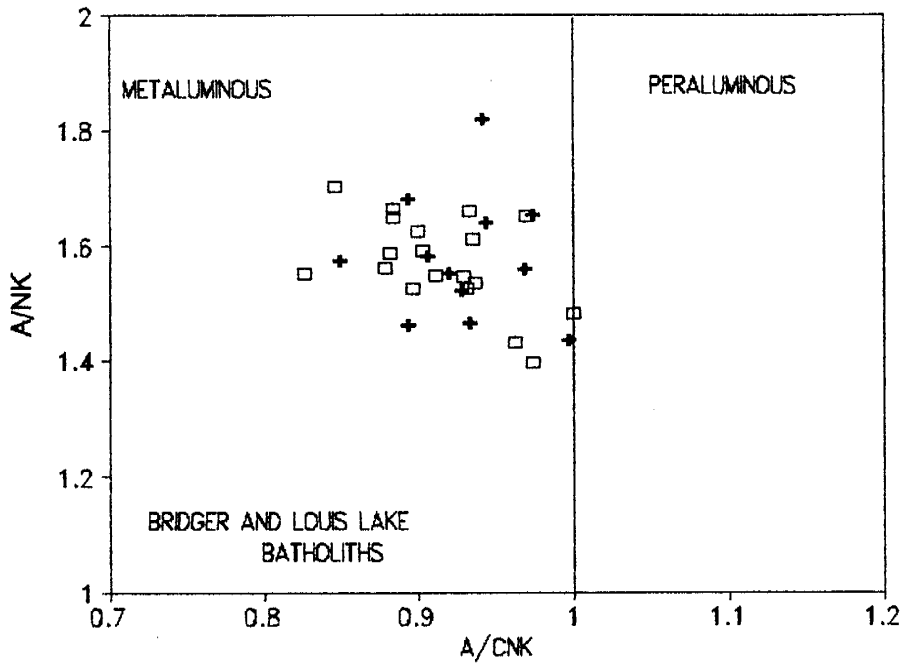


Figure 3.8: Shand's index for the Bridger (+) and Louis Lake (□) batholiths.

Table 3.3: Average major and trace element contents of granites from Bridger and Louis Lake batholiths.

Sample	Bridger Batholith		Louis Lake Batholith	
	n=12	STD	n=15	STD
SiO <sub>2</sub>	65.44	3.61	64.84	2.40
TiO <sub>2</sub>	0.55	0.13	0.66	0.13
Al <sub>2</sub> O <sub>3</sub>	16.85	0.91	16.25	0.60
Fe <sub>2</sub> O <sub>3</sub> -T	4.15	1.07	4.85	0.82
MgO	1.58	0.64	1.90	0.35
CaO	3.78	1.21	4.22	0.71
Na <sub>2</sub> O	5.52	1.21	4.79	0.38
K <sub>2</sub> O	1.72	0.67	2.21	0.49
MnO	0.05	0.02	0.07	0.01
P <sub>2</sub> O <sub>5</sub>	0.21	0.08	0.27	0.06
LOI	0.80	0.49	0.64	0.25
TOTAL	100.64	0.88	100.69	0.49
Rb	55.72	20.06	55.64	13.37
Ba	619.14	332.11	1294.03	537.46
Cs	0.51	0.28	1.46	0.95
Sr	550.22	245.34	769.19	90.72
Pb	14.17	4.31	17.73	4.25
Th	7.84	3.40	9.03	2.89
U	1.15	0.78	2.02	1.30
Sc	5.83	3.11	8.03	2.12
V	66.77	17.83	85.32	12.39
Cr	13.18	5.37	19.43	8.45
Co	8.94	3.06	11.11	2.04
Cu	5.87	11.76	5.35	9.02
Zn	72.36	28.68	84.41	14.00
Ga	24.83	2.95	21.94	3.11
Y	15.40	8.21	18.47	5.97
Zr	165.95	36.79	197.86	32.54
Nb	7.20	2.84	8.35	2.56
Hf	5.14	1.71	6.32	1.02
Ta	0.65	0.96	0.63	0.33

Sample	Bridger		Louis Lake	
	n=12	STD	n=15	STD
La	42.16	20.10	52.31	9.85
Ce	83.30	38.89	108.49	19.25
Nd	34.75	16.09	48.15	9.38
Sm	6.52	3.15	9.12	1.92
Eu	1.45	0.60	2.14	0.28
Tb	0.57	0.30	0.71	0.16
Yb	1.23	0.72	1.75	0.47
Lu	0.23	0.26	0.27	0.17
K <sub>2</sub> O/Na <sub>2</sub> O	0.34	0.15	0.47	0.14
K/Rb	330.92	257.32	337.58	56.48
Ba/Sr	1.08	0.47	1.67	0.67
Rb/Sr	0.11	0.04	0.07	0.02
La/Yb	39.13	20.65	33.11	13.89
La/Sm	6.47	2.10	5.73	2.35
Eu/Eu*	0.76	0.09	0.80	0.25

Table 3.3 cont'd: Average major and trace element contents for granites from Bridger and Louis Lake batholiths.  
 BD=Below detection  
 STD=1 standard deviation of the mean

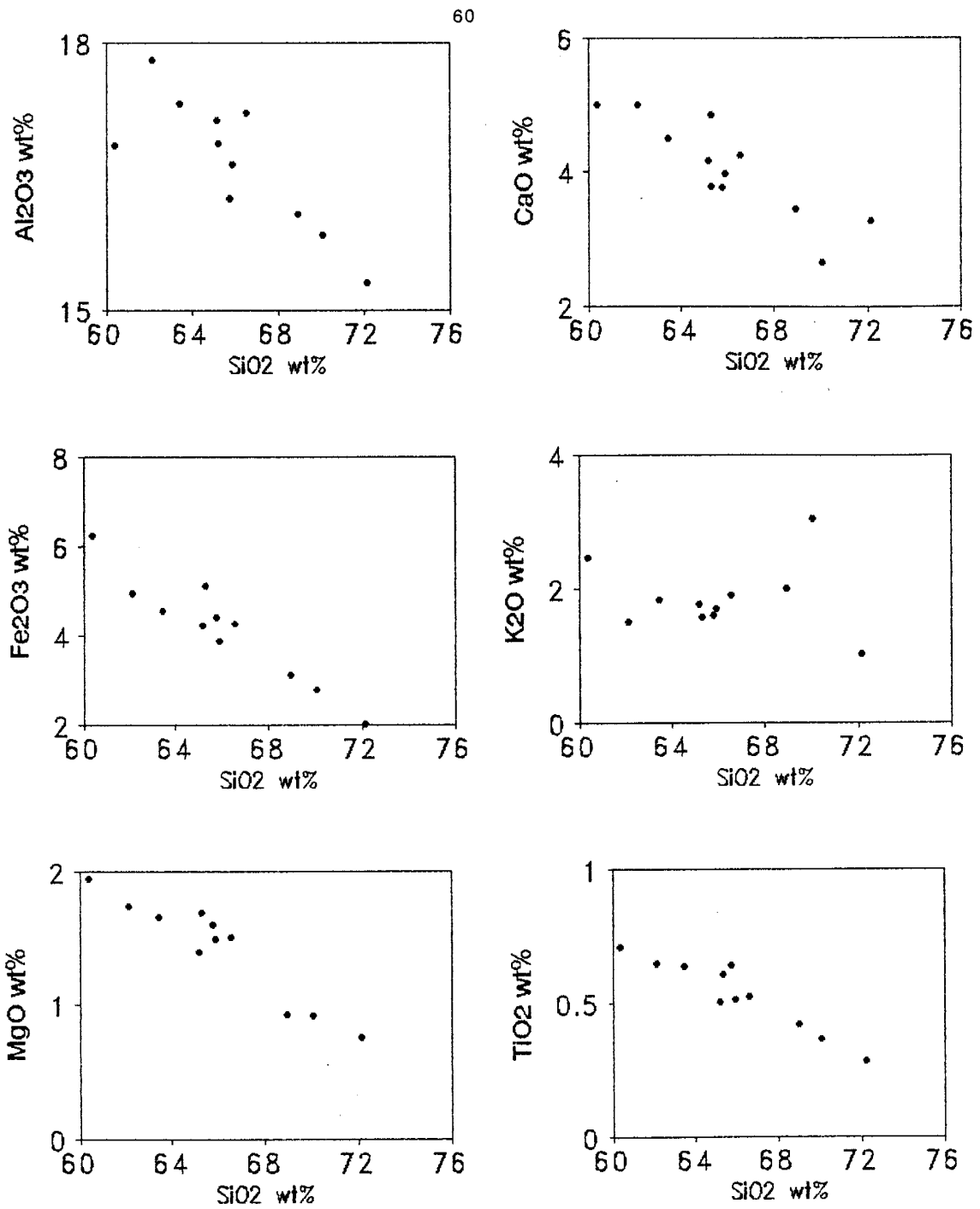


Figure 3.9: Harker variation diagrams showing the distribution of major elements in the Bridger batholith

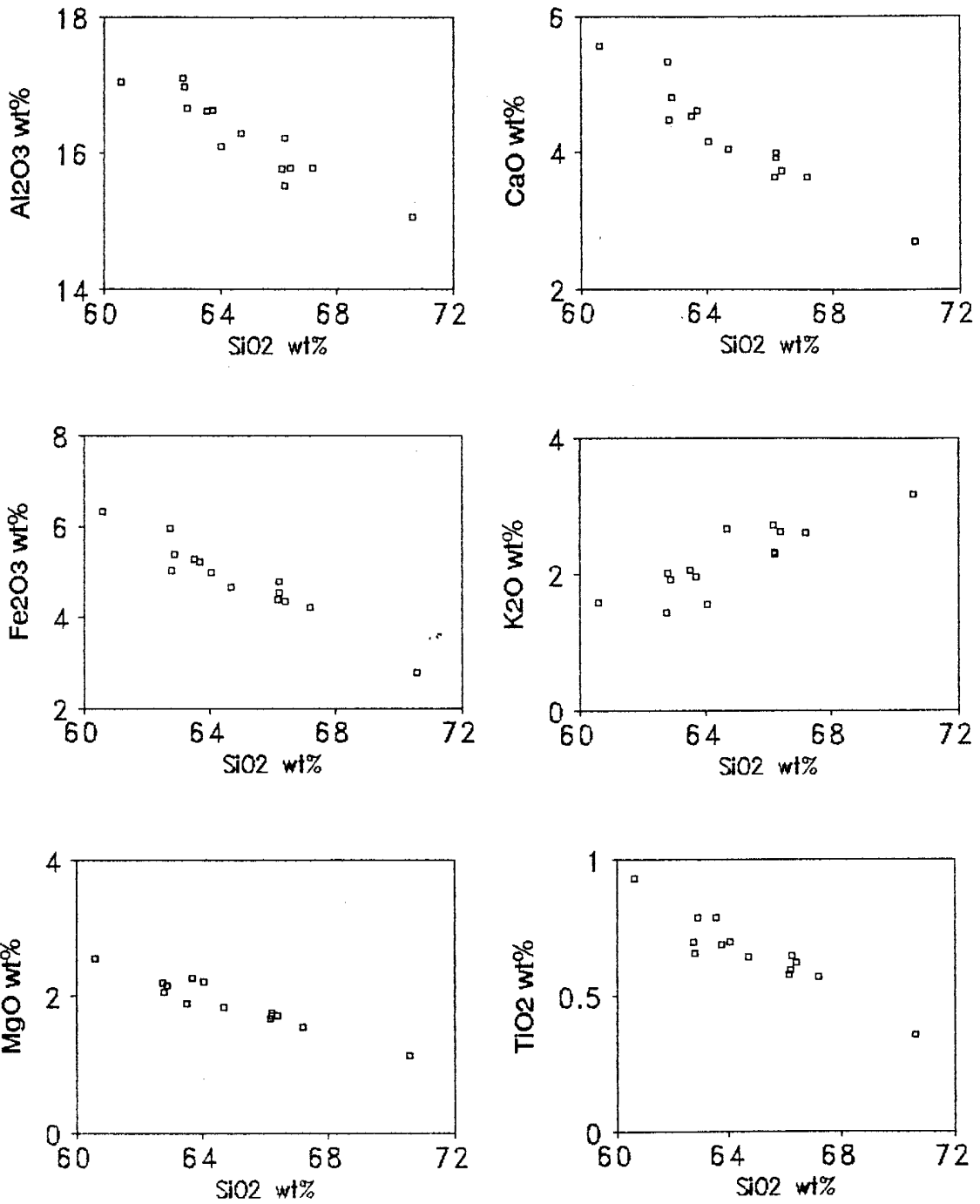


Figure 3.10: Harker variation diagrams showing the distribution of major elements in Louis Lake batholith.

correlation between all the major elements and  $\text{SiO}_2$  content ( $R=.86 \text{ TiO}_2$ ,  $R=.86 \text{ Al}_2\text{O}_3$ ,  $R=.92 \text{ Fe}_2\text{O}_3$ ,  $R=.91 \text{ MgO}$ ,  $R=.91 \text{ CaO}$ ,  $R=.74 \text{ K}_2\text{O}$ ) (Figure 3.10), implying that fractionation occurred subsequent to the genesis of the magma. This is an I-type granite with relatively high  $\text{Na}_2\text{O}$  content ( $>3.2\text{wt}\%$ ),  $\text{Mol Al}_2\text{O}_3/(\text{Na}_2\text{O}+\text{K}_2\text{O}+\text{CaO}) <1.1$  and CIPW normative corundum  $<1\%$  (Table 3.2)

The variation seen in both the Bridger and Louis Lake batholiths in part reflects the composite nature of these units. The samples cover a wide area (900  $\text{km}^2$  for Bridger batholith, 1000  $\text{km}^2$  for Louis Lake batholith) and represent multiple plutons.

### 3.4: Trace Element Data

#### Late Archean K-rich granites

#### Middle Mountain, Dome Peak and Mount Owen Plutons

Middle Mountain, Dome Peak and Mount Owen granites all have high Ba/Sr ratios (Table 3.1), consistent with the retention of plagioclase in their source, although K-feldspar and biotite fractionation can also control this ratio (Hanson, 1978). Their high K/Rb ratios are consistent with the evolved nature of the granites. On Harker Variation diagrams (Figures 3.11-3.13) showing the abundances of some LILE (Ba, Rb, Sr) and highly charged cations (Ce, Zr), Middle Mountain granite only shows fair linear correlation for Zr ( $R=.64$ ) with  $\text{SiO}_2$  content, Dome Peak shows good linear correlation for Sr ( $R=.91$ ), and Mount Owen shows moderate linear correlation for Ce ( $R=.64$ ). These data would indicate that fractionational crystallisation has occurred in all three plutons subsequent to their melting, which is in agreement with the major element data. The scatter in some of the LILE plots is not surprising as Ba, Rb, and Sr are relatively mobile. Scatter in Zr plots may be due to entrainment of restite zircon.

Chondrite-normalised REE plots (Figure 3.14a-c, normalising values from Evenson et al., 1978) show that Middle Mountain and Dome Peak plutons have highly fractionated patterns ( $\text{La/Yb}=40.68$  Middle Mountain,  $\text{La/Yb}=58.76$  Dome Peak)

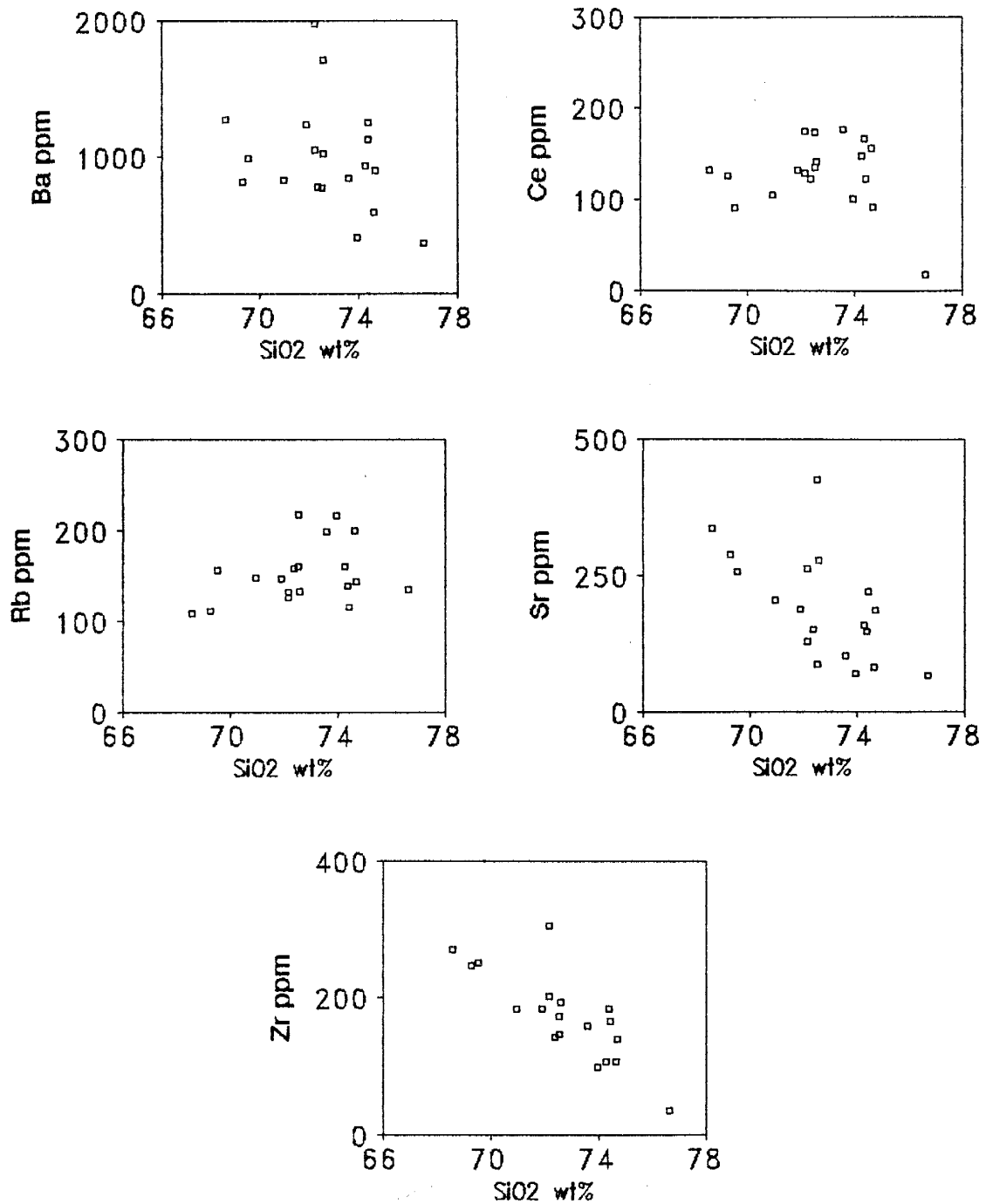


Figure 3.11: Harker variation diagrams showing the distribution of some LILE (Ba, Rb, Sr) and highly charged cations (Ce, Zr) in Middle Mountain pluton.



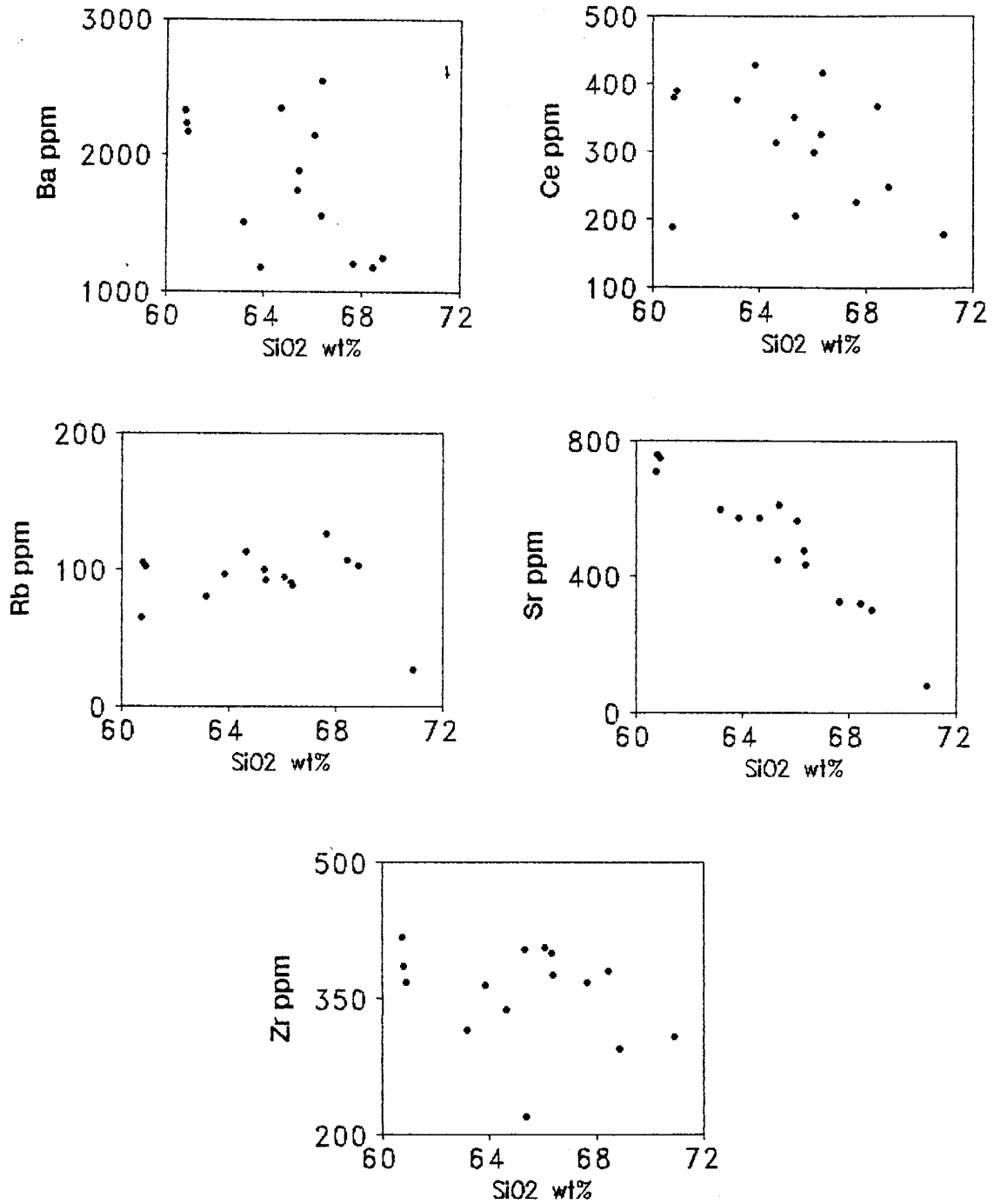


Figure 3.12: Harker variation diagrams showing the distribution of some LILE (Ba, Rb, Sr) and highly charged cations (Ce, Zr) in Dome Peak pluton.

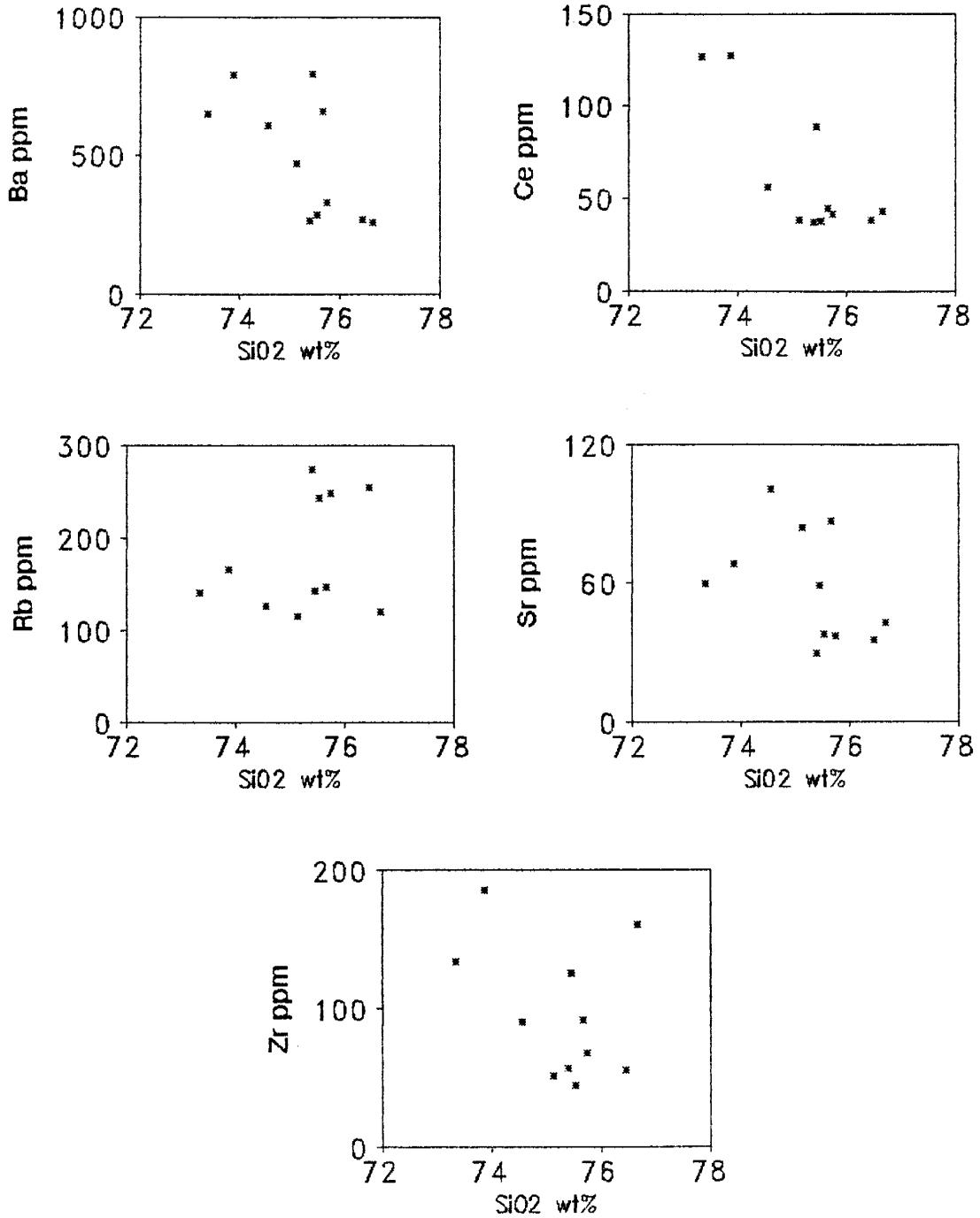


Figure 3.13: Harker variation diagrams showing the distribution of some LILE (Ba, Rb, Sr) and highly charged cations (Ce, Zr) in Mount Owen pluton.

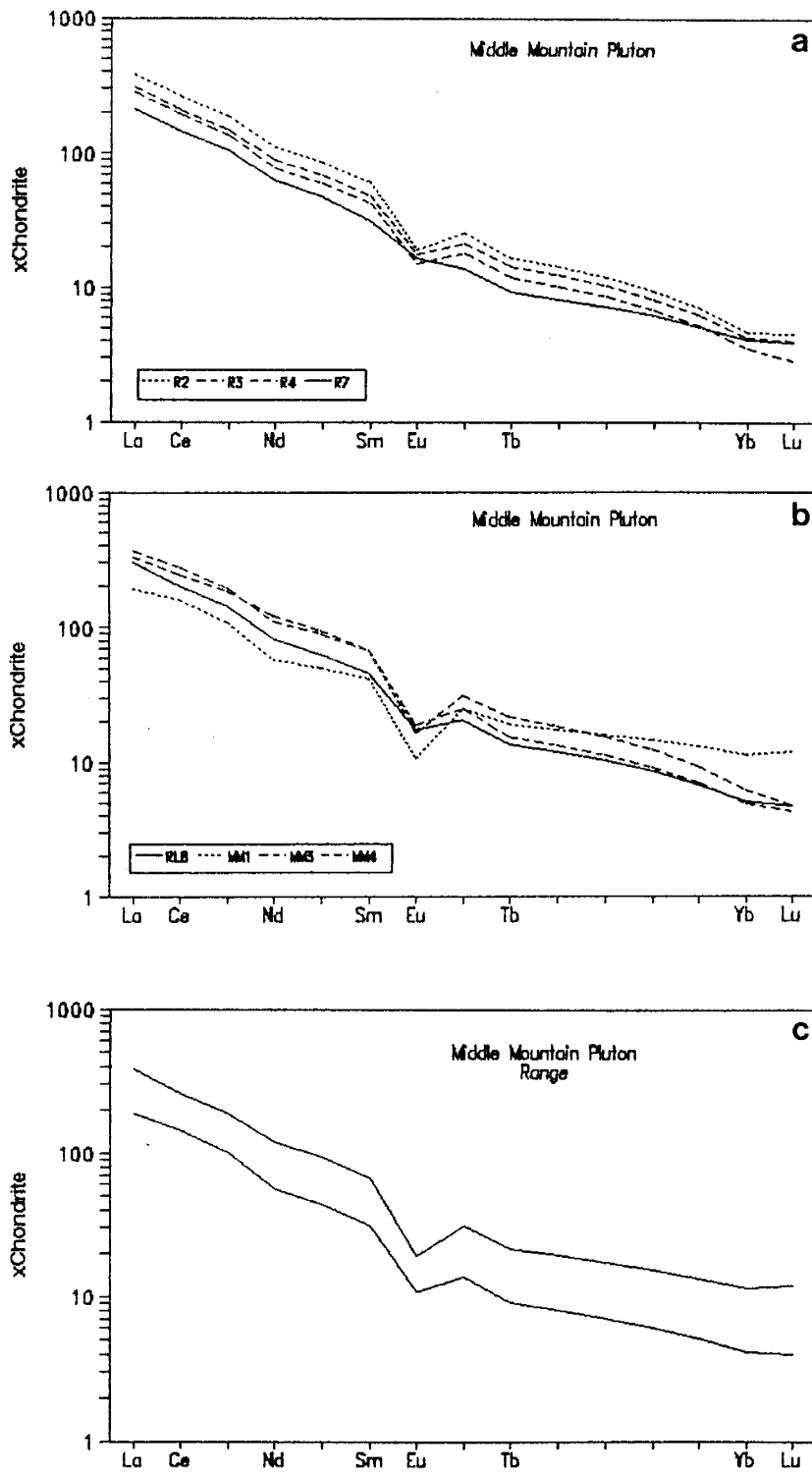


Figure 3.14a: REE plots for Middle Mountain pluton. a) and b) REE plots of representative samples, c) Range of REE values. For all REE plots data points are for elements shown on the horizontal scale. Chondrite-normalising values from Evenson et

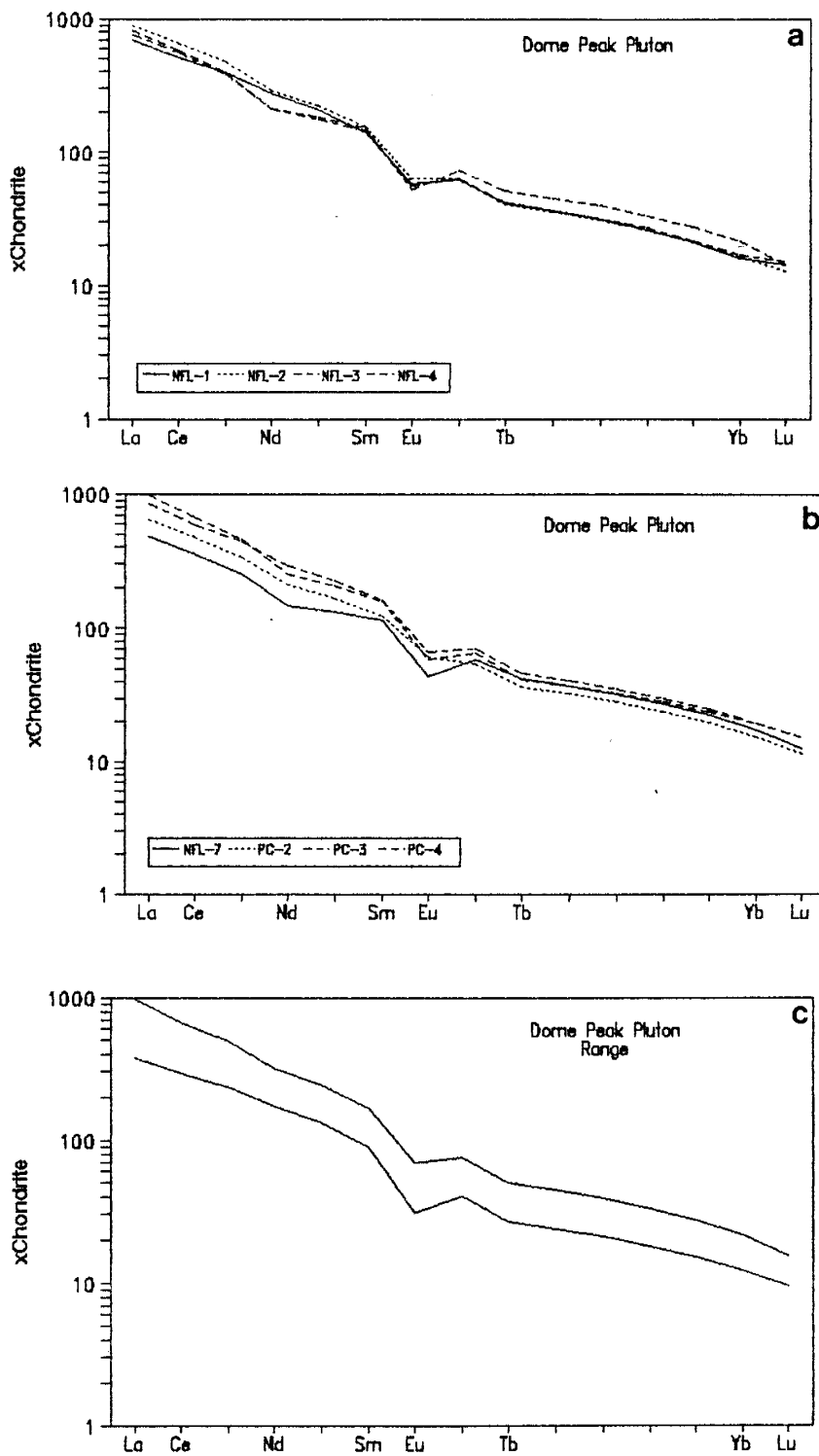


Figure 3.14b: REE plots for Dome Peak pluton. a) and b) plots of representative samples, c) Range of REE values.

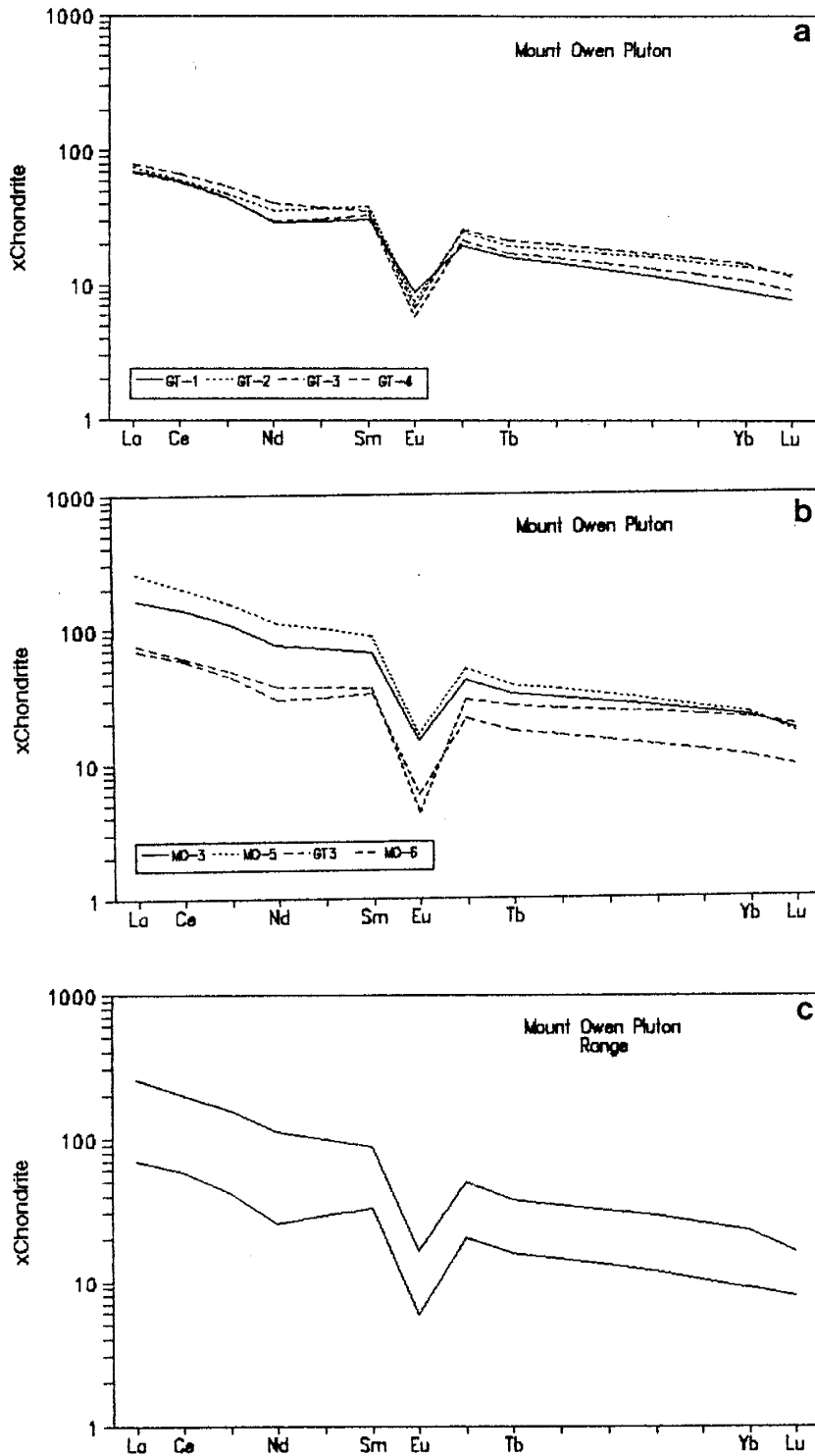
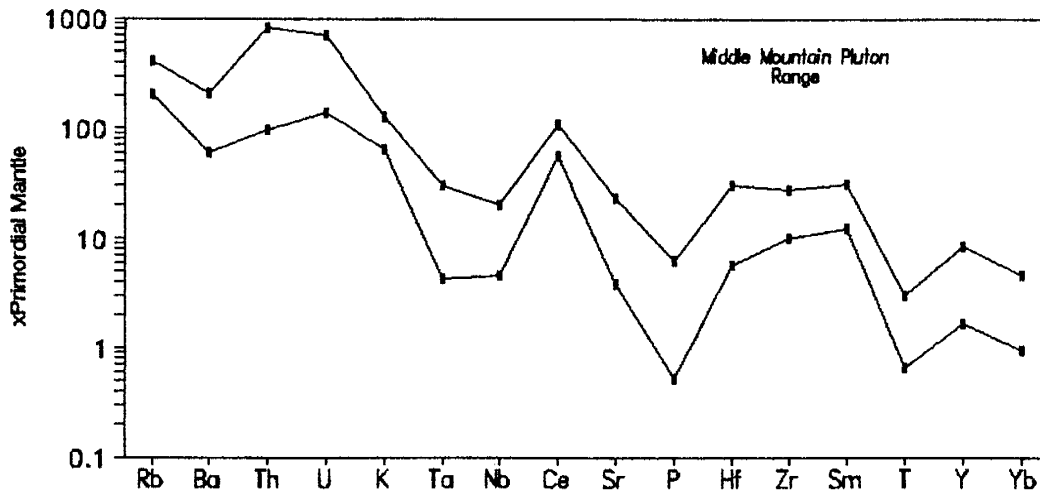
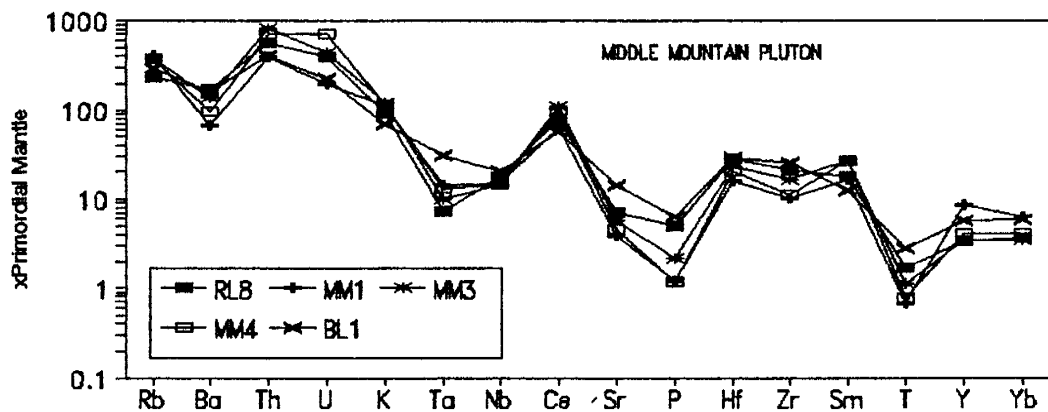
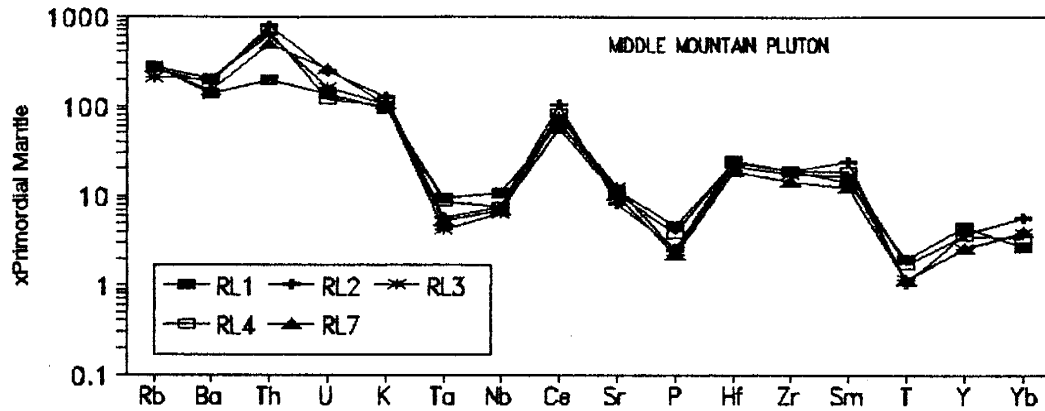


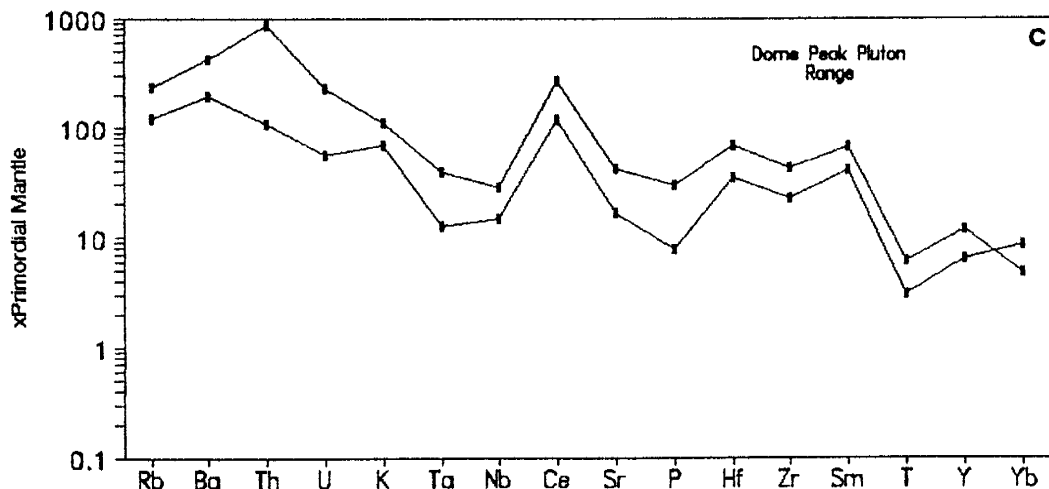
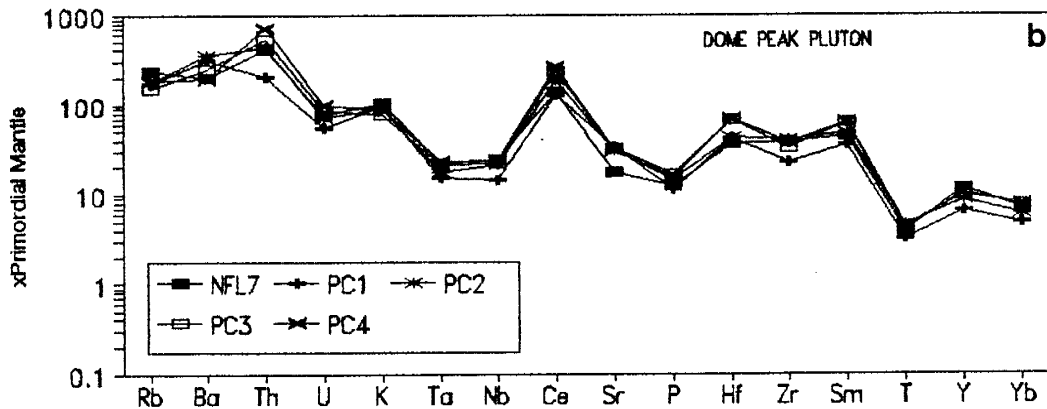
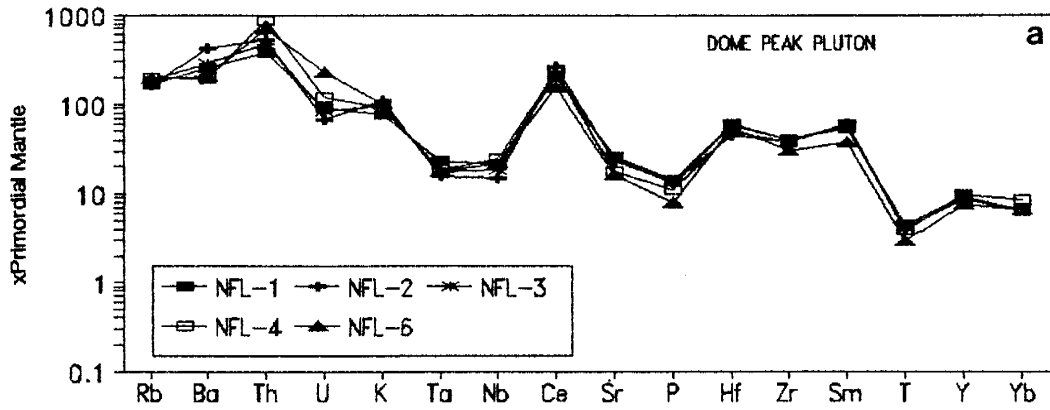
Figure 3.14c: REE plots for Mount Owen pluton. a) and b) plots of representative samples, c) Range of values.

with moderate Eu anomalies ( $\text{Eu}/\text{Eu}^* = .60$  Middle Mountain,  $\text{Eu}/\text{Eu}^* = .57$  Dome Peak), whilst Mount Owen pluton has only a moderately fractionated REE pattern ( $\text{La}/\text{Yb} = 12.25$ ) but a pronounced Eu anomaly ( $\text{Eu}/\text{Eu}^* = .37$ ). Dome Peak pluton is substantially more enriched in REE than either Middle Mountain or Mount Owen plutons.

Data for the three plutons are plotted on primordial mantle-normalised graphs (Figure 3.15a-c, normalising values from Hofmann, 1988). The elements are arranged in order of increasing bulk partition coefficient (D) for mantle mineralogies (Wood, 1979), modified from Brown et al. (1984); This gives an indication of element fractionations that have occurred since separation from the mantle. Middle Mountain and Dome Peak plutons have high Th contents, and Mount Owen pluton moderate Th content. Middle Mountain and Dome Peak plutons both have pronounced Ta-Nb anomalies, a characteristic of magmas generated in subduction zone environments (Pearce et al., 1983). Mount Owen pluton has only a slight Ta-Nb negative anomaly for samples MO-3, RM-2 and RM-3A, while most of the samples show decoupling between Ta and Nb. Garnet and clinopyroxene are two minerals both capable of fractionating these elements, with Ta having about a 3-fold greater compatibility than Nb in both phases (Green et al., 1989). This suggests that either garnet or clinopyroxene was present in the source and contributed to fractionating these elements in the melt. The decoupling however may reflect analytical

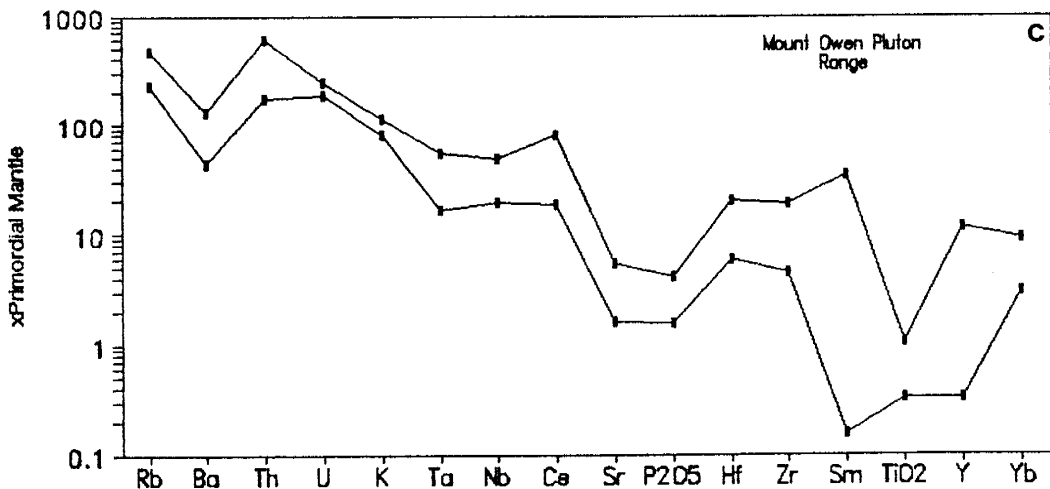
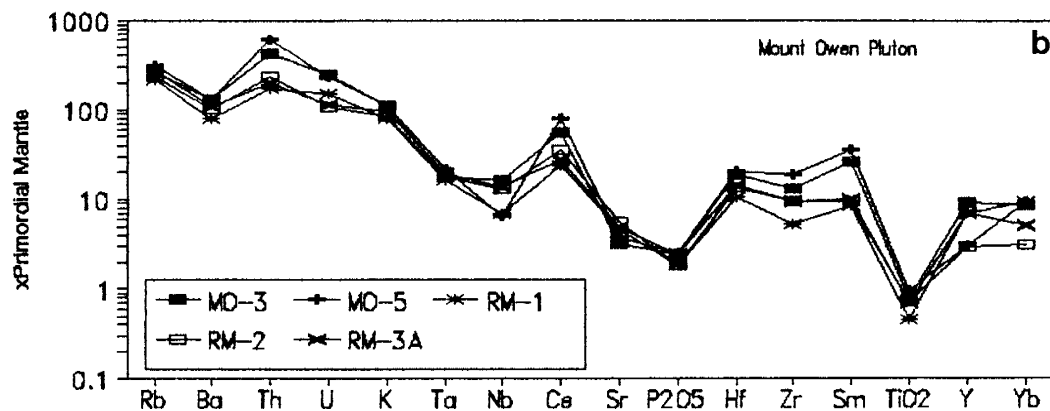
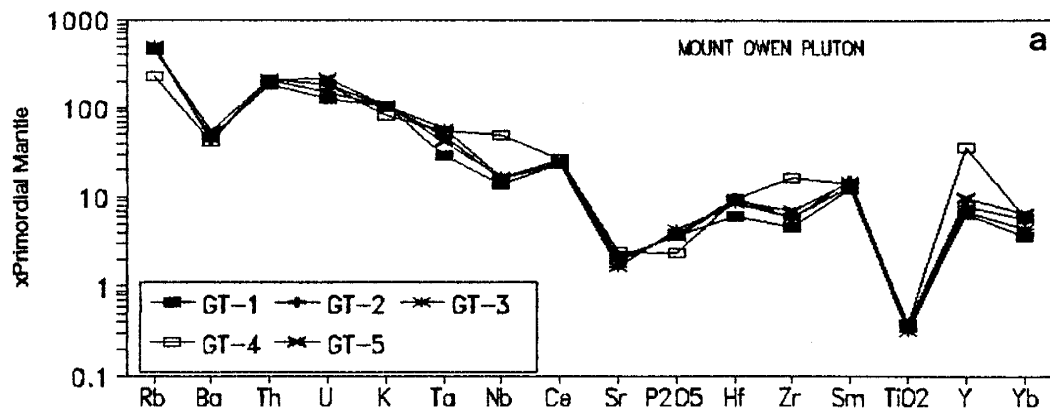


3.15a: Primordial mantle-normalised plots for Middle Mountain pluton. a) and b) plots of representative samples, c) Range of values. For all primordial mantle-normalised plots, normalising values are from Hofmann (1988). P= $P_2O_5$  and T= $TiO_2$ .



3.15b: Primordial mantle-normalised plots for Dome Peak pluton. a) and b) plots of representative samples, c) Range of values.





3.15c: Primordial mantle-normalised plots for Mount Owen pluton. a) and b) plots of representative samples, c) Range of values.

error in determining Nb content, as the values in Mount Owen pluton are close to the lower limit of determination for Nb (3.0 ppm, Table C1).

Mount Owen pluton also is depleted in Sr relative to Middle Mountain and Dome Peak plutons. All three plutons have  $P_2O_5$  and  $TiO_2$  negative anomalies due either to the retention of P/Ti-rich phases such as apatite (P), ilmenite (Ti) and magnetite (Ti) in the source, or by later fractional crystallisation of these phases.

## **Older Granitoids**

### **Bridger and Louis Lake Batholiths**

Both Bridger and Louis Lake batholiths have low Rb/Sr and Ba/Sr ratios (Table 3.3) which implies that plagioclase retention in their source was not a major factor in their genesis, although subsequent fractionation of K-feldspar and biotite could lower this ratio (Hanson, 1978). On Harker variation diagrams none of the trace elements show good linear correlation with  $SiO_2$  for the Bridger batholith (Figure 3.16), whilst for Louis Lake batholith the trace elements Rb and Zr show fair correlation with  $SiO_2$  ( $R=.61$  Rb,  $R=.69$  Zr). The variability in the older granitoids suggests that the LILE which are relatively mobile, have indeed been mobilised.

REE plots (Figure 3.18a-b) show that both the Bridger and Louis Lake batholiths have fractionated REE patterns (La/Yb=39.13 Bridger batholith, La/Yb=33.25 Louis Lake

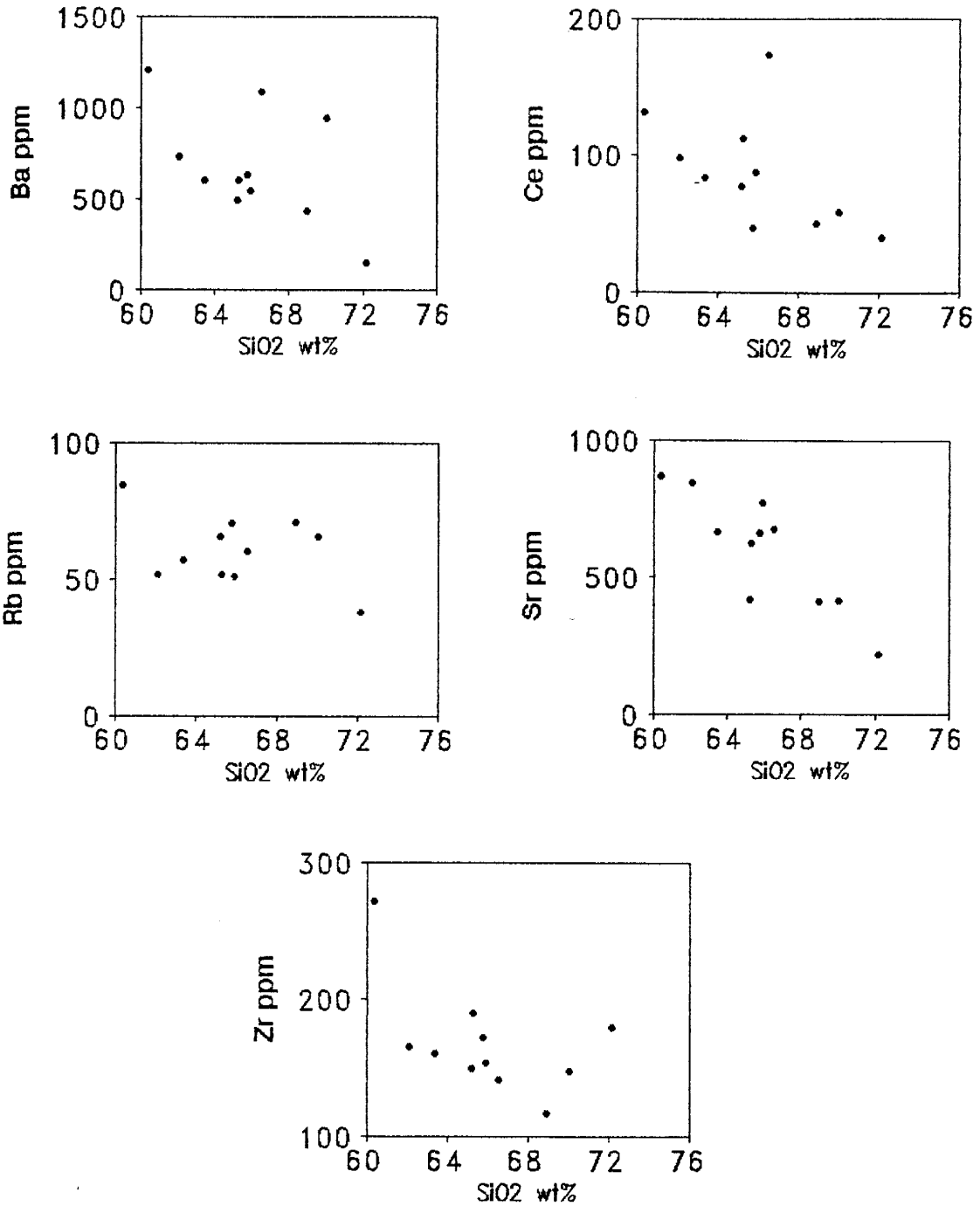


Figure 3.16: Harker variation diagrams showing the distribution of some LILE (Ba, Rb, Sr) and highly charged cations (Ce, Zr) in the Bridger batholith.

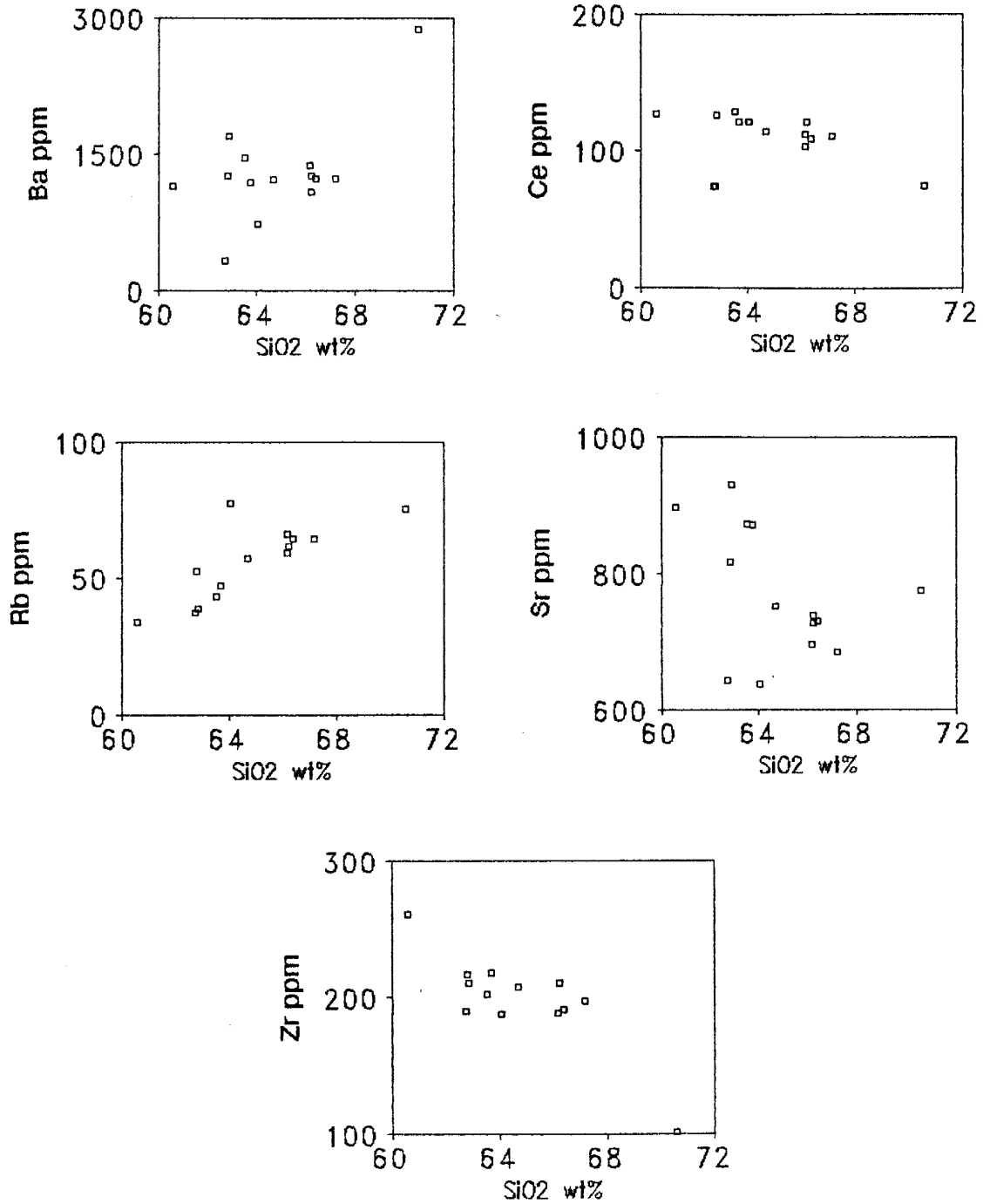


Figure 3.17: Harker variation diagrams showing the distribution of some LILE (Ba, Rb, Sr) and highly charged cations (Ce, Zr) in the Louis Lake batholith.

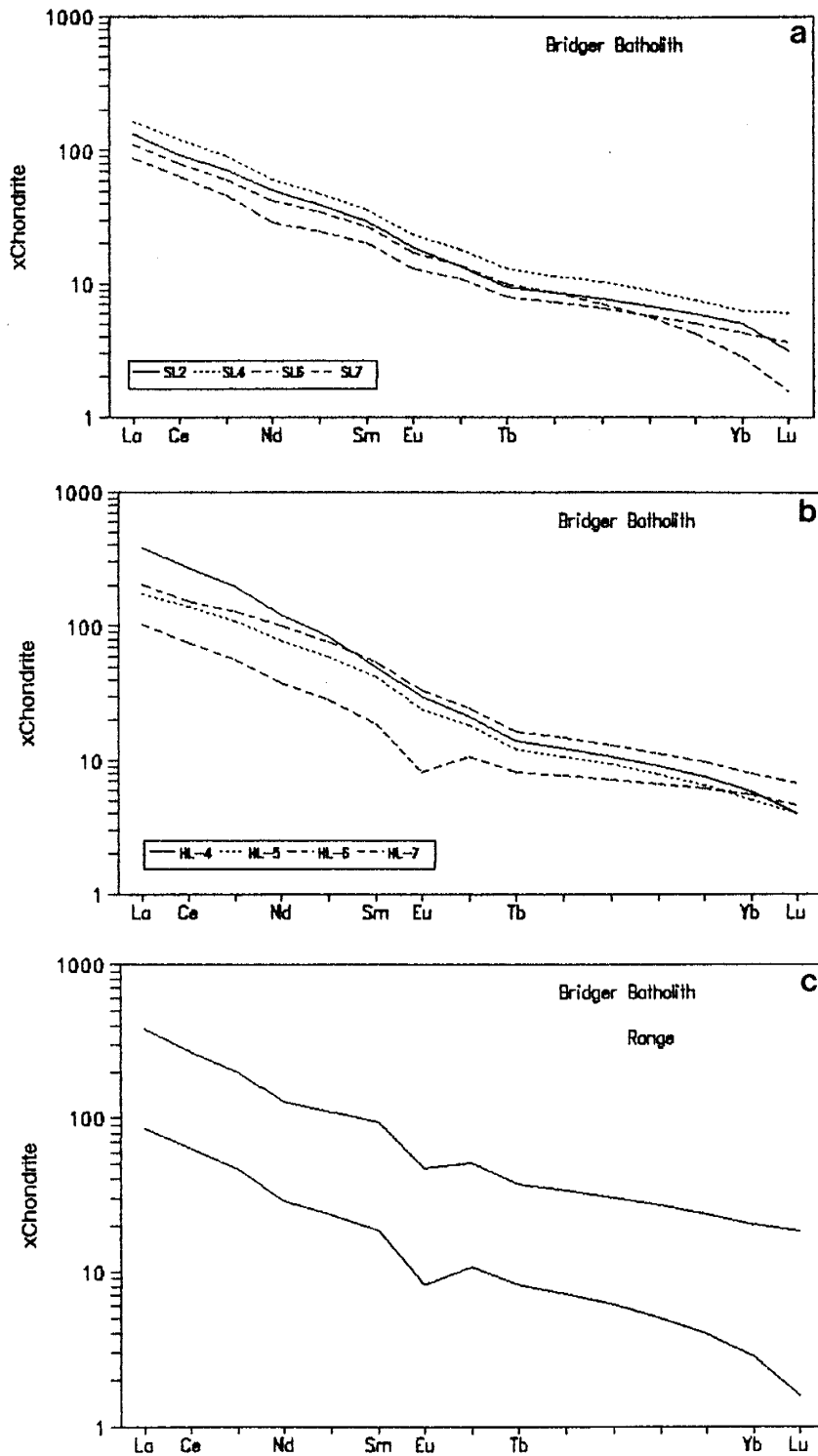


Figure 3.18a: REE plots for the Bridger batholith. a) and b) REE plots of representative samples, c) Range of REE values.

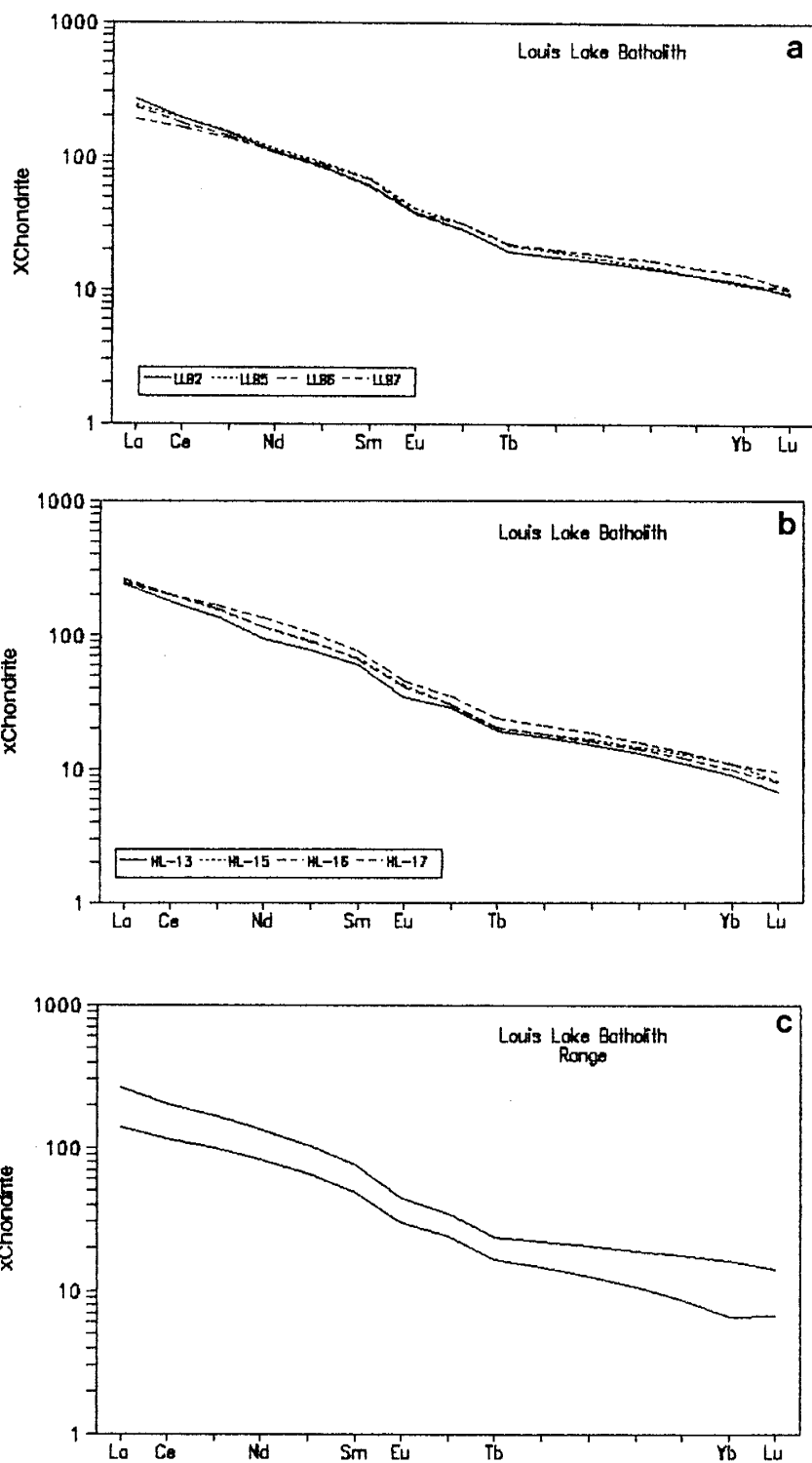
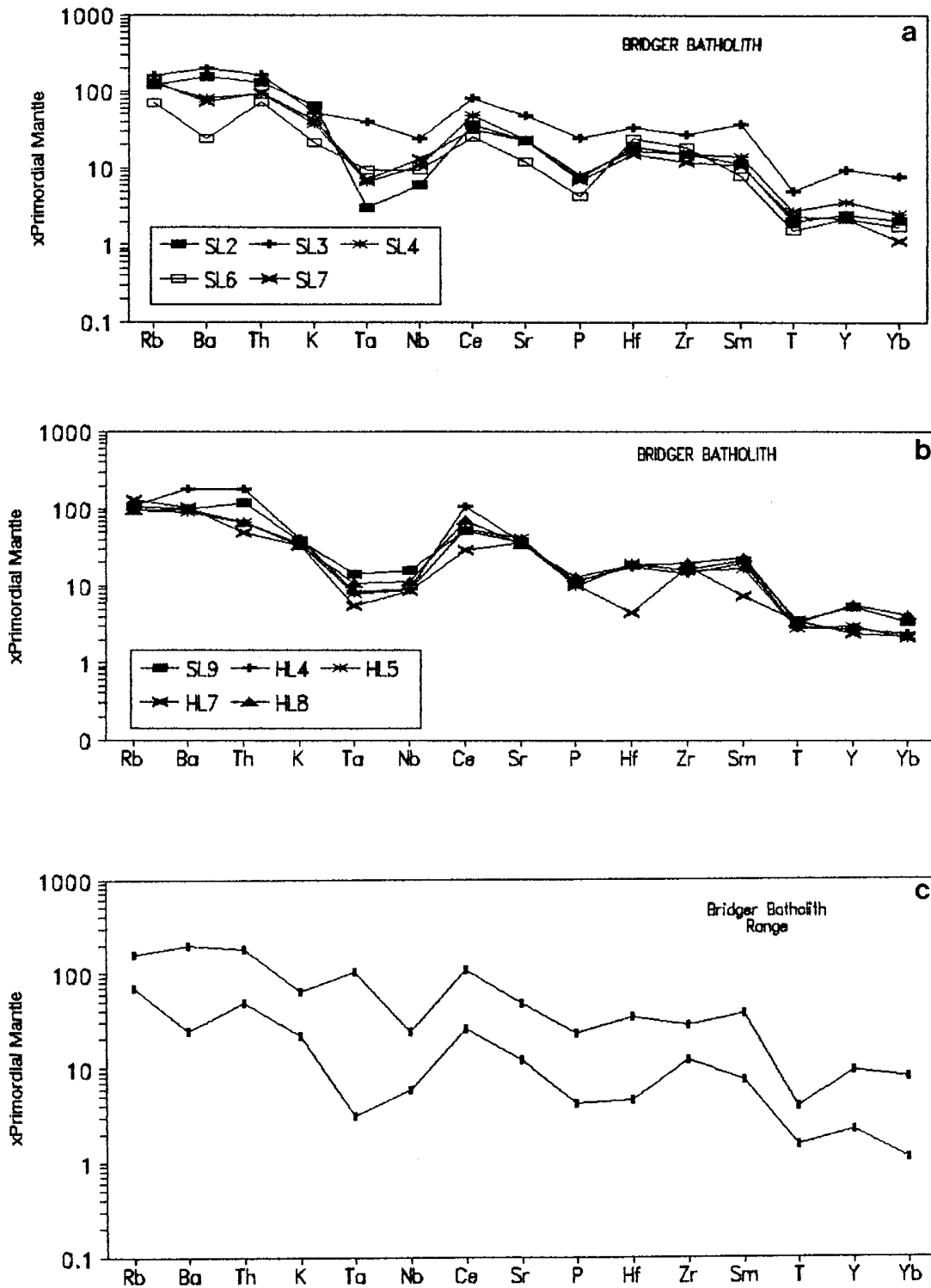


Figure 3.18b: REE plots for the Louis Lake batholith. a) and b) REE plots of representative samples, c) Range of REE values

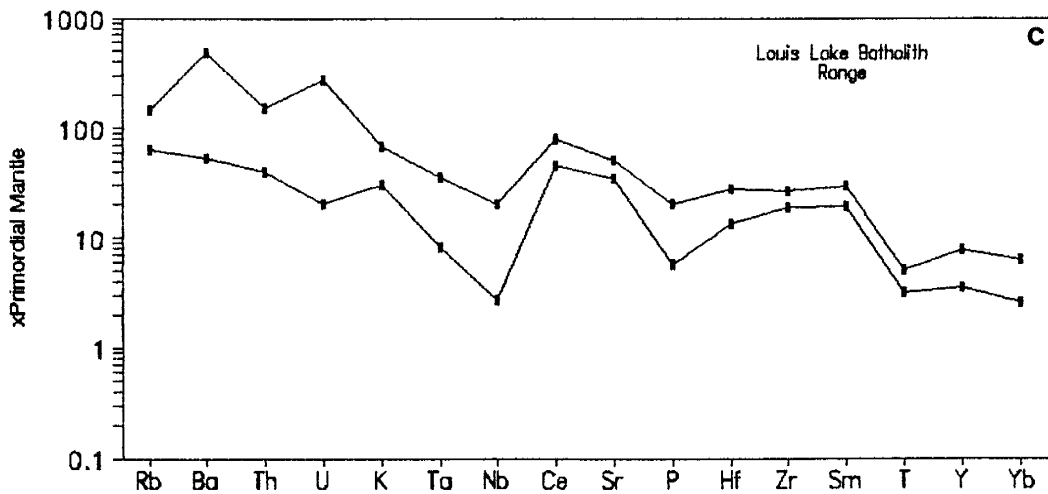
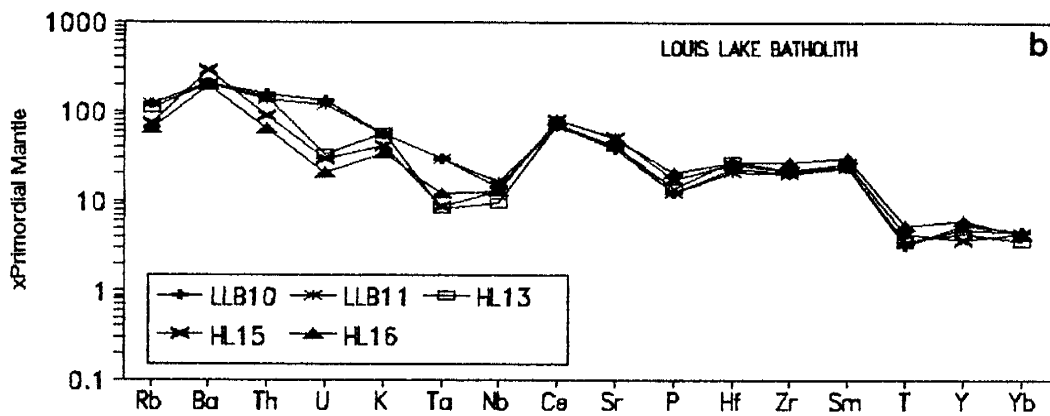
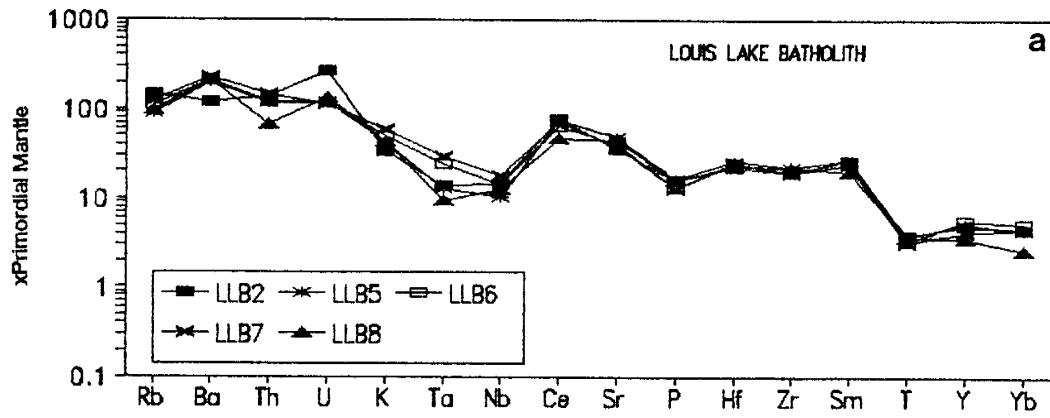
batholith) and slight Eu anomalies ( $\text{Eu}/\text{Eu}^* = .76$  Bridger batholith,  $\text{Eu}/\text{Eu}^* = .80$  Louis Lake batholith) characteristic of Archean trondhjemites and tonalites. They are slightly less fractionated than Middle Mountain and Dome Peak plutons. The range of REE values is more restricted for the Louis Lake batholith than the Bridger batholith, reflecting the more homogeneous nature of this batholith.

On primordial mantle-normalised plots (Figure 3.19a-b) the Bridger and Louis Lake batholiths are less fractionated than Middle Mountain and Dome Peak, with lower Ba, Th and HFSE (high field strength elements, Ta, Nb, Hf, Y, Zr) and with less pronounced Ta-Nb,  $\text{P}_2\text{O}_5$  and  $\text{TiO}_2$  negative anomalies. The Bridger batholith exhibits a greater range of values reflecting both the composite heterogeneous nature of this batholith and possible element mobilisation during deformation and metamorphism. Louis Lake batholith by comparison has a relatively restricted range and has not been intensely deformed like the Bridger batholith. Both batholiths show evidence of decoupling between Ta and Nb. In the Bridger batholith SL-3 is enriched in Ta relative to Nb, whilst SL-2 and to a lesser degree SL-4, SL-7 and HL-7 are depleted in Ta relative to Nb. For the Louis Lake batholith, LLB-6 and LLB-7 like Mount Owen pluton show decoupling of Ta and Nb which may be due to the assimilation and partial melting of a garnet or clinopyroxene-rich source. The depletion of Ta relative to Nb in the Bridger batholith may be due to the retention and



3.19a: Primordial mantle-normalised plots for the Bridger batholith. a) and b) plots of representative samples, c) Range of values.





3.19b: Primordial mantle-normalised plots for the Louis Lake batholith. a) and b) plots of representative samples, c) Range of values.

absence of melting of garnet in the source region, which has been proposed by numerous authors as a model to generate HREE depleted tonalites and trondhjemites (Arth et al., 1978; Martin, 1987; Rudnick and Taylor, 1987). The decoupling may also reflect analytical error in Nb concentration, which is close to the lower limits of determination by X-ray fluorescence (3.0 ppm).

### 3.5: Tectonic Discriminant Diagrams

Granites carry a major and trace element signature indicative of source region, which also generally characterises tectonic environment. Utilising major and trace elements, tectonic discriminant diagrams have been devised to distinguish between distinct tectonic settings (Pearce et al., 1984; Harris et al., 1986;). The fields on geochemical discriminant diagrams reflect source regions and melting and crystallisation histories rather than tectonic setting. However, reasonable discrimination can be made for Phanerozoic granites (Pearce et al., 1984) as distinct environments (such as ocean ridge, subduction zones and continental rifts) have distinct P/T conditions of granite generation. However caution must be used in applying these diagrams in the Precambrian, specifically in the Archean when the mantle was 200-300°C hotter and similar tectonic environments may have had different P/T conditions, reflecting the hotter mantle temperatures.

Rb-Nb-Y discriminant plots distinguish between granites generated in subduction zones (VAG) from those in collisional (syn-COLG), ocean ridge (ORG) and within plate (WPG) environments (Pearce et al., 1984). Rb-Hf-Ta plots further separate collisional granites into syn-collisional (II) and post-collisional (III) groups (Harris et al., 1986). Middle Mountain, Dome Peak and Mount Owen plutons all lie in the volcanic arc and syn-collisional fields on Rb-Nb-Y plots

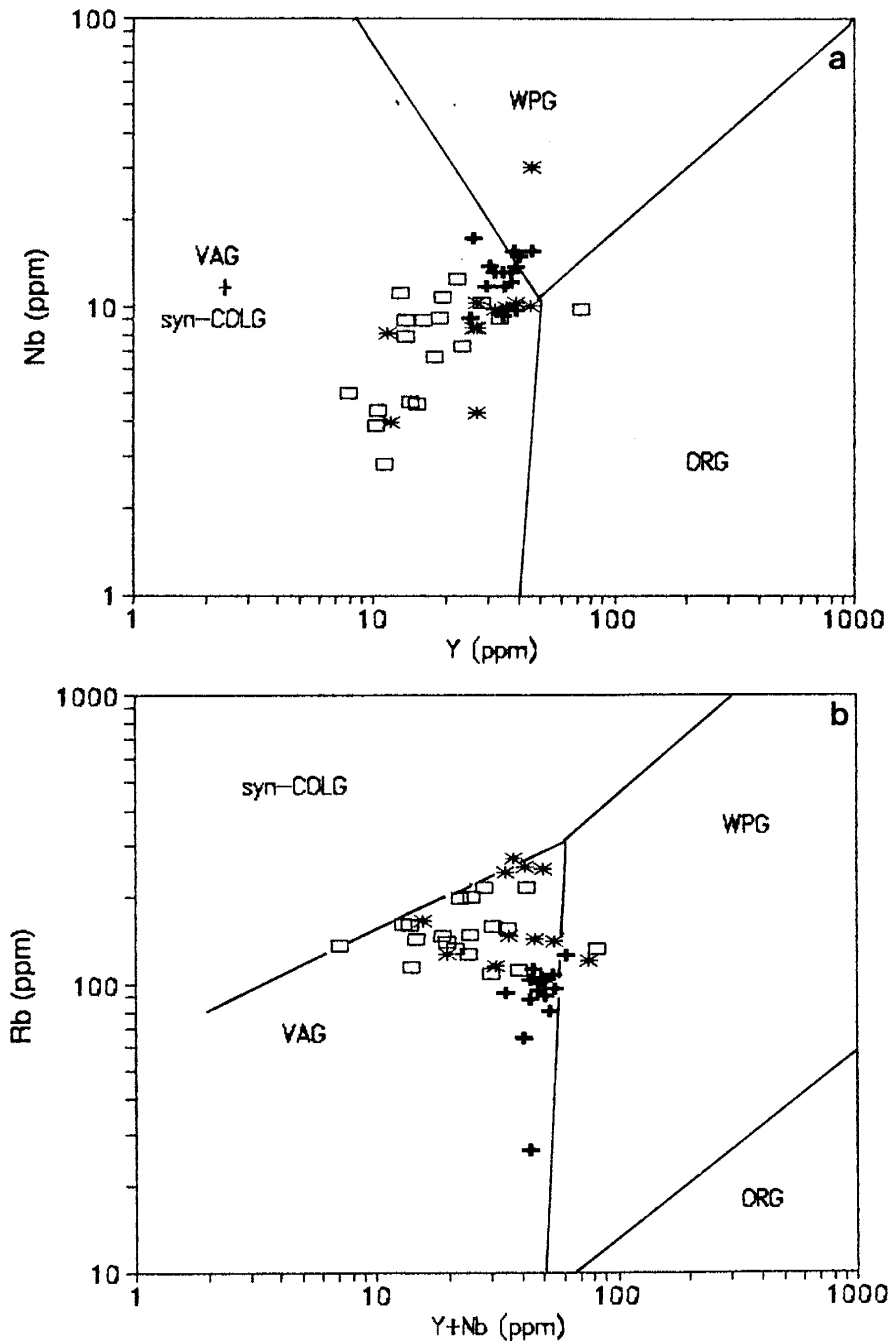


Figure 3.20: Rb-Y-Nb tectonic discriminant diagrams from Pearce et al. (1984). WPG=Within Plate Granites, VAG=Volcanic Arc Granites, syn-COLG=syn-Collisional Granites, ORG=Ocean Ridge Granites. a) and b) (□)=Middle Mountain, (+)=Dome Peak and (\*)=Mount Owen plutons.

(Figure 3.20). Their source region was not enriched in high field strength elements (Ta, Nb, Hf, Y) and reflects a source generated from a subduction zone environment. Some samples from both Middle Mountain and Mount Owen plutons straddle the VAG and syn-COLG fields.

On Rb-Hf-Ta plots Middle Mountain pluton lies in the volcanic arc (VA) field with a trend towards the syn-collisional field (II) (Figure 3.21a). Dome Peak pluton lies in the volcanic arc field (Figure 3.21b). Mount Owen pluton forms two distinct populations, one in the volcanic arc (VA) field, and one in the collisional fields (II and III) (Figure 3.21c). The samples in fields II and III are located well away from the pluton's margins, and are interpreted to reflect magma sources. The samples in the volcanic arc (VA) field come from close to the pluton's margins and may reflect assimilation of material generated in an arc environment (such as older tonalite-trondhjemite orthogneisses).

The older Bridger and Louis Lake batholiths lie in the volcanic arc fields on both Rb-Nb-Y and Rb-Hf-Ta plots (Figure 3.22 and 3.23), which supports the model for their genesis as partial melts derived from subducted oceanic crust (Martin, 1987).

In Proterozoic and Phanerozoic terranes, A-type granites with high  $\text{SiO}_2$ ,  $\text{Na}_2\text{O}+\text{K}_2\text{O}$ ,  $\text{Fe}/\text{Mg}$ ,  $\text{Ga}/\text{Al}$ , Zr, Nb, Ga, Y and Ce, low CaO and Sr are recognised (Collins et al., 1982; Anderson, 1983; Whalen et al., 1987), thought to be generated by either

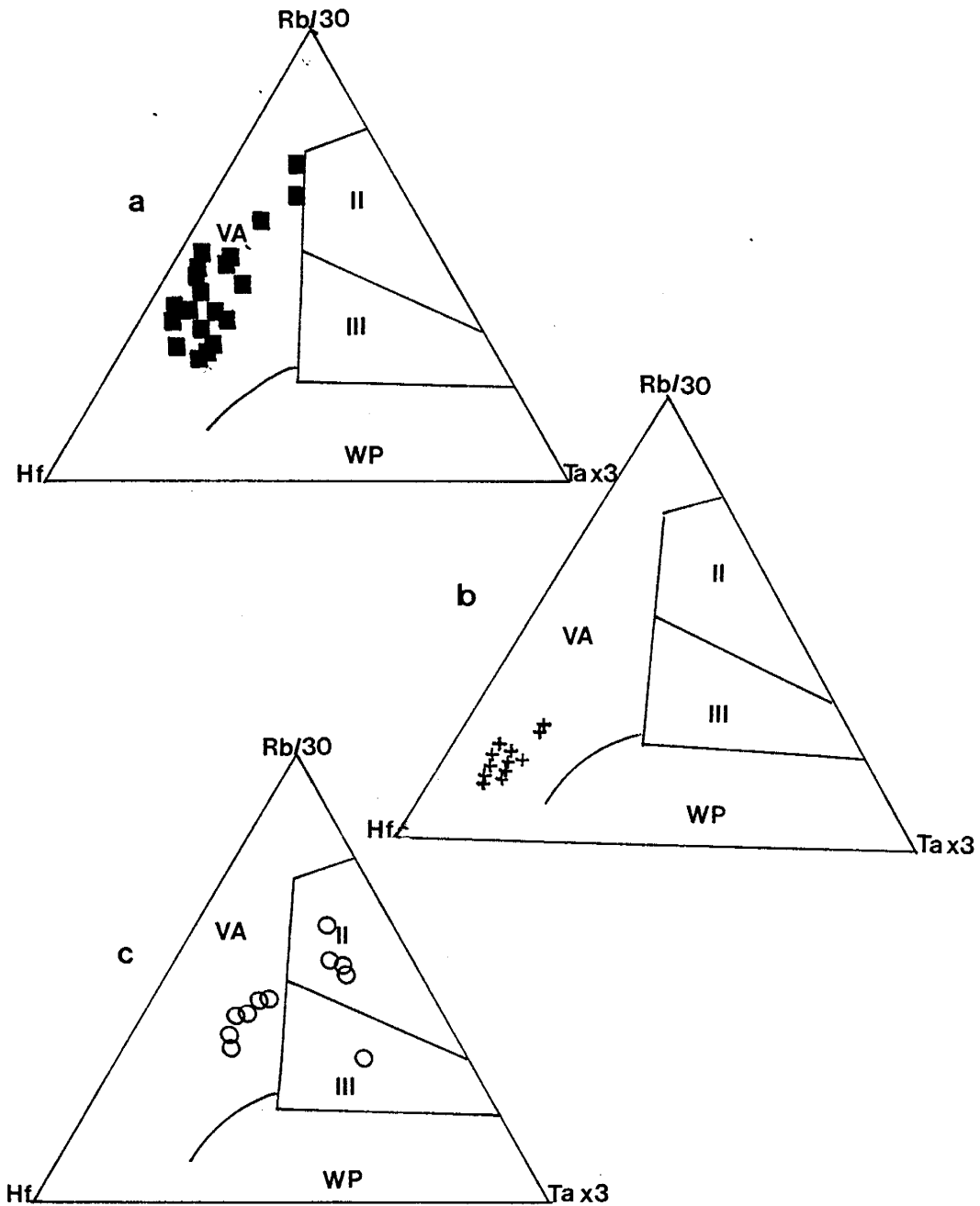


Figure 3.21: Rb-Hf-Ta plot from Harris et al. (1986). VA=Volcanic arc granites, WP=Within plate granites, II=Syn-collisional granites, III=Post-collisional granites. a) Middle Mountain pluton, b) Dome Peak pluton and c) Mount Owen pluton.

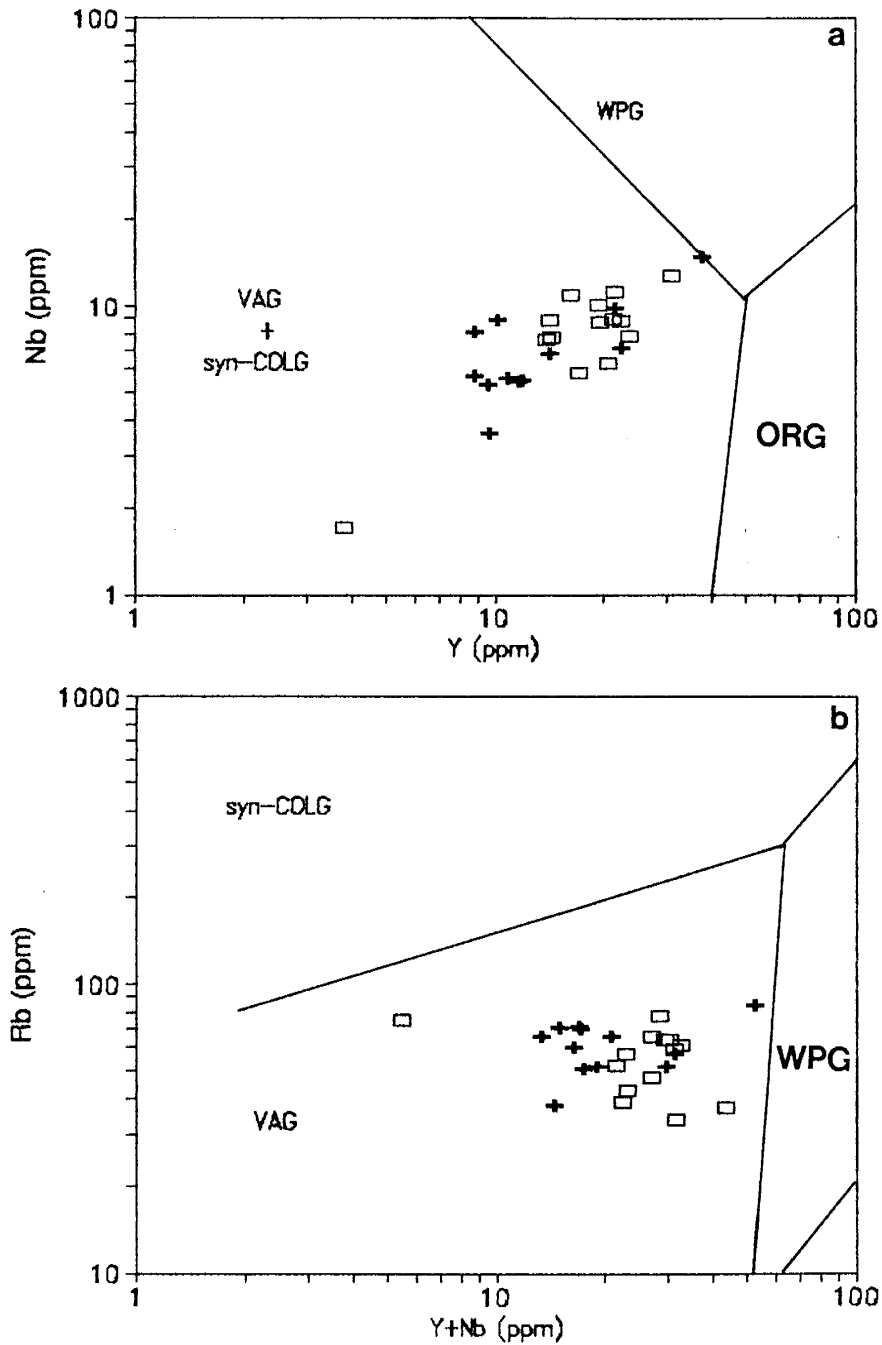


Figure 3.22: Rb-Y-Nb tectonic discriminant diagrams from Pearce et al. (1984). WPG=Within Plate Granites, VAG=Volcanic Arc Granites, syn-COLG=syn-Collisional Granites, ORG=Ocean Ridge Granites. a) and b) (+)=Bridger and (□)=Louis Lake batholiths.

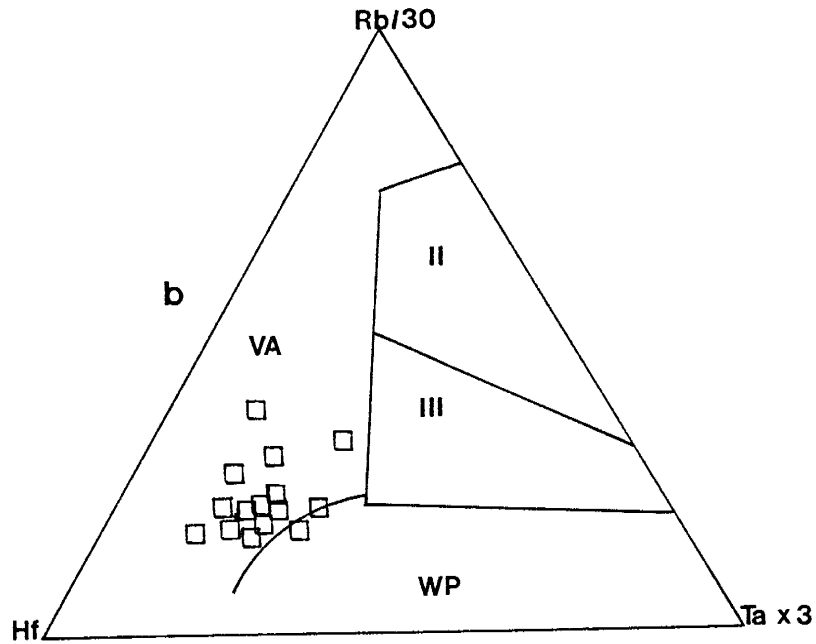
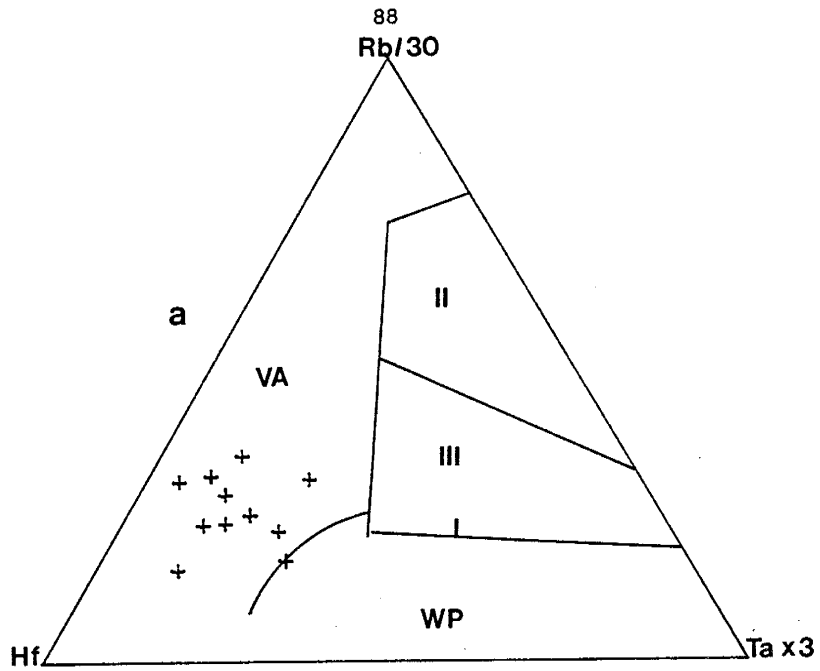


Figure 3.23: Rb-Hf-Ta plot from Harris et al. (1986). VA=Volcanic arc granites, WP=Within plate granites, II=Syn-collisional granites, III=Post-collisional granites. a) Bridger batholith and b) Louis Lake batholith.



melting a F and/or Cl enriched dry granulite residue remaining in the crust after the extraction of an orogenic granite (Whalen et al., 1987) or melting a charnockite source (Anderson, 1983). On plots employing Ga/Al against Y, Ce, Nb, Zr and  $\text{Na}_2\text{O}+\text{K}_2\text{O}$ , discrimination between A-type granites and most orogenic granites (M, I, and S-types) is obtained (Whalen et al., 1987). Figure 3.24 and 3.25 show selected trace element I-S-A grantoid discriminant plots for Middle Mountain, Dome Peak and Mount Owen plutons. All three plutons straddle the boundaries of I/S and A-type granites. For trace element content (Zr, Ce, Y, Nb) Dome Peak shows the clearest separation from the I/S fields, exhibiting A-type characteristics (Figure 3.25b). But as stated earlier Dome Peak pluton also is classified as an I-type granite (Table 3.2). This apparent contradiction in part reflects two different classification schemes, the I/S-type classification (Chappell and White, 1974) is based on major element and isotopic data, whereas the A-type classification (Collins et al., 1982; Whalen et al., 1987) is based on both major and trace element data. Also, the sources and therefore the geochemical signatures (major and isotopic) for A-type granites can be both igneous and sedimentary (Whalen et al., 1987). The A-type classification in effect is superimposed on the I/S-type classification.

The older granitoids, the Bridger and Louis Lake batholiths, also straddle the boundaries between I/S and A-

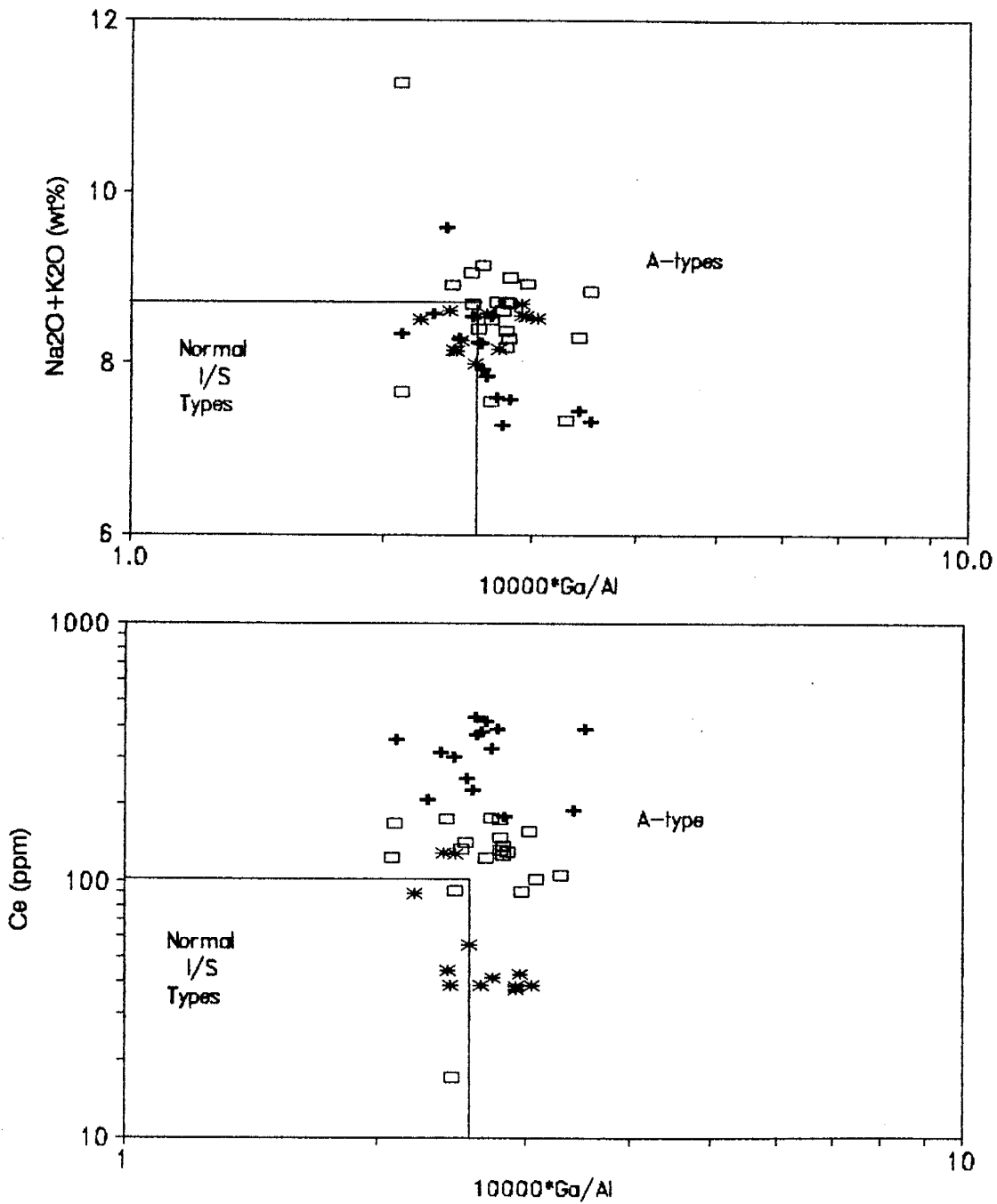


Figure 3.24: Trace element discriminant diagrams from Whalen et al. (1987). Normal I/S-types refer to the field occupied by ocean ridge, orogenic and syn-collisional granites of igneous and sedimentary origin. A-types plot outside this box. ( $\square$ )=Middle Mountain, (+)=Dome Peak and (\*)=Mount Owen plutons.

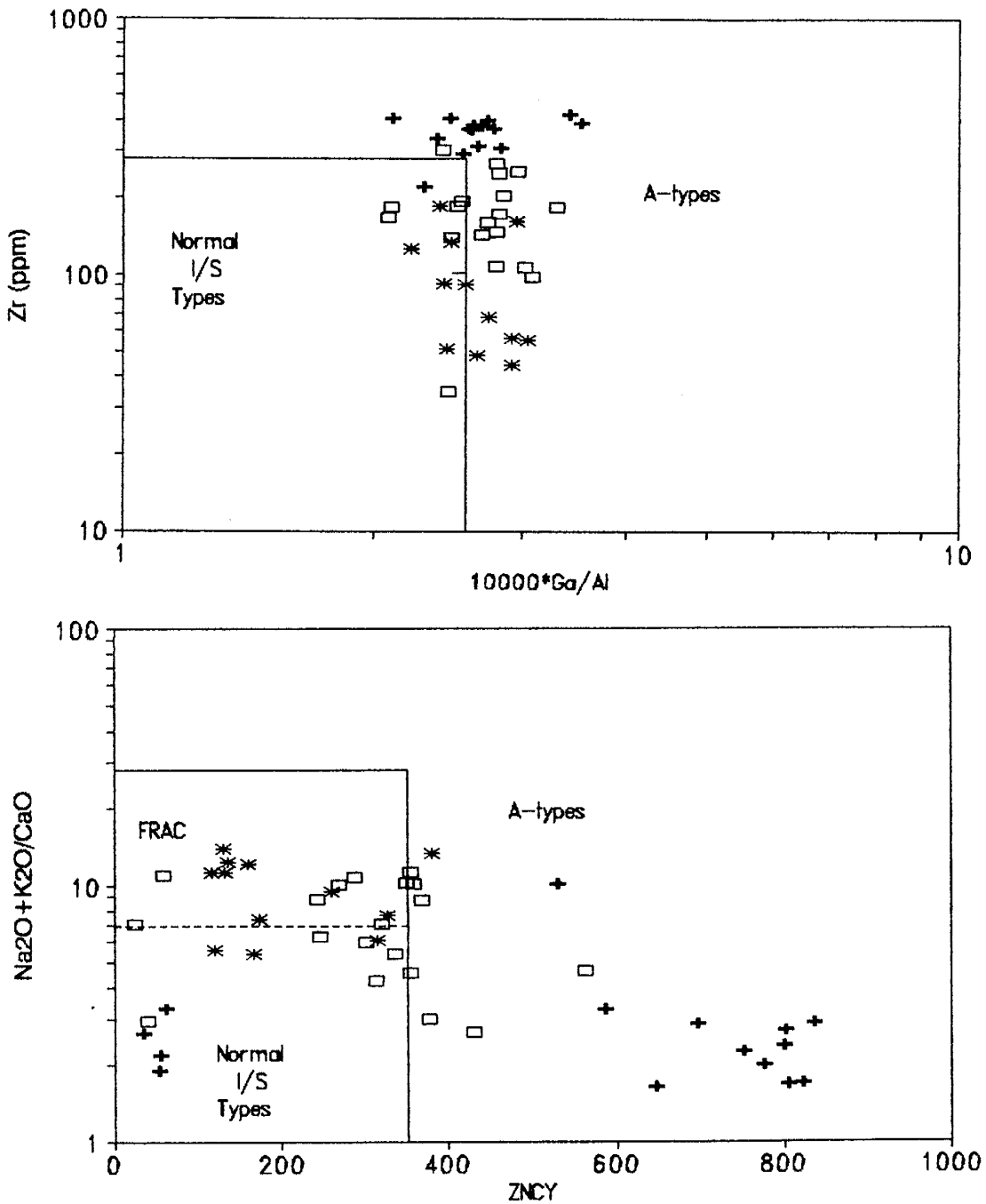


Figure 3.25: Trace element discriminant diagrams from Whalen et al. (1987). Normal I/S-types is the field occupied by ocean ridge, orogenic and syn-collisional granites of igneous and sedimentary origin. FRAC is the field of fractionated I/S-type granites. A-type plot outside these fields. ( $\square$ )=Middle Mountain, (+)= Dome Peak and (\*)=Mount Owen plutons.

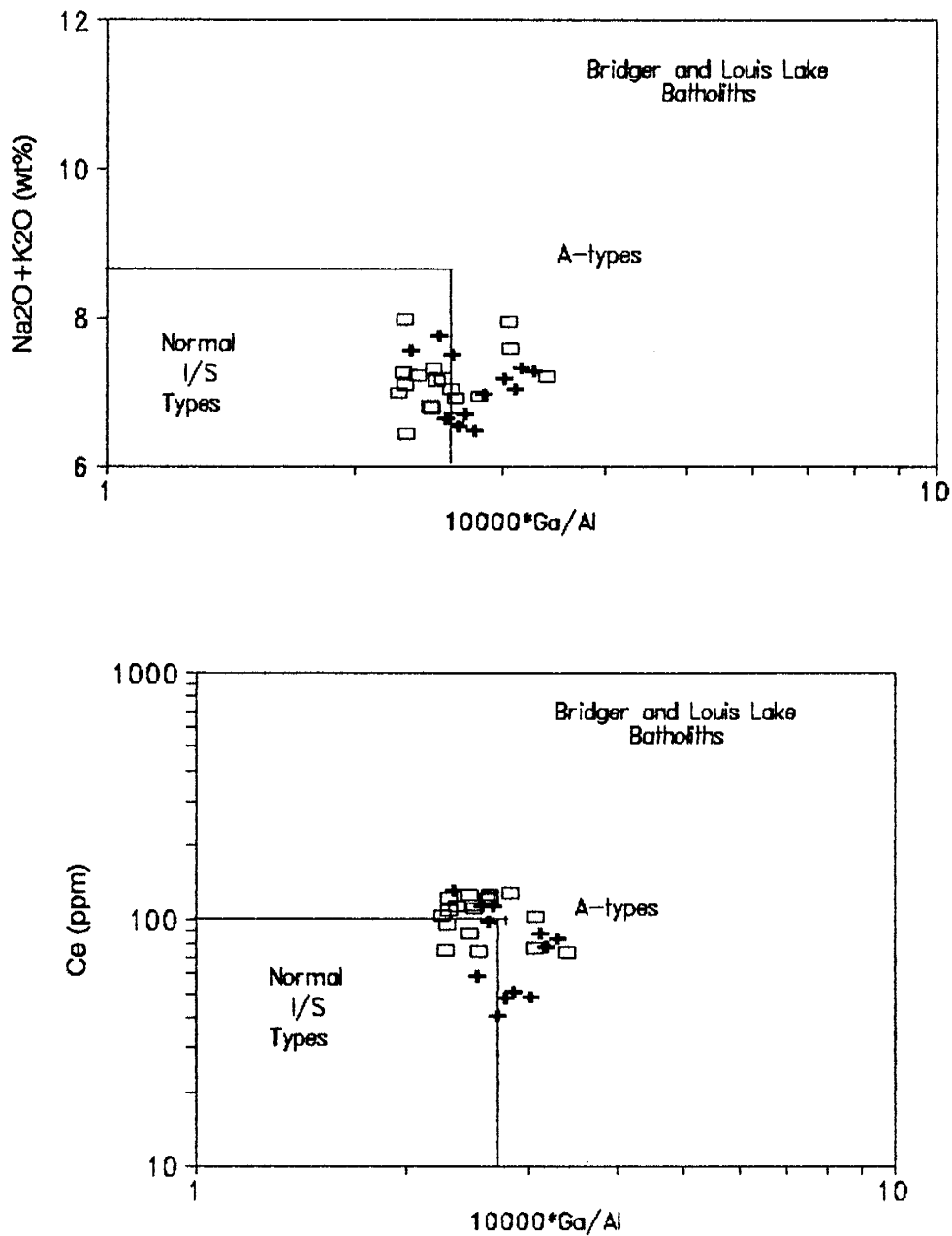


Figure 3.26: Trace element discriminant diagrams from Whalen et al. (1987). Normal I/S-types refer to the field occupied by ocean ridge, orogenic and syn-collisional granites of igneous and sedimentary origin. A-types plot outside this box. (+)=Bridger and ( $\square$ )=Louis Lake batholiths.

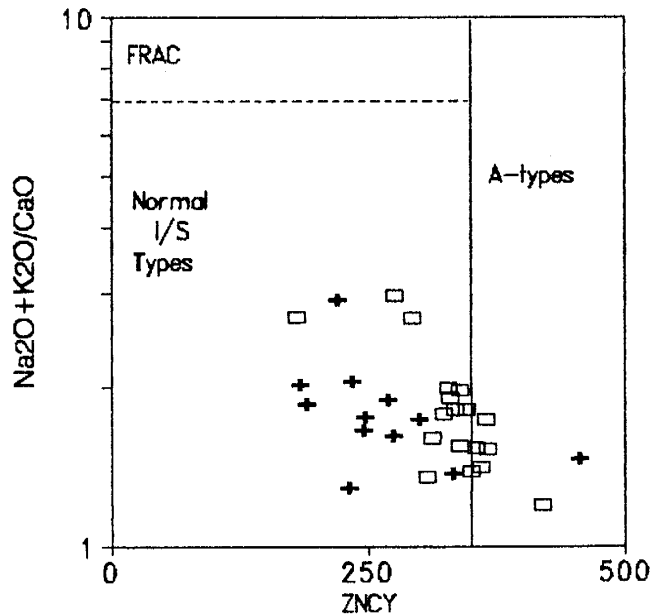
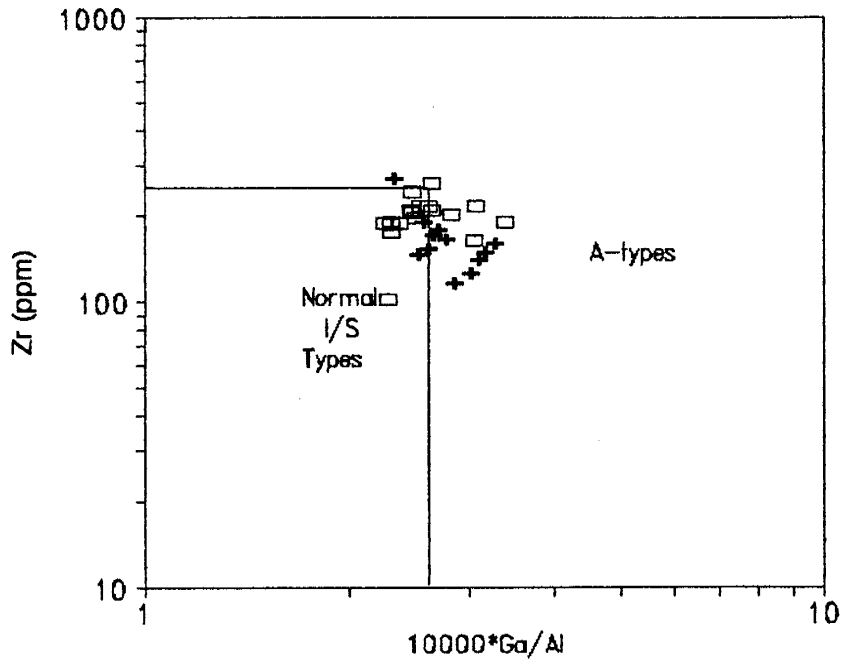


Figure 3.27: Trace element discriminant diagrams from Whalen et al. (1987). Normal I/S-types is the field occupied by ocean ridge, orogenic and syn-collisional granites of igneous and sedimentary origin. FRAC is the field of fractionated I/S-type granites. A-type plot outside these fields. (+)=Bridger and ( $\square$ )=Louis Lake batholiths.

type granite (Figure 3.26-3.27).

### 3.6: Comparison to other Late Archean granites and Post Archean granites

Most Archean cratons record a major episode of K-rich granitic plutonism between 2700-2500 Ma. Figure 3.28 shows the range of REE patterns for some Late Archean granites from the Wyoming craton (Laramie, Beartooth, Middle Mountain, Dome Peak and Mount Owen granites), Pilbara craton (Shaw batholith) and Zimbabwe craton (Salisbury and Chilimanzi granites). Data for the Wyoming craton are from this study and Montgomery (1989), for the Pilbara craton from Bickle et al. (1989) and the Zimbabwe craton from K.C. Condie (1989, unpublished data). The granites display a range of REE contents but the dominant feature is their HREE depletion, although some of them like the Mount Owen, Chilimanzi and Cooglegong granites have flatter REE patterns. The Late Archean granites also have a moderate range of major and trace element composition reflected in the tectonic discriminant diagrams shown in Figure 3.29 and 3.30. This indicates that the sources for these granites were variable, but does not constrain tectonic environment. The HREE-depleted granites may be generated from an already HREE-depleted source such as HREE-depleted tonalites (Arth et al., 1978; Martin, 1987; Rudnick and Taylor, 1987), which are a dominant component of the Archean

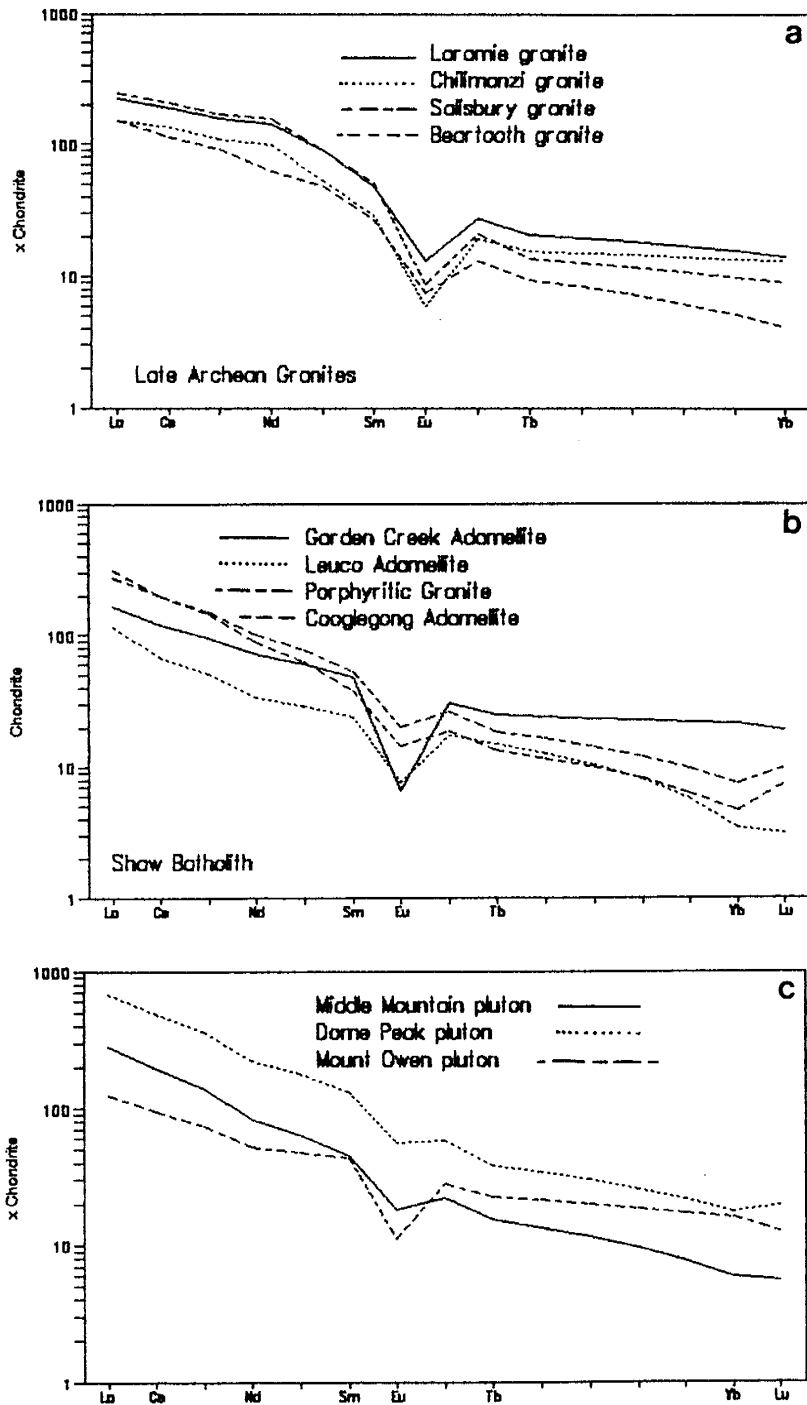


Figure 3.28: REE plots for late Archean granites. a) Laramie and Beartooth granites, Wyoming craton (Montgomery, 1989), and Salsbury and Chilimanzi granites, Zimbabwe craton (Condie, unpublished data, 1989). b) Shaw batholith granites, Pilbara craton (Bickle et al., 1989). c) Middle Mountain, Dome Peak and Mount Owen plutons (this study).

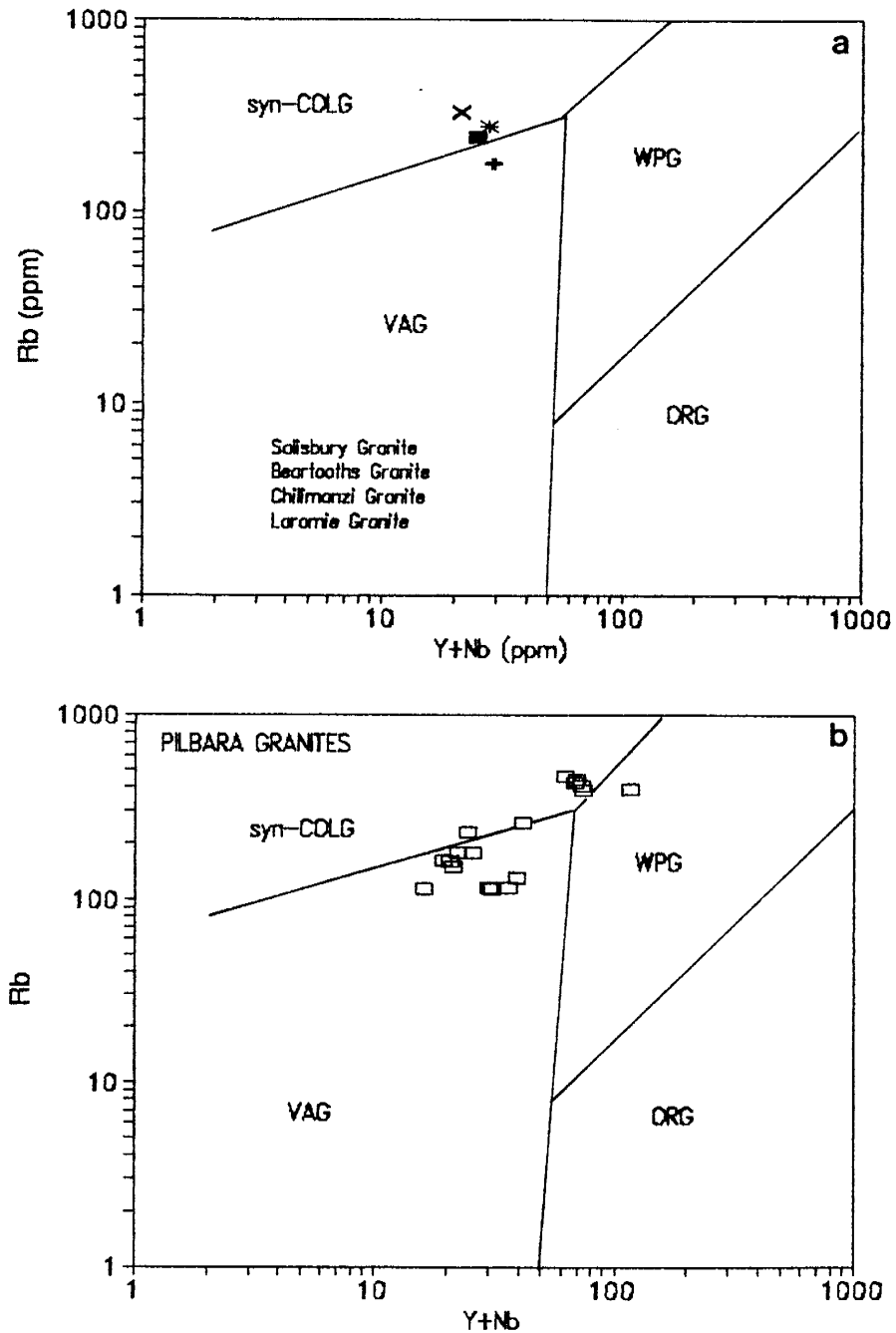


Figure 3.29: Rb-Y-Nb tectonic discriminant diagrams from Pearce et al. (1984), for late Archean granites. a) Laramie and Beartooth granites, Wyoming craton (Montgomery, 1989), and Salsibury and Chilimanzi granites, Zimbabwe craton (Condie, unpublished data, 1989). b) Shaw batholith granites, Pilbara craton (Bickle et al., 1989). WPG=Within Plate Granites, VAG=Volcanic Arc Granites, syn-COLG=syn-Collisional Granites, ORG=Ocean Ridge Granites.



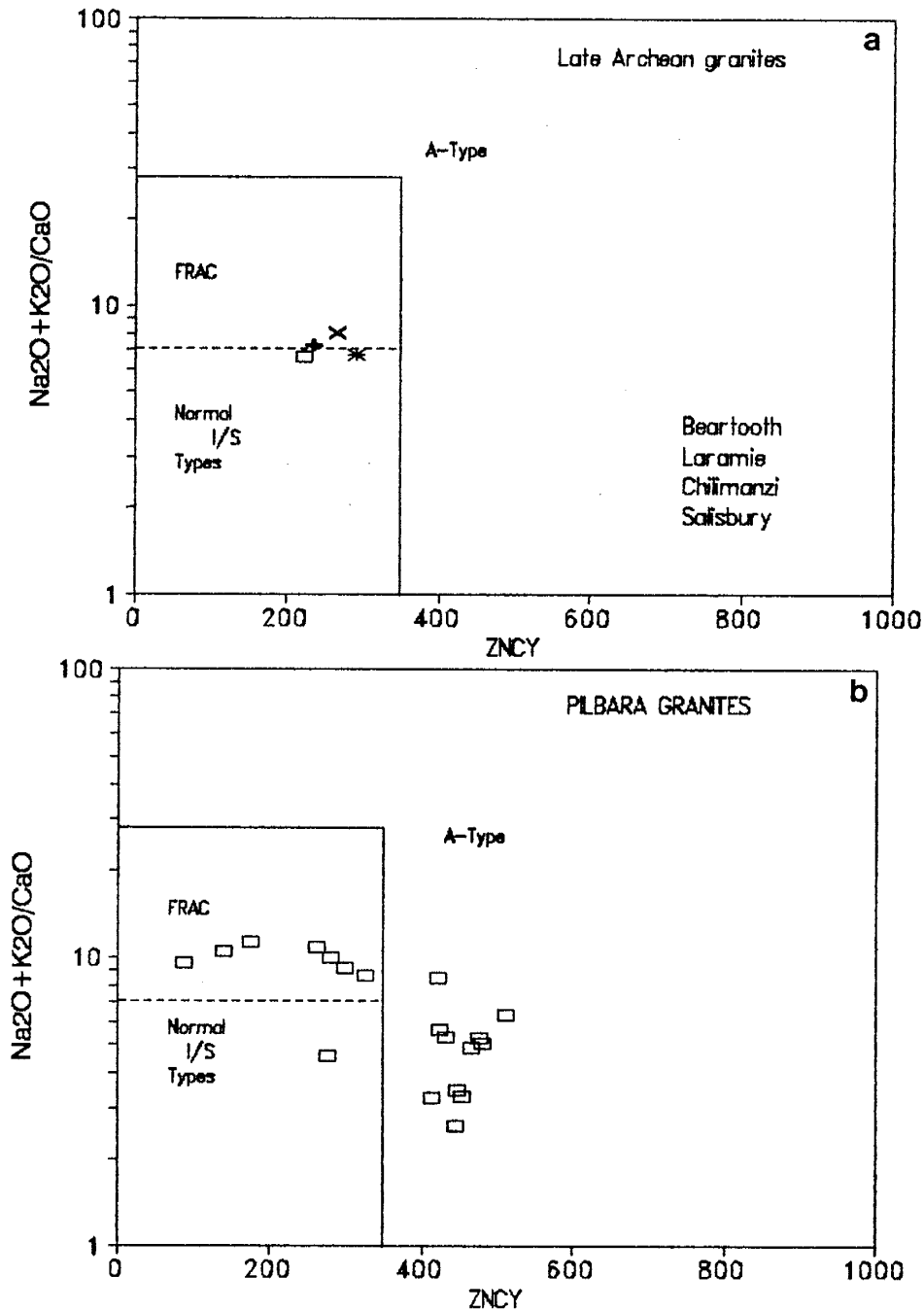


Figure 3.30:  $\text{Na}_2\text{O} + \text{K}_2\text{O} / \text{CaO}$  v  $\text{ZNCY}$  plots from Whalen et al. (1987) for late Archean granites. a) Laramie and Beartooth granites, Wyoming craton (Montgomery, 1989), and Salisbury and Chilimanzi granites, Zimbabwe craton (Condie, unpublished data, 1989). b) Shaw batholith granites, Pilbara craton (Bickle et al., 1989). Fields same as Figure 3.25.

crust. Less depleted granites may be generated from partial melts of undepleted tonalites and metasediments or by fractional crystallisation from a more basaltic precursor (Condie, 1981; Taylor and McClennan, 1985). To better constrain the origin of individual granites combined stable and radiogenic isotope data along with major and trace element data are required.

The early to mid-Proterozoic was another major period (1800-1300 Ma) of granite plutonism (at least in Laurentia). Figure 3.31 shows the range of some 1650-1450 Ma granites from the southwest U.S.A. In Figure 3.31a the granites have been divided by major and trace element content into five groups (Condie, 1978). Only the High-Ca group (1.7-4.0wt% CaO), represented by the Priest pluton and Penasco pluton (Figure 3.31b) have highly fractionated REE pattern. As can be seen there is no longer a dominance of HREE depleted granites, reflecting perhaps the lack of suitable source rocks (*i.e.*, HREE-depleted Archean tonalites). The differences between Archean and Proterozoic granites are less pronounced on a Primordial Mantle normalised plot (Figure 3.32). The range of LILE and HFSE in Middle Mountain, Dome Peak and Mount Owen plutons brackets the range of both 1680 Ma orogenic granites (Puntiagudo Granite Porphyry, Rana Quartz Monzonite) and the 1450 Ma anorogenic granite (Penasco Quartz Monzonite). Apart from the HREE depleted character of many Late Archean granites their overall geochemistry is similar to the range of post-

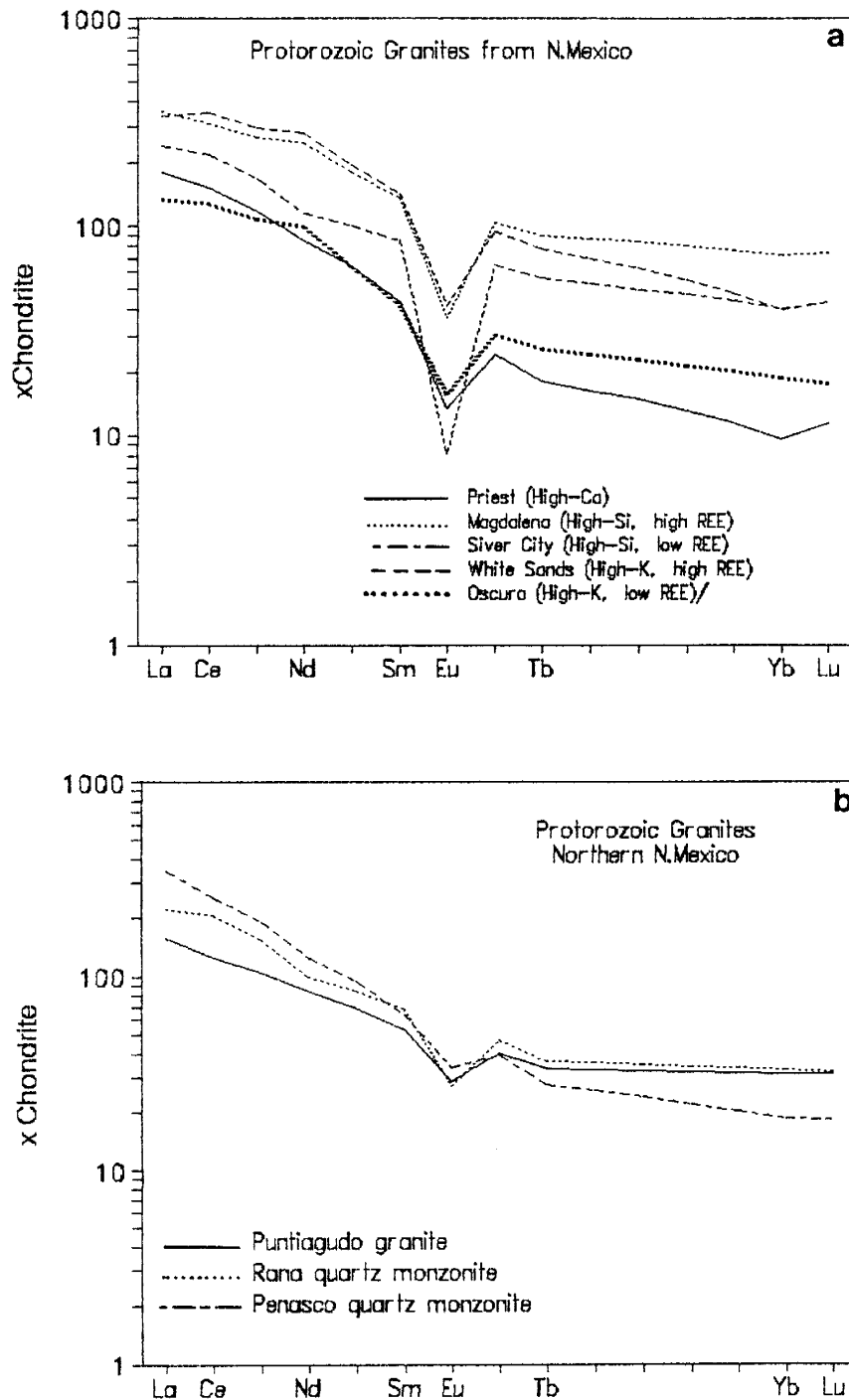


Figure 3.31: REE plots for Proterozoic granites.  
 a) Representative granites from the five subgroups exposed in New Mexico from Condie (1978). b) Three granites from the Picuris mountains, northern New Mexico.

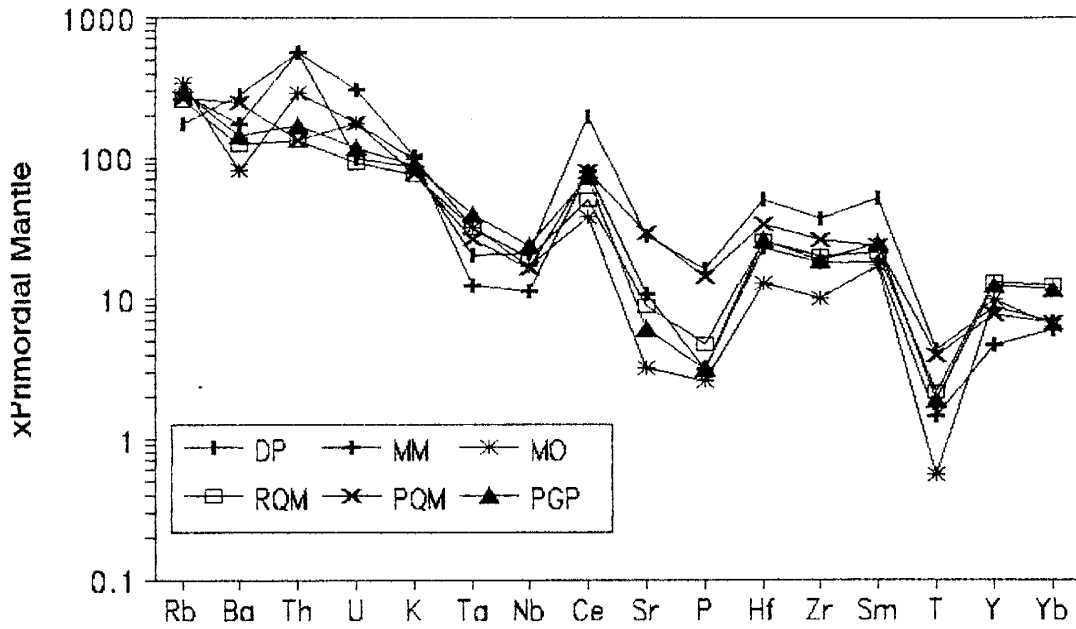


Figure 3.32: Proterozoic granites from Figure 3.31b plotted along with the late Archean granites of this study on a primitive mantle-normalized plot. DP=Dome Peak pluton, MM=Middle Mountain pluton, MO=Mount Owen pluton, RQM=Rana pluton, PQM=Penasco pluton and PGP=Puntiagudo pluton.

Archean K-rich granites.

### 3.7: **Conclusion**

The Middle Mountain pluton is a slightly peraluminous granite, depleted in the HREE, enriched in Th, Ba, Sr, moderately enriched in Zr, with a mixed I/S-type signature. It shows fair linear correlations between both major and trace elements and SiO<sub>2</sub> content indicating some degree of fractional crystallisation subsequent to magma genesis.

Dome Peak pluton is a metaluminous quartz monzonite, enriched in the REE with a relative depletion in the HREE, enriched in Th, Ba, Sr, Zr, with a mixed I/A-type signature. Like Middle Mountain pluton it shows moderate linear correlations on Harker diagrams indicating some degree of fractional crystallisation subsequent to magma genesis.

Mount Owen pluton is a peraluminous quartz monzonite, with moderate enrichment in the LREE and a flatter HREE pattern than either Middle Mountain or Dome Peak plutons. The pluton has an S-type composition and shows moderately linear correlations on Harker diagrams indicating some degree of fractional crystallisation subsequent to magma genesis.

On tectonic discriminant diagrams, all three plutons plot dominantly in the Volcanic Arc-Syn Collisional fields. However the central part of Mount Owen pluton has a collisional

signature, lying in fields II and III on a Rb-Hf-Ta plot, whilst closer to the margins the pluton has an volcanic arc signature, plotting in the VA field. Although the tectonic discriminant diagrams reflect the geochemical signature of the source environment (Pearce et al., 1984), they do not precisely constrain the environment in which these granites formed.

## Chapter 4

### Petrogenesis

#### 4.1: Introduction

The final chemical and isotopic composition of granitic magmas depends on a complex array of processes, which include source composition, pressure, temperature, volatile phase, magma underplating, and assimilation-fractionation cooling processes. The production of voluminous granitic batholiths requires substantial melting of crustal material at crustal depths (Clemens and Vielzeuf, 1987). Although the processes of granite genesis may be diverse, they tend to evolve towards a similar end member (Pitcher, 1987), which can often result in a non-unique petrogenetic model.

#### 4.2: Constraints on Petrogenetic Models

Numerous geochemical models were evaluated (partial melt, fractional crystallisation, assimilation and fractional crystallisation) to constrain the petrogenesis of Middle Mountain, Dome Peak and Mount Owen Plutons. Field observations and isotopic data combined with major and trace element data (Chapter 3) help to further constrain geochemical models.

##### 4.2.1: Field Evidence

Middle Mountain, Dome Peak and Mount Owen plutons are all relatively large (>100 km<sup>2</sup>) plutons lacking associated intermediate and mafic rocks, which one may expect to see if

fractional crystallisation from a more mafic parent was the preferred petrogenetic model.

In the southern Wind River Range, which is dominated by plutons of the Louis Lake and Bears Ear batholiths, the contacts between individual plutons are often diffuse (Pearson et al., 1971, this study), which raises the possibility that the Bears Ear batholith may in some places be a late stage fractional crystallisation product from the Louis Lake batholith. Although this may be possible, there is clear evidence around Atlantic Lake (S.E. Wind Rivers, Popo Agie Wilderness) that the Bears Ear batholith intrudes the Louis Lake batholith (Plate 2. ). It is also possible that the older Bridger and Louis Lake batholiths have partially melted to form the Bears Ear batholith. In the northern Wind River Range neither Middle Mountain or Dome Peak plutons (phases of the Bears Ear batholith) are associated with the Louis Lake batholith, both are intrusive into the the older gneiss terrane.

#### **4.2.2: Major and Trace Element Constraints**

From the Harker plots for both major and trace elements (Figures 3.4,5,6,10-12) it is clear that all three plutons have undergone varying degrees of fractional crystallisation subsequent to magma genesis. Although there is scatter in these plots, all three plutons show an overall decrease of Sr and Ba content and increase in Rb and K with increasing  $\text{SiO}_2$



content, indicating that both plagioclase and K-feldspar + biotite were crystallising phases. All three plutons show a range in REE content (Figures 3.14a-c) which is to be expected if fractional crystallisation occurred.

The HREE-depleted pattern of Middle Mountain and Dome Peak plutons is similar to the HREE-depleted pattern of Archean tonalites and trondhjemites suggesting these as possible source rocks, as partial melting of tonalite/trondhjemite does not fractionate the REE (plagioclase, K-feldspar and quartz do not fractionate the REE). However, accessory minerals (e.g. zircon, allanite, sphene) can exert a considerable control on the slope of the REE pattern (section 4.3.3.4, appendix G).

Mount Owen pluton has an S-type composition (Table 3.2), with a flatter HREE pattern than either Middle Mountain or Dome Peak plutons. On a Rb-Hf-Ta discriminant plot, samples from the central part of the pluton lie in the collisional field (Figure 3.21c). This suggests a metasedimentary composition as a viable source rock for the pluton (Harris et al., 1986)

#### **4.2.3: Isotopic Constraints**

There has been limited isotopic work in both the Wind River and Teton Ranges. Table 4.1 is a summary of all available isotopic data for the Wind River Range.

Table 4.1: Summary of isotopic data for the Wind River Range

SAMPLE	Rb	Sr	$^{87}\text{Rb}/^{86}\text{Sr}$	$^{87}\text{Sr}/^{86}\text{Sr}$	$^{17}\text{Sr}/^{86}\text{Sr}$	Sample
GPA10 <sup>1</sup>	166	144	3.37400	0.82410	0.69997	Middle Mountain
GPA12 <sup>1</sup>	157	100	4.63900	0.87250	0.70183	pluton
GPA5 <sup>1</sup>	233	109	6.32200	0.98040	0.74781	"
GPA6 <sup>1</sup>	114	520	0.63600	0.72680	0.70340	"
GPA11 <sup>1</sup>	172	69	7.42600	0.94850	0.67530	"
BW15 <sup>1</sup>	118	359	0.95170	0.73800	0.70299	Dome Peak pluton
FPS84-2 <sup>2</sup>	59	578	0.29430	0.71336	0.70207	Bridger batholith
FPS84-5 <sup>2</sup>	75	353	0.61690	0.72740	0.70364	"
FPS84-10 <sup>2</sup>	112	372	0.87380	0.73441	0.70090	"
BL83-22 <sup>2</sup>	135	1387	0.28170	0.71372	0.70292	"
BL83-24 <sup>2</sup>	49	1265	0.11110	0.70716	0.70290	"
BL83-25 <sup>2</sup>	106	300	1.02800	0.74412	0.70470	"

	Sm	Nd	$^{143}\text{Nd}/^{144}\text{Nd}$	$^{144}\text{Sm}/^{144}\text{Nd}$	$E_{\text{Nd}}$	
BL83-22 <sup>2</sup>	37	246	0.51084	0.09208	+0.62	Bridger batholith
BL83-24 <sup>2</sup>	20	117	0.51091	0.10372	-2.04	"
BL83-25 <sup>2</sup>	6	43	0.51069	0.08652	-0.44	"
BL83-21 <sup>2</sup>	4	14	0.51074	0.08358		"
RGW9-1 <sup>2</sup>	2	9	0.51099	0.10144		"
RGW9-2 <sup>2</sup>	3	15	0.51115	0.10109		"
4CF8 <sup>2</sup>	3	18	0.51076	0.10740	-6.28	Medina Mountain
4CF37 <sup>2</sup>	9	52	0.51109	0.10757	+0.29	Supracrustals
4CF53 <sup>2</sup>	7	35	0.51096	0.11615	-5.27	"

	U ppm	Th ppm	Pb ppm	$^{206}\text{Pb}/^{204}\text{Pb}$	$^{207}\text{Pb}/^{204}\text{Pb}$	$^{208}\text{Pb}/^{204}\text{Pb}$
GPA-1 <sup>1*</sup>	3	29	33	18.455	15.801	42.031
GPA-6 <sup>1*</sup>	3	19	30	17.356	15.612	39.198

References: 1. Stuckless et al., 1985; 2. Koesterer et al., 1987.  
 \* = Middle Mountain pluton

The work of Aleinikoff et. al (1989) has demonstrated the existence of 3.4Ga crust in the central Wind River Range. The heterogeneous Bridger batholith has variable initial Sr isotopic ratios from 0.701 to 0.704 and initial  $\epsilon_{Nd}$  values from +3.95 to -3.35 (Hulsebosch and Frost, 1989). Initial Sr isotope ratios of 0.701 and  $\epsilon_{Nd}$  values of +3.95 are close to the depleted mantle values at 2.7 Ga, the U-Pb zircon age of the Bridger batholith (Aleinikoff et al., 1989). The batholith is interpreted as derived from depleted mantle with up to 30% contamination from evolved older upper crust (Hulsebosch and Frost, 1989). Stuckless et al. (1985) carried out an extensive U-Pb-Th and Rb-Sr isotopic study of the Louis Lake and Bears Ear batholiths. All isotopic systems indicate an age of  $2630 \pm 20$  Ma for the Louis Lake batholith. The initial Sr isotopic ratio is  $0.7017 \pm 0.0005$ , which is within the range for model Archean mantle Sr isotope ratios proposed by Hart and Brooks (1977) and Peterman (1979b). The protolith for the Louis lake batholith could be of mantle or crustal affinity and of any age from earliest Archean to only slightly older than the batholith (Stuckless et al., 1985). Apparent ages for the Bears Ear batholith range from  $2504 \pm 40$  Ma to  $2575 \pm 50$  Ma. The initial Sr isotopic ratio of  $0.7038 \pm 0.0018$  is higher than Archean depleted mantle (DM) ratio at this time (0.7011) (Stuckless et al., 1985). These data rule out a depleted mantle as a possible source for the Bears Ear batholith.

It is clear from this study that the Bears Ear batholith is

made up of at least two petrographically and geochemically distinct plutons (e.g. Middle Mountain, Dome Peak) and may represent a prolonged period of plutonism. In the southern Wind River Range the individual plutons of the Bears Ear batholith have assimilated extensive blocks of country rock (e.g. around Deep Lake and Temple Lake). The Sr isotopic data allow the Bears Ear batholith to be derived from the older Louis Lake/ Bridger batholiths (Stuckless et al., 1985). However the average U-Pb-Th isotopic values for the Bears Ear batholith do not allow derivation from the Louis Lake batholith. Stuckless et al. (1985) point out that the scatter in ages may be explained by both a significant component of inherited zircons, and multiple intrusive and metasomatic events that occurred about  $2545 \pm 30$  Ma.

In conclusion, the isotopic data presented do not uniquely constrain the protoliths for either the Louis Lake or Bears Ear batholiths. The Bridger and Louis Lake batholiths are metaluminous tonalites to granodiorite in composition and appear to have a depleted mantle component ( $\epsilon_{Nd} +3.95$ ,  $^{87}Sr/^{86}Sr_1=0.701$ ) at the time of emplacement. The Bears Ear batholith is more evolved ( $^{87}Sr/^{86}Sr_1=0.7038$ ) and requires an older more evolved (crustal) source. The stable isotopic data support the above conclusion but again do not uniquely constrain the pluton protoliths. The  $\delta^{18}O$  values for Louis Lake Batholith range from 6.8 to 8.0 per mil (Stuckless et al., 1985; Cheang et al., 1986). These only slightly overlap oxygen

isotope values from the upper mantle which are restricted to the range of 5.5 to 7.0 per mil (Taylor, 1978). Longstaff and Schwarcz (1977) report oxygen isotope data for trondhjemite to tonalite gneisses from 6.1 to 7.8 per mil. The Louis Lake batholith is enriched in  $\delta^{18}\text{O}$  relative to a mantle source, but is similar to Archean mantle derived tonalite-trondhjemite suites. The  $\delta^{18}\text{O}$  values for the Bears Ear batholith are only slightly higher than the Louis Lake batholith (7.1 to 8.0 per mil), which is to be expected if the protolith was an older tonalite-trondhjemite.

Table 4.2 is a summary of all the available isotopic data for the Teton Range. The older gneisses into which the Mount Owen Pluton was emplaced yield a high-grade metamorphic age of 2.9 Ga, with an initial Sr isotopic ratio (0.701), within the same range as the mantle at 2.9 Ga. Reed and Zartman (1973) conclude that the original rocks were removed from the mantle only shortly before the episode of high-grade metamorphism. The extremely high initial Sr ratio of the Mount Owen Pluton ( $0.7320 \pm 0.009$ ) could not have been derived directly from a depleted mantle source at 2495 Ma, the age of the pluton. This coupled with the peraluminous nature of the granite rules out fractional crystallisation from a depleted mantle source at 2495 Ma. None of the older rocks have initial Sr ratios as high as Mount Owen pluton by 2.5 Ga, and hence it was not derived by partial melting of any of the exposed country rocks (Reed and Zartman, 1973). This is supported by field

observations. There is no evidence of partial melting of the wall rocks; rather Mount Owen pluton was emplaced into a brittle regime at shallow depths.

#### 4.3: Models

Partial melt and fractional crystallisation models were evaluated to determine the origin of Middle Mountain, Dome Peak and Mount Owen plutons. To quantitatively evaluate the genesis of these three plutons the following equations were used.

The behaviour of trace elements during batch (equilibrium) partial melting is given by (Schilling and Winchester, 1967; Hanson, 1978):

$$C_1 = C_0 / (F + D(1-F)) \quad (1)$$

where  $C_1$  is the concentration of the trace element in the melt,  $C_0$  is the initial concentration of the trace element in the source,  $D$  is the bulk distribution coefficient of the trace element in the residue at the time of melt removal, and  $F$  is the fraction of melt.

Trace element behaviour during fractional crystallisation of the parent melt ( $C_0$ ) relative to the differentiated melt ( $C_1$ ) is described by the Rayleigh fractionation law (Rayleigh, 1896) as applied by Neuman et al. (1954):

$$C_1 = C_0 (F^{D-1}) \quad (2)$$

where  $F$  is the fraction of melt remaining and  $D$  is the bulk distribution coefficient of the crystals being removed from

the melt.

The two models outlined above, batch melting and fractional crystallisation are relatively simple models which idealise the stages in generation and evolution of a magma. A model which addresses the extent to which magmas are modified during ascent and emplacement is the assimilation fractional crystallisation (AFC) model of De Paolo (1981), modified by Reagan et al. (1987) :

$$C_1 = C_0 F^{-z} + (x C_a + y C_i) * (1 - F^{-z}) / z \quad (3)$$

where  $C_1$  is the trace element concentration in the magma,  $C_0$  is the initial trace element concentration,  $C_a$  the trace element concentration in the assimilant and  $C_i$  the trace element concentration in the intrusive magma.

$$x = r_1 / (r_1 - r_2 + r_3 - 1)$$

$$y = r_3 / (r_1 - r_2 + r_3 - 1)$$

$$z = (r_1 + r_3 + D - 1) / (r_1 - r_2 + r_3 - 1)$$

$r_1$  = Assimilation Rate / Crystallisation Rate

$r_2$  = Extrusion Rate / Crystallisation Rate

$r_3$  = Intrusion Rate / Crystallisation Rate

$D$  = Bulk partition coefficient for the crystals being separated.

For the case considered in the generation of these plutons

$r_2 = r_3 = 0$  and equation (3) becomes

$$C^1 = C_0 F^{-D} + (x C_a (1 - F^{-D}))$$

The amount of material assimilated is a function of the temperature of the magma and intruded rocks, and the composition of the intruded rocks. Assimilation is greatest

when the intruded rocks are near their melting point, and they have a large proportion of a low melting fraction. Huppert and Sparks (1985) estimate that a komatiite, with an eruptive temperature of 1600°C, can assimilate up to 30% crustal material. It is unlikely that more evolved, cooler felsic magmas will assimilate more than this amount (Philpotts, 1990).

All models were tested using the spreadsheet modelling program MODULUS, developed by Knoper (1990).

#### **4.3.1: Controls on Models**

In determining the origin of any rock, it is important to understand the effect of the intensive parameters on the model. The following section and associated appendices evaluates the effect of the more important parameters on any one model.

##### **4.3.1.1: Partition Coefficients ( $K_d$ )**

Almost all geochemical petrogenetic models are based on the concept of an equilibrium partition coefficient ( $K_d$ ) between the mineral and melt. The partition coefficient is the ratio of the concentration of a trace element in the mineral to the concentration of the trace element in the melt. The  $K_d$  value can vary with pressure, temperature and composition of the phases (Allegre and Minster, 1978).

In Appendix D (Table D1), the average range of felsic  $K_d$



values for major minerals involved in granitic genesis are given. In Table D2 the range of  $K_D$  values for the REE in the major minerals is given. The effect of the range in  $K_D$  values on REE concentration in a melt for a given batch melt model is shown in figure D1. The higher  $K_D$  values result in a lower concentration of trace elements in the melt (Figure D1). The effect of composition of both melt and crystals might be the most important parameter for the quantitative use of partition coefficients (Allegre and Minster, 1978), i.e. the increase of  $D_{Sr}^{Plag/Liq}$  with Na content of plagioclase and with acidic aspect of the melt has been observed (Schnetzler and Philpotts, 1968; Noble and Hedge, 1970). The effect of oxygen fugacity on Eu partitioning and the  $Eu^{2+}/Eu^{3+}$  ratio is well documented (Weill and Drake, 1973). Under extreme reducing conditions,  $D_{Eu}(Plag)$  approaches the value of  $D_{Sr}(Plag)$  (Drake, 1975). The effect of varying the  $K_D$  for Eu in plagioclase is shown in Figure D2. The larger the  $K_D$  value the more pronounced the Eu anomaly and from the work of Drake and Weill (1975) the more reducing the conditions of magma genesis.

#### 4.3.1.2: Source and Melt Modes

Not only is the composition of the source of critical importance in the above models, but the proportion and composition of major minerals in both the source and melt for partial melt models and crystallising minerals for fractional crystallisation models an important constraint on the

composition of magma generated. This has been shown to be true for the genesis of HREE depleted Archean tonalites (Barker and Arth, 1976; Arth et al., 1978; Martin, 1987), where the presence or absence of garnet and /or amphibole in the source will control the concentration of HREE elements, as these two minerals preferentially concentrate the HREE (Hanson, 1978).

In the case of partial melt models, Hanson (1978) has shown that the K/Rb ratio of a granitic melt is dependent on whether K-feldspar or biotite is a residual phase. If K-feldspar is in the residue this would lead to a dramatic reduction of the K/Rb ratio in the melt as  $K_d$ 's for Rb are quite small. Biotite as a residual phase could lead to either a higher or lower K/Rb ratio depending on the stability of biotite (Hanson, 1978). In Appendix E the effect of varying the source mode is evaluated.

#### **4.3.1.3: Melt Fraction-F**

The melt fraction (degree of partial melt) is an important parameter in any petrogenetic model. Small degrees (<1%) of partial melt will be enriched in incompatible elements; however, the experimental work of van der Molen and Paterson (1979) indicates that not until 30-35% melting in a crustal environment is achieved will separation of melt from the source occur. Wickham (1987) showed from both field observations and theoretical calculations that low melt fractions are unlikely to be extracted to form large

(kilometer-size) bodies, because of limited separation efficiency. He determined the critical melt fraction (CMF) at which separation will occur as between 30-50% melt.

The experimental work (Arzi, 1978; van der Molen and Paterson, 1979) was performed on fine grained equigranular granitic rocks (0.5mm diameter) and the CMF value may be as low as 20% for partially melted rocks in a source region with a wide range in grain size (van der Molen and Paterson, 1979).

For this study melt fractions between 20-40% were considered reasonable values based on the above studies. Appendix F illustrates the effect on REE of changing F (degree of melt) for a partial melt model. As can be seen (Figure F1) the smaller the value of F the greater the overall REE content.

#### **4.3.1.4: Accessory Phases**

In the genesis of granites accessory phases such as zircon, apatite, allanite, sphene and monazite crystallise out and trace elements that in more mafic systems behave as incompatible elements become compatible and preferentially enter these accessory phases. Because these minerals preferentially concentrate REE and HFSE (high field strength elements, Ta, Nb, Zr, Y, Hf) they can exert a significant control on the slope of REE pattern (Hellman and Green, 1979; Miller and Mittlefehldt, 1982; Watson and Harrison, 1983; Sawka et al., 1984; Fujimaki, 1986; Rapp and Watson, 1986). For this

reason in modelling granites, it is also important to monitor the behaviour of the LILE elements (Ba, K, Rb, Sr) in the system even though these are relatively mobile elements and are not controlled by accessory phases (Hanson, 1978).

As zircon, apatite, sphene and allanite are all observed in thin section in both the older Bridger and Louis Lake batholiths and younger Bears Ear batholith and Mount Owen pluton, the effects of varying the modes in both source and melt has been evaluated in Appendix G. Monazite was also evaluated, even though it was not observed in thin section.

In partial melt models, a question that has to be addressed is whether these accessory phases contribute to the early stages of partial melting. If they do not, then the residue will be relatively enriched in REE and HFSE. The experimental work of Watson et al. (1989) has shown that accessory minerals tend to be situated at major phase grain boundaries and are involved in crustal melting. Accessory grains isolated from the melt inclusion within residual grains are common, but their generally small size results in only a minor contribution to the bulk rock budget. Susuki et al. (1990) show that some of the REE, particularly the LREE are concentrated at grain boundaries, and for small degrees of melting the REE pattern will be controlled by the pattern of that of the grain boundary phases.

On the basis of results in Appendix G coupled with petrographic observations, sources and melt modes for the

models were determined. Ultimately these are fine tuned to the model (Appendix H). It should be emphasized at this point that the  $K_d$  values for some accessory minerals are poorly known, especially for sphene, allanite and monazite.

#### 4.4.1: Results

##### Middle Mountain Pluton

As Middle Mountain and Dome Peak Plutons have similar REE distributions to Archean HREE-depleted tonalites/trondhjemites and isotopic and field evidence cannot unequivocally rule out the older Bridger and Louis Lake Batholiths as possible sources, their composition was first tested as a possible source. Parameters used in the models to generate Middle Mountain pluton are given in Appendix I.

Figure 4.1a and b show that the range of REE and HFSE for Middle Mountain pluton falls within the range generated by 40% partial melting of the maximum and minimum values of the Bridger and Louis Lake batholiths. Only  $TiO_2$  and  $P_2O_5$  content of Middle Mountain pluton lie below the values generated by partial melting the older tonalitic batholiths. This may be due to either the retention of a  $P_2O_5$  and  $TiO_2$ -rich phase (i.e. apatite, ilmenite, rutile) in the source, or the early crystallisation of these phases from the magma.

Harker diagrams of major elements (Figure 3.4) show that subsequent to the formation of the magma, fractional crystallisation has taken place. 40% partial melt of an

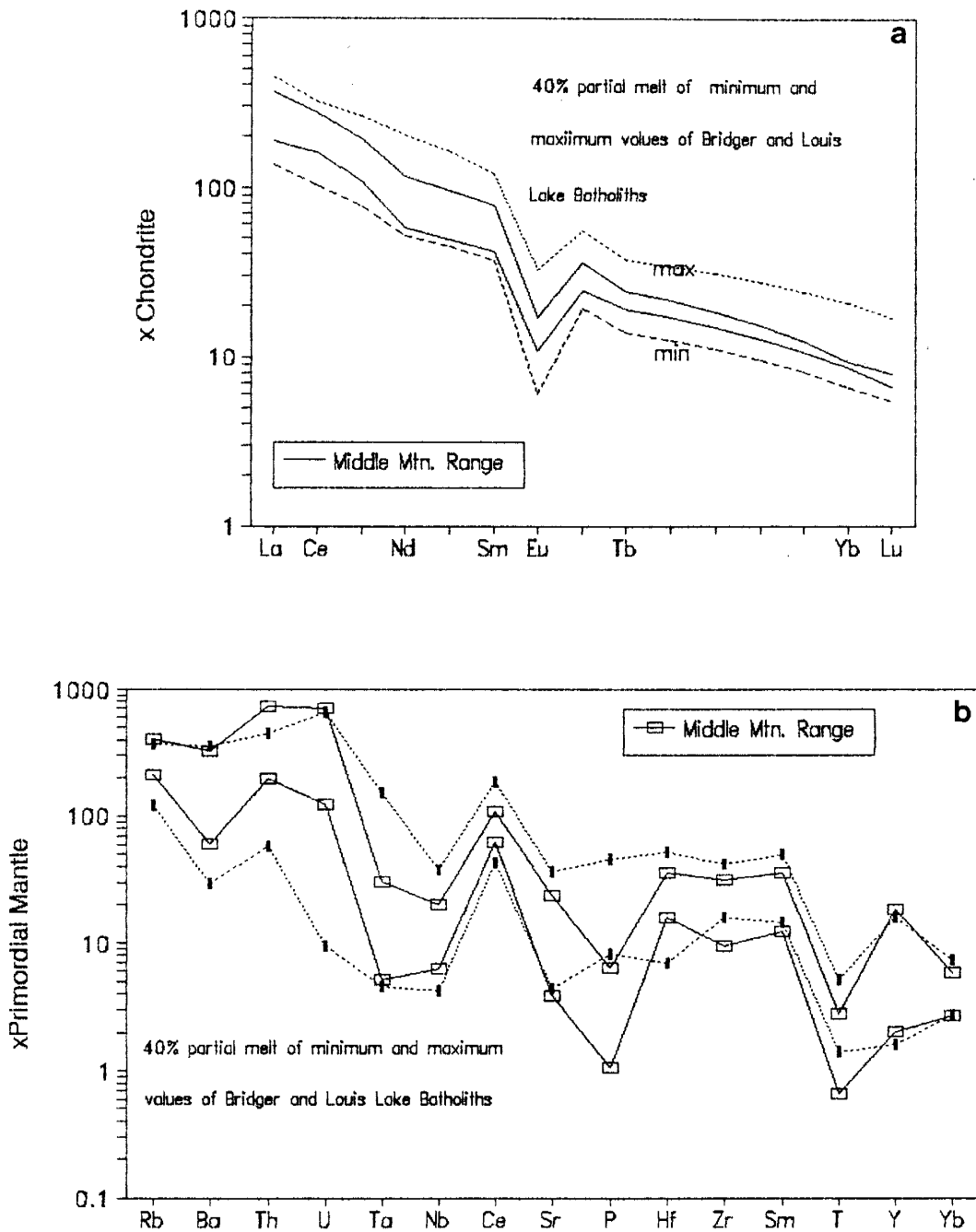


Figure 4.1: a) REE element and b) Primordial mantle-normalised plots for the range of melts produced by 40% batch melting of the minimum and maximum values of the Bridger/Louis Lake batholiths. Range of REE values for Middle Mountain pluton also plotted. Melting parameters given in Appendix I.

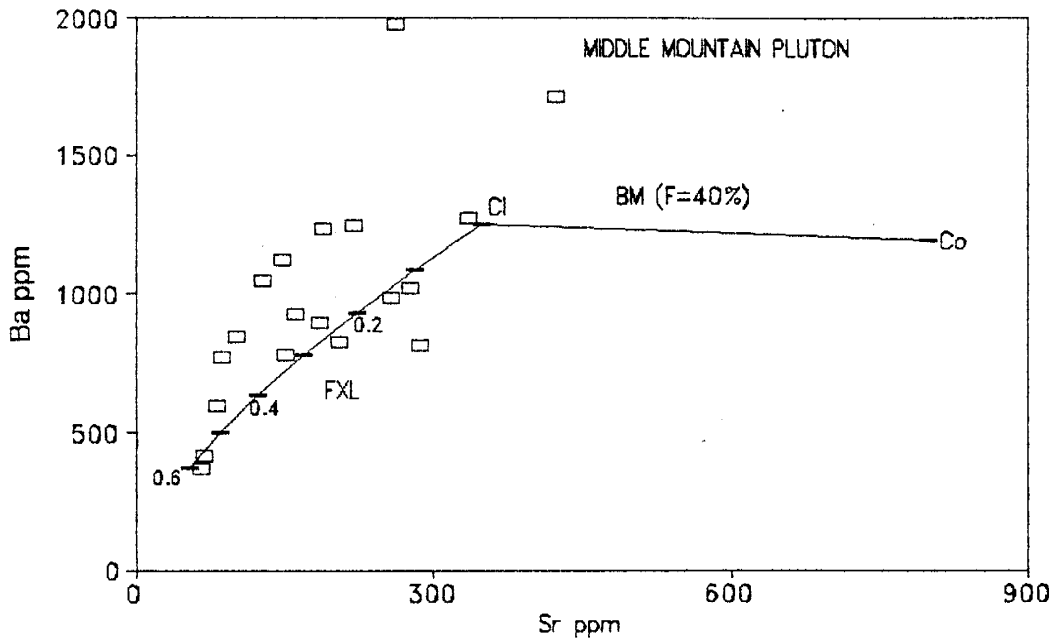


Figure 4.2: Ba versus Sr plot of the fractional crystallisation trend of a melt Cl produced by 40% batch melting (BM) of a tonalite source, Co (Bridger/Louis Lake batholith). Melting parameters given in Appendix I.

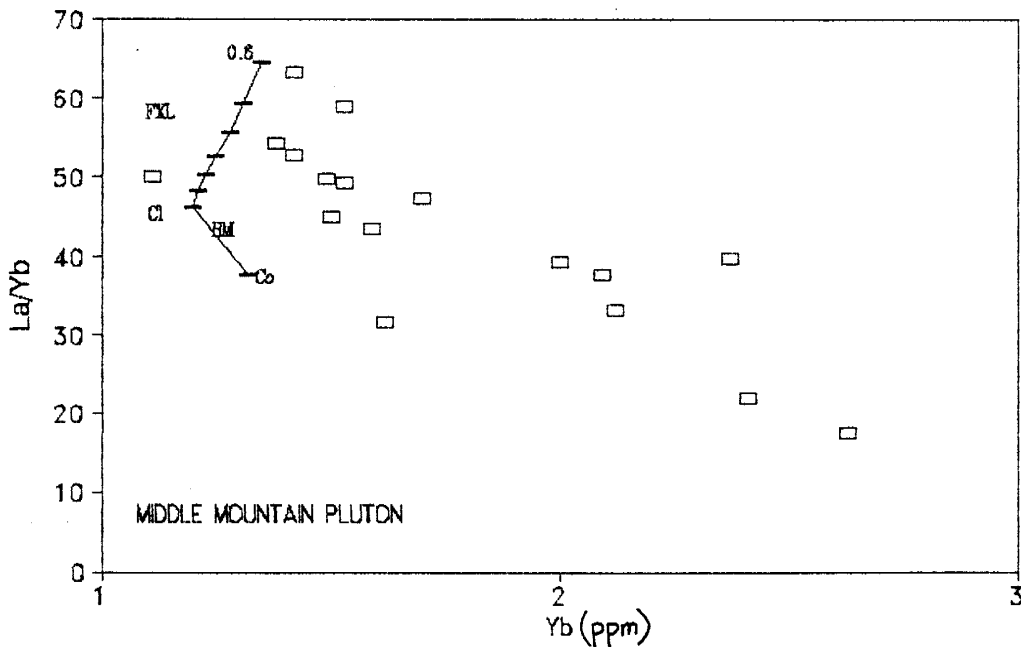


Figure 4.3: La/Yb versus Yb plot for a fractional crystallisation trend from a melt (Cl) produced by 40% batch melting (BM) of a tonalite source (Co-Bridger/Louis Lake batholiths). Melting parameters given in Appendix I.

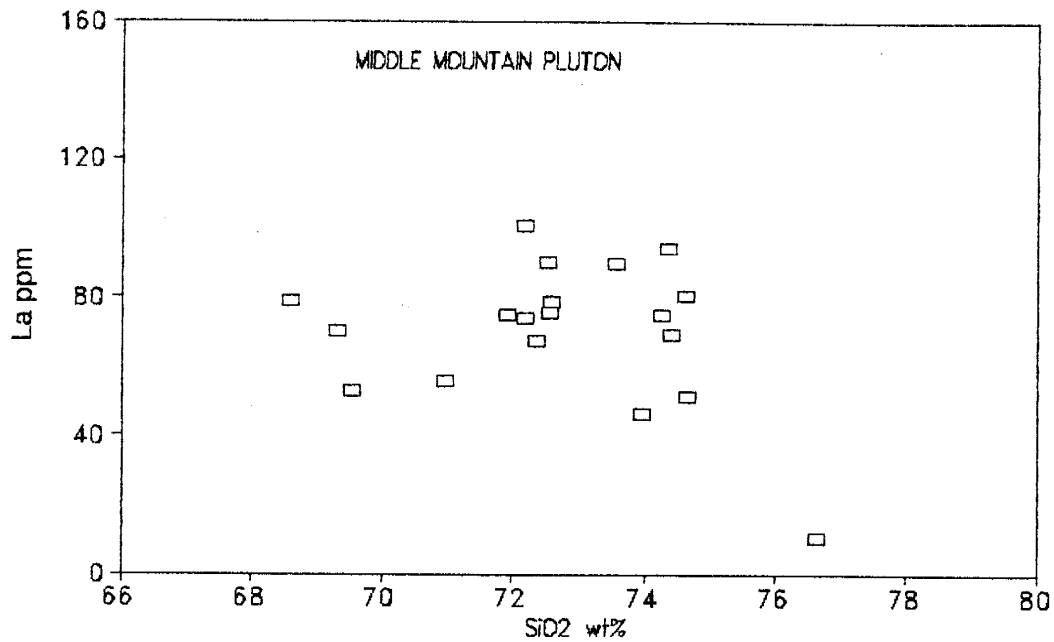


Figure 4.4a: Plot of La versus SiO<sub>2</sub> for Middle Mountain pluton

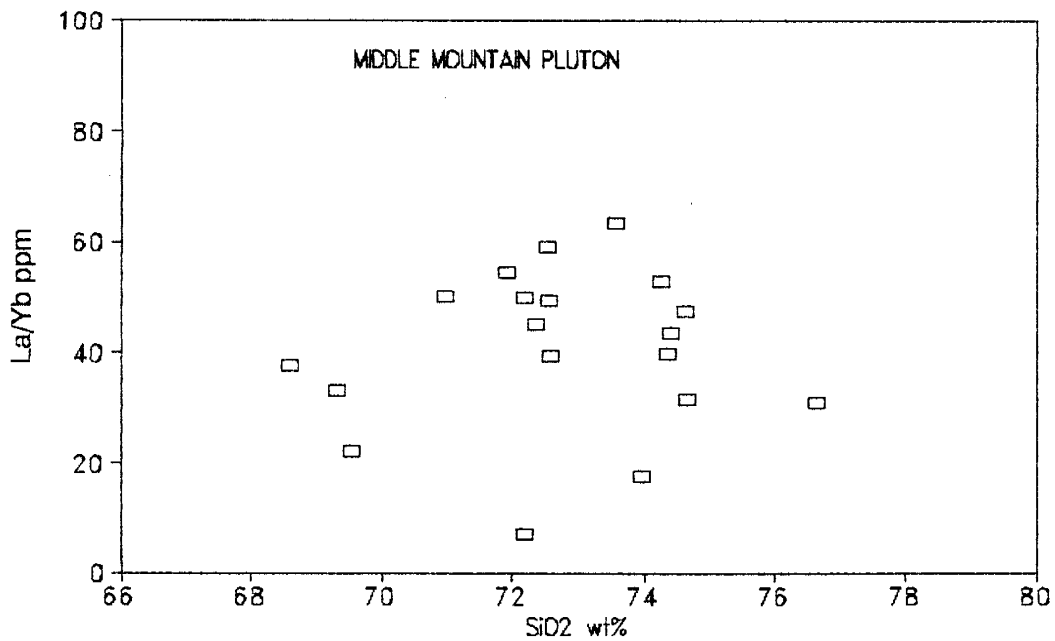


Figure 4.4b: Plot of La/Yb versus SiO<sub>2</sub> content for Middle Mountain pluton.



average value of the Bridger/Louis Lake batholiths will generate the lowest REE values of Middle Mountain pluton. Then, simple fractional crystallisation (Kspar, plag, quartz-Appendix I) can generate the range in LILE content (Figure 4.2). However partial melting followed by fractional crystallisation will not generate the range in REE values (Figure 4.3). On a Harker plot for La and La/Yb versus SiO<sub>2</sub> (Figure 4.4a and b), it can be seen that in fact the REE do not show any correlation with SiO<sub>2</sub> content.

The variable La/Yb values may reflect variable assimilation of supracrustal (metasediments and metavolcanics) and/or felsic orthogneisses with lower La/Yb ratios. The pluton intrudes mafic amphibolites, therefore a mafic assimilant was tested, where the assimilation rate/crystallisation ( $r^1$ ) was equal to 0.10. For a felsic melt to assimilate mafic material a maximum assimilation rate/crystallisation rate of 0.10 is considered a reasonable value (Philpotts, 1989) (Appendix I, Table I1). As can be seen Figure 4.5, the AFC model shows that the low La/Yb values can be explained by variable degrees of contamination, whereas the higher La/Yb values are more readily explained by simple partial melting followed by fractional crystallisation. Interestingly, the samples with the lower La/Yb values come from the margins of the pluton, where it intrudes a dominantly amphibolite gneiss terrane. These samples (BL-1, BL-4, BL-5) also have lower SiO<sub>2</sub> values (< 70%), higher Fe<sub>2</sub>O<sub>3</sub> values

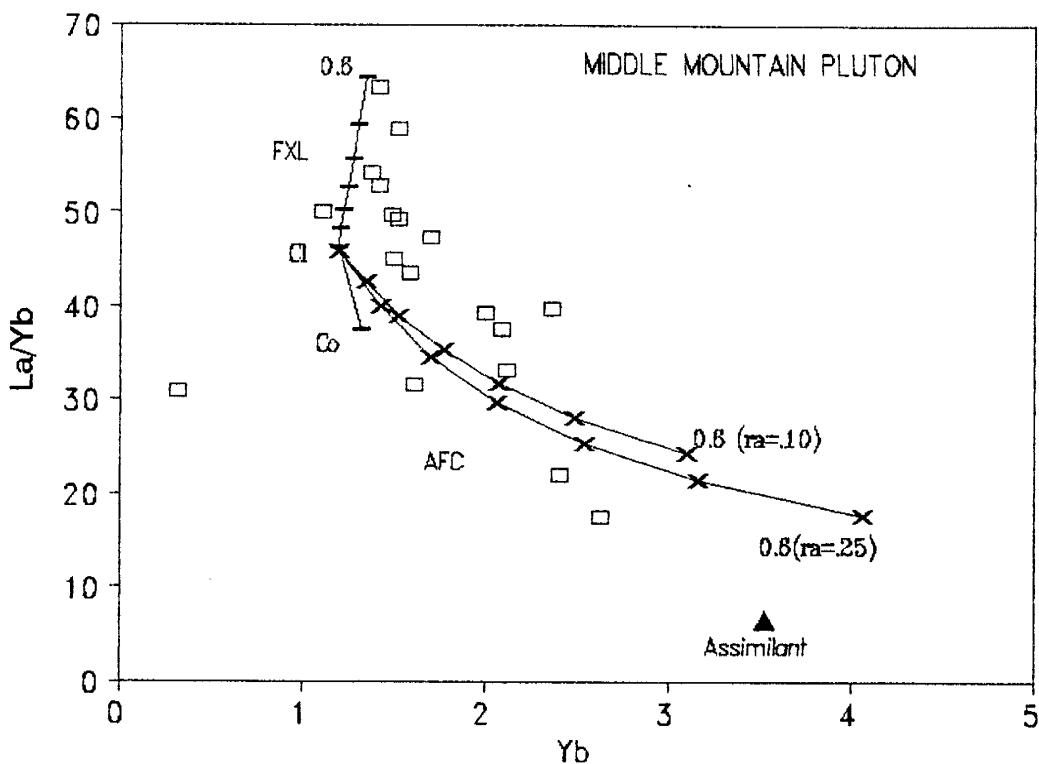


Figure 4.5: La/Yb versus Yb plot, where;  
 Co= Source (Tonalite-Bridger/Louis Lake batholiths)  
 Cl= 40% partial melt of Co.  
 + = Fractional crystallisation trend of Cl.  
 x = Assimilation fractional crystallisation trends of Cl.  
 ra= rate of assimilation/rate of crystallisation.  
 Tick marks at intervals of 10% Model parameters given in  
 Appendix I.

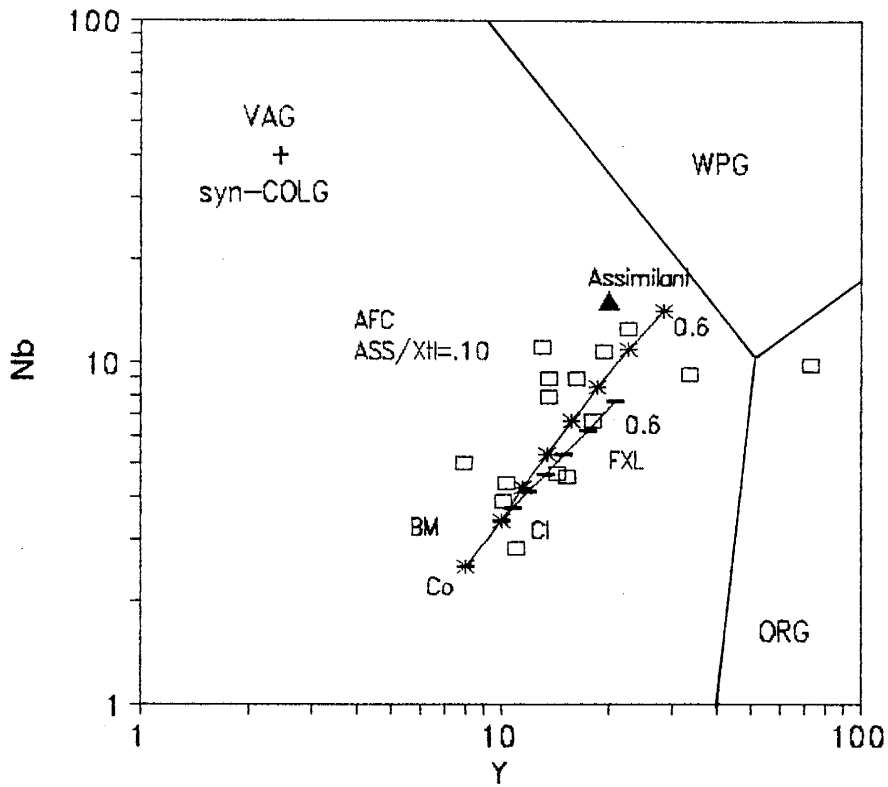


Figure 4.6: Nb versus Y tectonic discriminant plot from Pearce et al. (1984), where;

Co = Source (Tonalite-Bridger/Louis Lake batholiths).

Cl = 40% batch melt (BM) of Co.

+ = Fractional crystallisation (FXL) trend of Cl.

\* = Assimilation fractional crystallisation (AFC) trend.

VAG/syn-COLG=Volcanic arc and syn-Collisional granites;

WPG=Within-plate granites; ORG Ocean ridge granites.

Tick marks at 10% intervals. Model parameters given in Appendix I.

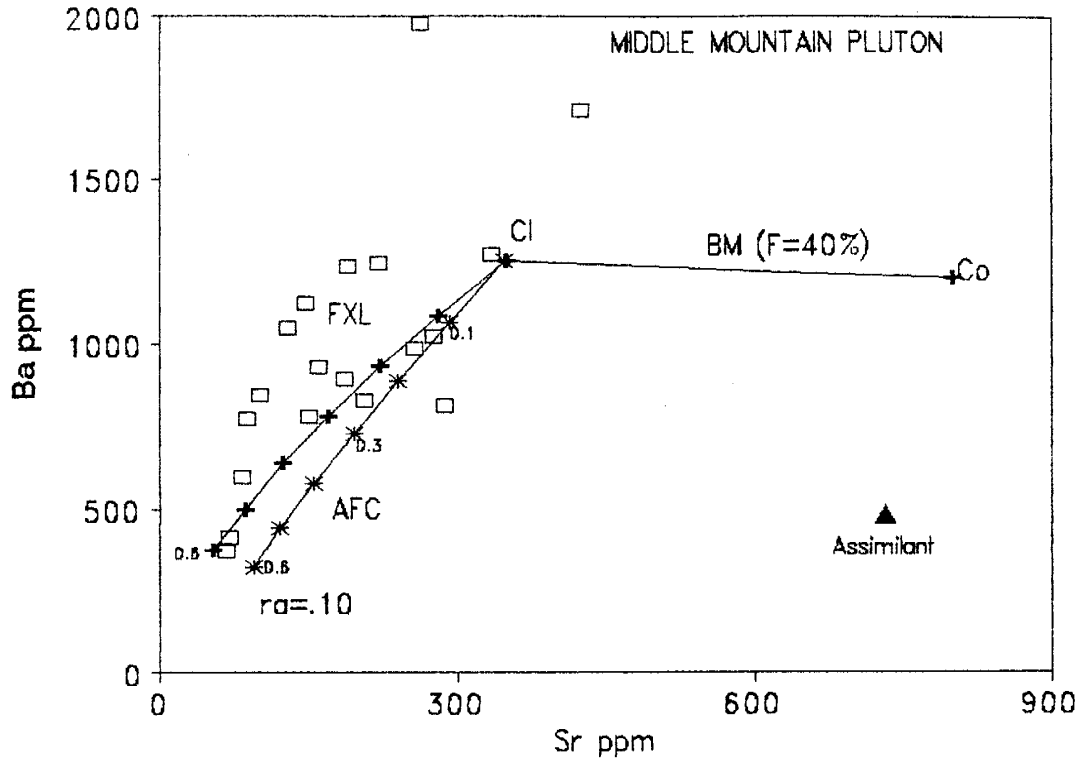


Figure 4.7: Plot of Ba versus Sr, where;  
 Co= Source (Tonalite-Bridger/Louis Lake batholiths)  
 Cl= 40% batch melt of source.  
 + = Fractional crystallisation trend of Cl (10% intervals).  
 \* = Assimilation fractional crystallisation trend (10% intervals).  
 ra= rate of assimilation/rate of crystallisation  
 Model parameters given in Apeendix I.

(>2.5wt%) and Zr content, >200ppm (avg=173). On a Nb versus Y tectonic discriminant plot (Figure 4.6) the spread in the data cannot be explained by simple fractional crystallisation, however additional assimilation and fractional crystallisation of amphibolite can generate the range of values. The AFC model has little effect on the LILE content (Figure 4.7).

### **Dome Peak Pluton**

The highest REE content of Dome Peak pluton cannot be generated by 40% partial melting of the older granitoids followed by fractional crystallisation. However 20% partial melting of the maximum and minimum values of the Bridger/Louis Lake batholiths will generate the lowest REE content observed for Dome Peak pluton (Figure 4.8a). The parameters used in the models to generate Dome Peak pluton are given in Appendix J.

Figure 4.8b shows the range of HFSE, LILE and REE for Dome Peak pluton lies within the range generated by 20% partial melting of the minimum and maximum values of the Bridger/Louis Lake batholiths. Partial melting (F=20%) of an average value of Bridger/Louis Lake batholiths will generate the lowest REE contents in Dome Peak pluton. A further 50% fractional crystallisation (K-feldspar, plagioclase, quartz) can produce the observed LILE concentration (Figure 4.9) and REE concentrations (Figure 4.10) unlike Middle Mountain pluton. Figure 4.11a and b, shows that for La and La/Yb versus SiO<sub>2</sub> plots there is fair linear correlation for Dome Peak, and an

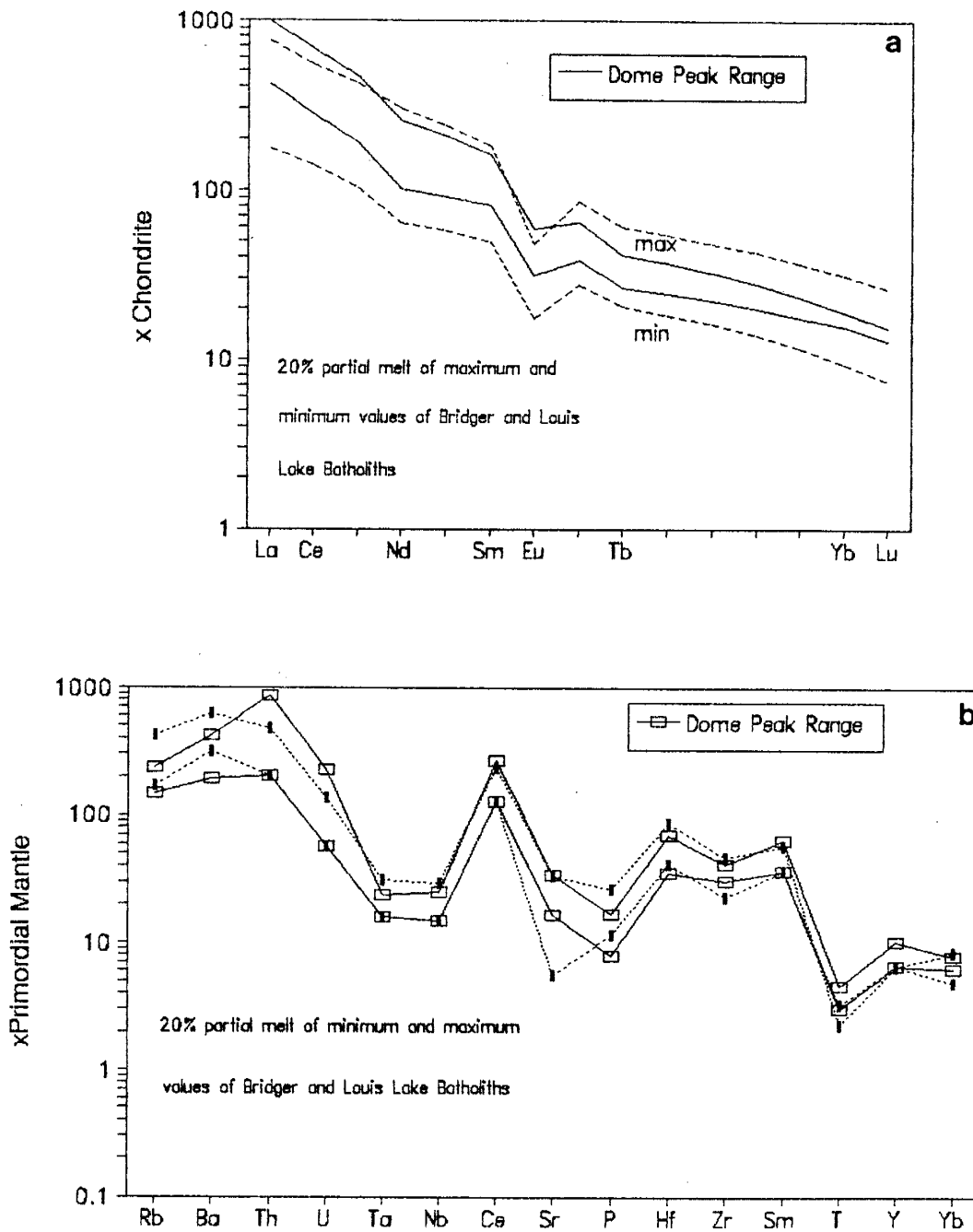


Figure 4.8: a) REE element and b) Primordial mantle-normalised plots for the range of melts produced by 20% batch melting of the minimum and maximum values of the Bridger/Louis lake batholiths. Range of REE values for Dome Peak pluton are also plotted.

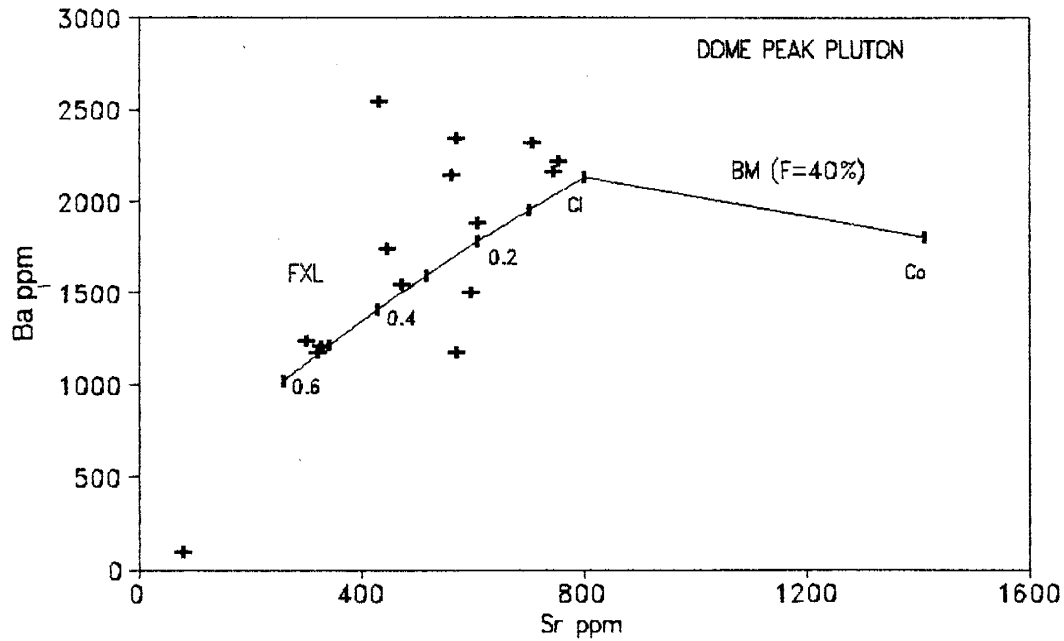


Figure 4.9: Ba versus Sr plot of the fractional crystallisation trend (FXL) of a melt (Cl), produced by 20% batch melting (BM) of a tonalite source (Co-Bridger/Louis Lake batholiths). Model parameters are given in Appendix J.

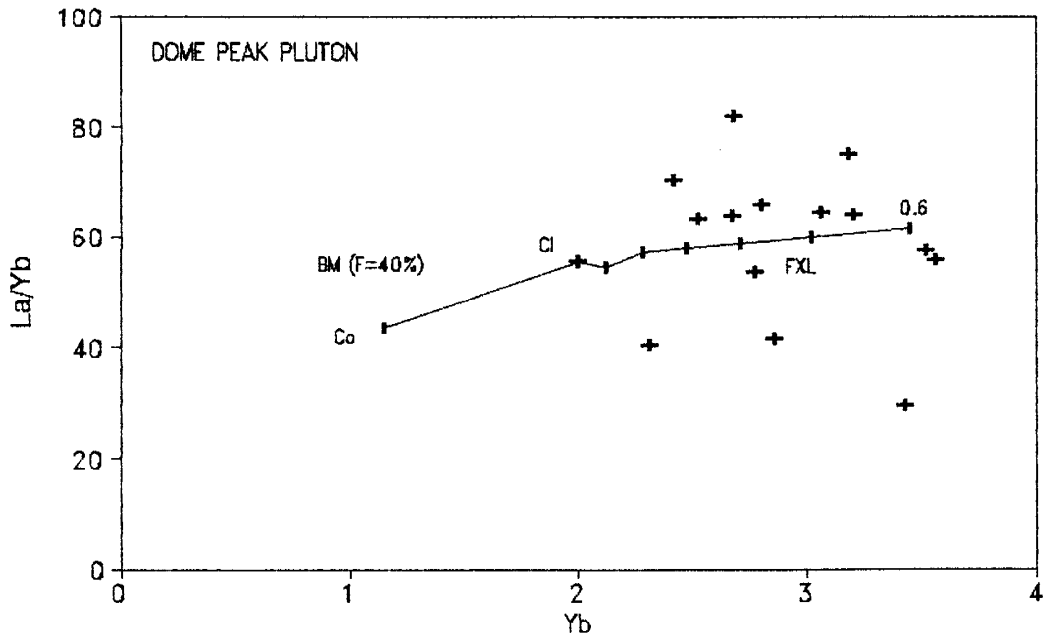


Figure 4.10: La/Yb versus Yb plot of a fractional crystallisation trend (FXL) from a melt (Cl) produced by 20% batch melting (BM) of a tonalite source (Co-Bridger/Louis Lake batholiths). Labelled samples refer to text. Model parameters in Appendix J.

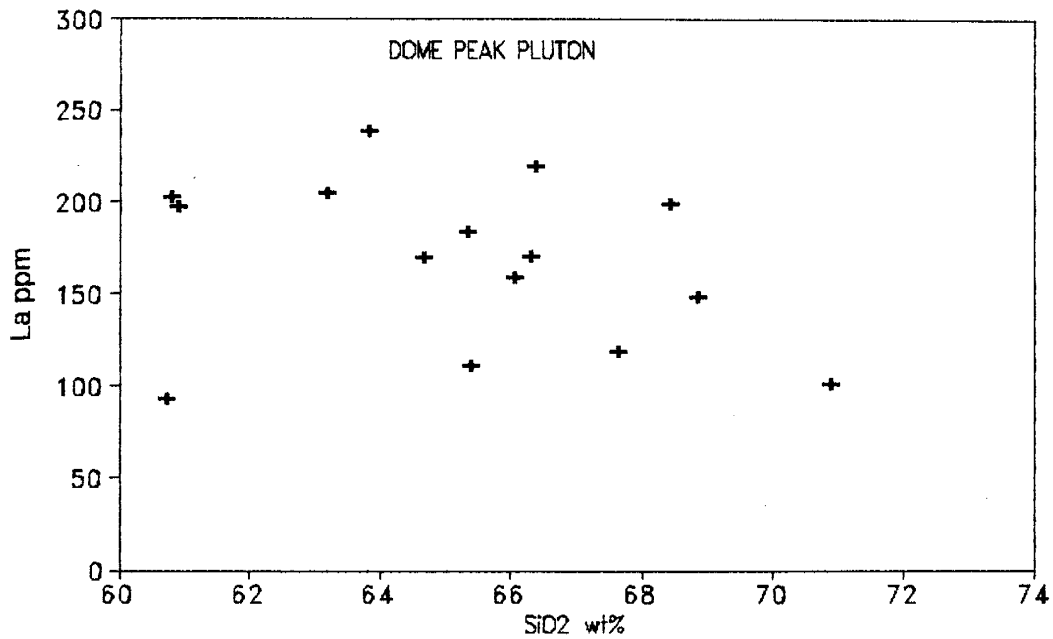


Figure 4.11a: Plot of La versus SiO<sub>2</sub> for Dome Peak pluton

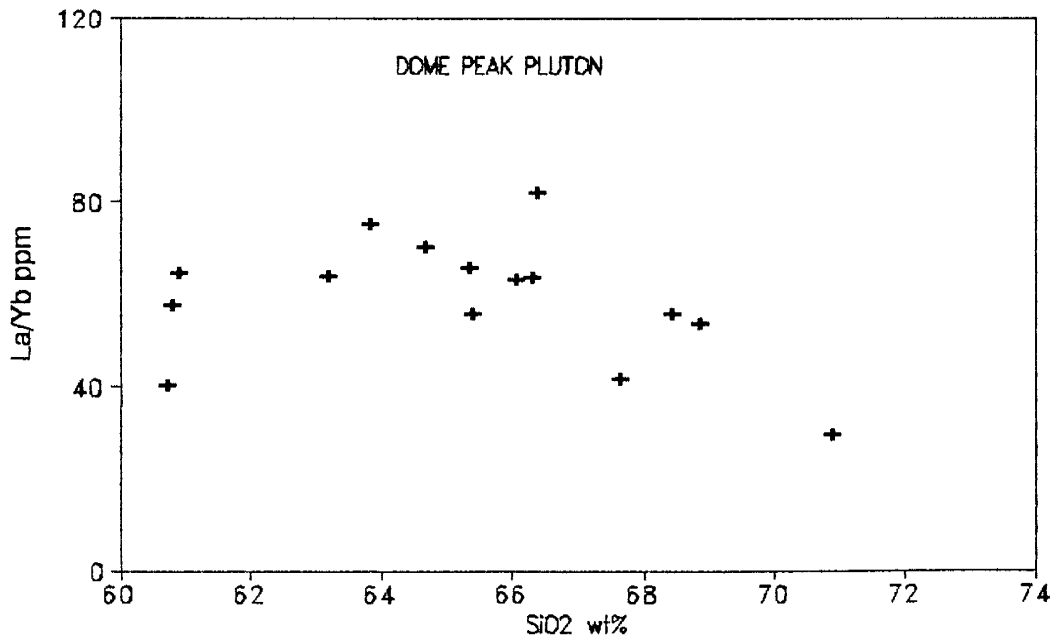


Figure 4.11b: Plot of La/Yb versus SiO<sub>2</sub> content for Dome Peak pluton.



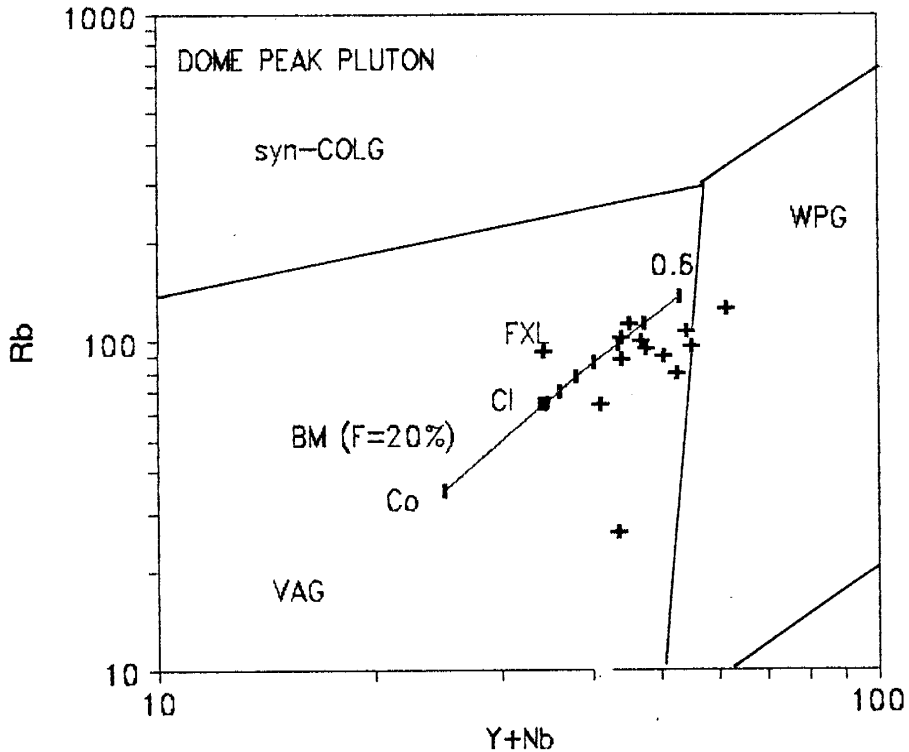


Figure 4.12: Rb-Y-Nb tectonic discriminant diagram from Pearce et al. (1984).

Co =Source (Tonalite-Bridger/Louis lake batholiths)

Cl = 20% batch melt (BM) of Co

=Fractional crystallisation (FXL) trend of Cl.

VAG=Volcanic arc granites, syn-COLG=syn-Collisional granites, WPG=Within plate granites and ORG=Ocean ridge granites.

Tick intervals at 10% Model parameters given in Appendix J.

AFC model is not needed to explain the major REE trend. Three samples fall below the fractional crystallisation trend (Figure 4.10). The lowest is an altered sample (NFL-5) where the feldspars have a milky white appearance, and the other two may represent contamination by greenstone material with a lower La/Yb value. On a Rb-Y-Nb plot, the trend can be explained by simple fractional crystallisation.

### Mount Owen Pluton

The 2-mica peraluminous Mount Owen Pluton with a flatter REE pattern than Middle Mountain and Dome Peak plutons, is classified as an S-type granite (Table 3.2), with the implication that its source was sedimentary rocks (Chappell and White, 1974). Miller (1985) has shown that weakly peraluminous granites can be derived from both igneous and sedimentary sources, and that most are derived from crustal sources with a pelitic component. A metasedimentary source seems likely for the Mount Owen pluton for the following reasons:

1. The samples that come from the center of the pluton all plot in the sedimentary source fields on a Rb-Hf-Ta plot (Figure 3.21).
2. These samples all have >1.25wt% normative corundum.
3. The high initial  $^{87}\text{Sr}/^{86}\text{Sr}$  isotopic ratio (0.7320-Table

Table 4.2: Summary of isotopic data from the Teton Range

Rock type	Rb	Sr	Rb/Sr	$^{87}\text{Sr}/^{86}\text{Sr}_*$
Biotite Gneiss	68	220	0.309	0.7049
Amphibolite Gneiss	12	98	0.122	0.7019
Rendezvous Metagabbro	23	185	0.124	0.7019
Webb Canyon Gneiss	69	87	0.793	0.7127
Mount Owen pluton	201	44	4.57	0.7320

All data from Reed and Zartman (1973).

\*= $^{87}\text{Sr}/^{86}\text{Sr}$  at 2.5Ga.

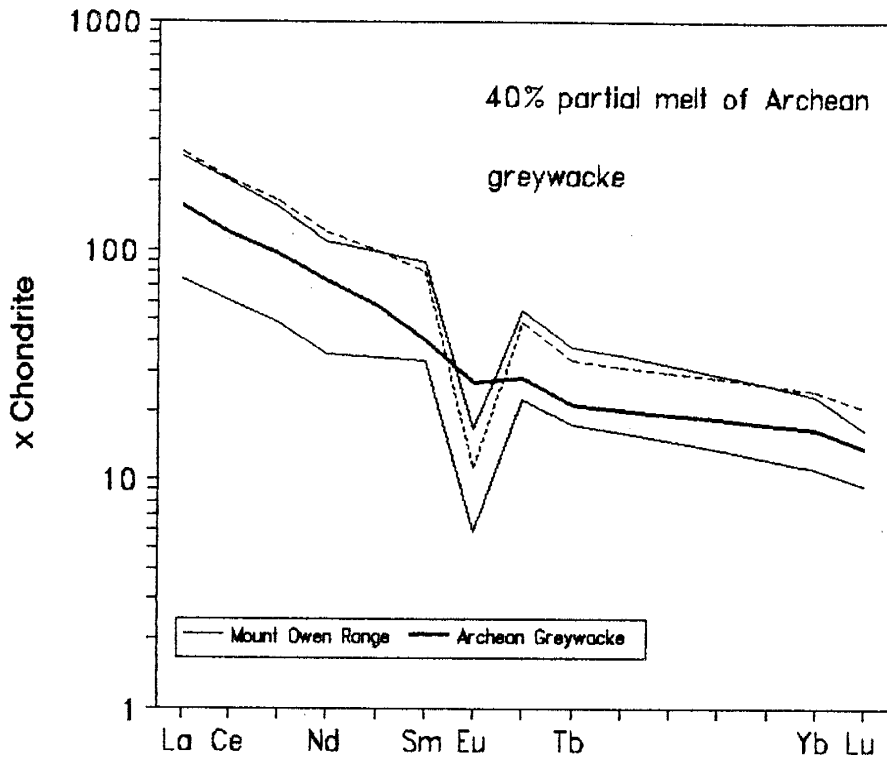


Figure 4.13: Plot of the REE element concentration produced by 40% batch melting of an Archean greywacke. The range of REE element content for Mount Owen pluton is also shown. Melting parameters are given in Appendix K.

4.2) is characteristic of S-type granites because the Rb/Sr ratio of pelites are much higher than those of average crustal rocks (0.5-1) (Miller, 1985).

4. The rocks in which Mount Owen pluton is emplaced had Sr isotopic ratios characteristic of a depleted mantle source at 2.5Ga (Table 4.2), suggesting that there was not an anomalous enriched mantle reservoir at depth in the lower crust.

The pluton was modelled by partial melting an Archean greywacke. The parameters used in the models to generate Mount Owen pluton are given in Appendix K. Figure 4.13 shows that the highest REE content observed in the pluton can be generated by 40% partial melting of an Archean greywacke. The range in REE content can be generated by subsequent fractional crystallisation (up to 50%) with monazite as a crystallising phase (Figure 4.13).

The range of LILE, however can not be accounted for even by 50% fractional crystallisation (Figure 4.14). Likewise on a plot of La/Yb versus Yb it can be seen that fractional crystallisation can not generate the observed REE distributions (Figure 4.15).

The samples that do not follow the fractional crystallisation trend all have lower Yb values, and variable La/Yb values suggesting contamination by a felsic orthogneiss with a low Yb relative to La/Yb content. An AFC model was

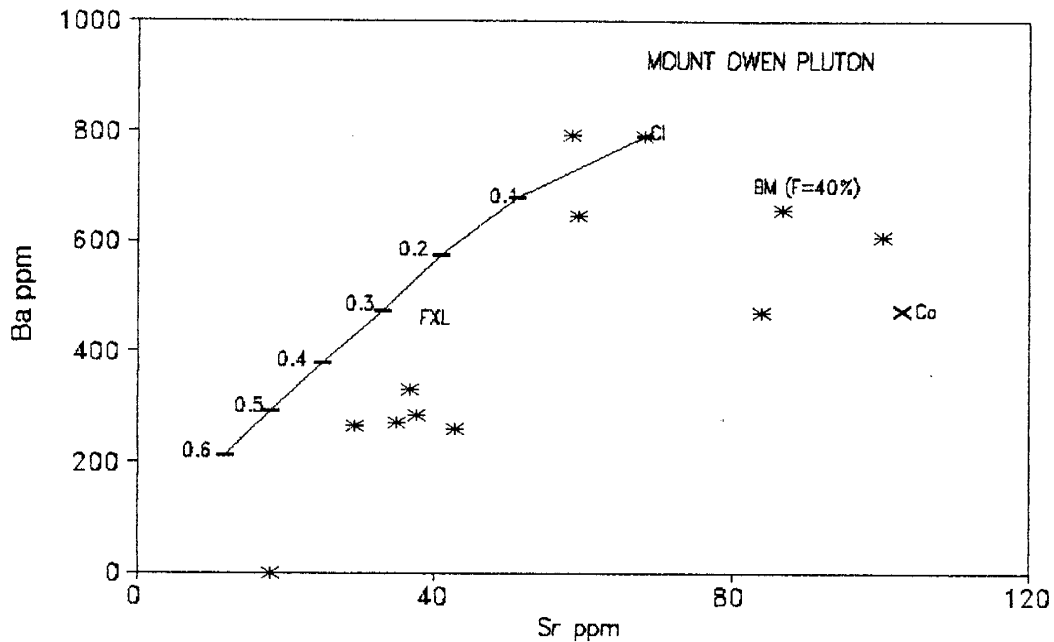


Figure 4.14: Fractional crystallisation trend of a melt (Cl) produced by 40% batch melting of an Archean greywacke (Co) on a Ba versus Sr diagram. Tick intervals at 10% Model parameters given in Appendix K.

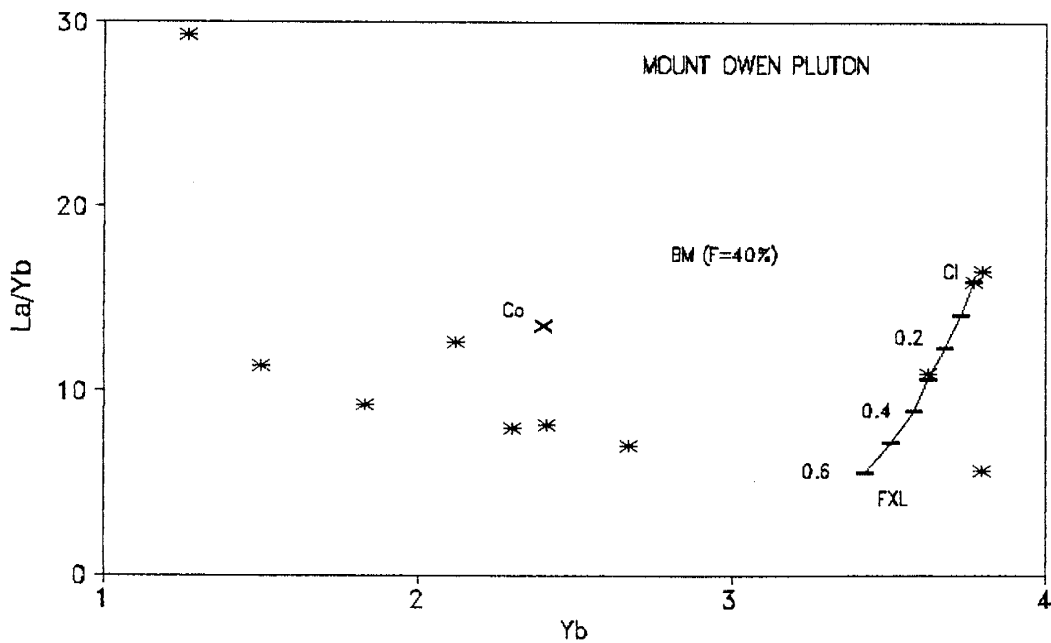


Figure 4.15: Plot to show the fractional crystallisation trend of a melt (Cl) produced by 40% batch melting of an Archean greywacke (Co) on a La/Yb versus Yb diagram. Tick intervals at 10% Model parameters given in Appendix K.

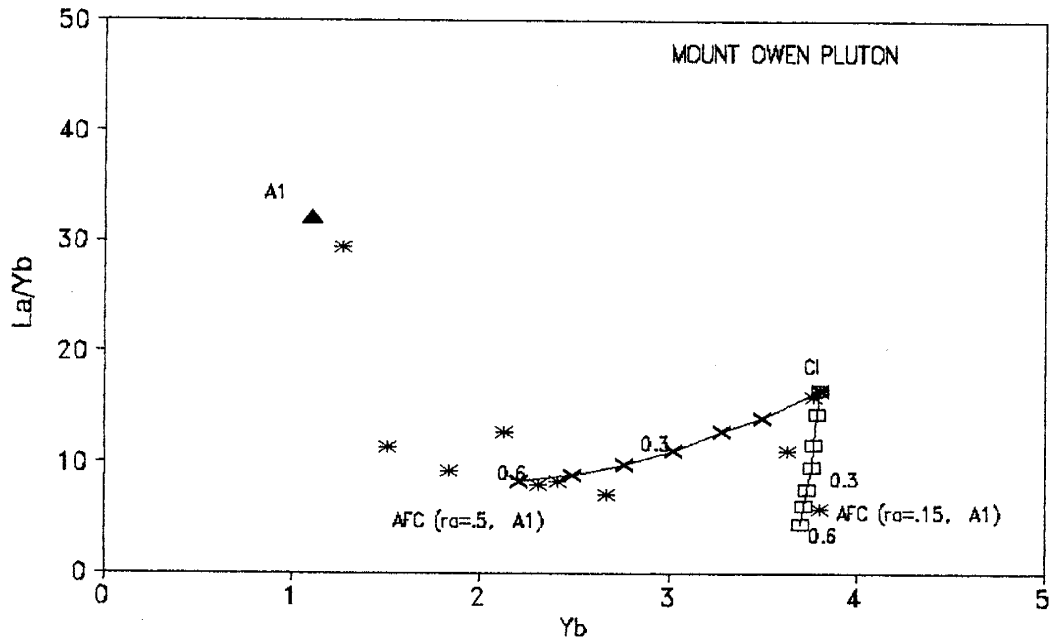


Figure 4.16a: Plot showing the AFC trend for a felsic orthogneiss assimilant A1 (Appendix K) and varying assimilation/crystallisation rates ( $r_a$ ) on a La/Yb versus Yb diagram. Model parameters given in Appendix K.

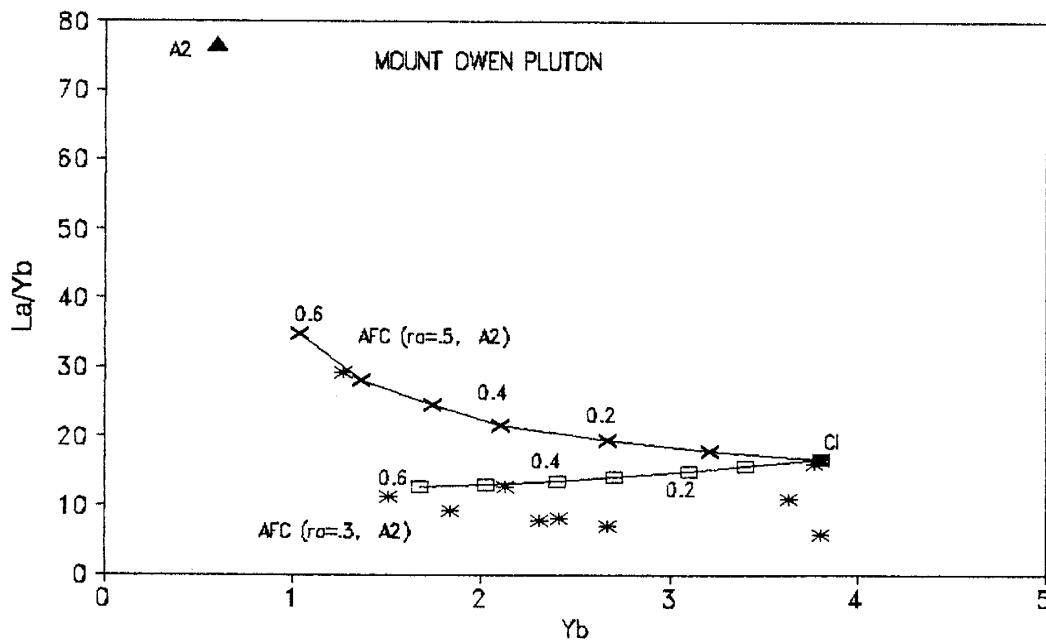


Figure 4.16b: Plot showing the AFC trend for a felsic orthogneiss assimilant A2 (Appendix K) with varying assimilation/crystallisation rates ( $r_a$ ) on a La/Yb versus Yb diagram. Model parameters given in Appendix K.

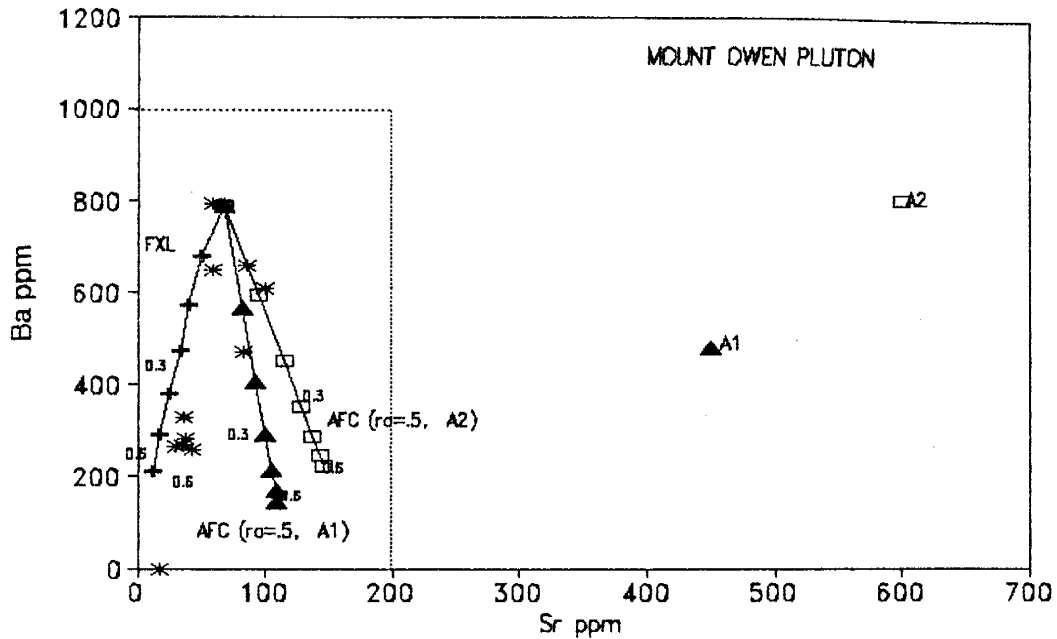


Figure 4.17a: Plot to show the AFC trends for the two different assimilants A1, A2 ( $r_a=0.5$ , assimilation rate/crystallisation rate) on a Ba versus Sr diagram. The FXL trend is also drawn. Model parameters given in Appendix K.

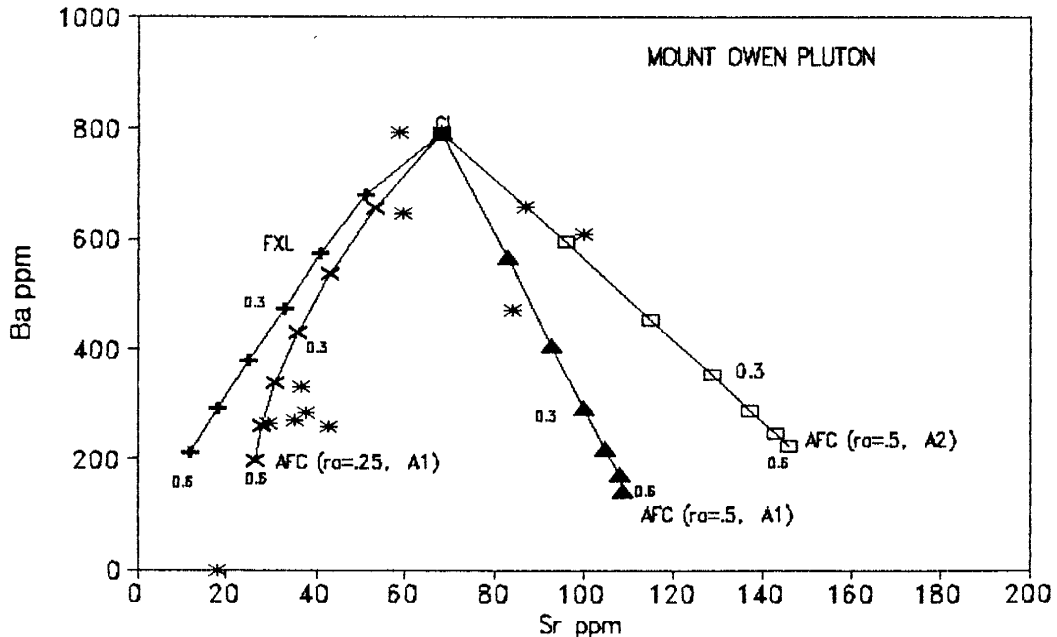


Figure 4.17b: Expanded box of 4.17a, also shown is the FXL trend.



tried where the contaminant is a felsic orthogneiss from the Wind River Range (Aleinikoff et al., 1989), with a La/Yb ratio of 32.2 and Yb content of 1.1 (A1-Appendix K). As can be seen from Figure 4.16a neither fractional crystallisation nor an AFC model with a rate of assimilation/rate of crystallisation of up to .50 can generate all the data points. This is considered a maximum assimilation/crystallisation rate, and a more reasonable value would be .25 (Philpotts, 1990). Another contaminant was tested (A2-Appendix K) with a La/Yb ratio of 76.4 and Yb content of .59, this corresponds to a composition of the older granitoids (Bridger and Louis lake batholiths) in the Wind River Range. The assimilants were chosen from the Wind River Range as there were no detailed geochemical analyses of felsic orthogneisses from the Teton Range.

One can generate the range of Mount Owen pluton with variable rates of assimilation versus crystallisation (Figure 4.16b). Figure 4.17a and b show the effects of the two AFC models (A1, A2) on the Ba and Sr contents of the pluton. As can be seen, the Mount Owen pluton data lie within the range of AFC and FXL model trends can generate the data range. On a Rb-Y-Nb plot most of the samples can be generated by variable degrees of AFC. However, three samples (labelled) fall below the AFC and FXL trends and Rb may have been lost from these samples (Figure 4.18).

In conclusion, Mount Owen pluton can be generated from a felsic (metasedimentary) source with variable degrees of AFC

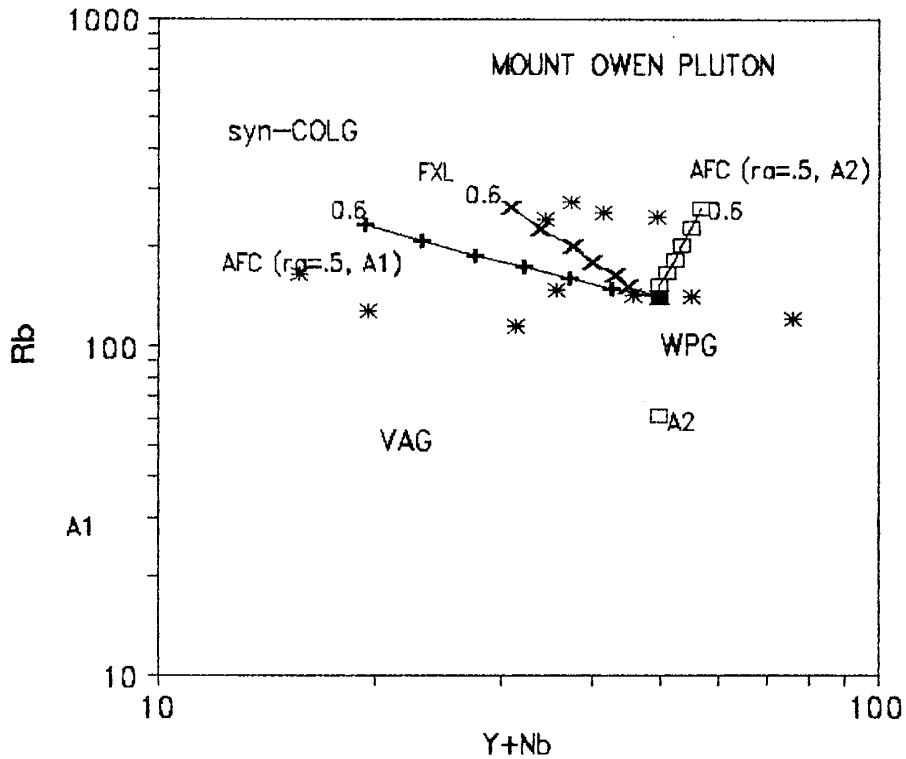


Figure 4.18: Plot of the AFC and FXL trends on a Rb-Y-Nb discriminant plot after Harris et al. (1986).

ra=assimilant rate/crystallisation rate

A1(+)=Contaminant 1 (Appendix K)

A2( )=Contaminant 2 (Appendix K)

VAG=Volcanic arc granites, syn-COLG=syn-Collisional granites, WPG=Within plate granites and ORG=Ocean ridge granites.

Tick intervals at 10% Model parameters given in Appendix K.

involving heterogeneous orthogneisses.

#### 4.5: Conclusion

Based on combined field observations (lack of intermediate-mafic associated rocks, size of plutons, cross-cutting intrusive relationships), isotopic data (i.e. relatively high initial  $^{87}\text{Sr}/^{86}\text{Sr}$  isotopic ratios for all three plutons) and geochemical modelling, the preferred petrogenetic models for the three plutons are as follows:

1) Middle Mountain Pluton: Partial melt ( $F=.4$ ) of an older HREE depleted tonalite/trondhjemite source (similar to the Bridger and Louis Lake batholiths) followed by assimilation or mixing with amphibolite (greenstone) and up to 50% fractional crystallisation.

2) Dome Peak Pluton: Partial melt ( $F=.2$ ) of an older HREE depleted tonalite/trondhjemite source (similar to the Bridger and Louis Lake batholiths) followed by up to 50% fractional crystallisation.

3) Mount Owen Pluton: Partial melt ( $F=.4$ ) of an Archean metasediment (probably greywacke) followed by variable degree of assimilation and up to 50% fractional crystallisation.

## CHAPTER 5

## DISCUSSION

In the absence of any associated supracrustal rocks, it is hard to uniquely determine the tectonic setting for the late Archean granites in western Wyoming. Possibilities include overthickening of continental crust in a collisional setting (continent-continent, continent-arc, or arc-arc) (England and Thompson, 1986), or in an extensional setting due to either relaxation of overthickened crust or large scale mantle upwelling (Anderson, 1983; White and Mckenzie, 1989).

In the Wind River Range, the older tonalite-granodiorite Louis Lake batholith is interpreted as intrusive into the South Pass greenstone belt (Bayley et al., 1973). Harper (1986) interpreted the greenstone belt as a dismembered ophiolite. The metadiabase and pillow lavas are similar to modern enriched mid-ocean ridge basalts (Harper, 1986), however there is no sheeted dike complex and associated gabbro cumulates characteristic of Proterozoic and Phanerozoic ophiolites.

In the Archean when the Earth's mantle was up to 200-300°C hotter (Richter, 1985), the environments of crust formation may have been different than those observed today and recorded in the Phanerozoic and Proterozoic record. The higher heat flow could have been dissipated by:

- 1) Faster spreading (Bickle, 1978);

- 2) Increased length of spreading ridges (Hargraves, 1986);
- 3) Thicker oceanic crust (Sleep and Windley, 1982); or
- 4) Increase in mantle plumes (Fyfe, 1978).

Each of these mechanisms of heat dissipation has a direct bearing on crustal processes. Faster spreading will result in the subduction of relatively hot and therefore buoyant crust which will subduct at shallower angles (Coney and Reynolds, 1977), with a reduction in volcanic activity (Abbott and Hoffman, 1984). Most of the igneous activity caused by subduction of young oceanic lithosphere is either siliceous plutonism or bimodal tholeiitic-rhyolite volcanism (Abbott and Hoffman, 1984). Increasing the length of ridges would result in many smaller plates and micro-continental collisions may have been more common in the Archean. Both (1) and (2) are inefficient mechanisms to dissipate heat (Wilks, 1988), although they may have operated locally. Wilks (1988) showed that with thicker oceanic crust, tonalites could be generated in oceanic-oceanic collisions and at the base of thickened oceanic crust. Increases in the number of plumes is similar to (3) above in that thickened oceanic crust is formed. The main difference is that the plumes will erupt through either continental or oceanic crust.

Today less than 5% of the Earth's surface is covered by plumes (e.g. Yellowstone, Hawaii, Iceland) (Fyfe, 1978). This could have been much higher in the Archean. In the Yilgarn Craton (Australia), the close temporal and spatial

relationship between the greenstone sequences and the granitoids indicates that all were formed in response to the same thermal event (Hill et al., 1990). There is a 20-30 Ma time gap between the initiation of basaltic volcanism and the onset of voluminous crustally derived magmatism. There is then a further time gap of about 20 Ma between the older granitoids and intrusion of younger K-rich granites. The entire thermal event spans about 100 Ma. All time scales can be related to the conduction of heat from a starting plume of anomalously hot mantle (Campbell and Hill, 1988). The presence of a hot plume is indicated by both the large volume of basaltic volcanism and the presence of komatiites within the basaltic sequence (Campbell et al., 1989).

Two plausible tectonic environments for the three late Archean granites studied are outlined below.

1) Plume environment

Upwelling of mantle asthenosphere through older (middle-late Archean) crust produced basaltic volcanism as seen in the South Pass Greenstone Belt. Heat from the plume melted the base of the thickened basaltic pile and/or the older crust to produce the Bridger and Louis Lake Batholiths. The generation of less dense felsic tonalites/granodiorites acted as a barrier to the more dense mafic magmas, which ponded at the base of the crust. Continued heat conduction into the lower-middle crust melted the recently formed tonalites and older

felsic crust to generate the Bears Ear Batholith and Mount Owen Pluton. Middle Mountain and Dome Peak Plutons represent the partial melt of an older tonalite source. Mount Owen Pluton represents the partial melt of a middle-lower crust dominated by metasediments. However to get metasediments to these depths requires crustal thickening and it is possible that during a thickening event (collision-overthrusting) melting could have occurred.

The isotopic dates in the Wind River Range do not adequately constrain this or any other model. However, the southern Wyoming Province is similar to the central Slave Craton in that it is dominated by late Archean granites.

Detailed field and isotopic data have revealed that the central Slave Craton is a late granite greenstone terrane consisting of an assemblage of metamorphosed volcanic, pluton and sedimentary rocks (2670-2650 Ma) intruded by syn-post tectonic granitoid rocks representing 65% of exposed crust in the area, emplaced within a short time interval (30 Ma) (Davis et al., 1990). These post-date the volcano-plutonic assemblage by 40-70 Ma. The granites evolve from early tonalites and quartz diorites through to late peraluminous granodiorites and granites.

The temporal and spatial relationship of the central Slave Craton can be explained by an upwelling mantle plume.

## 2) Subduction zone

Although the South Pass Greenstone Belt has an enriched mid-ocean or back-arc basin signature the contact with the younger Louis Lake batholith is highly tectonised and may in fact be a fault contact (Bayley et al., 1973; Harper, 1986). In this case the Bridger and Louis Lake batholiths are interpreted as subduction derived melts, with subduction taking place under a micro-continent (indicated by the presence of older Archean crust in the central Wind River Range). As subduction prograded, secondary partial melts are generated in the thickened accretionary wedges in the forearc producing dominantly peraluminous S-type granites (Mount Owen pluton) and in the overthickened magmatic pile producing dominantly I-type true granites (Middle Mountain and Dome Peak plutons).

### Discussion

At the end of the Archean all cratons experienced major anatexic melting. This worldwide magmatism is not a unique phenomena confined to the end of the Archean. In the middle Proterozoic (1800-1300 Ma) Laurentia was intruded by K-rich anorogenic granites, mafic dyke swarms and anorthosites (Anderson, 1983). The granite plutonism followed 200-300 Ma after a major period (1900-1700 Ma) of juvenile crustal accretion to the Archean cratons. Recent work in the Andes and Antarctica (Kay et al., 1989) has revealed a vast region of upper Paleozoic to Middle Jurassic (300-150 Ma) silicic



magmatic rocks that erupted in-board of the Gondwana margin. The magmas appear to be melts of crust that represent magmatic terranes accreted to the continental margin of Gondwana 200-300 My earlier.

The origin of both the Mid-Proterozoic and Paleozoic-Mesozoic felsic plutonism is uncertain but two overlapping models have been proposed.

1) Extension following a major period of crust formation.

When rapid convergence and terrane accretion ceases, a compressive stress system is replaced by an extensional one and extension related basalt causes melting in the lower crust (Anderson, 1983; Kay et al., 1989). However, the time lag between accretion and silicic volcanism indicates that heat must be added to the crust. The source for this heat may come from either of the following:

a) Cessation of subduction and resultant removal of slabs from beneath continental margins will lead to higher subcrustal temperatures as asthenospheric flow is renewed, as in the Tertiary of the Western U.S.A. (Kay et al., 1989).

b) During stationary periods for supercontinents heat is trapped in and beneath continents, leading to higher geothermal gradients.

2) Formation of supercontinents.

The amalgamation of all the continents to form one supercontinent will act as a thermal lid over the mantle resulting in the build up of heat beneath it (Anderson, 1982). Eventually the mantle becomes hot enough to melt its way through the continental lithosphere and produce extensive basaltic volcanism followed by felsic volcanism and plutonism as the base of the lower crust begins to melt (White and Mckenzie, 1989). Hoffman (1989) has argued that one large mantle plume was responsible for the Mid-Proterozoic anorogenic magmatism.

However, the mid-Proterozoic and Phanerozoic granite-ryholite magmatism differs from the Late Archean magmatism in that it follows at least 200 Ma after a major period of crustal accretion. The Late Archean felsic magmatism where isotopic are well constrained (Slave, Superior and Yilgarn Cratons) follows within 50 Ma of basaltic volcanism. The short time scale for magmatic events on individual cratons may be a function of the higher mantle temperatures in the Archean, but it also lends support to major deep mantle plume activity at the end of the Archean due to core-mantle cooling effects ( ).

The Late Archean event is further complicated by the scattered outcrops of Archean Cratons. By the mid-Proterozoic the geological record allows us to better reconstruct the position of continents and determine whether supercontinents

were in existence. It cannot be ruled out that a major Late Archean supercontinent was accreted at 2900-2700 Ma ago, and that the Late Archean granites which span from 2600-2500 Ma represent the collapse of this supercontinent by extension, mantle upwelling and lower crustal delamination.

## Chapter 6

### Conclusions

Middle Mountain, Dome Peak and Mount Owen plutons are all interpreted as crustally derived melts. They each have distinct geochemical signatures which reflect differences in their source and the conditions of melting and cooling histories. Middle Mountain and Dome Peak pluton both are depleted in the HREEs, whereas Mount Owen pluton has a much flatter HREE pattern.

Middle Mountain pluton has a mixed I/S-type composition and can be generated by partially melting ( $F=.4$ ) an older tonalite/trondhjemite source followed by variable degrees of assimilation of greenstone rocks along with up to 50% fractional crystallisation. Dome Peak pluton which is significantly enriched in the REEs has a mixed I/A-type composition and can be generated by partially melting ( $F=.2$ ) an older tonalite/trondhjemite with minimal degrees of assimilation of surrounding country rock and up to 50% fractional crystallisation. Mount Owen pluton has a S-type composition and can be generated by partially melting ( $F=.4$ ) an older metasedimentary source followed by variable degrees of assimilation of older greenstones and felsic gneisses along with up to 50% fractional crystallisation.

The major and trace element geochemistry cannot be used within the framework of Phanerozoic granitoid tectonic

discriminant diagrams to confidently determine their environment of genesis.

The worldwide Late Archean felsic plutonism may be due to the accretion of magmatic terranes to older Archean crust and the resultant formation of a supercontinent. With the cessation of compressive accretion, an extensional environment followed with localised asthenospheric upwelling causing anatectic melting in the lower crust. Additional heat may have been supplied by heat trapped in and beneath a supercontinent. Alternatively, the end of the Archean may represent a major period of mantle overturn with extensive upwelling of deep mantle plumes, perhaps a result of core-mantle cooling. These mantle plumes would, like localised asthenospheric upwelling cause anatectic melting in the lower crust. The plume model also can explain the presence of Late Archean komatiites, which require partial melts generated at depths in excess of 200km (Arndt, 1986). In all likelihood given the diversity of tectonic processes operating on the Earth today, it is probable that the Late Archean felsic plutonism represents both combined accretionary/collisional plate tectonics and plume tectonics.

## References

- Abbott, D.H. and Hoffman, S.E., 1984, Archean plate tectonics revisited: heat flow, spreading rate and the age of subducting oceanic lithosphere and their effects on the origin and evolution of continents. **Tectonics**, 3, 429-448.
- Aleinikoff, J.N., Williams, I.S., Compston, W., Stuckless, J.S. and Worl, R.G., 1989, Evidence for an Early Archean component in the Middle to Late Archean gneisses of the Wind River Range, west-central Wyoming: conventional and ion microprobe U-Pb data. **Contrib. Mineral. Petrol.**, 101, 198-206.
- Allegre, C.J. and Minster, J.F., 1978, Quantitative models of trace element behaviour in magmatic processes. **Earth Planet. Sci. Lett.**, 38, 1-25.
- Allen, P., Condie, K.C. and Bowling, G.P., 1986, Origins of the Southern Closepet Batholith. **Journal of Geology**, 94, 283-299.
- Anderson, D.L., 1983, Hotspots, polar wander, mesozoic convection, and the geoid. **Nature**, 97, 391-393.
- Anderson, C.I., 1986, Geology and Petrography of the ultramafics of Lake Victor, Horseshoe Lake Quadrangle, Bridger Wilderness, Wind river Mountains, Wyoming. **M.A. Thesis**, Idaho State University, 120 pp. (unpublished).
- Anderson, J.L., 1983, Proterozoic anorogenic granite plutonism of North America, in Medaris, L.G., Byers, C.W., Mickleson, D.M. and shanks, W.C., eds., **Proterozoic Geology**, Geol. Soc. Amer. Mem., 161, 133-154.
- Anderson, J.L. and Cullers, R.L., 1978, Geochemistry of the Wolf River batholith, a late Precambrian rapakivi massif in north Wisconsin, USA. **Contrib. Miner. Petrol.**, 74, 311-328.
- Arndt, N.T., 1986, Komatiites: a dirty window to the Archean mantle. **Terra Cognita**, 6, 59-66.
- Arth, J.G. and Hanson, G.N., 1975, Geochemistry and origin of the early Precambrian crust of northeastern Minnesota. **Geochim. Cosmochim. Acta**, 39, 325-362.
- Arth, J.G., Barker, F. and Stern, T.W., 1980, Geochronology of Archean gneisses in the Lake Helen area, southwestern Big

Horn Mountains, Wyoming. **Precamb. Res.**, 11, 11-22.

- Arth, J.G., Barker, F., Peterman, Z.E. and Friedman, I, 1978. Geochemistry of the Gabbro-Diorite-Tonalite-Trondhjemite Suite of southwest Finland and it's implication for the origin of Tonalitic and Trondhjemitic Magmas. **Journal of Petrology**, 19, 289-316.
- Arzi, A.A., 1978, Critical phenomena in the rheology of partially melted rocks. **Tectonophysics**, 44, 173-184.
- Barker, F., 1979, Trondhjemite: Definition, Environment and Hypotheses of Origin. in Barker, F., (ed) **Trondhjemites, dacites and related rocks**, Elsevier, 1-12.
- Barker, F. and Arth, J.G., 1976, Generation of trondhjemitic-tonalitic liquids and Archean bimodal trondhjemite-basalt series. **Geology**, 4, 596-600.
- Barker, F., Millard, H.T., Jr. and Lipman, P.W., 1979, Four low-K siliceous rocks of the western U.S.A. in Barker, F. (ed) **Trondhjemites, dacites and related rocks**, Elsevier, Amsterdam, 415-433.
- Barth, T.F.W., 1959, Principles of Classification and Norm Calculations of Metamorphic Rocks. **Journal of Geology**, 67, 135-152.
- Bayley, R.W., 1965a, Geologic map of the Miners delight quadrangle, Fremont County, Wyoming. **U.S. Geol. Surv. Geologic Quadrangle Map GQ-460**, scale 1:24,000.
- Bayley, R.W., 1965b, Geologic map of the Louis Lake quadrangle, Fremont County, Wyoming. **U.S. Geol. Surv. Geologic Quadrangle Map GQ-461**, scale 1:24,000.
- Bayley, R.W., 1965c, Geologic map of the South Pass quadrangle, Fremont County, Wyoming. **U.S. Geol. Surv. Geologic Quadrangle Map GQ-458**, scale 1:24,000.
- Bayley, R.W., 1965d, Geologic map of the Atlantic City quadrangle, Fremont County, Wyoming. **U.S. Geol. Surv. Quadrangle Map GQ-459**, scale 1:24,000.
- Bayley, R.W., Proctor, P.D. and Condie, K.C., 1973, Geology of the South Pass area, Fremont County, Wyoming. **U.S. Geol. Surv. Prof. Paper 793**, 39pp.
- Benedict, J.F., 1982, The Geology and Mineral Potential of the Schiestler Peak Area, Temple Peak Quadrangle, Wyoming. **M.A. Thesis**, University of Wyoming, 119 pp. (unpublished).

- Bickle, M.J., 1978, Heat loss from the Earth: A constraint on Archean tectonics from the relation between geothermal gradients and the rate of plate production. **Earth Sci. Planet. Lett.**, 40, 301-315.
- Bickle, M.J., 1982, In Arndt, N.T and Nisbet, E.G. (eds), **Komatiites**, Unwin, London, 479-494. Bickle, M.J., Bettenay, L.F., Chapman, H.C., Groves, D.I., McNaughton, N.J., Campbell, I.H. and de Laeter, J.R., 1989, The age and origin of younger granitic plutons of the Shaw Batholith in the Archean Pilbara Block, Western Australia, **Contrib. Mineral. Petrol.**, 101, 361-376.
- Bickle, M.J., Bettenay, L.F., Chapman, H.J., Groves, D.I., McNaughton, N.J., Campbell, I.H. and de Laeter, J.R., 1989, the age and origin of younger granitic plutons of the Shaw Batholith in the Archean Pilbara Block, Western Australia. **Contrib. Mineral. Petrol.**, 101, 361-376.
- Bickle, M.J., 1990, Archean magmatism. Abstr. in **Third International Archean Symposium**, Perth, 143-146.
- Bradley, F.H., 1873, Report of Frank H. Bradley, geologist of the Snake River Division, in Hayden, F.V., **6th Annual Report of the U.S. Geol. Surv. of the Territories**, 189-271.
- Brooks, C.K., Henderson, P. and Ronsbo, J.G., 1981, Rare-earth partition between allanite and glass in the obsidian of Sandy Braes, Northern Ireland. **Min. Mag.**, 44, 157-160.
- Brown, G.C., Thorpe, R.S. and Webb, P.C., 1984, The geochemical characteristics of granitoids in contrasting arcs and comments on magma sources. **J. Geol. Soc. London**, 141, 413-426.
- Campbell, I.H. and Hill, R.I., 1988, A two-stage model for the formation of the granite-greenstone terrains of the Kalgoorlie-Norseman area, Western Australia. **Earth Planet. Sci. Lett.**, 90, 11-25.
- Campbell, I.H., Griffiths, R. and Hill, R.I., 1989, Melting in an Archean mantle plume: heads its basalts, tails its komatiites. **Nature**, 339, 697-699.
- Chappell, B.W. and Hergt, J.W., 1989, The use of known Fe content as a flux monitor in neutron activation analysis. **Chem. Geology**, 78, 151-158.
- Chappell, B.W. and White, A.J.R., 1974, Two Contrasting Granite Types. **Pacific Geology**, 8, 173-174.



- Cheang, K.K., Wenner, D.B. and Stuckless, J.S., 1986, Oxygen isotopic constraints on the origin of the Precambrian granites from the southern Wind River Range and the Granite Mountains, Central Wyoming. **U.S. Geol. Surv. Bull.**, 1622, 109-129.
- Clemens, J.D. and Vielzeuf, D., 1987, Constraints on melting and magma production in the crust. **Earth Planet. Sci Lett.**, 86, 287-306.
- Collins, W.J., 1988, Genesis of Archean Granitoids in the Pilbara Block and implications for crustal growth. In **Workshop on the Growth of Continental Crust** (L.D.Ashwal, ed), LPI Tech Rpt. 88-02. Lunar and Planetary Institute, Houston, 49-50.
- Collins, W.J., Beams, S.D., White, A.J.R. and Chappell, B.W., 1982, Nature and origin of A-type granites with particular reference to southeastern Australia. **Contrib. Mineral. Petrol.**, 80, 189-200.
- Condie, K.C., 1978, Geochemistry of Proterozoic granitic plutons from New Mexico, U.S.A. **Chem. Geology**, 21, 131-149.
- Condie, K.C., 1981, **Archean greenstone belts**. Amsterdam, Elsevier.
- Coney, P.J. and Reynolds, S.J., 1977, Cordilleran Benioff zones. **Nature**, 270, 403-406.
- Cullers, R.L., Medaris, L.G. and Haskin, L.A., 1973, Experimental studies of the distribution of rare earths as trace elements among silicate minerals and liquids and water. **Geochim. Cosmochim. Acta**, 37, 1499-1512.
- Davies, W.J., King, J., Fryer, B.J. and van Breeman, O., 1990. Petrogenesis and evolution of late-Archean granitoids in the central Slave Province: Implications for the tectonic development of the Slave Province, Canada. Abstr. in **Third International Archean Symposium**, Perth, 185-188.
- DePaolo, D.J., 1981, Trace element and isotopic effects of combined wallrock assimilation and fractional crystallisation. **Earth Planet. Sci. Lett.**, 53, 189-202.
- Drake, M.J., 1975, The oxidation state of europium as an indicator of oxygen fugacity. **Geochim. Cosmochim. Acta**, 39, 55-64.
- Drake, M.J. and Weill, D.F., 1975, Partition of Sr, BA, Ca, Y,  $\text{Eu}^{2+}$ ,  $\text{Eu}^{3+}$ , and other REE between plagioclase feldspar and

- magmatic liquid: an experimental study. **Geochim. Cosmochim. Acta**, 39, 689-712.
- Dubendorfer, E.M. and Houston, R.S., 1986, Kinematic history of the Cheyenne belt: a Proterozoic suture in southeastern Wyoming. **Geology**, 14, 171-174.
- England, P.C. and Thompson, A., 1986, Some thermal and tectonic models for crustal melting in continental collision zones. in Coward, M.P. and Ries, A.C. eds., **Collision Tectonics**, Geol. Soc. Spec. Publ., 19, 83-94.
- Evenson, N.M., Hamilton, P.J. and O'Nions, R.K., 1978, Rare-earth abundances in chondritic meteorites. **Geochem. Cosmochim. Acta**, 42, 1199-1212.
- Fujimaki, H., 1986, Partition coefficients of Hf, Zr, and REE between zircon, apatite, and liquid. **Contrib. Mineral. Petrol.**, 94, 42-45.
- Eyfe, W.S., 1978, The evolution of the Earth's crust: modern plate tectonics to ancient hot spot tectonics. **Chem. Geol.**, 23, 89-114.
- Govindaraju, K., 1989, **Geostandards Newsletter**, 13.
- Gromet, L.P. and Silver, L.T., 1983, Rare earth element distributions among minerals in a granodiorite and their petrogenetic implications. **Geochim. Cosmochim. Acta**, 47, 925-939.
- Granger, H.C., McKay, E.J., Mattick, R.E., Patten, L.L. and McIlroy, P., 1971, Mineral resources of the Glacier Primitive Area, Wyoming. **U.S. Geol. Surv. Bull.** 1319-F, 113pp.
- Green, T.H., Sie, S.H., Ryan, C.G. and Cousens, D.R., 1989, Proton microprobe-determined partitioning of Nb, Ta, Zr, Sr and Y between garnet, clinopyroxene and basaltic magma at high pressure and temperature. **Chem. Geology**, 74, 201-216.
- Gurnis, M., 1988, Large-scale mantle convection and the aggregation and dispersal of supercontinents. **Nature**, 332, 695-699.
- Hanson, G.N., 1978, The application of trace elements to the petrogenesis of igneous rocks of granitic composition. **Earth Planet. Sci. Lett.**, 38, 26-43.
- Hargraves, R.B., 1986, Faster spreading or greater ridge length in the Archean. **Geology**, 14, 750-752.

- Harper, G.D., 1986, Dismembered Archean ophiolite in the southeastern Wind River Mountains, Wyoming-Remains of Archean oceanic crust. in de Wit, M.J. and Ashwal, L.D. (eds), **Workshop on Tectonic Evolution of Greenstone Belts**, LPI Tech. Rpt. 86-10, 108-110.
- Harris, N.B.W., Pearce, J.A. and Tindle, A.G., 1986, Geochemical characteristics of collision-zone magmatism. in Coward, M.P. and Ries, A.C. (eds), **Collision Tectonics**, Geol. Soc. Sp. Publ., 19, 67-81.
- Harrison, T.M. and Watson, E.B., 1984, The behaviour of apatite during crustal anatexis: Equilibrium and kinetic considerations. **Geochim. Cosmochim. Acta**, 48, 1467-1477.
- Hart, S.R. and Brooks, C., 1977, The geochemical evolution of the early Precambrian mantle. **Contrib. Min. Pet.**, 61, 109-128.
- Hellman, P.L. and Green, T.H., 1979, The role of sphene as an accessory phase in the high-pressure partial melting of hydrous mafic compositions. **Earth Planet. Sci. Lett.**, 42, 191-201.
- Henry, D.J., Mueller, P.A., Wooden, J.L, Warner, J.L. and Lee-Berman, R., 1982, Granulite grade supracrustal assemblages of the Quad Creek area, eastern Beartooth Mountains, Montana. **Montana Bureau of Mines and Geology Spec. Pub.**, 84, 147-156.
- Hill, R.I., Campbell, I.H. and Compston, W., 1990, Crustal growth, crustal reworking, and granite genesis in the southeastern Yilgarn Block, Western Australia. abstr. in **Third International Archaean Symposium, Perth**, 473-475.
- Hoffman, P.F., 1980, Wopmay Orogen: a Wilson cycle of early Proterozoic age in the northwest of the Canadian Shield, in D.W. Strangway, ed., **The Continental Crust and its Mineral Deposits**, Geol. Assoc. Can. Spec. Pap. 20, 5223-549.
- Hoffman, P.F., 1989, Speculations on Laurentia's first gigayear (2.0 to 1.0 Ga). **Geology**, 1989, 17, 135-138.
- Hofmann, A.W, 1988, Chemical differentiation of the Earth: the relationship between mantle, continental crust, and oceanic mantle. **Earth Planet. Sci. Lett.**, 90, 297-314.
- Hulsebosch, T.P. and Frost, C.D., 1989, Evidence for depleted mantle in late Archean rocks of the Wind River Mountains, Wyoming. **Abstr in Geol. Soc. Amer. Ann. Meeting**, 21.

- Huppert, H.E. and Sparks, R.S.J., 1985, Cooling and contamination of mafic and ultramafic magmas during ascent through continental crust. **Earth Planet. Sci. Lett.**, 74, 371-386.
- Hurich, C.A and Smithson, S.B., 1982, Gravity interpretations of the southern Wind River mountains, Wyoming. **Geophysics**, 47, 1550-1561.
- Jensen, B.B., 1973, Patterns of trace element partitioning. **Geochim. Cosmochim. Acta**, 37, 2227-2242.
- Karlstrom, K.E. and Houston, R.S., 1984, The Cheyenne Belt: analysis of a Proterozoic suture in southern Wyoming. **Precamb. Res.**, 25, 415-446.
- Kay, S.M., Ramos, V.A., Mpodozis, C. and Sruoga, P., 1989, Late Paleozoic to Jurassic silicic magmatism at the Gondwana margin: Analogy to the Middle Proterozoic in North America? **Geology**, 17, 324-328.
- Knoper, M.W., 2000,
- Koesterer, M.E., 1986, Archean history in the Medina Mountain area, Wind River Range, Wyoming. **M.A. Thesis**, University of Wyoming, 99 pp. (unpublished).
- Koesterer, M.E., Frost, C.D., Frost, B.R., Hulsebosch, T.P., Bridgewater, D. and Worl, R.G., 1987, Development of the Archean Crust in the Medina Mountain Area, Wind River Range, Wyoming (U.S.A.). **Precambrian Res.**, 37, 287-304.
- Kusky, T.M., 1989, Accretion of the Archean Slave Province. **Geology**, 17, 63-67.
- Leeman, W.P. and Phelps, D.W., 1981, Partitioning of rare earths and other trace elements between sanidine and coexisting volcanic glass. **J. Geophys. Res.**, 86, 10193-10199.
- Lindstrom, D.J. and Korotev, R.L., 1982, TEABAGS: Computer programs for instrumental neutron activation analysis. **J. Radioanal. Chem.**, 70, 439-458.
- Link, P.K., Anderson, C.I., Hengesh, J.V. and Worl, R.G., 1985, Geologic map of the Horseshoe Lake quadrangle, Sublette County, Wyoming. **U.S. Geol. Surv. Open-File Report 85-0449**.
- Long, P.E., 1978, Experimental determination of partition coefficients for Rb, Sr, and Ba between alkali feldspar and silicate liquid. **Geochim. Cosmochim. Acta**, 42, 833-

846.

- Longstaff, F.J. and Schwarcz, H.P., 1977,  $^{18}\text{O}/^{16}\text{O}$  of Archean clastic metasedimentary rocks: a petrogenetic indicator for Archean gneisses. **Geochem. Cosmochim. Acta**, 41, 1303-1312.
- Love, J.D. and Reed, J.C., 1968, Creation of the Teton landscape-The geologic story of the Grand Teton National park: Moose, Wyoming, **Grand Teton Nat. History Assoc.**, 120p.
- Mahood, G. and Hildreth, W., 1983, Large partition coefficients for trace elements in high silica rhyolites. **Geochim. Cosmochim. Acta**, 47, 11-30.
- Marshall, D.M., 1987, Structure and Petrology of an Archean Shear Zone, Crescent Lake Area, Wind River Mountains, Wyoming. **M.A. Thesis**, University of Wyoming, 132pp. (unpublished).
- Martin, H., 1987, Petrogenesis of Archean Trondhjemites, Tonalites, and Granodiorites from Eastern Finland: Major and Trace Element Geochemistry. **Journal of Petrology**, 28, 921-953.
- Miller, C.F., 1985, Are strongly peraluminous magmas derived from pelitic sedimentary sources? **Journal of Geology**, 93, 673-689.
- Miller, C.F. and Mittlefehldt, D.W., 1982, Depletion of light rare-earth elements in felsic magmas. **Geology**, 10, 129-133.
- Mitra, G. and Frost, B.R., 1981, mechanisms of deformation within Laramide and Precambrian deformation zones in basement rocks of the Wind River mountains. **Contributions to Geology**, University of Wyoming, 19, 161-173.
- Mogk, D.W., Mueller, P.A. and Wooden, J.L., 1988, Archean tectonics of the North Snowy Block, Beartooth Mountains, Montana. **Journal of Geology**, 96, 125-141.
- Mueller, P.J., Wooden, J.L., Odom, A.L. and Bowes, D.R., 1982, Geochemistry of the Archean rocks of the Quad Creek and Hellroaring Plateau areas of the eastern Beartooth Mountains. **Montana Bur. Mines and Geology Spec. Publ.**, 84, 60-82.
- Montel, J., 1986, Experimental determination of the solubility of Ce-monazite in  $\text{SiO}_2\text{-Al}_2\text{O}_3\text{-K}_2\text{O-Na}_2\text{O}$  melts at 800°C, 2kb, under  $\text{H}_2\text{O}$ -saturated conditions. **Geology**, 14, 659-662.

- Nagasawa, H. and Schnetzler, C.C., 1971, Partitioning of rare earth, alkali and alkaline earth elements between phenocrysts and acidic igneous magma. **Geochim. Cosmochim. Acta**, 35, 953-968.
- Nash, W.P. and Crecraft, H.R., 1985, Partition coefficients for trace elements in silicic magmas. **Geochim. Cosmochim. Acta**, 49, 2309-2322.
- Naylor, R.S., Steiger, R.H. and Wasserburg, G.J., 1970, U-Th-Pb and Rb-Sr systematics in  $2700 \times 10^9$ -year old plutons from the southern Wind River Range, Wyoming. **Geochim. Cosmochim. Acta**, 4, 1133-1159.
- Neuman, H., Mead, J. and Vitaliano, C.J., 1954, Trace element variations during fractional crystallisation as calculated from the distribution law. **Ibid.**, 44, 933-941.
- Nisbet, E.G., 1987, *The Young Earth*, Allen and Unwin, 402p.
- Noble, D.C. and Hedge, C.E., 1970, Distribution of rubidium between sodic-sanidine and natural silicic liquid. **Contrib. Mineral. Petrol.**, 29, 234-245.
- Norrish, K. and Chappell, B.W., 1977, An accurate X-ray fluorescence spectrographic method for the analysis of a wide range of geologic samples. **Geochim. Cosmochim. Acta**, 33, 67-76.
- Norrish, K. and Hutton, J.T., 1969, X-ray fluorescence spectrometry: in Zussman, J. (ed.) **Physical Methods in Determinative Mineralogy**, London, Academic Press.
- Oak, K.A. and Friend, C.R.L., 1990, The Closepet Granite, Karnataka, South India: Post-Collisional Crustal Anatexis? in **Third International Archean Symposium**, Perth, 165-168.
- Pearce, J.A., 1983, Role of the sub-continental lithosphere in magma genesis at active continental margins. In Hawkesworth, C.J. and Norry, M.J. eds., **Continental basalts and mantle xenoliths**, Shiva, 230-249.
- Pearce, J.A., Harris, N.B.W. and Tindle, A.G., 1984, Trace Element Discriminant Diagrams for the Tectonic Interpretation of Granitic Rocks. **Journal of Petrology**, 25, 956-983.
- Pearson, R.C., Kiilsgaard, T.H., Patten, L.L. and Mattick, R.E., 1971, Mineral resources the Popo Agie Primitive Area, Fremont and Sublette counties, Wyoming. **U.S. Geol. Surv. Bull.** 1353-B, 55pp.

- Perry, K., 1965, High Grade Regional Metamorphism of Precambrian Gneisses and Associated Rocks, Paradise Basin Quadrangle, Wind River Mountains, Wyoming. **Phd Thesis**, Yale University, 190pp. (unpublished).
- Peterman, Z.E., 1979a, Geochronology and the Archean of the United States. **Economic Geology**, 74, 1544-1562.
- Peterman, Z.E., 1979b, Strontium isotope geochemistry of late Archean to late Cretaceous Tonalites and Trondhjemites. in Barker, F. ed., **Trondhjemites, Dacites, and Related Rocks**. Elsevier, Amsterdam, 133-147.
- Peterman, Z. E., 1982, Geochronology of the southern Wyoming age province—a summary. **1982 Archean Geochemistry Field conference Part 1**. Guide to Field Trips. Golden, Colo. School Mines, 1-23.
- Philpotts, A.J., 1990, **Principles of Igneous and Metamorphic Petrology**. Prentice Hall, New Jersey.
- Philpotts, J.A. and Schnetzler, C.C., 1970, Phenocryst-matrix partition coefficients for K, Rb, Sr and Ba, with applications to anorthosite and basalt genesis. **Geochim. Cosmochim. Acta**, 34, 307-322.
- Pitcher, W.S., 1982, Granite Type and Tectonic Environment. in Hsu, K.J., ed **Mountain Building Processes**, Academic Press, 19-40.
- Pitcher, W.S., 1987, Granites and yet more granites forty years on. **Geologische Rundschau**, 76/1, 51-79.
- Rapp, R.P. and Watson, E.B., 1986, Monazite solubility and dissolution kinetics: implications for the thorium and light rare earth chemistry of felsic magmas. **Contrib. Mineral. Petrol.**, 94, 304-316.
- Rayleigh, J.W.S., 1896, Theoretical considerations respecting the separation of gases and similar processes. **Phil. Mag.**, 42, 77-107.
- Reagan, M.K., Gill, J.B., Malavassi, E. and Garcia, M.O., 1987, Changes in magma composition at Arenal volcano, Costa Rica, 1968-1985: Real-time monitoring of open-system differentiation. **Bull. Volcanol.**, 49, 415-434.
- Reed, J.C. Jr., 1963, Structure of Precambrian Crystalline Rocks in the Northern part of Grand Teton National Park, Wyoming. **U.S. Geol. Surv. Prof. Paper 475-C**, C1-C6.
- Reed, J.C. and Zartman, R.E., 1973, Geochronology of

- Precambrian Rocks of the Teton Range, Wyoming. **Geol. Soc. America Bull.**, 84, 561-582
- Reid, F., 1983, Origin of the rhyolitic rocks of the Taupo Volcanic Zone, New Zealand. **J. Volcan. Geothermal Res.**, 15, 315-338.
- Richter, F.M., 1985, Models for the Archaean thermal regime. **Earth Planet. Sci. Lett.**, 73, 350-360.
- Rudnick, R.L. and Taylor, S.R., 1986, Geochemical constraints on the origin of Archaean tonalitic-trondhjemitic rocks and implications for lower crustal composition. in **The Nature of the Lower Crust**, Dawson, J.B., Carswell, D.A., Hall, J. and Wedepohl, K.H. (eds), **Geol. Soc. Spec. Publ.** No 24, 179-191.
- St. John, O., 1878, Report on the geology of the Wind River District, in Hayden, F.V., **12th Annual Report of the U.S. Geol. and Geograph. Surv. of the Territories: Wyoming and Idaho.** 173-255.
- St. John, O., 1879, Report of Orestes St. John, geologist of the Teton Division, in Hayden, F.V., **11th Annual Report of the U.S. Geol. and Geograph. Surv. of the Territories,** 321-508.
- Sawka, W. N., Chappell, B.W. and Norrish, K., 1984, Light-rare-earth element zoning in sphene and allanite during granitoid fractionation. **Geology**, 12, 131-134.
- Schilling, J.G. and Winchester, J.W., 1967, Rare earth fractionation and magmatic processes. in Runcorn, S.K. (ed.) **Mantles of the Earth and Terrestrial Planets.** London, Interscience, 267-283.
- Schnetzer, C.C. and Philpotts, J.A., 1968, Partition coefficients of rare earth elements and barium between igneous matrix material and rock forming mineral phenocrysts, I. in Ahrens, L.H. (ed.) **Origin and Distribution of the Elements**, Pergamon, Oxford, 929.
- Schnetzer, C.C. and Philpotts, J.A., 1970, Partition coefficients of rare-earth elements between igneous matrix material and rock-forming mineral phenocrysts-II. **Geochim. Cosmochim. Acta**, 34, 331-340.
- Sleep, N. and Windley, B.F., 1982, Archean plate tectonics: constraints and inferences. **Journal of Geology**, 90, 363-379.
- Streckeisen, A., 1976, To each plutonic rock its proper name.



**Earth Science Reviews, 12, 1-33.**

- Stuckless, J.S., 1989, Petrogenesis of Two Contrasting, Late Archean Granitoids, Wind River Range, Wyoming. **U.S. Geol. Surv. Prof. Paper 1491**. 38pp.
- Stuckless, J.S., Miesch, A.T. and Wenner, D.B., 1986, Geochemistry and petrogenesis of an Archean granite from the Owl Creek mountains, Wyoming. **U.S. Geol. Surv. Prof. Paper 1388-A**, 1-21.
- Stuckless, J.S., Hedge, C.E., Worl, R.G., Simmons, K.R., Nkomo, I.T and Wenner, D.B., 1985, Isotopic studies of the late Archean plutonic rocks of the Wind River Range, Wyoming. **Geological Soc. America Bull.**, 96, 850-860.
- Sun, C., Williams, R.J. and Sun, S., 1974, Distribution coefficients of Eu and Sr for plagioclase-liquid and clinopyroxene-liquid equilibria in oceanic ridge basalt: an experimental study. **Geochim. Cosmochim. Acta**, 38, 1415-1433.
- Susuki, K., Adachi, M. and Yamamoto, K., 1990, Possible effects of grain-boundary REE on the REE distribution in felsic melts derived by partial melting. **Geochemical Journal**, 24, 57-74.
- Taylor, H.P., Jr., 1978, Oxygen and hydrogen isotope studies of plutonic granitic rocks. **Earth Planet. Sci. Lett.**, 38, 177-210.
- Taylor, S.R. and McLennan, S.M., 1985, *The Continental Crust: Its composition and Evolution*, Blackwell, London, 312p.
- van der Molen, I. and Paterson, M.S., 1979, Experimental deformation of partially-melted granite. **Contrib. Mineral. Petrol.**, 70, 299-318.
- Watson, E.B. and Capobianco, C.J., 1981, Phosphorous and the rare earth elements in felsic magmas: an assessment of the role of apatite. **Geochim. Cosmochim. Acta**, 45, 2349-2358.
- Watson, E.B. and Harrison, T.M., 1983, Zircon saturation revisited: temperature and composition effects in a variety of crustal magma types. **Earth Planet. Sci. Lett.**, 64, 295-304.
- Watson, E.B., Vicenzi, E.P. and Rapp, R.P., 1989, Inclusion/host relations involving accessory minerals in

high-grade metamorphic and anatexitic rocks. **Contrib. Mineral. Petrol.**, 101, 220-231.

- Weill, D.F. and Drake, M.J., 1973, Europium anomaly in plagioclase feldspar: experimental results and semi-quantitative model. **Science**, 180, 1059-1060.
- Whalen, J.B., Currie, K.L. and Chappell, B.W., 1987, A-type granites: geochemical characteristics, discrimination and petrogenesis. **Contrib. Min. Pet.**, 95, 407-419.
- White, E.W. and Johnson, G.G., 1970, X-ray absorption wavelengths and two-theta tables. American Society for testing and material-Data series DS 37A, 2nd ed., 293p.
- White, R. and McKenzie, d., 1989, Magmatism at rift zones: the generation of volcanic continental margins and flood basalts. **J. Geophy. Res.**, 94, 7685-7729
- Whitney, J.A., 1988, The origin of granite: The role and source of water in the evolution of granitic magmas. **Geol. Soc. Amer. Bull.**, 100, 1886-1897.
- Wickham, S.M., 1987, The segregation and emplacement of granitic magmas. **J. Geol. Soc. London**, 144, 281-297.
- Wilks, M.E., 1988, The Himalayas-a modern analogue for Archean crustal evolution. **Earth Planet. sci Lett.**, 87, 127-136.
- Windley, B.F., 1984, The Evolving continents, John Wiley, 399p.
- Winkler, H.G.F., 1979, **Petrogenesis of Metamorphic Rocks**, Springer-Verlag, 348pp.
- Wood, D.A., 1979, A variably veined suboceanic upper mantle--Genetic significance for mid-ocean ridge basalts from geochemical evidence. **Geology**, 7, 499-503.
- Worl, R.G., Koesterer, M.E. and Hulsebosch, T.P., 1986, Geologic map of the Bridger Wilderness and the Green-Sweetwater Roadless area, Sublette and Fremont Counties, Wyoming. **U.S. Geol. Surv. Misc. Field Studies Map MF-1636-B**.

## Appendix A

Major, trace element and CIPW data for  
Middle Mountain, Dome peak and Mount Owen plutons  
and  
The Bridger and Louis Lake batholiths

BD=Below detection  
Oxides in wt%  
Trace elements in ppm

## MIDDLE MOUNTAIN PLUTON

SAMPLE	RL-1	RL-2	RL-3	RL-4	RL-5	RL-7	RL-8	MM-1
SiO2	70.98	74.36	74.42	71.91	76.63	74.66	72.19	73.95
TiO2	0.36	0.19	0.21	0.32	0.04	0.21	0.30	0.12
Al2O3	15.37	14.64	15.45	14.82	14.05	15.26	15.64	14.04
Fe2O3-T	2.10	1.56	1.65	2.10	0.37	1.42	2.22	1.33
MgO	0.82	0.47	0.50	0.65	0.20	0.51	1.09	0.06
CaO	1.92	1.02	1.42	1.53	0.80	1.32	0.78	1.03
Na2O	3.73	2.95	3.49	3.50	2.75	3.47	4.43	3.73
K2O	4.45	5.97	5.01	4.77	5.95	4.91	4.26	5.32
MnO	0.04	0.03	0.03	0.03	0.02	0.03	0.03	0.01
P2O5	0.09	0.05	0.05	0.07	0.01	0.04	0.10	0.02
LOI	0.66	0.50	0.52	0.62	0.38	0.47	1.08	0.33
TOTAL	100.52	101.74	102.75	100.32	101.18	102.29	102.10	99.95
Rb	148	139	114	147	134	144	126	216
Ba	829	1121	1246	1234	368	894	1049	414
Cs	0.74	0.86	0.51	0.51	0.39	0.56	0.30	0.85
Sr	205	147	220	189	66.0	187	129	69.7
Pb	35	49	39.4	47	52	41	24	55
Th	16	65	50	57	7.7	41	47	32
U	2.8	5.1	3.3	2.5	3.7	5.4	8.0	4.1
Sc	3.80	2.33	2.26	3.34	0.46	2.45	3.27	2.75
V	25.6	20.4	16.0	28.2	4.54	23.1	31.2	5.23
Cr	13.7	2.56	17.2	5.15	3.91	1.78	23.8	18.6
Co	3.6	2.0	2.0	2.8	BD	2.1	2.6	0.80
Cu	BD	BD	BD	BD	BD	BD	BD	BD
Zn	46	28	29	39	13	32	29	11
Ga	26.9	16.2	17.0	19.7	18.3	20.0	23.6	23.0
Y	18	15	10	14	6.6	10	13	33
Zr	183	183	166	184	35	139	201	98
Nb	6.7	4.6	3.9	4.7	0.56	4.4	11	9.1
Hf	6.2	6.8	5.7	6.7	1.5	5.0	7.5	4.3
Ta	0.33	0.20	0.15	0.30	0.41	0.18	0.25	0.50

MIDDLE	MOUNTAIN	PLUTON						
SAMPLE	RL-1	RL-2	RL-3	RL-4	RL-5	RL-7	RL-8	MM-1
La	55.5	94.1	69.1	74.9	10.2	51.2	74.1	46.1
Ce	104	165	122	131	17.0	91.9	128	101
Nd	33.0	51.8	36.9	41.8	4.84	29.5	38.6	26.9
Sm	5.50	9.30	6.47	7.30	0.77	4.79	6.91	6.34
Eu	1.49	1.11	0.87	1.02	0.39	0.96	1.01	0.62
Tb	0.47	0.62	0.44	0.53	0.11	0.34	0.51	0.71
Yb	0.86	0.76	0.39	0.70	0.16	0.68	0.51	1.9
Lu	0.14	0.12	0.07	0.10	0.04	0.10	0.12	0.30
K <sub>2</sub> O/Na <sub>2</sub> O	1.19	2.02	1.43	1.36	2.16	1.42	0.96	1.43
K/Rb	248.71	355.31	361.71	269.09	366.19	283.41	279.35	204.41
Ba/Sr	4.03	7.60	5.66	6.53	5.59	4.79	8.11	5.95
Rb/Sr	0.72	0.94	0.52	0.78	2.04	0.77	0.98	3.10
La/Yb	64.53	123.82	177.18	107.00	63.75	75.29	145.37	24.50
Eu/Eu*	0.92	0.42	0.47	0.48	1.56	0.69	0.50	0.32
CIPW	NORM							
Q	26.97	30.99	30.38	29.07	35.52	31.44	26.52	29.55
C	1.14	1.57	1.78	1.29	1.64	1.90	2.54	0.32
Or	26.33	34.85	28.96	28.27	34.87	28.49	24.91	31.56
Ab	31.60	24.66	28.89	29.70	23.08	28.83	37.08	31.68
An	8.95	4.68	6.57	7.16	3.87	6.17	3.18	5.00
Di	-	-	-	-	-	-	-	-
Hy	2.59	1.68	1.75	2.21	0.65	1.67	3.36	0.64
Mgn	1.53	1.12	1.17	1.53	0.27	1.01	1.59	0.97
Il	0.69	0.36	0.39	0.61	0.08	0.39	0.56	0.23
Ap	0.21	0.11	0.11	0.16	0.02	0.09	0.23	0.05

MIDDLE	MOUNTAIN			PLUTON				
SAMPLE	MM-3	MM-4	MM-5	BL-1	BL-2	BL-4	BL-5	GL-1
SiO2	73.56	74.63	72.53	69.54	72.35	69.30	68.60	74.25
TiO2	0.20	0.14	0.17	0.50	0.26	0.41	0.54	0.19
Al2O3	13.66	13.69	14.50	16.55	15.19	16.24	16.03	14.19
Fe2O3-T	1.33	1.30	1.66	3.41	1.51	2.61	3.34	1.21
MgO	0.20	0.09	0.00	0.98	0.31	0.70	0.99	0.11
CaO	0.88	0.82	0.84	2.75	1.23	2.54	2.89	0.91
Na2O	3.32	3.45	2.99	5.06	3.58	4.45	4.68	3.84
K2O	5.59	5.37	5.61	3.24	5.12	3.09	2.98	5.30
MnO	0.02	0.02	0.03	0.03	0.02	0.03	0.02	0.01
P2O5	0.04	0.02	0.05	0.12	0.07	0.12	0.12	0.03
LOI	0.60	0.68	0.68	0.40	0.85	0.77	0.70	0.47
TOTAL	99.95	100.21	99.05	102.57	100.47	100.25	100.88	100.50
Rb	198	200	217	155	158	111	108	160
Ba	847	595	777	985	778	814	1271	930
Cs	0.71	0.50	0.71	1.89	0.78	1.59	1.35	0.55
Sr	102	82.5	87.9	256	151	287	335	160
Pb	43	52	51	30	41	38	36	63
Th	67	59	59	34	42	39	37	55
U	9.1	14	3.8	4.7	7.4	4.63	3.22	9.67
Sc	3.48	2.99	3.47	4.20	3.34	4.67	5.42	2.14
V	13.1	13.1	13.0	45.8	13.7	42.3	49.8	8.78
Cr	BD	1.79	BD	7.06	3.89	8.43	3.68	2.93
Co	1.5	1.0	1.3	6.4	2.1	4.6	6.0	1.1
Cu	BD	BD	BD	BD	BD	BD	BD	BD
Zn	13	BD	13	31	8.4	18	38	5.7
Ga	19.8	22.0	21.5	26.1	21.6	24.2	23.8	21.0
Y	14	16	19	23	14	29	19	11
Zr	159	106	147	250	143	246	269	107
Nb	9.0	8.9	9.2	12	7.3	10	11	2.9
Hf	6.4	5.5	6.3	7.8	5.3	7.4	8.2	4.5
Ta	0.35	0.46	0.31	1.1	0.66	0.75	0.72	0.39

MIDDLE	MOUNTAIN	PLUTON						
SAMPLE	MM-3	MM-4	MM-5	BL-1	BL-2	BL-4	BL-5	GL-1
La	89.9	80.5	90.2	52.8	67.5	70.3	78.71	75.05
Ce	175	155	173	90.2	122	125	130.88	146.51
Nd	51.9	56.5	54.4	26.8	42.1	40.4	39.70	45.01
Sm	10.3	10.4	12.1	4.76	7.22	7.72	6.54	7.44
Eu	1.07	0.95	0.98	1.17	1.00	1.39	1.55	0.91
Tb	0.58	0.80	0.91	0.50	1.3	0.86	0.65	0.45
Yb	0.81	1.0	0.72	1.9	1.2	1.9	1.54	0.70
Lu	0.07	0.06	0.11	0.30	0.15	0.28	0.21	0.06
K2O/Na2O	1.68	1.55	1.88	0.64	1.43	0.69	0.64	1.38
K/Rb	234.12	222.94	214.48	172.61	268.02	230.07	228.63	274.87
Ba/Sr	8.31	7.22	8.78	3.84	5.15	2.84	3.79	5.80
Rb/Sr	1.94	2.42	2.47	0.61	1.05	0.39	0.32	1.00
La/Yb	111.01	79.66	125.26	28.09	57.73	36.98	51.11	107.21
Eu/Eu*	0.37	0.31	0.28	0.80	0.41	0.58	0.78	0.43
CIPW								
Q	30.99	32.12	32.25	19.01	28.97	25.26	22.23	29.45
C	0.65	0.76	2.14	0.01	1.70	1.25	0.14	0.55
Or	33.43	31.88	33.70	18.38	30.36	18.35	17.58	31.31
Ab	28.43	29.33	25.72	41.10	30.40	37.85	39.52	32.48
An	4.15	3.96	3.90	12.34	5.67	11.88	13.53	4.32
Di	-	-	-	-	-	-	-	-
Hy	0.89	0.69	0.63	4.23	1.15	2.45	3.29	0.59
Mgn	0.98	0.95	1.22	3.77	1.10	1.90	2.42	0.88
Il	0.38	0.27	0.33	0.91	0.50	0.78	1.02	0.36
Ap	0.09	0.05	0.12	0.27	0.16	0.28	0.28	0.07

MIDDLE	MOUNTAIN	PLUTON			
SAMPLE	GL-2	GL-3	GL-4	AVG n=19	
SiO2	72.54	72.58	72.19	72.69	2.00
TiO2	0.28	0.33	0.24	0.26	0.12
Al2O3	14.69	14.83	14.60	14.92	0.81
Fe2O3-T	2.38	1.87	2.01	1.86	0.72
MgO	0.51	0.61	0.82	0.51	0.33
CaO	1.28	1.91	1.81	1.46	0.66
Na2O	4.39	4.22	3.87	3.78	0.60
K2O	4.61	4.46	4.52	4.76	0.87
MnO	0.02	0.02	0.02	0.02	0.01
P2O5	0.09	0.05	0.04	0.06	0.03
LOI	0.64	0.47	0.57	0.60	0.17
TOTAL	101.43	101.34	100.68	100.96	0.97
Rb	160	132	131	153	32.40
Ba	1711	1024	1975	993	381.98
Cs	1.16	1.03	1.87	0.89	0.47
Sr	424	277	262	191	95.06
Pb	54	41	51	44	9.43
Th	54	53	57	46	15.38
U	10	4.6	7.9	6.0	3.04
Sc	2.28	3.00	3.84	3.13	1.05
V	3.75	26.09	29.59	21.51	13.32
Cr	6.63	2.26	5.34	7.14	6.51
Co	2.3	2.9	3.0	2.3	1.89
Cu	BD	BD	BD	----	----
Zn	14	18	19	21	12.16
Ga	21.9	19.9	18.7	21.3	2.77
Y	8.0	14	73	18	14.90
Zr	173	192	304	173	63.21
Nb	5.0	7.9	9.8	7.3	3.13
Hf	6.6	6.6	9.5	6.2	1.67
Ta	0.41	0.63	0.54	0.45	0.23



MIDDLE	MOUNTAIN	PLUTON			
SAMPLE	GL-2	GL-3	GL-4	AVG n=19	STD
La	75.5	78.7	101	70.3	20.12
Ce	134	141	174	127	36.69
Nd	41.2	45.0	55.8	40.1	12.19
Sm	5.44	6.22	13.7	7.32	2.83
Eu	1.38	1.22	2.52	1.14	0.42
Tb	0.27	0.37	2.86	0.70	0.57
Yb	0.66	1.1	14	2.4	2.91
Lu	0.10	0.16	2.17	0.25	0.46
K2O/Na2O	1.05	1.06	1.17	1.32	0.42
K/Rb	237.98	279.85	284.73	264.02	51.31
Ba/Sr	4.03	3.69	7.53	5.75	1.75
Rb/Sr	0.38	0.48	0.50	1.13	0.81
La/Yb	114.35	70.22	6.93	40.68	14.08
Eu/Eu*	0.91	0.69	0.52	0.60	0.30
CIPW					
Q	25.56	25.85	27.07	27.98	
C	0.36	-	0.15	1.03	
Or	27.03	26.13	26.68	27.91	
Ab	36.85	35.39	32.71	31.73	
An	5.72	8.28	8.71	6.80	
Di	-	0.63	-	-	
Hy	2.03	1.64	2.69	2.50	
Mgn	1.71	1.34	1.46	0.83	
Il	0.53	0.62	0.46	0.49	
Ap	0.21	0.12	0.09	0.14	

DOME PEAK PLUTON

SAMPLE	NFL-1	NFL-2	NFL-3	NFL-4	NFL-5	NFL-6	NFL-7	PC-1
SiO2	66.32	66.37	65.34	68.44	70.88	68.84	67.63	65.39
TiO2	0.82	0.75	0.76	0.72	0.60	0.55	0.70	0.58
Al2O3	15.56	15.57	15.65	14.53	13.75	14.94	15.09	16.92
Fe2O3-T	5.00	4.80	5.15	4.41	3.57	3.57	3.97	3.29
MgO	1.76	1.52	1.69	1.29	2.09	1.28	1.14	0.99
CaO	3.81	2.93	3.52	2.90	0.75	2.59	2.58	3.25
Na2O	4.01	3.33	3.86	3.61	6.87	3.79	3.38	3.95
K2O	3.60	5.21	4.48	4.31	0.71	4.74	4.85	4.61
MnO	0.05	0.03	0.05	0.04	0.01	0.04	0.06	0.05
P2O5	0.27	0.26	0.24	0.21	0.16	0.15	0.23	0.22
LOI	0.59	0.97	1.00	0.67	1.31	1.02	0.70	0.47
TOTAL	101.78	101.73	101.74	101.13	100.70	101.51	100.32	99.71
Rb	90.3	88.3	100	107	26.3	102	125	93
Ba	1552	2540	1741	1174	93.0	1244	1207	1882
Cs	BD	BD	BD	0.46	BD	BD	0.29	0.20
Sr	474	432	446	320	80.1	301	327	609
Pb	28	14	24	31	6.6	28	29.4	27.3
Th	30	42	38	70	116	56.4	33.7	16.6
U	1.8	1.4	1.7	2.4	4.5	4.6	1.6	1.1
Sc	9.28	9.56	9.61	9.47	7.70	6.39	6.86	6.07
V	70.3	76.4	71.9	54.6	54.2	45.7	58.2	61.2
Cr	12.8	12.9	16.8	10.6	4.57	7.82	10.8	12.5
Co	11	9.9	11	8.6	4.1	6.3	7.2	7.5
Cu	4.1	22	22	BD	BD	BD	BD	BD
Zn	57	11	61	46	ND	17.6	49.4	52.8
Ga	22.1	22.1	17.4	20.3	20.6	20.2	20.4	20.6
Y	37.1	34.8	35.2	38.6	26.2	30.3	46.2	25.3
Zr	400	375	403	379	308	294	367	219
Nb	13.1	9.3	11.8	15.5	17.4	13.7	15.6	9.1
Hf	16.3	12.3	15.6	13.2	9.7	14.8	9.9	11.2
Ta	0.83	0.56	0.61	0.66	1.4	0.63	0.78	0.55

DOME PEAK		PLUTON						
SAMPLE	NFL-1	NFL-2	NFL-3	NFL-4	NFL-5	NFL-6	NFL-7	PC-1
La	170	219	183	198	101	148	118	111
Ce	326	416	351	368	177	248	225	205
Nd	130	138	99.2	99.2	47.5	69.6	69.3	79.4
Sm	21.2	23.9	22.3	23.1	12.5	14.7	17.5	13.9
Eu	3.35	3.65	3.22	2.97	1.81	2.61	2.53	2.86
Tb	1.5	1.5	1.5	1.9	1.0	1.1	1.6	1.0
Yb	2.7	2.68	2.80	3.56	3.43	2.77	2.86	2.00
Lu	0.37	0.33	0.39	0.37	0.33	0.36	0.32	0.24
K2O/Na2O	0.90	1.57	1.16	1.19	0.10	1.25	1.43	1.17
K/Rb	330.55	489.67	370.11	333.32	223.41	383.43	319.66	411.74
Ba/Sr	3.27	5.88	3.90	3.66	1.16	4.13	3.69	3.09
Rb/Sr	0.19	0.20	0.22	0.33	0.33	0.34	0.38	0.15
La/Yb	63.69	81.81	65.64	55.85	29.45	53.48	41.50	55.67
Eu/Eu*	0.55	0.54	0.50	0.44	0.49	0.61	0.49	0.71
CIPW	NORM							
Q	19.10	18.69	16.40	23.29	23.70	22.31	22.48	16.72
C	-	-	-	-	0.70	-	0.14	0.05
Or	21.02	30.55	26.28	25.35	4.22	27.60	28.77	27.45
Ab	33.53	27.96	32.42	30.41	58.49	31.60	28.71	33.67
An	13.66	12.06	12.06	10.66	2.68	9.61	11.34	14.80
Di	2.62	0.55	2.99	1.84	-	1.67	-	-
Hy	4.33	4.73	4.18	3.42	6.07	3.30	3.81	3.29
Mgn	3.58	3.45	3.71	3.18	2.60	2.55	2.89	2.40
Il	1.54	1.41	1.43	1.36	1.15	1.03	1.33	1.11
Ap	0.62	0.60	0.55	0.48	0.37	0.34	0.54	0.51

DOME PEAK		PLUTON					
SAMPLE	PC-2	PC-3	PC-4	PC-5	FL-1	FL-1A	FL-7
SiO2	66.05	63.19	63.84	64.67	60.82	60.91	60.74
TiO2	0.82	0.80	0.77	0.67	1.11	1.10	1.03
Al2O3	16.21	17.24	17.02	16.50	15.37	15.36	16.67
Fe2O3-T	4.98	4.69	4.15	4.00	6.60	6.55	6.37
MgO	1.52	1.46	1.34	1.14	2.56	2.51	2.15
CaO	3.68	4.11	3.74	3.32	4.32	4.33	4.57
Na2O	3.98	4.24	4.04	4.56	3.45	3.43	4.23
K2O	4.29	3.60	4.18	5.01	3.87	3.83	3.21
MnO	0.05	0.06	0.05	0.04	0.08	0.08	0.09
P2O5	0.28	0.32	0.29	0.22	0.56	0.56	0.47
LOI	0.43	0.34	0.54	0.64	0.98	0.75	0.36
TOTAL	102.29	100.05	99.96	100.77	99.72	99.40	99.89
Rb	94.8	80.1	96.5	113	104	102	64.6
Ba	2144	1506	1174	2341	2225	2161	2321
Cs	0.28	0.36	0.28	0.37	0.59	0.53	0.38
Sr	562	597	572	572	757	745	708
Pb	28	28	30	30	25	23	16
Th	35	43	58	37	48	45	8.8
U	1.4	1.8	2.0	1.5	1.7	1.3	1.3
Sc	7.57	10.5	8.13	6.8	12.0	11.9	10.3
V	69.8	61.2	74.8	57.1	106	103	98.6
Cr	23.3	13.7	10.1	12.2	34.0	67.5	22.9
Co	9.5	8.2	9.6	7.5	15.8	15.8	12.6
Cu	BD	3.9	BD	0.13	6.4	18.8	BD
Zn	65	67	59	48	104	100	98
Ga	21.2	24.3	23.6	20.8	28.7	22.6	30.3
Y	34.5	38.8	40.0	32.1	39.1	37.7	29.4
Zr	405	314	364	338	385	367	417
Nb	13.1	13.6	14.9	13.1	9.73	12.1	11.7
Hf	11.6	17.7	18.5	9.3	13.7	11.4	14.7
Ta	0.62	0.77	0.81	0.72	0.49	0.45	0.58

DOME PEAK      PLUTON

SAMPLE	PC-2	PC-3	PC-4	PC-5	FL-1	FL-1A	FL-7
La	158	204	238	169	202	197	93
Ce	300	377	428	314	388	389	188
Nd	98.8	136	120	122	150	151	82.2
Sm	18.9	24.6	24.6	19.1	25.4	25.2	15.9
Eu	3.53	3.86	3.37	3.48	3.94	4.03	3.59
Tb	1.4	1.7	1.6	1.32	1.6	1.7	1.1
Yb	2.52	3.20	3.18	2.42	3.52	3.06	2.31
Lu	0.29	0.39	0.39	0.29	0.32	0.32	.27
K2O/Na2O	1.08	0.85	1.03	1.10	1.12	1.12	0.76
K/Rb	375.46	372.62	359.50	367.77	306.16	310.16	412.18
Ba/Sr	3.81	2.52	2.05	4.09	2.94	2.90	3.28
Rb/Sr	0.17	0.13	0.17	0.20	0.14	0.14	0.09
La/Yb	63.07	63.84	75.04	70.20	57.47	64.41	40.26
Eu/Eu*	0.64	0.54	0.48	0.63	0.54	0.56	0.78
CIPW							
Q	16.83	14.39	14.97	11.46	14.48	14.88	12.04
C	-	-	-	-	-	-	-
Or	24.89	21.34	24.84	29.57	23.16	22.94	19.06
Ab	33.06	35.98	34.38	38.53	29.56	29.41	35.97
An	13.45	17.43	16.05	9.74	15.21	15.41	17.10
Di	2.15	0.74	0.56	4.23	2.22	2.12	2.08
Hy	3.92	4.45	4.01	1.80	7.07	6.99	6.07
Mgn	3.54	3.41	3.02	2.90	4.84	4.81	4.63
Il	1.53	1.52	1.47	1.27	2.14	2.12	1.97
Ap	0.64	0.74	0.68	0.51	1.31	1.31	1.09

DOME PEAK		PLUTON
SAMPLE	AVG n=13	STD
SiO2	65.29	2.93
TiO2	0.79	0.17
Al2O3	15.76	0.96
Fe2O3-T	4.74	1.04
MgO	1.63	0.48
CaO	3.36	0.92
Na2O	4.05	0.83
K2O	4.03	1.04
MnO	0.05	0.02
P2O5	0.29	0.13
LOI	0.72	0.27
TOTAL	100.71	0.90
Rb	92.7	22.40
Ba	1687	625.53
Cs	0.25	0.20
Sr	500	181.05
Pb	25	6.72
Th	45	24.08
U	2.0	1.05
Sc	8.80	1.84
V	73.5	20.10
Cr	20.5	16.84
Co	10.1	3.48
Cu	5.2	8.26
Zn	55	29.67
Ga	22.4	3.23
Y	35.0	5.42
Zr	356	51.19
Nb	12.9	2.31
Hf	13.3	2.80
Ta	0.70	0.21

DOME PEAK    PLUTON

SAMPLE	AVG n=13	STD
La	168	43.51
Ce	313	82.34
Nd	106	31.12
Sm	20.2	4.32
Eu	3.25	0.59
Tb	1.4	0.26
Yb	2.87	0.44
Lu	0.50	0.60

K <sub>2</sub> O/Na <sub>2</sub> O	1.06	0.32
K/Rb	357.71	58.02
Ba/Sr	3.36	1.03
Rb/Sr	0.21	0.09
La/Yb	58.76	13.22
Eu/Eu*	0.57	0.09

CIPW

Q	16.48
C	-
Or	23.72
Ab	34.14
An	12.87
Di	1.51
Hy	6.27
Mgn	2.13
Il	1.50
Ap	0.67

## MOUNT OWEN PLUTON

SAMPLE	GT-1	GT-2	GT-3	GT-4	GT-5	MO-2	MO-3	MO-5
SiO2	75.54	76.45	75.39	76.66	75.73	73.34	75.44	73.88
TiO2	0.06	0.07	0.06	0.07	0.07	0.19	0.14	0.17
Al2O3	13.98	13.98	13.96	13.79	14.00	13.82	13.54	13.76
Fe2O3-T	1.05	1.18	1.03	1.14	1.02	1.76	1.64	1.74
MgO	0.28	0.30	0.24	0.25	0.24	0.48	0.16	0.25
CaO	0.77	0.69	0.61	0.64	0.67	1.36	0.90	1.12
Na2O	3.70	3.53	3.69	3.87	3.32	4.04	3.22	3.35
K2O	4.98	4.99	4.85	4.67	4.84	4.21	5.28	5.25
MnO	0.03	0.03	0.03	0.04	0.03	0.01	0.01	0.01
P2O5	0.07	0.07	0.08	0.04	0.07	0.04	0.05	0.05
LOI	0.57	0.54	0.69	0.08	0.63	0.52	0.52	0.45
TOTAL	100.85	101.81	100.63	102.00	100.62	99.77	100.89	100.02
Rb	243	253	273	120	247	140	142	164.85
Ba	282	267	263	256	329	646	792	789.33
Cs	5.6	6.8	6.9	10.4	6.5	1.5	1.2	2.07
Sr	37.7	35.1	29.5	42.8	36.8	59.6	58.6	68.38
Pb	40	38	36	16	42	61	57	51.09
Th	15	17	17	17	17	43	34	48.61
U	2.6	3.8	3.03	3.7	4.4	4.6	5.0	4.76
Sc	2.24	2.64	2.34	2.30	2.22	3.42	3.13	3.01
V	2.53	0.48	5.35	7.06	6.92	8.52	6.33	8.29
Cr	7.73	20.7	17.1	12.7	14.7	10.5	1.6	10.32
Co	0.74	0.59	0.59	0.71	0.83	2.12	1.38	2.06
Cu	ND	ND	ND	ND	ND	3.9	ND	ND
Zn	42	41	40	34	32	12	7.1	18.67
Ga	21.7	22.6	21.7	21.6	20.4	18.1	15.9	17.52
Y	26	31	27	45	39	45	36	11.79
Zr	45	55	56	160	68.1	133	126	185.10
Nb	8.5	9.8	10	30	10	10	10	4.0
Hf	1.6	2.6	2.2	2.5	2.4	5.3	5.1	5.3
Ta	1.1	1.7	2.0	1.9	1.5	0.69	0.63	0.76



MOUNT	OWEN	PLUTON						
SAMPLE	GT-1	GT-2	GT-3	GT-4	GT-5	MO-2	MO-3	MO-5
La	17.0	18.2	16.9	19.6	18.8	60.0	39.8	62.7
Ce	38.1	38.7	37.4	43.0	41.5	126	88.5	127
Nd	13.8	16.9	12.0	19.3	19.4	52.7	35.9	52.2
Sm	4.7	5.9	5.1	5.5	5.6	12.3	10.1	13.6
Eu	0.51	0.44	0.34	0.39	0.41	0.87	0.86	0.96
Tb	0.60	0.74	0.65	0.81	0.94	1.3	1.2	1.4
Yb	1.5	2.3	1.8	2.4	2.7	3.8	3.6	3.8
Lu	0.20	0.31	0.24	0.30	0.34	0.42	0.44	0.42
K2O/Na2O	1.35	1.42	1.31	1.21	1.46	1.04	1.64	1.57
K/Rb	170.12	163.06	147.07	321.45	162.09	248.42	306.34	264.43
Ba/Sr	7.49	7.63	8.95	6.00	8.95	10.85	13.52	11.54
Rb/Sr	6.45	7.23	9.29	2.81	6.74	2.36	2.44	2.41
La/Yb	11.33	7.91	9.23	8.13	7.04	15.92	10.97	16.51
Eu/Eu*	0.34	0.24	0.21	0.22	0.22	0.23	0.27	0.23
CIPW	NORM							
Q	32.72	34.41	33.73	34.01	36.10	30.17	34.07	31.53
C	1.27	1.66	1.72	1.29	2.25	0.24	1.01	0.65
Or	29.29	29.11	28.68	27.28	28.60	25.07	31.08	31.15
Ab	31.16	29.49	31.24	32.37	28.09	34.44	27.14	28.46
An	3.35	2.93	2.51	2.88	2.87	6.54	4.12	5.25
Di	-	-	-	-	-	-	-	-
Hy	1.18	1.27	1.08	1.14	1.05	1.80	1.01	1.24
Mgn	0.76	0.85	0.75	0.82	0.74	1.29	1.18	1.27
Il	0.11	0.13	0.11	0.13	0.13	0.36	0.27	0.32
Ap	0.16	0.16	0.19	0.09	0.16	0.09	0.12	0.17

MOUNT	OWEN		PLUTON			
	SAMPLE	RM-1	RM-2	RM-3A	AVG n=11	STD
	SiO2	75.15	74.56	75.66	75.25	0.95
	TiO2	0.08	0.13	0.13	0.10	0.04
	Al2O3	14.47	14.27	13.54	13.92	0.27
	Fe2O3-T	0.95	1.41	1.62	1.32	0.30
	MgO	0.05	0.17	0.29	0.24	0.10
	CaO	1.45	1.48	1.11	0.98	0.32
	Na2O	4.36	3.96	3.63	3.70	0.33
	K2O	3.77	4.02	4.51	4.67	0.47
	MnO	0.02	0.01	0.02	0.02	0.01
	P2O5	0.04	0.03	0.05	0.05	0.02
	LOI	0.38	0.35	0.41	0.47	0.16
	TOTAL	100.70	100.39	100.95	100.78	0.63
	Rb	115	126	146	180	58.51
	Ba	469	608	657	487	207.06
	Cs	2.04	1.44	2.46	4.25	2.95
	Sr	84.1	100	86.8	58.2	23.05
	Pb	39	44	47	42	11.46
	Th	14	19	16	23	11.77
	U	3.1	2.2	2.30	3.58	0.96
	Sc	1.93	2.78	2.94	2.63	0.44
	V	5.06	7.38	10.9	6.26	2.74
	Cr	10.9	BD	BD	9.65	6.53
	Co	0.66	1.5	1.5	1.2	0.56
	Cu	ND	ND	ND	0.35	1.12
	Zn	8.7	23	24	25	12
	Ga	18.8	19.5	17.4	19.5	2.10
	Y	27	11	27	39	35
	Zr	51	90	92	96	45.79
	Nb	4.3	8.1	8.4	10	6.7
	Hf	2.8	3.6	3.7	3.4	1.3
	Ta	0.58	0.63	0.69	1.1	0.54

MOUNT	OWEN	PLUTON			
SAMPLE	RM-1	RM-2	RM-3A	AVG n=11	STD
La	21.7	37.2	26.9	30.8	16.25
Ce	38.5	56.0	44.5	61.8	33.74
Nd	12.4	19.8	15.3	24.5	14.55
Sm	3.20	3.63	3.80	6.69	3.45
Eu	1.01	0.71	0.67	0.65	0.23
Tb	0.71	0.35	0.52	0.84	0.33
Yb	3.8	1.3	2.1	2.7	0.92
Lu	0.51	0.11	0.27	0.32	0.11
K <sub>2</sub> O/Na <sub>2</sub> O	0.86	1.01	1.24	1.28	0.23
K/Rb	271.74	263.15	254.72	233.87	59.21
Ba/Sr	5.59	6.06	7.57	8.56	2.41
Rb/Sr	1.37	1.26	1.69	4.01	2.71
La/Yb	5.71	29.29	12.67	12.25	6.32
Eu/Eu*	0.87	0.65	0.55	0.37	0.21
CIPW					
Q	32.01	32.56	34.14	32.86	
C	0.67	0.79	0.78	1.11	
Or	22.20	23.75	26.50	27.42	
Ab	36.77	33.49	30.54	31.11	
An	6.91	7.14	5.15	4.51	
Di	-	-	-	-	
Hy	0.51	0.94	1.34	1.63	
Mgn	0.69	1.02	1.17	0.59	
Il	0.15	0.25	0.25	0.19	
Ap	0.09	0.07	0.12	0.12	

## BRIDGER BATHOLITH

SAMPLE	SL-2	SL-3	SL-4	SL-6	SL-7	SL-9	HL-4	HL-5
SiO2	70.06	60.40	65.20	72.16	68.96	63.42	66.55	65.91
TiO2	0.37	0.71	0.50	0.28	0.42	0.64	0.52	0.51
Al2O3	15.84	16.85	17.13	15.31	16.08	17.31	17.21	16.63
Fe2O3-T	2.78	6.23	4.21	2.02	3.11	4.55	4.27	3.87
MgO	0.92	1.94	1.40	0.75	0.93	1.66	1.50	1.49
CaO	2.66	5.00	4.17	3.28	3.45	4.49	4.25	3.98
Na2O	4.70	4.68	5.54	5.67	4.95	5.44	5.12	5.79
K2O	3.05	2.48	1.77	1.03	2.00	1.83	1.90	1.70
MnO	0.04	0.11	0.06	0.04	0.04	0.06	0.06	0.06
P2O5	0.15	0.43	0.16	0.08	0.13	0.22	0.22	0.19
LOI	0.45	0.34	1.21	0.50	0.63	0.89	0.25	0.66
TOTAL	101.01	99.17	101.34	101.13	100.70	100.51	101.86	100.78
Rb	65.7	84.2	65.9	37.9	70.9	57.2	60.3	50.9
Ba	939	1205	494	147	434	602	1085	546
Cs	0.34	0.52	0.43	0.54	0.73	0.24	0.57	0.41
Sr	415	869	418	219	412	665	676	770
Pb	21	14	10.5	15	18	22	16	13
Th	10	13	7.6	6.0	7.7	9.7	15	5.4
U	1.2	2.4	0.81	1.4	0.64	0.75	0.80	0.59
Sc	1.90	10.5	9.50	3.56	2.52	7.93	4.96	3.77
V	60.0	101	65.7	31.1	43.1	84.8	77.7	59.9
Cr	2.9	18	21	7.4	15	20	14	9.3
Co	6.1	13	7.6	3.7	6.9	10	8.5	8.8
Cu	4.6	0.74	BD	BD	BD	0.36	2.1	BD
Zn	50	138	79	43	66	86	84	61
Ga	21.2	21.5	28.7	21.9	24.3	30.1	28.3	23.0
Y	9.7	38	14	8.8	8.8	21	11	12
Zr	147	271	149	179	116	160	141	153
Nb	3.6	15	6.8	5.7	8.1	9.8	5.6	5.5
Hf	5.0	9.1	4.5	6.5	4.0	5.0	4.7	5.3
Ta	0.11	1.4	0.23	0.33	0.25	0.49	0.30	0.28

## BRIDGER

SAMPLE	SL-2	SL-3	SL-4	SL-6	SL-7	SL-9	HL-4	HL-5
La	32.3	56.7	40.0	21.1	27.0	40.7	94.6	42
Ce	58.7	131.1	77.1	40.7	50.9	83.6	172.8	88
Nd	23.8	61.1	28.7	13.7	19.9	41.7	56.3	36
Sm	4.48	14.4	5.44	3.08	4.11	8.39	7.65	6.5
Eu	1.09	2.74	1.35	0.75	0.98	1.94	1.72	1.4
Tb	0.35	1.4	0.48	0.30	0.37	0.75	0.52	0.45
Yb	0.85	3.4	1.0	0.71	0.47	1.4	0.98	0.85
Lu	0.08	0.46	0.15	0.09	0.04	0.19	0.10	1.01
K <sub>2</sub> O/Na <sub>2</sub> O	0.65	0.53	0.32	0.18	0.40	0.34	0.37	0.29
K/Rb	385.24	244.01	223.40	226.22	234.03	265.59	261.67	277.27
Ba/Sr	2.26	1.39	1.18	0.67	1.05	0.91	1.60	0.71
Rb/Sr	0.16	0.10	0.16	0.17	0.17	0.09	0.09	0.07
La/Yb	38.09	16.93	38.46	29.72	57.53	28.26	96.53	49.55
Eu/Eu*	0.83	0.63	0.83	0.81	0.80	0.78	0.78	0.75
CIPW	NORM							
Q	23.87	11.38	15.62	27.39	22.85	13.48	18.12	17.48
C	0.33	-	-	-	-	-	-	-
Or	17.92	14.83	10.45	6.05	11.58	10.86	11.05	9.84
Ab	39.54	40.07	46.81	47.68	41.03	46.20	42.64	47.97
An	12.15	17.85	16.62	13.20	15.43	17.48	18.08	14.07
Di	-	3.56	2.41	1.97	0.42	2.76	1.01	3.25
Hy	3.14	5.38	3.73	1.54	3.99	4.19	4.58	3.28
Mgn	2.00	4.57	3.05	1.45	3.63	3.31	3.05	2.75
Il	0.70	1.36	0.95	0.53	0.78	1.22	0.97	0.95
Ap	0.35	1.01	0.37	0.18	0.30	0.51	0.50	0.43

## BRIDGER

SAMPLE	HL-6	HL-7	HL-8	AVG n=12	STD
SiO2	62.12	65.74	65.28	65.44	3.61
TiO2	0.65	0.64	0.61	0.55	0.13
Al2O3	17.80	16.25	16.87	16.85	0.91
Fe2O3-T	4.95	4.41	5.10	4.15	1.07
MgO	1.74	1.60	1.69	1.58	0.64
CaO	5.01	3.77	4.86	3.78	1.21
Na2O	4.96	4.92	5.06	5.52	1.21
K2O	1.51	1.60	1.58	1.72	0.67
MnO	0.06	0.06	0.06	0.05	0.02
P2O5	0.25	0.20	0.25	0.21	0.08
LOI	0.83	0.98	0.65	0.80	0.49
TOTAL	99.85	100.18	101.99	100.64	0.88
Rb	51.8	70.7	51.8	55.7	20.06
Ba	729	633	601	619	332.11
Cs	0.50	1.21	0.69	0.51	0.28
Sr	843	662	624	550	245.34
Pb	13	11	12	14	4.31
Th	6.1	13	5.6	7.8	3.40
U	0.55	3.1	0.84	1.2	0.78
Sc	7.76	10.4	10.7	5.83	3.11
V	72.9	65.4	78.6	66.8	17.83
Cr	11.8	10.2	9.18	13.2	5.37
Co	10	14	12	8.9	3.06
Cu	0.67	23	39	5.9	11.76
Zn	86	81	78	72	28.68
Ga	26.2	22.9	22.9	24.8	2.95
Y	10	9.6	22	15	8.21
Zr	165	172	190	165	36.79
Nb	8.9	5.3	7.1	7.2	2.84
Hf	6.0	4.0	5.1	5.1	1.71
Ta	3.6	0.62	0.38	0.65	0.96

## BRIDGER

SAMPLE	HL-6	HL-7	HL-8	AVG n=12	STD
La	49.6	85.4	57.5	42.2	20.10
Ce	97.8	161	112	83.3	38.89
Nd	47.2	60.7	52.8	34.8	16.09
Sm	8.30	9.79	9.07	6.52	3.15
Eu	1.94	1.53	1.94	1.45	0.60
Tb	0.61	1.0	0.81	0.57	0.30
Yb	1.3	3.2	1.8	1.2	0.72
Lu	0.17	0.40	0.23	0.23	0.26
K <sub>2</sub> O/Na <sub>2</sub> O	0.30	0.33	0.31	0.34	0.15
K/Rb	241.24	188.33	252.97	330.92	257.32
Ba/Sr	0.87	0.96	0.96	1.08	0.47
Rb/Sr	0.06	0.11	0.08	0.11	0.04
La/Yb	37.58	26.94	32.86	39.13	20.65
Eu/Eu*	0.81	0.54	0.72	0.70	0.09
CIPW					
Q	14.61	20.69	17.40	15.81	
C	-	0.05	-	-	
Or	9.01	9.53	9.21	10.13	
Ab	42.37	41.97	42.24	46.54	
An	22.06	17.54	18.40	16.06	
Di	1.12	-	3.04	1.03	
Hy	5.39	5.31	4.35	6.26	
Mgn	3.62	3.22	3.65	1.86	
Il	1.25	1.23	1.14	1.04	
Ap	0.58	0.47	0.57	.49	

## LOUIS LAKE BATHOLITH

SAMPLE	LLB-2	LLB-4	LLB-5	LLB-6	LLB-7	LLB-8	LLB-9	LLB-10
SiO2	64.04	70.59	63.71	66.20	66.14	62.80	66.22	67.18
TiO2	0.70	0.36	0.69	0.59	0.58	0.65	0.65	0.57
Al2O3	16.10	15.05	16.64	15.52	15.77	16.98	16.21	15.79
Fe2O3-T	4.99	2.78	5.21	4.54	4.39	5.03	4.77	4.20
MgO	2.20	1.14	2.26	1.71	1.67	2.06	1.75	1.54
CaO	4.15	2.69	4.61	3.92	3.63	4.47	3.99	3.62
Na2O	4.87	4.09	5.08	4.65	4.49	5.15	4.61	4.53
K2O	1.56	3.17	1.97	2.32	2.72	2.01	2.29	2.61
MnO	0.08	0.04	0.08	0.06	0.07	0.07	0.07	0.07
P2O5	0.30	0.11	0.31	0.25	0.24	0.30	0.27	0.23
LOI	1.33	0.47	0.76	0.89	0.42	0.67	0.48	0.49
TOTAL	100.31	100.49	101.29	100.63	100.12	100.20	101.31	100.63
Rb	77.5	75.3	47.2	59.1	66.1	52.5	61.7	64.5
Ba	725	2874	1191	1266	1380	1264	1087	1233
Cs	1.27	2.11	1.99	1.96	2.35	2.46	2.25	2.37
Sr	637	775	870	738	696	816	727	685
Pb	15	18	13	22	22	15	21	26
Th	11	7.5	9.5	9.7	12	5.6	13	13
U	5.5	2.3	2.5	2.4	2.3	2.7	2.5	2.6
Sc	8.81	2.87	9.10	7.54	6.50	8.94	7.00	6.43
V	99.3	63.8	98.0	85.5	68.0	83.3	80.83	89.0
Cr	23.1	4.34	22.8	12.5	11.5	20.3	15.96	16.4
Co	11	6.1	13	9.5	13	13	10	9.2
Cu	BD	BD	BD	ND	ND	1.9	ND	ND
Zn	92	47	85	81	82	88	88	71
Ga	19.7	18.2	22.9	18.5	19.8	22.8	22.7	20.9
Y	20	3.8	21	22	16	14	21	21
Zr	187	101	218	188	189	216	210	197
Nb	8.7	1.7	6.3	8.8	11	7.6	11	8.9
Hf	6.0	3.6	7.0	6.6	6.6	6.1	7.0	6.1
Ta	0.48	0.31	0.45	0.84	1.0	0.32	1.2	1.0



LOUIS	LAKE							
SAMPLE	LLB-2	LLB-4	LLB-5	LLB-6	LLB-7	LLB-8	LLB-9	LLB-10
La	64.4	45.1	58.3	46.1	56.4	33.7	55.1	47.8
Ce	121	74.8	121	103	112	73.9	121.5	111
Nd	51.2	22.4	54.1	51.5	50.4	40.5	54.7	46.4
Sm	9.35	3.10	10.5	10.3	9.25	7.58	10.5	8.95
Eu	2.21	1.52	2.34	2.18	2.15	1.94	2.40	2.04
Tb	0.72	0.18	0.80	0.82	0.72	0.62	0.82	0.74
Yb	1.9	0.59	1.8	2.2	1.9	1.1	2.0	1.9
Lu	0.24	0.06	0.25	0.27	0.26	0.21	0.30	0.27
K2O/Na2O	0.32	0.77	0.39	0.50	0.61	0.39	0.50	0.58
K/Rb	166.56	348.73	345.32	325.23	341.80	318.19	307.99	335.35
Ba/Sr	1.14	3.71	1.37	1.72	1.98	1.55	1.49	1.80
Rb/Sr	0.12	0.10	0.05	0.08	0.09	0.06	0.08	0.09
La/Yb	33.89	76.44	32.03	21.15	30.00	31.20	27.14	25.03
Eu/Eu*	0.81	1.74	0.76	0.72	0.80	0.87	0.78	0.77
CIPW	NORM							
Q	18.16	27.11	14.30	20.12	19.80	13.32	19.69	21.08
C	-	0.26	-	-	-	-	-	-
Or	9.31	18.72	11.58	13.74	16.12	11.94	13.42	15.37
Ab	41.62	34.60	42.74	39.44	38.11	43.79	38.68	38.20
An	17.64	12.62	16.69	14.66	14.89	17.36	16.64	14.99
Di	0.94	-	3.23	2.56	1.29	2.36	0.99	1.13
Hy	6.62	3.72	5.69	4.47	4.95	5.63	5.30	4.59
Mgn	3.65	2.02	3.76	3.30	3.19	3.66	3.43	3.04
Il	1.34	0.68	1.30	1.12	1.11	1.24	1.22	1.08
Ap	0.70	0.26	0.71	0.58	0.56	0.70	0.62	0.53

## LOUIS LAKE

SAMPLE	LLB-11	HL-13	HL-15	HL-16	HL-17	SC-7	AVG 15	STD
SiO2	66.39	64.68	62.87	60.60	63.53	62.74	64.84	2.40
TiO2	0.62	0.64	0.79	0.93	0.79	0.70	0.66	0.13
Al2O3	15.78	16.29	16.66	17.05	16.62	17.11	16.25	0.60
Fe2O3-T	4.34	4.66	5.37	6.33	5.28	5.96	4.85	0.82
MgO	1.72	1.83	2.16	2.55	1.90	2.19	1.90	0.35
CaO	3.73	4.04	4.80	5.56	4.53	5.32	4.22	0.71
Na2O	4.47	4.64	4.88	5.03	4.86	5.74	4.79	0.38
K2O	2.61	2.66	1.91	1.60	2.06	1.44	2.21	0.49
MnO	0.08	0.07	0.07	0.09	0.08	0.11	0.07	0.01
P2O5	0.24	0.26	0.32	0.39	0.32	0.26	0.27	0.06
LOI	0.49	0.53	0.57	0.83	0.74	0.33	0.64	0.25
TOTAL	100.46	100.31	100.40	100.95	100.70	101.90	100.69	0.49
Rb	64.5	57.2	38.9	34	43.0	37.4	55.6	13.37
Ba	1235	1218	1702	1152	1459	326	1294	537.46
Cs	2.47	0.21	0.22	0.26	0.33	0.17	1.46	0.95
Sr	730	751	929	896	872	642	769	90.72
Pb	20	20	12	12	13	21	18	4.25
Th	11	12	7.2	5.2	7.5	3.3	9.0	2.89
U	2.4	0.66	0.60	0.41	0.90	0.61	2.0	1.30
Sc	6.80	8.24	9.11	10.4	8.29	12.4	8.03	2.12
V	84.9	68.9	75.1	103	94.7	99.9	85.3	12.39
Cr	24.2	17.5	22.8	24.6	13.9	42.2	19.4	8.45
Co	9.5	11	12	14	11	13	11	2.04
Cu	BD	26	1.6	24	5.2	16	5.4	9.02
Zn	72	79	94	102	100	100	84	14.00
Ga	19.2	21.4	21.7	23.8	24.8	30.7	21.9	3.11
Y	19	17	14	23	14	30	18	5.97
Zr	191	207	210	260	202	190	198	32.54
Nb	10	5.8	7.8	7.9	8.9	13	8.4	2.56
Hf	5.6	7.5	6.9	7.2	7.4	4.9	6.3	1.02
Ta	1.0	0.29	0.30	0.42	0.33	0.76	0.63	0.33

LOUIS	LAKE							
SAMPLE	LLB-11	HL-13	HL-15	HL-16	HL-17	SC-7	AVG	STD
La	47.6	58.9	61.7	59.6	64.0	33.6	52.3	9.85
Ce	108	114	126	127	128	73.7	108	19.25
Nd	48.5	44.1	53.3	63.5	54.5	39.0	48.2	9.38
Sm	8.96	9.25	10.0	11.5	10.0	8.36	9.12	1.92
Eu	2.11	1.96	2.43	2.59	2.35	1.72	2.14	0.28
Tb	0.70	0.71	0.75	0.88	0.75	0.78	0.71	0.16
Yb	1.8	1.5	1.8	1.8	1.6	2.7	1.8	0.47
Lu	0.27	0.17	0.20	0.24	0.20	0.36	0.27	0.17
K2O/Na2O	0.58	0.57	0.39	0.32	0.42	0.25	0.47	0.14
K/Rb	336.01	386.35	408.38	388.36	397.15	320.72	337.58	56.48
Ba/Sr	1.69	1.62	1.83	1.29	1.67	0.51	1.67	0.67
Rb/Sr	0.09	0.08	0.04	0.04	0.05	0.06	0.07	0.02
La/Yb	25.87	40.07	34.47	34.06	39.51	12.63	33.11	13.89
Eu/Eu*	0.81	0.73	0.83	0.77	0.81	0.69	0.79	0.25
CIPW	NORM							
Q	20.29	16.81	14.72	11.02	15.70	10.55	16.46	
C	-	-	-	-	-	-	-	
Or	15.43	15.76	11.31	9.44	12.18	8.38	13.01	
Ab	37.83	39.35	41.36	42.50	41.13	47.82	40.38	
An	15.29	15.80	17.94	19.19	17.46	16.41	16.25	
Di	1.32	2.07	3.05	4.64	2.35	6.35	2.33	
Hy	4.97	5.01	5.47	5.95	5.12	4.35	6.89	
Mgn	3.15	3.39	3.90	4.58	3.83	4.25	2.17	
Il	1.18	1.22	1.50	1.76	1.50	1.31	1.25	
Ap	0.56	0.60	0.74	0.90	0.74	0.59	0.62	

## Appendix B

## Sample locations in UTM\* coordinates

Middle Mountain pluton

Sample	Grid Location	Sample	Grid Location
RL-1 <sup>a</sup>	480608mN 60850mE	MM-1 <sup>c</sup>	480575mN 61300mE
RL-2 <sup>a</sup>	480625mN 60845mE	MM-2 <sup>c</sup>	480560mN 61290mE
RL-3 <sup>a</sup>	480632mN 60842mE	MM-3 <sup>c</sup>	480525mN 61245mE
RL-4 <sup>a</sup>	480640mN 60842mE	MM-4 <sup>c</sup>	480550mN 61250mE
RL-5 <sup>a</sup>	480638mN 60870mE	MM-5 <sup>c</sup>	480625mN 61312mE
RL-6 <sup>a</sup>	480700mN 60950mE	BL-1 <sup>b</sup>	480062mN 61331mE
RL-7 <sup>a</sup>	480710mN 60951mE	BL-2 <sup>b</sup>	480100mN 61331mE
RL-8 <sup>a</sup>	480715mN 60952mE	BL-3 <sup>b</sup>	480130mN 61335mE
GL-1 <sup>b</sup>	480055mN 61460mE	BL-4 <sup>b</sup>	440152mN 61352mE
GL-2 <sup>b</sup>	480112mN 61450mE	BL-5 <sup>b</sup>	480212mN 61354mE
GL-3 <sup>c</sup>	480435mN 61485mE	GL-5 <sup>c</sup>	480535mN 61450mE
GL-4 <sup>c</sup>	480450mN 61465mE		

a=samples from Simpson Lake 7.5 Minute Series, Wyoming

b=samples from Ink Wells 7.5 Minute Series, Wyoming

c=samples from Torrey Lake 7.5 Minute Series, Wyoming

\* Universal Transverse Mercator grid coordinates.

Dome Peak Pluton

Sample	Grid Location	Sample	Grid Location
NFL-1 <sup>a</sup>	477754mN 59376mE	PC-2 <sup>a</sup>	478518mN 59277mE
NFL-2 <sup>a</sup>	477724mN 59375mE	PC-3 <sup>a</sup>	478560mN 59260mE
NFL-3 <sup>a</sup>	477700mN 59327mE	PC-4 <sup>a</sup>	478590mN 59255mE
NFL-4 <sup>a</sup>	477675mN 59278mE	PC-5 <sup>a</sup>	478678mN 59255mE
NFL-5 <sup>a</sup>	477675mN 59200mE	FL-1 <sup>c</sup>	
NFL-6 <sup>b</sup>	477665mN 59126mE	FL-1A <sup>c</sup>	
NFL-7 <sup>b</sup>	477590mN 59078mE	FL-7 <sup>c</sup>	
PC-1 <sup>a</sup>	478490mN 59270mE		

a=samples from Square Top Mountain 7.5 Minute Series, Wyoming.  
 b=samples from Kendall Mountain 7.5 Minute Series, Wyoming.  
 c=samples from Fremont Lake North 7.5 Minute Series, Wyoming.

Mount Owen Pluton

Sample	Grid Location	Sample	Grid Location
MO-2 <sup>a</sup>	484560mN 51695mE	GT-2 <sup>a</sup>	484895mN 51485mE
MO-2 <sup>a</sup>	484558mN 51728mE	GT-3 <sup>a</sup>	484880mN 51480mE
MO-3 <sup>a</sup>	484558mN 51750mE	GT-4 <sup>a</sup>	484875mN 51435mE
MO-4 <sup>a</sup>	484555mN 51775mE	GT-5 <sup>a</sup>	484890mN 51400mE
MO-5 <sup>a</sup>	484560mN 51800mE	RM-1 <sup>b</sup>	486180mN 50485mE
MO-6 <sup>a</sup>	484555mN 51835mE	RM-2 <sup>b</sup>	486185mN 50485mE
GT-1 <sup>a</sup>	484895mN 51495mE	RM-3 <sup>b</sup>	486200mN 50445mE

a=samples from Mount Moran 7.5 Minute Series, Wyoming.  
 b=samples from Rammel Mountain 7.5 Minute Series, Wyoming.

Bridger Batholith

Sample	Grid Location		Sample	Grid Location	
SL-1 <sup>a</sup>	476685mN	60825mE	SL-9 <sup>a</sup>	476375mN	60700mE
SL-2 <sup>a</sup>	476680mN	60827mE	LL8 <sup>a</sup>	476412mN	60650mE
SL-3 <sup>a</sup>	476675mN	60830mE	LL12 <sup>a</sup>	476390mN	60612mE
SL-4 <sup>a</sup>	476660mN	60825mE	HL-4 <sup>b</sup>	475610mN	62298mE
SL-5 <sup>a</sup>	476625mN	60810mE	HL-5 <sup>b</sup>	475615mN	62280mE
SL-6 <sup>a</sup>	476600mN	60812mE	HL-6 <sup>b</sup>	475630mN	62278mE
SL-7 <sup>a</sup>	476575mN	60808mE	HL-7 <sup>b</sup>	475645mN	62270mE
SL-8 <sup>a</sup>	476515mN	60800mE	HL-8 <sup>b</sup>	475660mN	62260mE

a=samples from Bridger Lakes 7.5 Minute Series, Wyoming.

b=samples from Halls Mountain 7.5 Minute Series, Wyoming.

Louis Lake Batholith

Sample	Grid Location		Sample	Grid Location	
LLB-1 <sup>a</sup>	47296mN	6725mE	LLB-9 <sup>a</sup>	47116mN	6804mE
LLB-2 <sup>a</sup>	47293mN	6724mE	LLB-10 <sup>a</sup>	47118mN	6807mE
LLB-3 <sup>a</sup>	47290mN	6726mE	LLB-11 <sup>a</sup>	47108mN	6806mE
LLB-4 <sup>a</sup>	47267mN	6740mE	HL-13 <sup>b</sup>	475055mN	61885mE
LLB-5 <sup>a</sup>	47240mN	6749mE	HL-15 <sup>b</sup>	474950mN	61975mE
LLB-6 <sup>a</sup>	47130mN	6790mE	HL-16 <sup>b</sup>	474945mN	61980mE
LLB-7 <sup>a</sup>	47125mN	6802mE	HL-17 <sup>b</sup>	474920mN	61990mE
LLB-8 <sup>a</sup>	47251mN	6744mE			

a=samples from Lander 1:100,000 Series, Wyoming.

b=samples from Horseshoe Lake 7.5 Minute Series, Wyoming.

**Appendix C****Analytical Methods****C1: Initial Sample Processing**

Samples are hand-trimmed in the field to remove weathering rinds. Due to the coarse grain size of some of the granites up to 1.5kg of rock is sampled. Weathered fragments if present, are handpicked and discarded during preliminary crushing stages. Samples are then pulverised (-200 mesh; <.004mm) in porcelain grinding disks. This grinding technique is preferred to eliminate possibilities of trace element contamination (Ta) from tungsten carbide grinding equipment. A sufficient quantity of each sample (0.5kg) is processed to insure against effects of rock heterogeneities.

**C2: X-Ray Fluorescence****a) Sample Preparation and Analytical Technique**

Major element concentrations were determined by X-ray fluorescence (XRF) on fused glass discs using an automated Rigaku 3064 XRF spectrometer. The fused discs are prepared (following the methods of Norrish and Hutton, 1969) from approximately 0.5 grams of powdered sample, about 2.7 grams of Spectoflux-105, and several beads of  $\text{NH}_4\text{NO}_3$  (oxidising agent). The mixture is then melted and heated in a Pt crucible for ten minutes, then molded and cooled in a mechanical heating press.

Trace element concentrations for Rb, Ba, Sr, Pb, Y, Zr,

Table C1: Information for X-Ray Fluorescence Analyses

Element	Electron Shell	Operating KV	Lower Limit Detection (ppm)	Lower Limit Determination (ppm)
Si	Ka 1,2	35	-	100
Ti	Ka 1,2	35	-	100
Al	Ka 1,2	35	-	100
Fe	Ka 1,2	35	-	20
Mg	Ka 1,2	35	-	100
Ca	Ka 1,2	35	-	100
Na	Ka 1,2	35	-	100
K	Ka 1,2	35	-	100
Mn	Ka 1,2	35	7.0	22
P	Ka 1,2	35	-	100
Rb	Ka 1,2	60	1.022	3.0
Sr	Ka 1,2	60	0.94	3.0
Pb	Ka 1,2	60	3.28	9.8
V	Ka 1,2	50	-	-
Ni	Ka 1,2	50	0.68	2.0
Y	Ka 1,2	60	1.08	3.2
Zr	Ka 1,2	60	0.78	2.5
Nb	Ka 1,2	60	2.0	3.0
Cu	Ka 1,2	60	1.70	5.1
Zn	Ka 1,2	60	2.04	6.1
Ga	Ka 1,2	60	.90	2.70

--not determined



Nb, Cu, Zn, Ga, Ni, V, and Cr are determined by XRF from pressed pellets. The pellets are prepared from about 8 grams of powdered sample containing 5 drops of polyvinyl alcohol (binding agent) and pressed with a boric acid backing. The pellet is then subjected to 10 tons of pressure under a hydraulic press for five minutes.

#### **b) Detection Limits**

A list of measured energies, detection limits and lower limits of determination are given in Table C1. Detection limits describe the minimum concentration of an element needed for qualitative analytical detection. Lower limit of determination describes the minimum concentration of an element needed for quantitative analytical determination.

#### **c) Accuracy and Precision**

Tables C2-C6 present individual values, mean and standard deviation values for standards run as unknown samples. Accepted element abundances (Govindaraju, 1989) also are given. Calculated accuracy (closeness of analytical value to an accepted value, calculated as % deviation from the accepted value) and precision (ability to repeat measurements, calculated as coefficient of variation) is also presented.

For BCR-1 the precision for  $\text{SiO}_2$ ,  $\text{TiO}_2$ ,  $\text{Al}_2\text{O}_3$ ,  $\text{Fe}_2\text{O}_3$ ,  $\text{MgO}$ ,  $\text{CaO}$ ,  $\text{K}_2\text{O}$  and  $\text{P}_2\text{O}_5$  is less than 1%, for  $\text{Na}_2\text{O}$  and  $\text{MnO}$  it is less than 2% (Table C2). For GS-N the precision for Rb, Ba, Sr, V,

Table C2: Major (XRF) and trace (INNA) element analyses of standard BCR-1 (basalt)

SAMPLE	BCR1-A	BCR1-B	BCR1-C	BCR1-D	BCR1-E	BCR1-F	BCR-1H
SiO2	54.13	54.21	53.91	54.14	54.22	54.05	54.13
TiO2	2.26	2.24	2.27	2.24	2.25	2.26	2.27
Al2O3	13.40	13.51	13.53	13.46	13.46	13.43	13.55
Fe2O3-T	13.16	13.17	13.15	13.17	13.17	13.16	13.16
MgO	3.73	3.71	3.72	3.77	3.68	3.76	3.76
CaO	7.09	7.12	7.01	7.11	7.08	7.09	7.04
Na2O	3.32	3.34	3.30	3.18	3.36	3.37	3.38
K2O	1.71	1.71	1.71	1.70	1.72	1.72	1.73
MnO	0.19	0.18	0.18	0.19	0.18	0.18	0.18
P2O5	0.36	0.36	0.36	0.36	0.36	0.37	0.36
LOI	0.62	0.62	0.62	0.62	0.62	0.62	0.62
TOTAL	99.96	100.15	99.76	99.94	100.09	100.01	100.18
Cs	0.9	0.97	1.0	0.9	0.9	0.9	0.97
Th	6.1	5.95	5.6	5.7	5.7	5.8	5.82
U	2.09	1.92	1.66	1.80	1.72	1.83	1.76
Sc	32.6	32.54	33.1	33.1	33.0	32.6	32.75
Hf	5.2	5.15	5.2	5.3	5.1	5.1	5.20
Ta	0.82	0.81	0.78	0.76	0.76	0.74	0.77
La	25.3	25.50	25.4	25.5	26.2	26.6	26.20
Ce	53.3	53.90	54.1	55.2	54.0	55.0	54.60
Nd	28.20	31.20	29.50	27.00	28.70	27.10	27.80
Sm	7.28	7.29	6.89	6.80	6.96	6.97	6.89
Eu	1.97	1.95	1.98	1.98	2.02	1.96	1.99
Tb	1.15	1.05	1.08	1.03	1.05	0.96	1.02
Yb	3.38	2.95	3.40	3.31	3.39	3.17	3.20
Lu	0.50	0.50	0.51	0.51	0.49	0.50	0.48

SAMPLE	BCR-1AP	BCR-1BP	AVG	STD	ACC	A%	P%	n
SiO2	54.10	54.14	54.11	0.09	54.06	0.10	0.16	9
TiO2	2.25	2.27	2.26	0.01	2.24	0.76	0.55	9
Al2O3	13.47	13.50	13.48	0.04	13.64	1.18	0.33	9
Fe2O3-T	13.17	13.19	13.16	0.01	13.41	1.83	0.08	9
MgO	3.79	3.70	3.74	0.03	3.48	7.35	0.92	9
CaO	7.07	7.07	7.08	0.03	6.95	1.82	0.45	9
Na2O	3.26	3.33	3.31	0.06	3.27	1.35	1.80	9
K2O	1.70	1.71	1.71	0.01	1.69	1.28	0.47	9
MnO	0.18	0.18	0.18	0	0.18	2.26	1.90	9
P2O5	0.36	0.36	0.36	0	0.36	0.19	0.70	9
LOI	0.62	0.62	0.62	0	1.56	60.26	0	9
TOTAL	99.97	100.05	100.01	0.12	100.84	0.82	0.12	9
Cs	0.77	1.04	0.93	0.07	0.96	3.12	7.75	9
Th	5.76	5.79	5.80	0.12	5.98	2.95	2.04	9
U	1.67	1.62	1.79	0.14	1.75	2.03	7.80	9
Sc	32.60	32.50	32.75	0.23	32.60	0.47	0.69	9
Hf	4.90	5.29	5.16	0.11	4.95	4.20	2.11	9
Ta	0.79	0.76	0.78	0.02	0.81	4.12	3.15	9
La	25.00	26.20	25.76	0.51	24.90	3.46	1.96	9
Ce	53.70	54.10	54.21	0.58	53.70	0.95	1.07	9
Nd	28.70	27.70	28.43	1.24	28.80	1.27	4.35	9
Sm	7.20	7.10	7.04	0.17	6.59	6.86	2.43	9
Eu	1.79	2.00	1.96	0.06	1.95	0.51	3.23	9
Tb	1.05	0.99	1.04	0.05	1.05	0.74	4.89	9
Yb	3.20	3.23	3.25	0.14	3.38	3.91	4.16	9
Lu	0.48	0.48	0.50	0.01	0.51	2.94	2.42	9

Table C.2 cont'd:

AVG=Average value (Major elements in wt%, trace elements in ppm)

STD=Standard deviation of mean value at 1 confidence interval

ACC=Accepted value (Govindaraju, 1989)

A%=Accuracy [(average-accepted)/accepted]x100

P%=Precision (STDx100)/AVG

n=number of samples analyzed

Table C3: Trace element analyses (XRF) of standard GS-N (granite)

	GS-N1	GS-N2	GS-N3	GS-N4	GS-N5	GS-N6
Rb	188	189	187	188	173	173
Ba	1439	1404	1394	1423	1388	1394
Sr	585	583	584	585	577	573
Pb	49	51	50	50	48	48
V	65.3	70.0	63.6	67.4	71.5	66.8
Cr	49	49	51	50	48	51
Cu	17	17	16	12	3.6	18
Zn	45	44	44	42	35	39
Ga	24.2	18.8	20.3	18.3	18.5	21.2
Y	23	21.7	22.32	21.29	17.91	17.42
Zr	219	216	217	218	209	209
Nb	21	21	21	21	24	23

	GS-N7	AVG	STD	ACC	A%	P%	n
Rb	173	181	7.4	185	1.72	4.09	7
Ba	1403	1407	16.7	1400	0.50	1.19	7
Sr	582	581	4.6	570	2.00	0.80	7
Pb	58	51	2.8	53	4.09	5.57	7
V	69.6	67.7	2.6	65	4.22	3.81	7
Cr	48.6	59.6	0.94	55	10.20	1.90	7
Cu	4.3	13	5.8	20	37.04	45.97	7
Zn	37	41	3.8	48	15.26	9.22	7
Ga	22.1	20.5	2.01	22	6.84	9.80	7
Y	17	20	2.3	19	5.59	11.65	7
Zr	209	214	4.2	235	8.79	1.95	7
Nb	24	22	1.4	21	6.98	6.11	7

AVG=Average value (All values in ppm)

STD=Standard deviation of mean value at 1 confidence interval

ACC=Accepted value (Govindaraju, 1989)

A%=Accuracy [(average-accepted)/accepted]x100

P%=Precision (STD/AVG)x100

n=number of samples analyzed

Table C4: Trace element analyses (XRF) of standard AN-G (anorthosite)

	AN-G	AN-G1	AN-G2	AN-G3	AN-G4	AN-G5	AN-G6	AN-G7
Rb	2.7	2.5	2.4	1.9	2.7	2.2	2.4	0.9
Ba	36.8	24.8	29.1	29.5	36.8			
Sr	77.2	77.9	76.8	77.1	77.2	75.8	74.9	77.2
Pb	5.2	7.7	6.5	4.4	5.2	4.2	8.4	4.0
V	72.3	82.6	75.9	77.4	72.3			
Cr	74.6	68.5	63.4	64.6	74.6			
Cu	26.6	25.4	25.46	25	0.65	23	1.4	18
Zn	25	25	25	27	21	23	2.3	20
Ga	17.1	18.5	17.6	23.1	18.9	20.3	1.4	18.4
Y	8.7	9.0	8.0	8.7	8.7	9.9	.26	6.3
Zr	18.9	19.4	19.2	19.4	18.9	17.1	2.1	26.6
Nb	2.6	3.0	3.1	3.1	2.6	2.8	.31	1.3

	AN-G8	AN-G9	AVG	STD	ACC	A	P	n
Rb	0.9	2.7	2.00	0.94	1	46.8	99.6	10
Ba			31.4	4.70	34	15.0	7.7	5
Sr	75.1	76.1	76.5	0.97	76	1.3	0.7	10
Pb	BD	0.4	4.6	2.6	2	56.4	129.3	10
V			76	3.8	70	56	8.7	5
Cr			69.1	4.79	50	6.9	38.3	5
Cu	18	18	18	9.0	19	50	4.7	10
Zn	21	23	23	1.9	20	8.1	17	10
Ga	18.4	19.2	19.0	1.54	18	8.1	5.7	10
Y	9.5	7.0	8.4	1.0	8	12	4.8	10
Zr	27.9	27.1	22.3	4.26	15	19.2	48.3	10
Nb	3.1	3.2	2.8	0.54	2	19	40	10

AVG=Average value (All values in ppm)

STD=Standard deviation of mean value at 1 confidence interval

ACC=Accepted value (Govindaraju, 1989)

A%=Accuracy [(average-accepted)/accepted]x100

P%=Precision (STD/AVG)x100

n=number of samples analyzed

Table C5: Trace element analyses (XRF) of standard NIM-G (granite)

	NIM-G	NIM-G	NIM-G	NIM-G	NIM-G
Rb	325	326	323	325	315
Ba	103	103	97.2	99.7	101
Sr	10.9	11.0	10.7	11.6	12.9
Pb	35	38	35	38	42
V	BD	BD	0.6	BD	BD
Cr	1.6	3.3	3.6	3.6	3.4
Cu	4.2	3.1	5.6	6.7	2.1
Zn	51	55	56	53	55
Ga	27.9	29.1	28.9	29.0	29.5
Y	140	140	142	142	160
Zr	267	269	266	270	247
Nb	48	48	48	48	46

	AVG	STD	ACC	A%	P%	n
Rb	329	4.39	320	0.89	1.36	5
Ba	100	2.37	120	16.15	2.35	5
Sr	11.4	0.81	10	14.24	7.09	5
Pb	38	2.46	40	6.03	6.55	5
V	0.15	0.26	2	93.63	173.21	5
Cr	3.01	0.81	12	74.92	26.81	5
Cu	4.3	1.67	12	63.85	38.50	5
Zn	54	1.78	50	7.25	3.33	5
Ga	28.8	0.53	27	6.83	1.84	5
Y	143	3.54	143	0.13	2.48	5
Zr	264	8.69	300	12.03	3.29	5
Nb	48	0.79	53	10.21	1.66	5

AVG=Average value (All values in ppm)  
 STD=Standard deviation of mean value at 1 confidence interval  
 ACC=Accepted value (Govindaraju, 1989)  
 A%=Accuracy  $[(\text{average}-\text{accepted})/\text{accepted}]\times 100$   
 P%=Precision  $(\text{STD}/\text{AVG})\times 100$   
 n=number of samples analyzed  
 BD=Below detection

Table C6: Trace element analyses (XRF) of standard W2 (diabase)

	W2-1	W2-2	W2-3	W2-4	W2-5	W2-6
Rb	19.9	20.7	20.6	21.1	18.0	18.5
Ba	195	186	193	200	196	191
Sr	200	200	200	200	197	196
Pb	9.7	12	10	11	9.6	12
V	270	270	265	270	267	264
Cr	101	100	99.5	102	82.7	80.3
Cu	84	84	85	82	86	71
Zn	78	82	76	77	83	78
Ga	19.9	20.3	20.3	15.8	18.1	19.9
Y	22	23	24	22	24	23
Zr	95	96	96	95	93	93
Nb	8.6	9.3	8.6	8.5	9.9	10

	W2-7	AVG	STD	ACC	A%	P%	n
Rb	17.4	19.4	1.40	20	2.92	7.23	7
Ba	188	192	4.41	182	5.90	2.29	7
Sr	195	198	2.08	194	2.26	1.05	7
Pb	12	10	0.87	9	16.44	8.00	7
V	262	267	3.12	262	1.87	1.17	7
Cr	82.5	92.5	9.31	93	0.49	10.06	7
Cu	71	81	5.98	103	21.64	7.41	7
Zn	76	78	2.42	77	2.26	3.08	7
Ga	20.3	19.2	1.57	20	3.97	8.20	7
Y	24	23	0.79	24	3.02	3.41	7
Zr	93	95	1.38	94	0.70	1.45	7
Nb	9.4	9.2	0.58	8	16.29	6.27	7

AVG=Average value (All values in ppm)  
 STD=Standard deviation of mean value at 1 confidence interval  
 ACC=Accepted value (Govindaraju, 1989)  
 A%=Accuracy [(average-accepted)/accepted]x100  
 P%=Precision (STD/AVG)x100  
 n=number of samples analyzed

Cr and Zr is less than 5% For Pb, Zn, Ga and Nb it is less than 10% For Y the precision is less than 15% (Table C3).

The poor precision of AN-G for Rb, Pb, Zn, Zr and Nb may be due to the accepted values being close to the lower limits of determination for those elements (Table C4). The precision for NIM-G is less than 5% for Rb, Ba, Zn, Ga, Y, Zr, and Nb. For Sr and Pb the precision is less than 10% V, Cu and Cr show poor precision due to their accepted values being close to the lower limits of determination for these elements (Table C5). The precision for W-2 is less than 5% for Ba, Sr, V, Zn, Y, and Zr. For Rb, Pb, Cr, Cu, Ga and Nb it is less than 10% (Table C6).

As this study concentrated on the petrogenesis of granites, the precision of the trace elements analysed by XRF is reported for the two granite standards GS-N and NIM-G, where the lower precision value is reported (i.e. higher number).

The precision for Rb, Ba, V, Cr, Zr is less than 5% Sr, Pb, Zn, Ga, and Nb have precision less than 10% The precision for Y is less than 12%

### **C3: Instrumental Neutron Activation Analyses**

#### **a) Sample preparation and analytical technique**

Hf, Ta, Sc, Cr, Co, Ba, Cs, Th, U and eight REE (La, Ce, Nd, Sm, Eu, Tb, Yb, Lu) are analysed by instrumental neutron activation analyses (INNA) using a Nuclear Data 6600 gamma-ray



Table C7: Information for instrumental neutron activation

Parent Nuclide	Daughter Nuclide	KeV	Count Time in days	Detection Limit-ppm	Determination Limit-ppm
Ba-130	Ba-131	373	7	2.0	25.0
		496*			
Ce-140	Ce-141	145*	7	0.12	1.5
Co-59	Co-60	1173*	7,40	0.05	1.0
		1332			
Cr-50	Cr-51	320*	7,40	0.3	1.0
Cs-133	Cs-134	605	7,40	0.04	0.5
		796			
Eu-151	Eu-152	245	40	0.02	0.15
		344*			
		779			
		1408*			
Hf-180	Hf-181	482*	40	0.02	0.1
La-139	La-140	329*	7	-	0.9
		487*			
		816			
		1596			
Lu-176	Lu-177	208*	7	-	0.04
Nd-146	Nd-147	91	7	-	2.5
		531			
Sc-45	Sc-46	889*	7,40	0.2	0.5
		1121*			
Sm-152	Sm-153	103*	7	-	0.5
Ta-181	Ta-182	1189*	40	0.002	0.04
		1221*			
		1231			
Tb-159	Tb-160	299*	7,40	0.01	0.05
		879			
		966*			
		1178			
Th-232	Pa-232	312*	40	0.04	0.1
U-238	Np-239	228	7	0.017	0.02
		278*			
Yb-174	Yb-175	177*	7	0.017	0.02
		198			

\*preferred keV

spectrometer connected to twin high-purity Ge detectors. Approximately 300 milligram sample splits are sealed in polyvinyl containers and irradiated at the Annular Core Research Reactor at Sandia National Laboratory, Albuquerque, New Mexico. All samples are irradiated

Air blowing into the irradiation chamber should assure that a constant neutron flux of  $2.7 \times 10^{13}$  passes through each sample. Two counts of released gamma rays are made 7 and 40 days after irradiation. Data for the elements Ba, U, La, Ce, Nd, Sm, Yb and Lu are taken off the short (7 day) count, Eu, Hf, Ta and Th are taken off the long (40 day) count, and Sc, Cr, Co, Cs and Tb are averaged between the short and long counts. Reference samples of fly ash standard NBS-1633 are irradiated in triplicate; two are used as calibrating standards and one is run as an unknown. The data is reduced using TEABAGS (Trace Element Analysis By Automated Gamma-ray Spectrometry, Lindstrom and Korotev, 1982) software.

#### **b) Flux correction**

During the irradiation there is no control on the absolute flux that each sample receives which could lead to significant errors in individual instrumental neutron activation analyses. Chappell and Hergt (1988) have shown that for rock samples containing >3% total FeO, the Fe content can be determined by XRF with a precision close to 0.25% (BCR1=0.08%). In INNA, the two strong Fe peaks at 1099 and

1292 keV can be measured with comparable precision. The Fe content determined by XRF can therefore be used to correct for the effects of flux gradient. The correction factor is given by;  $\text{Fe}_2\text{O}_3\text{-T(XRF)}/\text{FeO(INNA)} \times 1.111^*$ . For Ba, U, La, Ce, Nd, Sm, Yb and Lu the FeO(INNA) value will be the average FeO from the short count. For Th, Eu, Hf and Ta the FeO(INNA) value is the average FeO from the long count and for Sc, Co, Tb, Cr and Cs the correction factor is the average of the short and long correction factor. An example of this correction factor is given in Table C7. All samples are corrected for flux variation. For 90% of the samples the correction factor was between 1.03--0.97.

\*1.1111 conversion factor, FeO to  $\text{Fe}_2\text{O}_3\text{-T}$

#### c) Detection Limits

A list of parent nuclides, daughter nuclides, decay energies, detection limits and lower limits of determination are presented in Table C8.

#### d) Accuracy and Precision

Tables C2, C9-C11 present analyses of standards run as unknowns. Also presented are the mean values, standard deviation, accuracy and precision. For BCR-1, the precision for Th, Sc, Hf, La, Ce, Sm and Lu is <3% For Ta, Nd, Eu, Tb and Yb the precision is <5% For Cs, and U the precision is <10% (Table C2). For the Fly Ash run as an unknown the

Table C8: Trace element analyses (INNA) of standard BCR-1(AP) showing uncorrected and corrected data (ppm).

		7-Day	40-Day	Uncorrected	Corrected	Accepted
Cs-A	FA-1	.53	1.06	.774	.76	.96
	FA-2	.54	1.02			
Th-A/L	FA-1	5.51	6.09	L=6.0	L=5.76	5.98
	FA-2	5.62	5.91	A=5.78	A=5.69	
U-S	FA-1	1.66		1.67	1.69	1.75
	FA-2	1.67				
Sc-A	FA-1	32.02	33.46	32.96	32.43	32.60
	FA-2	32.87	33.47			
Hf-L	FA-1	5.20	5.63	5.28	5.07	4.95
	FA-2	5.21	5.38			
Ta-L	FA-1	.77	.84	.82	.79	.81
	FA-2	.79	.802			
La-S	FA-1	25.57		25.90	26.16	24.90
	FA-2	26.22				
Ce-S	FA-1	51.3		52.3	52.82	53.70
	FA-2	53.2				
Nd-S	FA-1	23.8		23.6	23.84	28.80
	FA-2	23.3				
Sm-S	FA-1	7.09		7.20	7.27	6.59
	FA-2	7.30				
Eu-L	FA-1	1.94	2.10	2.07	1.99	1.95
	FA-2	1.95	2.04			
Tb-A	FA-1	.98	1.03	1.01	.99	1.05
	FA-2	1.03	.98			
Yb-S	FA-1	3.0	3.50	3.45	3.31	3.38
	FA-2	2.81	3.39			
Lu-S	FA-1	.465		.479	.48	.51
	FA-2	.49				
FeOwt%	FA-1	11.76	12.70			Fe <sub>2</sub> O <sub>3</sub> -T*
	FA-2	12.24	12.46			13.41

S=value calculated from short count, L=value calculated from long count, A=value calculated from average of short and long count.

FA-1/2 refers to value from either Fly ash standard 1 or 2.

Short count correction factor:  $13.41 / ((11.76 + 12.24) / 2) \times 1.111 = 1.006$

Long count correction factor:  $13.41 / ((12.70 + 12.46) / 2) \times 1.111 = .96$

Average count correction factor:  $(1.006 + 0.96) / 2 = .983$

\*=Accepted XRF value in wt% (Govindaraju, 1989).

Table C9: Trace element analyses (INNA) of Fly Ash standard NBS1633a

	FA-1	FA-2	FA-3	FA-4	AVG	STD	ACC	A%	P%	n
Cs	9.44	10.8	10.92	10.68	10.46	0.59	10.42	0.38	5.69	4
Th	21.50	24.60	24.70	24.40	23.80	1.33	24.0	0.83	5.50	4
U	8.11	11.4	11.4	10.86	10.44	1.36	10.3	1.36	13.07	4
Sc	38.5	38.3	38.4	38.4	38.40	0.07	38.60	0.52	0.18	4
Hf	7.19	7.24	7.33	7.65	7.35	0.18	7.29	0.82	2.43	4
Ta	1.70	2.08	2.02	2.03	1.96	0.15	1.93	1.55	7.68	4
La	81.2	80.48	79.5	79.56	80.19	0.70	79.1	1.38	0.88	
Ce	168	172	170.1	168.7	169.70	1.53	168.3	0.83	0.90	4
Nd	73.5	84.1	73.1	76.2	76.73	4.42	75.7	1.36	5.76	4
Sm	15.3	17.7	17.4	17.35	16.94	0.95	16.83	0.65	5.64	4
Eu	3.56	3.53	3.6	3.6	3.57	0.03	3.58	0.28	0.83	4
Tb	2.23	2.52	2.65	2.72	2.53	0.19	2.38	6.30	7.41	4
Yb	6.93	7.06	7.54	7.37	7.23	0.24	7.50	3.60	3.35	4
Lu	1.03	1.08	1.06	1.07	1.06	0.02	1.08	1.85	1.76	4

AVG=Average value (All values in ppm)

STD=Standard deviation of mean value at 1 confidence interval

ACC=Accepted value (Govindaraju, 1989)

A%=Accuracy [(average-accepted)/accepted]x100

P%=Precision (STDx100)/AVG

n=number of samples analyzed

Table C10: Trace element analyses (INNA) of standard G-2 (granite)

	G-2A	G-2B	G-2C	AVG	STD	ACC	A%	P%	n
Cs	1.42	1.36	1.41	1.40	0.03	1.34	4.48	0.63	3
Th	25.5	25.06	25.66	25.41	0.25	24.70	2.87	0.33	3
U	2.17	2.46	2.70	2.44	0.22	2.07	17.87	2.96	3
Sc	3.41	3.40	3.45	3.42	0.02	3.5	2.29	0.21	3
Hf	8.96	8.60	9.01	8.86	0.18	7.90	12.15	0.69	3
Ta	0.86	0.85	0.88	0.86	0.01	0.88	2.27	0.48	3
La	87.5	89.0	90.70	89.07	1.31	89.0	0.08	0.49	3
Ce	168.6	165.0	170.30	167.97	2.35	160.0	4.98	0.47	3
Nd	56.90	48.40	58.40	54.57	4.40	55.0	0.78	2.69	3
Sm	8.17	7.87	8.01	8.02	0.12	7.2	11.39	0.51	3
Eu	1.30	1.45	1.39	1.38	0.06	1.4	1.43	1.49	3
Tb	0.47	0.50	0.47	0.48	0.01	0.48	0.00	0.98	3
Yb	1.10	1.06	1.24	1.13	0.08	0.80	41.25	2.27	3
Lu	.10	.10	.10	0.10	0.01	0.11	9.09	0.01	3

AVG=Average value (All values in ppm)  
 STD=Standard deviation of mean value at 1 confidence interval  
 ACC=Accepted value (Govindaraju, 1989)  
 A%=Accuracy [(average-accepted)/accepted]x100  
 P%=Precision (STDx100)/AVG  
 n=number of samples analysed

Table C11: Trace element analyses (INNA) of standard AGV-1 (Andesite)

	AGV1	AGV	AGV	AVG	STD	ACC	A%	P%	n
Cs	1.39	1.30	1.32	1.34	0.04	1.28	4.69	0.96	3
Th	6.5	6.06	6.45	6.34	0.20	6.50	2.46	1.03	3
U	2.09	1.95	2.1	2.05	0.07	1.92	6.77	1.12	3
Sc	11.96	11.98	11.99	11.98	0.01	12.20	1.80	0.03	3
Hf	5.40	5.47	5.49	5.45	0.04	5.10	6.86	0.24	3
Ta	0.90	0.84	0.89	0.88	0.03	0.90	2.22	1.00	3
La	38.3	39.3	38.34	38.65	0.46	38.00	1.71	0.40	3
Ce	71.4	69.8	72.5	71.23	1.11	67.00	6.31	0.52	3
Nd	32.6	32.00	32.90	32.50	0.37	33.00	1.52	0.38	3
Sm	6.60	6.20	6.58	6.46	0.18	5.90	9.49	0.95	3
Eu	1.62	1.65	1.63	1.63	0.01	1.64	0.61	0.25	3
Tb	0.67	0.62	0.67	0.65	0.02	0.70	7.14	1.20	3
Yb	1.68	1.68	1.66	1.67	0.01	1.72	2.91	0.19	3
Lu	0.25	0.25	0.24	0.25	0.01	0.27	7.41	0.64	3

AVG=average value (All values in ppm)

STD=standard deviation of mean value at 1 confidence interval

ACC=Accepted value (Govindaraju, 1989)

A%=Accuracy [(average-accepted)/accepted]x100

P%=Precision (STDx100)/AVG

n=number of samples analyzed

precision for Sc, Hf, La, Ce, Eu and Lu is <3% For Cs, Th, Nd, Sm, and Yb the precision is <6% For Ta and Tb the precision is <10% and for U <15% (Table C9). For G-2 the precision is <2% for Cs, Th, Sc, Hf, Ta, La, Ce, Sm, Eu, Tb and Lu and is <3% for U, Nd and Yb (Table C10). For AGV-1 (andesite) the precision is <2% for all the elements (Table C11).

The reported precision for this study is taken from all the standards analysed. For Sc, La and Ce the precision is <2%, for Hf and Lu <3%, for Eu and Yb <5%, for Th, Nd, Sm, Cs, Ta and Tb <10% and for U < 15%



**Appendix D****Distribution Coefficients**

The distribution coefficient ( $K_D$ ) is the ratio of a trace element in the mineral to the concentration of the trace element in the melt. The majority of reported  $K_D$  values have been determined on volcanic rocks, where the groundmass matrix is assumed to represent the melt. There has been limited work on determining  $K_D$  values for plutonic rocks as it is difficult to determine the composition of the melt from which a particular phase separated. The effect of temperature on  $K_D$  values depends strongly on the element and mineral considered. However, for most incompatible elements effects of temperature (1100-1300°C for basaltic cases, 650-800°C for granitic cases) are minor (Allegre and Minster, 1978). Major element partition coefficients used in this study are those presented in the program MODULUS (Knoper, unpublished). These values correspond with the average range of published felsic  $K_D$  values (Table D1). Table D2 shows the range in  $K_D$  values for the REE. Figure D1 shows the effect the  $K_D$  values have on a partial melt model. As can be seen the higher the  $K_D$  values the lower the overall REE concentration in the melt. Figure D2 shows the effect of varying only the  $K_D$  (Eu/Plag). The maximum  $K_D$  (Eu/Plag) results in a pronounced Eu anomaly and indicates more reducing conditions (Drake, 1975).

Table D1

 $K_p$  values

	Plag	Kspar	Biot	Opx	Amph	Qtz	Cord
La	.3	.05	.11	.1	.33	.012	.9
Ce	.25	.04	.32	.15	1.5	.006	.85
Nd	.20	.025	.30	.22	4.3	.009	.92
Sm	.13	.02	.26	.27	7.8	.008	.86
Eu	1.5	2.0	.25	.17	5.0	.031	.32
Tb	.09	.01	.35	.65	12.	.007	.45
Yb	.06	.01	.44	.86	8.0	.012	.97
Lu	.06	.008	.33	.90	5.5	.002	1.19
Rb	.06	.031	2.24	.003	.014	.012	0.0
Ba	.63	5.0	5.6	.003	.044	.004	.62
Th	.03	.01	.09	.11	.07	.006	1.85
U	.05	.008	.1	.12	.45	.014	1
K	.19	1.4	3.5	.001	.01	.014	0.0
Ta	.02	.001	1.2	.9	1.02	.007	.85
Nb	.02	.001	4.0	.8	1.5	0.0	.8
Sr	6.8	4.5	.12	.085	.022	0.0	1.3
P	.01	.01	.1	.03	.005	0.0	0.0
Hf	.06	.005	.44	.2	.84	.018	1.2
Zr	.04	.01	.79	.2	.72	0.0	1.0
Ti	.05	.05	2.5	.4	7	.015	1.0
Y	.04	.1	1.3	1	8	0.0	1.0
Ref	1-7	1-3,8,9	2,3,5-7	1-3,5,7	1-3,7,10	5,10	11

## References:

1. Nagasawa and Schnetzler, 1971;
2. Philpotts and Schnetzler, 1970;
3. Schnetzler and Philpotts, 1970;
4. Sun et al., 1974;
5. Nash and Crecraft, 1985;
6. Gromet and Silver, 1983;
7. Arth and Hanson, 1975;
8. Leeman and Phelps, 1981;
9. Long, 1978;
10. Cullers et al., 1973;
12. Reid, 1983

Table D2: Range of published  $K_D$  values for the REEMinimum  $K_D$  values

	Plag	Kspar	Biot	Opx	Amph	Qtz	Cord
La	.28	.03	.76	.10	.08	.012	.90
Ce	.21	.018	.30	.13	.43	.006	.85
Nd	.14	.009	.29	.20	1.03	.009	.92
Sm	.11	.012	.24	.25	1.61	.008	.86
Eu	.89	1.8	.24	.15	1.39	.031	.32
Tb	.09	.01	.30	.60	2.0	.007	.45
Yb	.06	.01	.40	.80	1.89	.012	.97
Lu	.06	.008	.30	.85	1.75	.002	1.19

Maximum  $K_D$  values

	Plag	Kspar	Biot	Opx	Amph	Qtz	Cord
La	.45	.15	15.1	7.7	40	.018	.9
Ce	.34	.095	11.0	7.7	40.9	.018	.85
Nd	.29	.09	5.7	4.46	52	.024	.92
Sm	.23	.946	4.3	1.7	18.5	.017	.86
Eu	7.9	9.56	4.7	.84	5.9	.08	.32
Tb	.19	.04	3.9	17	13	.026	.45
Yb	.13	.04	3.0	17.1	8.7	.025	.97
Lu	.13	.04	3.4	2.5	6.3	.024	1.19
Ref	1-7	1-3,8,9	2,3,5-7	1-3,5,7	1-3,7,10	5,10,	11

## References:

1. Nagasawa and Schnetzler, 1971; 2. Philpotts and Schnetzler, 1970; 3. Schnetzler and Philpotts, 1970;
4. Sun et al., 1974; 5. Nash and Crecraft, 1985; 6. Gromet and Silver, 1983; 7. Arth and Hanson, 1975;
8. Leeman and Phelps, 1981; 9. Long, 1978; 10. Cullers et al., 1973; 12. Reid, 1983

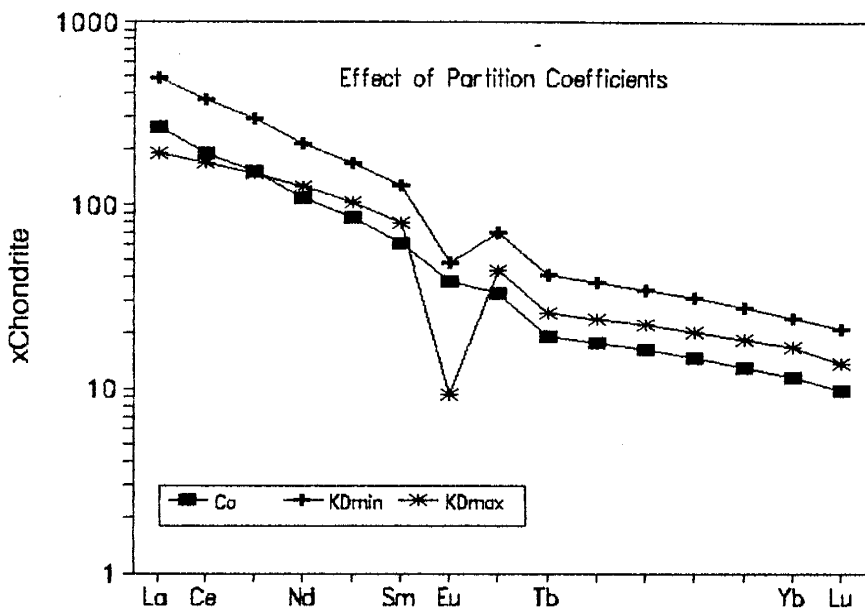


Figure D1: Effect of maximum and minimum  $K_D$  values on the REE concentration in the melt.

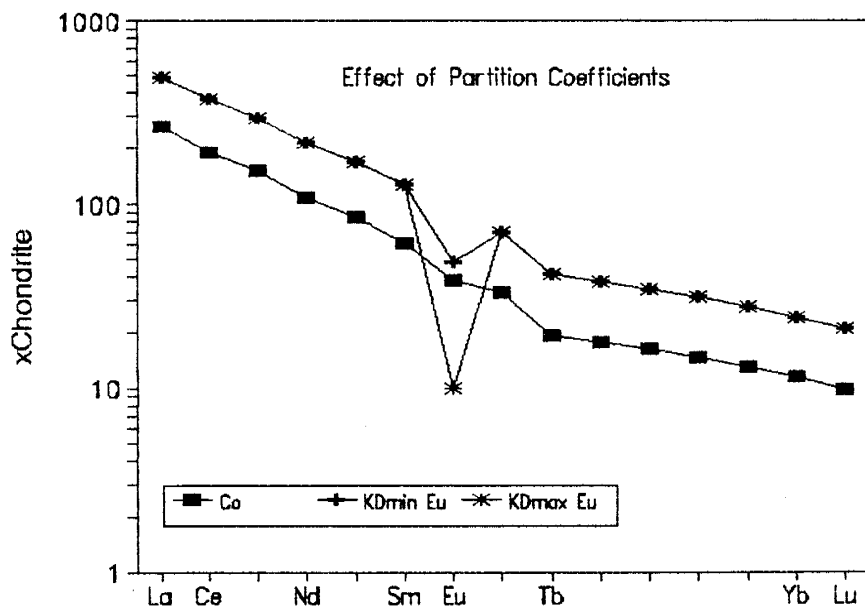


Figure D2: Effect of varying only the  $K_D(\text{Eu/Plag})$  on the REE concentration in the melt.

**Appendix E****Effects of source and melt modes on melt composition.**

Table E1 lists three source and melt modes tested as possible models for the genesis of the three granite plutons studied (Middle Mountain, Dome Peak and Mount Owen Plutons:

- A) Tonalite mode, no orthopyroxene or amphibole present.
- B) Felsic granulite mode, orthopyroxene but no K-feldspar in the source.
- C) Felsic granulite mode, amphibole but no orthopyroxene or K-feldspar in the source.

For 40% partial melting there is virtually no difference between a tonalite source mode and felsic granulite mode (OPX) in the concentration of REE in the melt (Figure E1). However if amphibole is present in the source and is not a major phase in the melt mode it's presence exerts a considerable control on the slope of the REE pattern. The light REE are still enriched relative to the source (Co), but there is no longer a Eu anomaly and the HREE are depleted relative to the source (Figure E2).

Table E1

A)

	MELT* (F=.2)	SOURCE	MELT (F=.4)	SOURCE
OPX	---	---	---	---
AMPH	---	---	---	---
PLAG	31%	57%	46%	65%
KSPAR	34%	8%	---	---
BIOT	4%	10%	6%	12%
QTZ	30%	22%	45%	20%
MGT	1%	2%	1.5%	2.3%

B)

OPX	1%	4%
AMPH	---	---
PLAG	47%	62%
KSPAR	---	---
BIOT	5%	7%
QTZ	46%	25%
MGT	1%	2%

C)

OPX	---	---
AMPH	2%	10%
PLAG	47%	48%
KSPAR	---	---
BIOT	5%	20%
QTZ	44%	20%
MGT	1%	2%

\* from Hanson (1978).

A) Tonalite mode for F=.2 and recalculated for F=.4 as Kspar is exhausted at 23% partial melting.

B) Felsic Granulite Mode with Opx

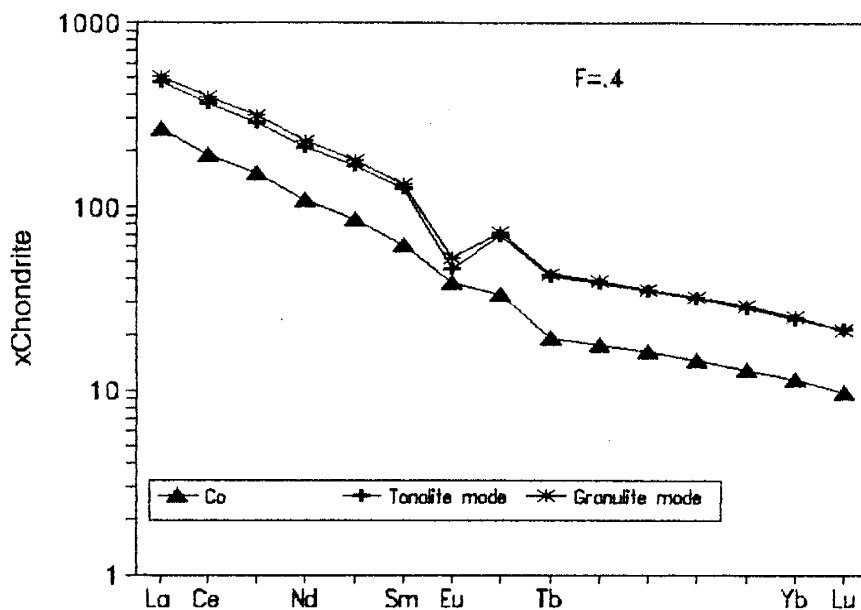


Figure E1: Effect of varying the source mode on the REE concentration in the melt.

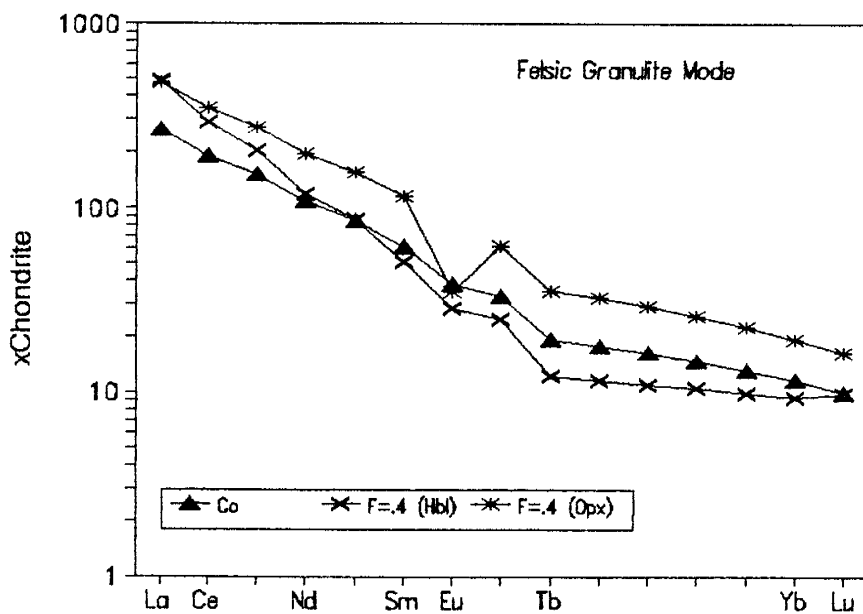


Figure E2: Effect of Opx (Mode B, Table E1) and Hbl (Mode C, Table E1) on the concentration of REE in the melt.

**Appendix F****Effect of Degree of Partial Melt on magma composition**

Figure F1 shows the effect of varying the degree of partial melt on the batch melting model of an Archean tonalite (Co). As can be seen the smaller the degree of partial melt the more enriched the melt in incompatible trace elements (REE, HFSE), however the slope of the REE pattern remains constant for varying degrees of partial melt. Similarly in fractional crystallisation models as the degree of crystallisation increases so too does the concentration of incompatible elements in the residual melt. For the purpose of this study melt ranges between 20-40% were considered reasonable based on the work of van der Molen and Paterson (1979) and Wickham (1987).



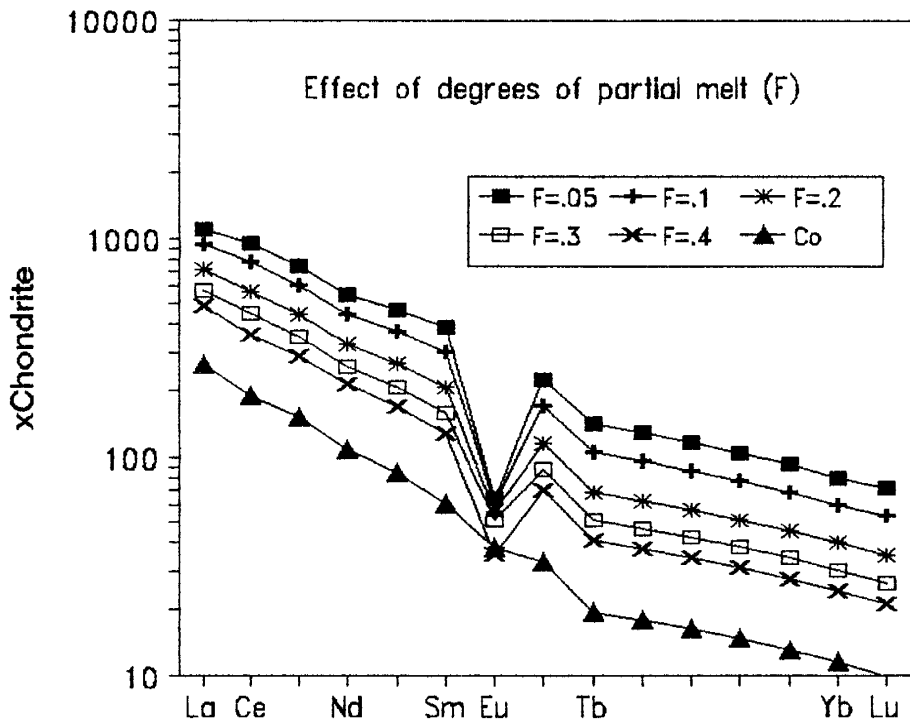


Figure F1: Effect of degree of partial melt on REE concentration in the melt.

## Appendix G

### Effects of Accessory phases on geochemical models.

Table G1 lists published REE  $K_D$  data for zircon, apatite, allanite, sphene and monazite. For each accessory mineral the effects of varying the source and melt modes are evaluated for 40% batch melting of an Archean tonalite at  $T=800^\circ\text{C}$  and  $P=10\text{Kb}$  (unless otherwise stated).

#### Zircon

Zircon,  $\text{ZrSiO}_4$  preferentially incorporates Zr, Hf, Nb, Ta, HREE, U and Th into its structure. The partition coefficient of Zr in Zircon has been determined experimentally by Watson and Harrison (1983),

$$\ln D_{\text{Zr}} (\text{Zircon/Melt}) = -3.80 - (.85(M-1)) + 12900/T \quad (\text{G1})$$

where  $M$  is the cation ratio  $(\text{Na}+\text{K}+2\text{Ca})/\text{Al}*\text{Si}$ , and  $T$  is the absolute temperature. Figure G1 taken from Watson and Harrison (1983) is a plot of zircon saturation/solubility experiments at various temperatures. For a given source rock one can determine the value of  $M$  and using Figure G1 to determine the solubility of zircon at various temperatures and calculate whether zircon will be left in the residue using the equation below:

$$C_m * F + C_s * (1-F) = C_o \quad (\text{G2})$$

Table G1:  $K_D$  values for REEs in Accessory Phases

Apatite	1	2	3 <sup>a</sup>	4
La	25.0	-	-	14.5
Ce	34.7	16.6	8.0	21.1
Nd	57.1	21.0	12	32.8
Sm	62.8	20.7	12	46
Eu	30.4	14.5	14	25.5
Tb	52.0*	-	12	40
Yb	23.9	9.4	12	15.4
Lu	20.2	7.9	12	13.8

Zircon	5	5	1	3	4
La	7.2	26.6	-	.65*	3.11
Ce	10	23.5	2.64	.65	3.49
Nd	4.6	22	2.20	.60	3.80
Sm	11.1	17.0	3.14	1.25	4.72
Eu	20	12.0	3.14	1.20	4.23
Tb	37	37.0	-	12	50
Yb	564	490	270	225	250
Lu	648	635	323	600*	330

Allanite	5	5	6	3
La	2827	2362	820	1000*
Ce	2494	2063	635	1000
Nd	1840	1400	463	640
Sm	977	756	205	300
Eu	100	122	81	125
Tb	311	235	71	90
Yb	37	24.5	8.9	16
Lu	44	22	7.7	16*

Table G1 cont.

Sphene	3 <sup>a</sup>	7	8 <sup>a</sup>
La	-	19	15
Ce	51.2	33.6	18
Nd	107	319	-
Sm	152	352	25
Eu	154	189	15.7
Tb	160	218	27.69
Yb	185	105	30
Lu	-	75	25.7

Monazite	9	10	11
La	10 <sup>3</sup> -10 <sup>4</sup>	10 <sup>3</sup> -10 <sup>4</sup>	10 <sup>4</sup> **
Ce	10 <sup>3</sup> -10 <sup>4</sup>	10 <sup>3</sup> -10 <sup>4</sup>	10 <sup>4</sup> **
Nd			-
Sm			3000**
Eu			1000**
Tb			1300**
Yb			200**
Lu			200**

\* Interpolated value

\*\* Theoretical value

a=  $K_D$  calculated as (element concentration in mineral/element concentration in whole rock).

- 1) Arth and Hanson, 1975.
- 2) Nagasawa and Schnetzler, 1971
- 3) Gromet and Silver, 1983.
- 4) Fujimaki, 1986.
- 5) Mahood and Hildreth, 1983.
- 6) Brooks et al., 1981.
- 7) Hellman and Green, 1978.
- 8) Cullers et al., 1987.
- 9) Miller and Mittlefehldt, 1982.
- 10) Rapp and Watson, 1986.
- 11) Condie, 1978.

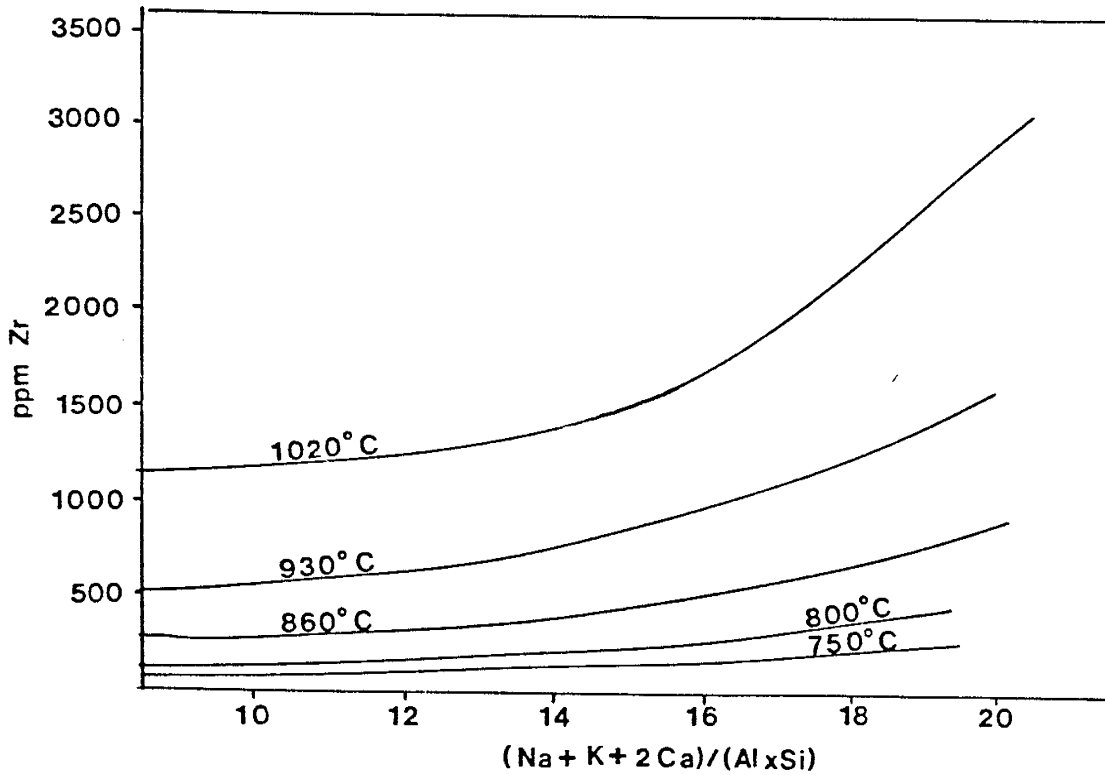


Figure G1: Results of hydrothermal zircon saturation/solubility experiments at temperatures of 1020°, 930°, 860° and 750°C, redrawn from Watson and Harrison, (1983). The residual zirconium concentration in the glass following zircon crystallisation is plotted here against a measure of the melt basicity, the cation ratio  $M = (Na + K + 2Ca)/(Al \cdot Si)$ .

Table G2

Calculation of whether zircon is a residual phase when an average composition of the Bridger/Louis Lake Batholiths is melted.

M	F	T°C	Solubility ppm	Zr (Co) ppm	Residue ppm
1.7	.4	750	100	190	250
1.7	.4	800	250	190	150
1.7	.4	850	500	190	-
1.7	.2	750	100	190	325
1.7	.2	800	250	190	110
1.7	.2	850	500	190	50
1.7	.2	930	1000	190	-

Table G3

Calculation of whether zircon is a residual phase when an Archrean greywacke is melted.

M	F	T°C	Solubility ppm	Zr (Co) ppm	Residue ppm
1.32	.4	750	50	150	325
1.32	.4	800	100	150	110
1.32	.4	850	250	150	50
1.32	.4	930	650	150	-

$M = (Na + K + 2Ca) / Al \times Si$

F = Degree of partial melt

where  $C_m$  is the solubility in the melt,  $C_s$  is the concentration in the residue and  $C_o$  is the total Zr in the system, i.e. the concentration in the source rock.

For the genesis of Middle Mountain and Dome Peak plutons the older Bridger and Louis Lake batholiths were considered as possible sources. Their average M value is 1.7 and Zr content is 190ppm. Table G2 shows the amount of zircon left in the residue for various temperatures of melting and degree of melt ( $F=.2$  and  $.4$ ). At  $850^\circ\text{C}$  there is no residual zircon left at  $F=.4$ . Not until temperatures of around  $950^\circ\text{C}$  are reached would all the zircon be melted for smaller degrees of melt ( $F=.2$ ).

For Mount Owen pluton a peraluminous S-type granite, an Archean greywacke was considered as a possible source with  $M=1.32$ , and a Zr content of 150ppm. Table G3 shows that there is residual zircon at temperatures up to around  $930^\circ\text{C}$ , at which point all the zircon will have melted.

All models were evaluated with zircon in the residue. For Middle Mountain, if the temperature of melting was greater than  $800^\circ\text{C}$  one may expect all the zircon to be melted. However within the range of Zr content (100-270ppm) for the Bridger and Louis Lake batholiths, this temperature may be extended to over  $850^\circ\text{C}$ . Also without Zircon in the residue the values of Zr in the melt are higher than those observed in Middle Mountain pluton.

Figure G2 shows the effect of varying the source and melt modes on the concentration of REE and Zr content in the melt.

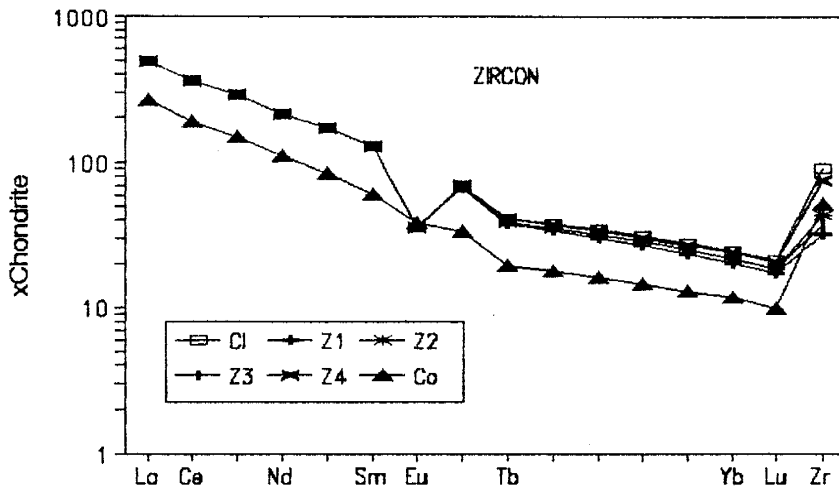


Figure G2: Effect of varying source and melt modes on the REE and Zr concentration in the melt.

Co=Source

Cl=No zircon in the residue (either it has all melted out or was never present in the source).

Z1=Source mode=.05wt% zircon, no zircon in the melt, M=1.7

Z2=Source mode=.05wt% zircon, Melt mode=.05wt% zircon, M=1.7

Z3=Source mode=.05wt% zircon, Melt mode=.05wt% zircon, M=1.4

Z4=Source mode=.01wt% zircon, Melt mode=.01wt% zircon, M=1.7

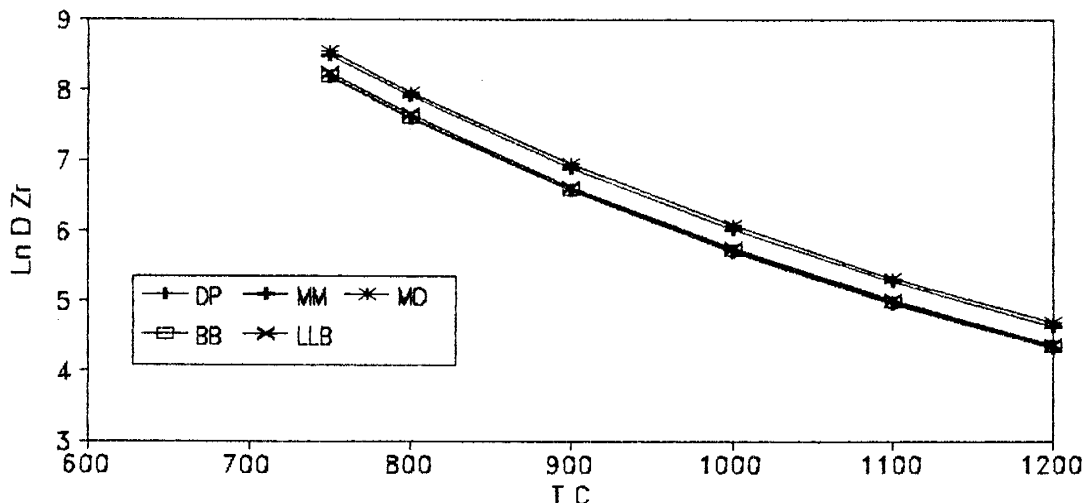


Figure G3: Plot of  $\ln D_{\text{zircon/melt}}$  for M values of 1.32 (Mmount Owen pluton), 1.38 (Middle Mountain pluton), 1.69 (Louis Lake batholith), 1.72 (Bridger batholith), and 1.76 (Dome Peak pluton).



C1 and Z1 are the extreme cases. No zircon in the residue will result in the highest concentration of both HREE and Zr in the melt. Zircon has little effect on the concentration of the LREE in the melt. Zircon in the residue, but not melting will result in the lowest concentration of HREE and Zr content in the melt. Decreasing the concentration of zircon in both the source and melt modes causes the concentration of the HREE and Zr to approach C1.

Changing M has no effect on the REE concentration but will lower the Zr content in the melt. For a given temperature the smaller the M value the larger  $\ln D_{Zr}$  (from equation G1). This is illustrated in Figure G3 which is a plot of  $\ln D_{Zr}$  against temperature for both the older granitoids (Bridger/Louis Lake batholiths) and younger granites (Middle Mountain, Dome Peak and Mount Owen plutons). As can be seen, Middle Mountain and Mount Owen plutons with smaller M values have larger  $K_p^{Zr/Melt}$  than the Bridger and Louis Lake batholiths and Dome Peak pluton.

## Apatite

Apatite ( $\text{Ca}_5(\text{PO}_4)_3(\text{OH}, \text{F}, \text{Cl})$ ) preferentially incorporates the REEs, U and P. The experimental work of Watson and Capobianco (1981) has shown that if the source  $\text{P}_2\text{O}_5$  content exceeds 0.14%, apatite must be residual for all degrees of melting, increasing in abundance as melting proceeds. The solubility of apatite has been determined experimentally by Harrison and Watson (1984) and is given by:

$$\ln D_p^{\text{apatite/melt}} = [8400 + ((\text{SiO}_2 - 0.5) 2.64 \times 10^4) / T] - 3.1 + 12.4 (\text{SiO}_2 - 0.5)$$

where T is the absolute temperature. Variations in pressure are unlikely to change significantly any solubility values.

Figure G4 shows the effect of varying the source and melt modes on the concentration of REE and  $\text{P}_2\text{O}_5$  content in the melt. Cl and AP1 are the extreme cases. Apatite in the source lowers the overall REE and P content in the melt and reduces the size of the Eu anomaly. A very small amount of apatite (.01wt%) in the source and melt modes has a negligible effect on the REE and P content.

Figure G5 shows the range of REE content for  $K_D$  values from Arth and Hanson (1975), Gromet and Silver (1983), and Fujimaki (1986). As can be seen the choice of  $K_D$  values will effect the overall concentration but not the distribution pattern of REE in the melt.

The average value of  $\text{P}_2\text{O}_5$  in the Bridger and Louis Lake

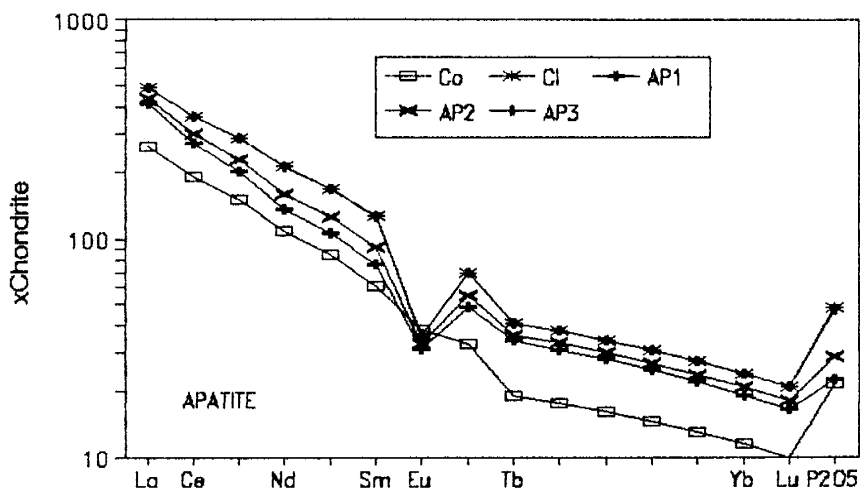


Figure G4: Effect of varying source and melt modes on the REE and  $P_2O_5$  concentration in melt.  $K_D$  values from Arth and Hanson (1975).

Co=Source

Cl=No apatite in the residue (either it has all melted or was never present in the source).

AP1=Source mode=.5wt% apatite, No apatite in the melt.

AP2=Source mode=.5wt% apatite, Melt mode=.5wt% apatite.

AP3=Source mode=.01wt% apatite, Melt mode=.01wt% apatite.

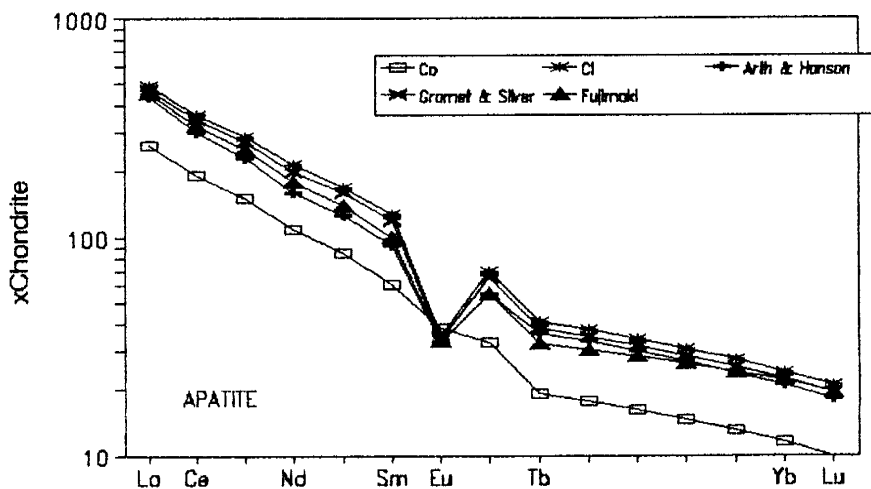


Figure G5: Effect of different apatite  $K_D$  values on REE content in the melt.

Co=Source

Cl=40% partial melt, no apatite in the source.

All other plots are for source and melt modes of .5wt% apatite ( $F=.4$ ).

batholiths is .24wt% and for the Archean greywacke .15wt%. Using the results of Watson and Capobianco (1981) and assuming that all  $P_2O_5$  forms apatite, then apatite is considered as a residual phase in generating Middle Mountain and Dome Peak plutons and as both a residual phase and exhausted phase in generating Mount Owen pluton.

A source mode of .5wt% apatite is considered to be a maximum value as likely sources (Bridger and Louis Lake batholiths, Archean greywacke) contain less than .5wt%  $P_2O_5$ .

## Allanite

Allanite  $(Ca, Ce)_2(Fe^{2+}, Fe^{3+})Al_2O.OH(Si_2O_7)(SiO_4)$  concentrates the REE, specifically the LREE, La and Ce. The only experimentally determined  $K_D$ s for allanite are for high silica rhyolites (Mahood and Hildreth, 1983) and rhyolite/obsidian glass (Brooks et al., 1981). The effect of temperature on the  $K_D$ s for allanite is unknown.

Figure G6 shows the effect of varying the source and melt modes for allanite on the concentration of the REE. Depending on how much allanite is in the source will determine whether the concentration of LREE in the melt is greater or less than the concentration in the source. All melts will have HREE concentrations greater than  $C_0$ , but for AL1 (no allanite in the melt) and AL2 (modal melting .05wt%) the HREE slope is flatter than both C1.

Figure G7 shows the effect of different  $K_D$  values of allanite on the concentration of REE in the melt. The  $K_D$  values of Brooks et al. (1981) and Gromet and Silver (1983) result in similar REE patterns, with a depletion in the LREEs relative to C1. The  $K_D$  values of Mahood and Hildreth (1983) produce a marked depletion in the LREE content relative to both C1 and C, these  $K_D$  values were determined for high silica (75-77wt%) rhyolites.

The presence of small amounts of allanite in the source can exert a considerable control on both the REE content and slope of the REE pattern. The effect of  $K_D$  values is also of

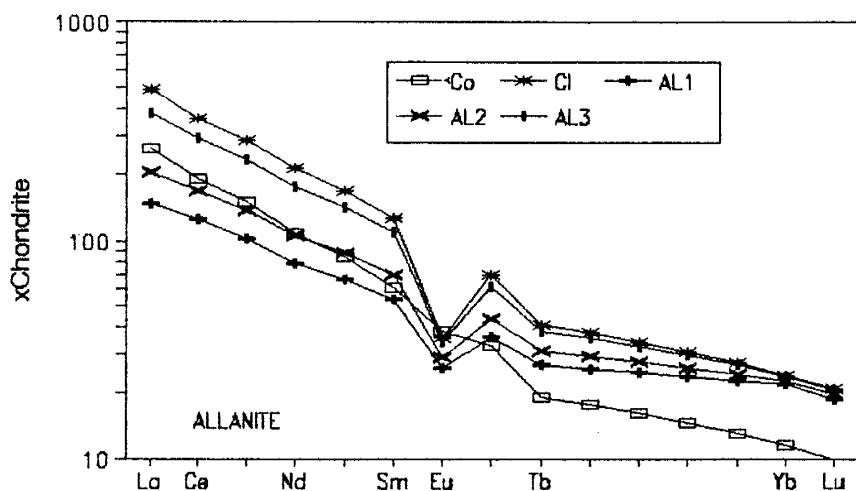


Figure G6: Effect of varying source and melt modes on the concentration of REE in the melt.  $K_D$  values from Mahood and Hildreth (1983).

Co=Source

Cl=No allanite in the source (either it has all melted out or was never present in the source).

AL1=Source mode=.05wt% allanite, No allanite in the melt.

AL2=Source mode=.05wt% allanite, Melt mode=.05wt% allanite,

AL3=Source mode=.01wt% allanite, Melt mode=.01wt% allanite,

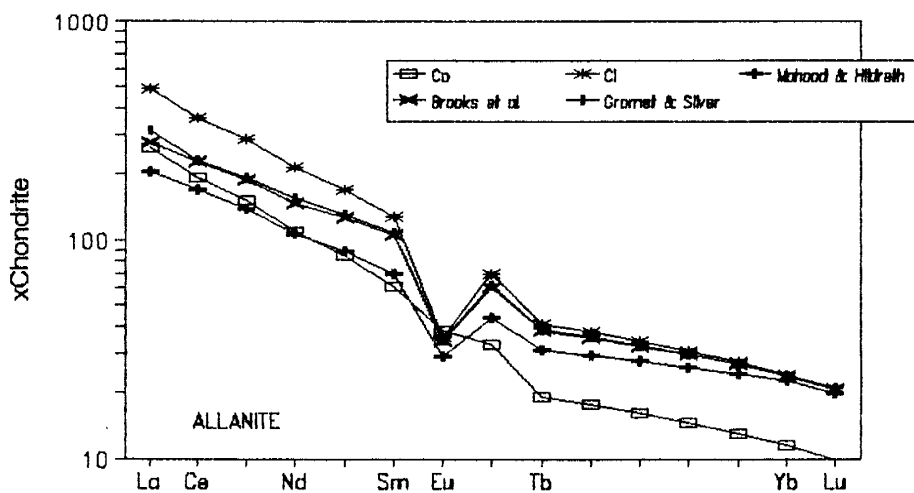


Figure G7: Effect of different  $K_D$  values for allanite on REE concentration in the melt.

Co=Source

Cl=40% partial melt, no allanite present.

All other plots are for a source and melt mode of .5wt% respectively. ( $F=.4$ )

extreme importance, as has been demonstrated in Appendix D.

For this study average values from Brooks et al. (1981) were used as these were determined on less evolved rhyolites ( $\text{SiO}_2=72-74\text{wt}\%$ ), which are compositionally closer to the granites analysed in this study.

**Sphene**

Sphene,  $\text{CaTi}(\text{SiO}_4)(\text{O},\text{OH},\text{F})$  preferentially concentrates the REEs, Th, Nb and Ta. Considering the ubiquitous presence of sphene in granitic rocks there is suprisingly little experimental  $K_D$  values for it.

Figure G8 shows the effect of different  $K_D$  values for sphene on the concentration of REEs in the melt. As can be seen there is an appreciable difference in the REE patterns for the different  $K_D$  values. The  $K_D$  values used in this study are derived from the results of Gromet and Silver (1983). The  $K_D$  value is calculated as the concentration of the element in sphene over the concentration of the element in the whole rock (granodiorite).



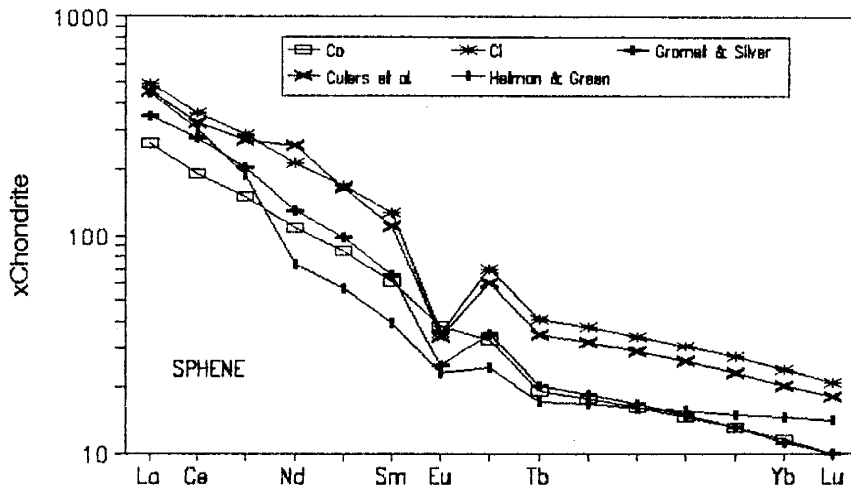


Figure G8: Effect of different  $K_D$  values for sphene on the REE concentration in the melt.

Co=Source

Cl=40% partial melt, no sphene in the source.

The other plots are for source and melt modes of .5wt% sphene respectively. ( $F=.4$ )

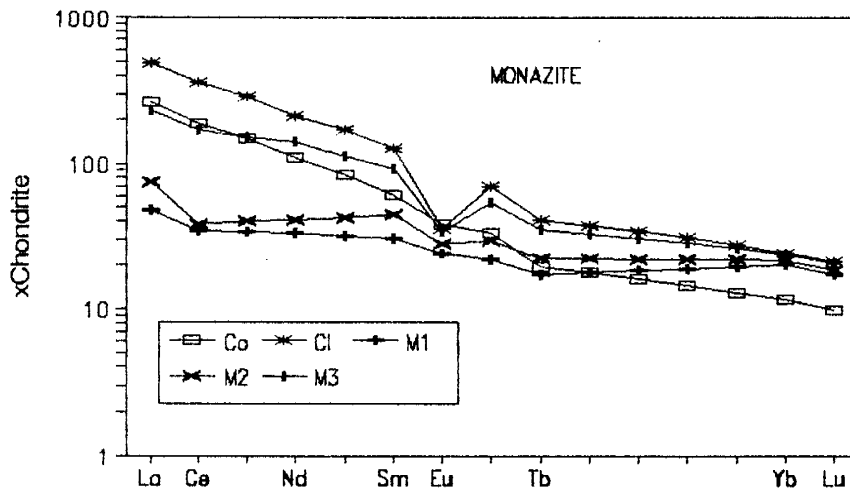


Figure G9: Effect of varying the source and melt modes of monazite on the REE concentration in the melt.

Co=Source

Cl=No monazite in the source (either it has all melted or was never present in the source).

M1=Source mode=.05wt% monazite, No monazite in the melt.

M2=Source mode=.05wt% monazite, Melt mode=.05wt% monazite.

M3=Source mode=.01wt% monazite, Melt mode=.01wt% monazite.

## Monazite

Monazite  $(\text{Ce,La,Th})\text{PO}_4$  concentrates the LREEs (La,Ce) and Th. Miller and Mittlefehldt (1982) recognised the importance of depleting LREEs in peraluminous magmas by crystallizing out allanite and monazite. Montel (1986) showed that at 2kb, 800°C the solubility of  $\text{CePO}_4$  is especially low in peraluminous liquids, favouring the precipitation of monazite. Rapp and Watson (1986) determined  $K_D$  values for the LREE as a group for monazite. Their results (Table G1-monazite, column 2) were consistent with estimates made by Condie (1978) and Miller and Mittlefehldt (1982).

Figure G9 shows the effect of varying the source and melt modes of monazite on the concentration of REE in the melt. It can be seen that the presence of a small amount (.05wt%) monazite in the source has a dramatic effect on the REE pattern. There is a dramatic drop in REE content, especially the LREE and a reduction in the size of the Eu anomaly, with a flattening out of the HREE. Only .01wt% in both the source and melt has a lesser effect on the MREE (Sm, Eu, Tb) and HREE (Yb, Lu), but still results in a lower LREE (La,Ce) content relative to the source.

**Appendix H****Fine-Tuning Geochemical Models**

For any given model the final source and melt modes for accessory phases was determined by varying the source and melt modes of the accessory phases. This is shown below for non-modal equilibrium partial melting of the older Bridger and Louis Lake batholiths. Table H1 lists the source and melt modes for major minerals and the range of source and melt modes for accessory phases tested.

Figure H1 shows the REE patterns produced by varying the source and melt modes for 40% batch melting of the older granitoids (Bridger and Louis Lake batholiths). The maximum REE content is achieved when there are no accessory phases in the source mode (T1). The minimum REE content is produced when no accessory phases enter the melt (T4) and from the work of Watson et al. (1985) and Susuki et al. (1990) this model is unlikely to occur as accessory phases are concentrated at grain boundaries, where early melting is likely to occur. In Figure H2 the REE distribution of the five different models are plotted along with the average value for Middle Mountain pluton. The slopes of models T3 and T5 are closest to that of the average value for Middle Mountain pluton; however, only model T5 is able to generate the Zr values for the melt (C1) which then crystallised to form Middle Mountain pluton.

## Appendix H

Table H1: Source, melt and restite modes (in fractions) for 40% batch melting of the older granitoids (Bridger and Louis Lake batholiths).

F=.40, T=850°C, P=10Kb, M=1.7

	Melt Mode <sup>a</sup>	Source Mode	Restite
OPX	.01		.05
PLAG	.47	.62	.66
BIOT	.05	.07	.08
QTZ	.45	.25	.20
MGT	.01	.02	.02
ZIR	.0001-.0005 (.0005)*	.0001-.0005 (.0002)*	.0001*
ALA	.0001-.0005 (.0005)*	.0001-.0005 (.0002)*	.0001*
APA	.0005-.005 (.005)*	.0005-.005 (.002)*	.001*
SPH	.005-.0005 (.004)*	.005-.0005 (.002)*	.0012*

a=From Hanson (1978).

\*=Preferred numbers; numbers for which the models fits the best.

M=Cation ratio (Na+K+2Ca)/(AlxSi) (Watson and Harrison, 1983).

OPX=Orthopyroxene

PLAG=Plagioclase

BIOT=Biotite

QTZ=Quartz

MGT=Magnetite

ZIR=Zircon

ALA=Allanite

APA=Apatite

SPH=Sphene

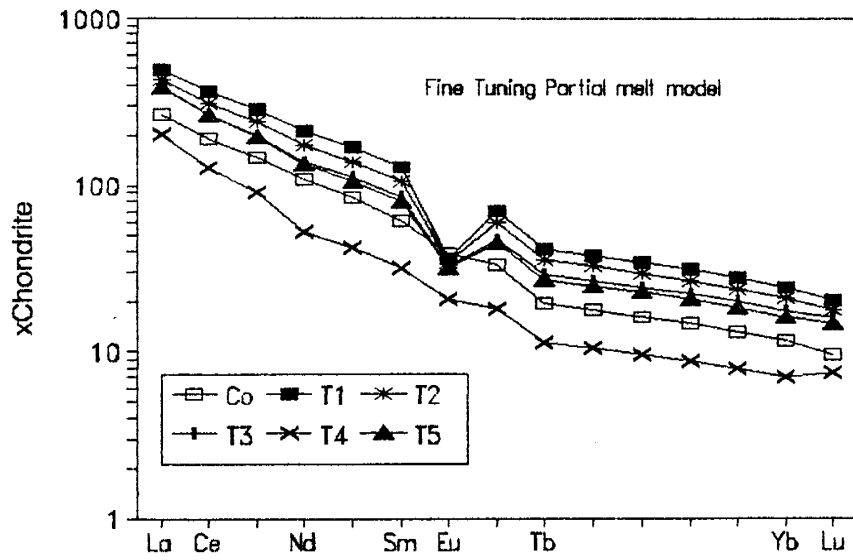


Figure H1: REE patterns produced by 40% batch melting of Co (Bridger/Louis Lake batholiths) with varying source and melt modes (fractions) of accessory phases.

	T1		T2		T3		T4		T5	
	Melt	Source	Melt	Source	Melt	Source	Melt	Source	Melt	Source
Zircon	----	----	.0001	.0001	.0002	.0001	-----	.0005	.0005	.0003
Allanite	----	----	.0001	.0001	.0002	.0001	-----	.0005	.0005	.0003
Sphene	----	----	.0005	.0005	.003	.002	-----	.005	.005	.003
Apatite	----	----	.0005	.0005	.003	.002	-----	.005	.005	.003

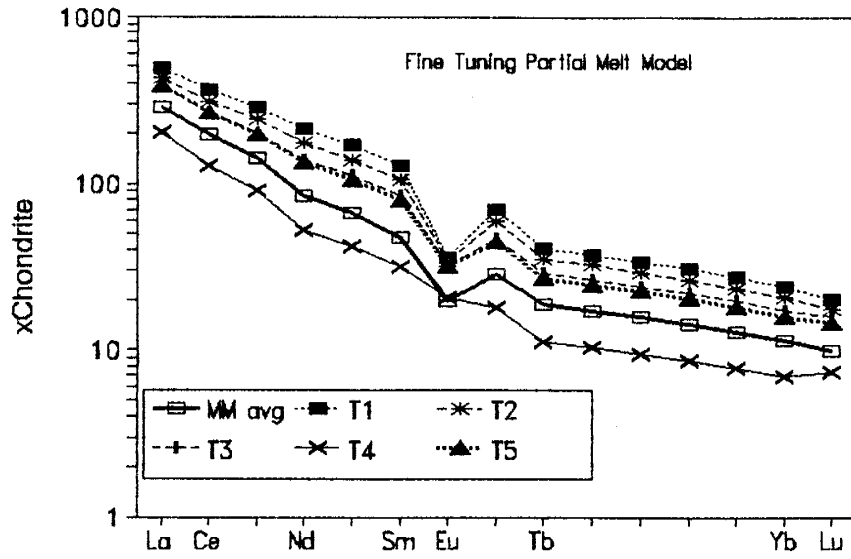


Figure H2: A REE plot of the previous patterns (T1-T5, Figure H1) with the average REE content of Middle Mountain pluton.

## Appendix I

## Element concentrations (in ppm) for geochemical models of Middle Mountain Pluton

Table I1: Composition of sources used in batch melting (columns 1,2), fractional crystallisation (column 3) and assimilation fractional crystallisation (columns 3,4) models.

	1	2	3	4
Rb	34.1	106	148	61
Sr	171	1410	349	732
Ba	147	1810	1250	480
Th	2.8	14.7	27	1.6
U	.08	5.5	1	0.33
La	32.3	64.4	55.5	23
Ce	58.7	121.8	104	55
Nd	23.8	51.2	33	26
Sm	4.5	9.4	5.5	4.9
Eu	1.09	2.21	1.49	1.41
Tb	0.35	0.72	0.47	0.81
Yb	0.47	1.9	1.2	3.5
Lu	0.08	0.24	.14	0.55
Y	3.8	37	18	4.0
P	0.08	0.45	1.8	0.12
Nb	1.7	14.8	6.7	3.1
Ta	0.11	3.64	0.33	0.17
Zr	101	271	150	110
Hf	1.2	9.1	3.3	3.3

1 and 2) Minimum and maximum source concentrations for batch melting models, compiled from the Bridger and Louis Lake batholiths.

3) The melt produced by 40% batch melting corresponding to sample RL-1, from the Middle Mountain pluton.

4) The assimilant used in the AFC model, an averaged from from Aleinikoff et al. (1989)

Table I2: Crystallisation modes (fractions) for FXL and AFC models.

F=40%, T=850°C, P=10kb, M=1.7

	FXL	AFC
AMP	.01-.05 (.0)*	.01-.05 (.0)*
PLAG	.30-.57 (.31)*	.30-.57 (.31)*
KSPAR	.08-.35 (.29)*	.08-.35 (.29)*
BIOT	.05-.10 (.07)*	.05-.10 (.07)*
QTZ	.20-.30 (.30)*	.20-.30 (.30)*
MGT	.02	.02
ZIR	.0001-.0005 (.0001)*	.0001-.0005 (.0003)*
ALA	.0001-.0005 (.0001)*	.0001-.0005 (.0002)*
APA	.0005-.005 (.001)*	.0005-.005 (.001)*
SPH	.0005-.005 (.004)*	.0005-.005 (.0001)*

\*=Preferred numbers; numbers for which the model works best.

FXL=Fractional crystallisation

AFC=Assimilation and fractional crystallisation

F=Degree of partial melt, P=Pressure (Kb), T=Temperature of melting (T°C).

M=Cation ration (Na+K+2Ca)/(Al\*Si) (Watson and Harrison, 1983)

AMP=Amphibole

PLAG=Plagioclase

KSPAR=K-feldspar

BIOT=Biotite

QTZ=Quartz

MGT=Magnetite

ZIR=Zircon

ALA=Allanite

APA=Apatite

SPH=Sphene



## Appendix J

## Element concentrations (in ppm) for geochemical models of Dome Peak Pluton

Table J1: Composition of sources used in batch melting (columns 1,2) and fractional crystallisation (column 3) models.

	1	2	3
Rb	34.1	106	64.6
Sr	171	1410	708
Ba	147	1810	2321
Th	2.8	14.7	8.8
U	.08	5.5	1.1
La	32.3	64.4	93
Ce	58.7	121.8	188
Nd	23.8	51.2	82
Sm	4.48	9.35	15.9
Eu	1.09	2.21	3.59
Tb	0.35	0.72	1.14
Yb	0.47	1.9	2.31
Lu	0.08	0.24	0.27
Y	3.77	37.54	25.31
P	0.08	0.45	0.22
Nb	1.7	14.8	9.1
Ta	0.11	3.64	0.55
Zr	101	271	219
Hf	1.2	9.1	11.2

1 and 2: Minimum and maximum source concentrations for batch melting compiled from the Bridger and Louis Lake batholiths.

3: The melt produced by 20% batch melting, corresponding to sample NFL-7 from Dome Peak pluton.

Table J2: Source and melt modes for batch melting of the older granitoids (Bridger and Louis Lake batholiths).

F=.40, T=850°C, P=10Kb, M=1.7

	Melt Mode	Source Mode	Restite
OPX	.01		.05
PLAG	.47	.62	.66
BIOT	.05	.07	.08
QTZ	.45	.25	.20
MGT	.01	.02	.02
ZIR	.0001-.0005 (.0005)*	.0001-.0005 (.0002)*	.0001*
ALA	.0001-.0005 (.0005)*	.0001-.0005 (.0002)*	.0001*
APA	.0005-.005 (.005)*	.0005-.005 (.002)*	.001*
SPH	.005-.0005 (.004)*	.005-.0005 (.002)*	.0012*

Table J3: Crystallising modes for FXL models.  
FXL

AMP	.01-.05 (.02)*
PLAG	.30-.57 (.31)*
KSPAR	.08-.30 (.30)*
BIOT	.05-.10 (.07)*
QTZ	.20-.30 (.30)*
MGT	.02
ZIR	.0001-.0005 (.0001)*
ALA	.0001-.0005 (.0001)*
APA	.0005-.005 (.001)*
SPH	.0005-.005 (.004)*

All abbreviations are the same as in Appendix I.

## Appendix K

## Element concentrations (in ppm) for geochemical models of Mount Owen Pluton

Table K1: Composition of sources used in batch melting an Archean greywacke (column 1), fractional crystallisation of a magma produced by batch melting a greywacke (column 2), and the contaminants used in AFC models of a magma produced by batch melting a greywacke (column 3,4).

	1	2	3	4
Rb	110	164	35	61
Sr	250	68.4	450	600
Ba	900	789	480	800
Th	15	40	1.6	1.6
U	1.5	1.2	0.3	0.3
La	25.3	62.7	35.4	45.1
Ce	45.7	127	56.7	74.8
Nd	25.8	52.2	21	22
Sm	4.4	13.6	3.5	3.2
Eu	1.28	0.96	1.01	1.52
Tb	0.54	1.46	0.47	0.18
Yb	1.6	3.8	1.1	0.59
Lu	0.28	0.42	0.21	0.06
Y	17	45	4.0	45
P	0.09	0.05	0.12	0.12
Nb	4.1	6.5	3.1	4.5
Ta	0.9	0.76	0.17	0.17
Zr	160	185	110	110
Hf	4.5	5.34	3.33	3.33

Column 1: Archean greywacke from Taylor and McClennan (1985).

Column 2: Concentration produced by 40% batch melting of the Archean greywacke, corresponding to sample MO-5 from Mount Owen pluton.

Column 3 and 4: Assimilants used in the AFC model, compiled

from the older granitoids in the Wind River Range (Bridger and Louis Lake batholiths and Aleinikoff et al. (1989).

Table K2: Source, melt, and restite modes (in fractions) for 40% batch melting an Archean greywacke from Arth and Hanson (1975), and Reid (1983).

F=.30, T=850°C, P=10Kb, M=1.38.

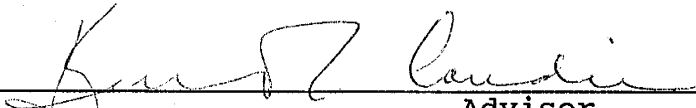
	Melt Mode	Source Mode	Restite
PLAG	.47	.46	.44
BIOT	.06	.136	.18
GARN	.015	.026	.03
CORD	.015	.026	.03
QTZ	.44	.35	.27
MGT	.01	.02	.03
ZIR	.0001-.0005 (.0001)*	.0001-.0005 (.0001)*	.0001*
APA	.0005-.005 (.0002)*	.0005-.005 (.0001)*	.0001*

Table K3: Crystallising modes for FXL and AFC models.

	FXL	AFC
AMP	.01-.05 (.02)*	.01-.05 (.02)*
PLAG	.30-.57 (.32)*	.30-.57 (.32)*
KSPAR	.08-.30 (.28)*	.08-.30 (.28)*
BIOT	.05-.10 (.07)*	.05-.10 (.07)*
MUSC	0-.01 (.01)*	0-.01 (.01)*
QTZ	.20-.30 (.22)*	.20-.30 (.22)*
MGT	.02	.02
ZIR	.0001-.0005 (.0001)*	.0001-.0005 (.0001)*
ALA	.0001-.0005 (.0002)*	.0001-.0005 (.0001)*
APA	.0005-.005 (.001)*	.0005-.005 (.0005)*
SPH	.0005-.005 (.0005)*	.0005-.005 (.003)*
MONAZ	.0001-.0005 (.0002)*	.0001-.0005 (.0002)*

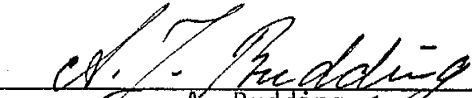
All abbreviations the same as Appendix I, additional abbreviations are; GARN=Garnet, CORD=Cordierite, MUSC=Muscovite and MONAZ=Monazite.

This dissertation is accepted on behalf of the faculty  
of the Institute by the following committee:

  
\_\_\_\_\_

Kent Condie

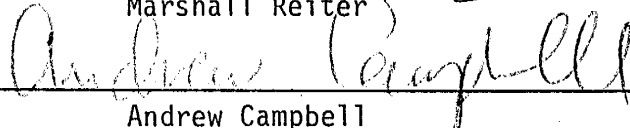
Adviser

  
\_\_\_\_\_

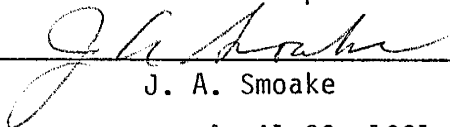
A. Budding

  
\_\_\_\_\_

Marshall Reiter

  
\_\_\_\_\_

Andrew Campbell

  
\_\_\_\_\_

J. A. Smoake

April 29, 1991

\_\_\_\_\_

Date